MODELLING STREAMFLOW VARIABILITY IN DRY AND WET ZONE RIVER BASINS IN SRI LANKA USING SATELLITE SOIL MOISTURE DATA

Utsab Phuyal

(208360T)

Degree of Master of Science

Department of Civil Engineering

University of Moratuwa
Sri Lanka

February 2022

MODELLING STREAMFLOW VARIABILITY IN DRY AND WET ZONE RIVER BASINS IN SRI LANKA USING SATELLITE SOIL MOISTURE DATA

Utsab Phuyal

(208360T)

Supervised by

Prof. R. L. H. L. Rajapakse

Thesis submitted in partial fulfillment of the requirements for the degree

Master of Science in Civil Engineering

UNESCO Madanjeet Singh Centre for

South Asia Water Management (UMCSAWM)

Department of Civil Engineering

University of Moratuwa

Sri Lanka

February 2022

DECLARATION OF THE CANDIDATE AND SUPERVISOR

"I declare that this is my own work and this thesis does not incorporate without acknowledgement any material previously submitted for a Degree or Diploma in any other University or institute of higher learning and to the best of my knowledge and belief it does not contain any material previously published or written by another person except where the acknowledgement is made in the text".

Also, I hereby grant to University of Moratuwa the non-exclusive right to reproduce and distribute my thesis/dissertation, in whole or in part in print, electronic or other medium. I retain the right to use this content in whole or part in future works (such as articles or books).

UOM Verified Signature

2022-02-06

------ ----------

Utsab Phuyal Date

The above candidate has carried out research for the Masters Dissertation under my supervision.

UOM Verified Signature

2022-02-06

. ----------

Porf. R. L. H. L. Rajapakse Date

ABSTRACT

Modelling Streamflow Variability in Dry and Wet Zone River Basins in Sri Lanka using Satellite Soil Moisture Data

Streamflow variability is important in basin water resources management to analyze and plan for the present and future hazards and vulnerabilities affecting effective water management. The unique feature of soil to hold the moisture regulates the precipitation falling on its surface generating the variability in streamflow. The lack of extensive data for distributed hydrological models restrains modelers to accurately simulate temporal and spatial variability of streamflow associated with the soil moisture (SM) in basin-scale. The present study is focused on the use of a simple hydrologic model to assess the impact of SM on the generation of streamflow variability in selected dry and wet zone river basins in Sri Lanka and enhance the model accuracy through the use of satellite soil moisture (SSM) data. The wet and dry zone river basins, Kalu Ganga and Kirindi Oya basins, respectively with a diverse streamflow variability were selected for this study. A semi-distributed hydrologic model was developed to model various events using Hydrologic Engineering Centre's Hydrologic Modelling System (HEC-HMS) with soil moisture accounting (SMA) as the loss method. The results obtained from the model are compared with model results forced with soil moisture active passive (SMAP) SM data to assess the impact of antecedent moisture on watershed hydrology.

Events of varying magnitude in terms of discharge and precipitation from both Maha and Yala seasons were selected considering different return period discharge to calibrate and validate the model performance. Both models developed for Kirindi Oya and Kalu Ganga performed well with an average Nash-Sutcliffe Efficiency (NSE) of above 0.73 for calibration and above 0.75 for validation along with average root mean square error (RMSE) and observed standard deviation ratio (RMSE std dev) below 0.55 for calibration and below 0.48 for validation. The average coefficient of determination (R^2) was obtained above 0.80 indicating a strong correlation. Initial use of SSM improved the model performance of the Kalu Ganga basin whereas deteriorated the performance of the Kirindi Oya basin. The performance was further enhanced by optimizing the soil storage and groundwater parameters yielding an average NSE higher than 0.80, an average R^2 of above 0.90 along with an average RMSE std dev below 0.35 in both basins. Further, the average variation in peak discharge and runoff volume was reduced to 6 % and 2 %, respectively for Kirindi Oya and 15 % and 10 %, respectively for Kalu Ganga basins. The overestimated peak discharge and runoff volume were reduced by 28 % and 18%, respectively upon increasing the soil storage parameters whereas the underestimated peak discharge and runoff volume were increased by 37 % and 43%, respectively by decreasing the soil storage parameters.

A minor adjustment in soil storage allowed to manipulate and fine-tune the peak discharge and runoff volume in the basin which substantiates that the runoff is directly associated with the basin SM. The findings of this study can be useful in basins with similar hydrological characteristics to understand the role of SM in runoff generation and for sustainable water management in the basin.

Keywords: Antecedent moisture condition (AMC), Event-based modelling, Soil moisture accounting (SMA), Soil moisture active passive (SMAP)

DEDICATION

I would like to dedicate this work to my

Father and Mother

The biggest treasure of my life who always taught me to do good and work hard. No words can explain their patience and sacrifices beyond everything just to shape my life.

To my amazing two

Sisters

For having faith in me and cheering me every time to work harder.

ACKNOWLEDGEMENTS

It is a genuine pleasure to express my deep sense of gratitude and warm appreciation to my supervisor Prof. Lalith Rajapakse for his persistent support in this study through his immense knowledge, motivation, and guidance. In every step of the study, he continually and convincingly conveyed a spirit of motivation to shape and reshape this valuable piece of work. Without his guidance, captivating words, and consistent help, this work would not have been possible.

I take this opportunity to convey my heartiest thanks to Prof. Sohan Wijesekera for conveying a deeper sense of knowledge through his teachings which were valuable in this study and steered me in the right direction of completing this work.

My gratitude is extended to Dr. Janaka Bamunawala for his continuous effort in helping out in any circumstances. Respected panel members are highly acknowledged for their constructive and valuable comments during every presentation that helped me shape this document.

A debt of profound gratitude is owed to my mentor, Mr. Wajira Kumarasinghe for his kind assistance throughout this course. It was his selfless support and encouragement that helped me to push myself further and make this dream a reality.

My sincere gratitude to the late Sri Madanjeet Singh for his vision and efforts to establish the UMCSAWM centre and I am highly indebted to South Asia Foundation (SAF) Nepal for bestowing me with this scholarship. My humble appreciation to Dr. Nishchal Nath Pandey, Chairperson, SAF Nepal Chapter for his kind help and support throughout this period.

I would like to convey my gratitude to all the staff of the centre for their kind assistance throughout this course. My special thanks to Irrigation Department for providing data useful for this study. My thanks and appreciation also goes to my colleagues who have willingly helped me out with their abilities and motivated me constantly.

Last but not the least, my grandparents, my father and mother, and my sisters owe loads of appreciation for providing me with continual support and encouragement throughout my life.

TABLE OF CONTENTS

LIST OF FIGURES

LIST OF TABLES

LIST OF ABBREVIATIONS

AM	-	Annual Maximum
AMC	-	Antecedent Moisture Condition
CDD	-	Consecutive dry days
CDS	-	Consecutive low-flow days
CWD	-	Consecutive wet days
CWS	-	Consecutive high-flow days
DC	-	Deficit and Constant
DEM	-	Digital Elevation Model
ESA	-	European Space Agency
ESRI	-	Environmental Systems Research Institute
ET	-	Evapotranspiration
FDC	-	Flow Duration Curve
FIT	-	First Inter Monsoon
HEC	-	Hydrologic Engineering Center
HMS	-	Hydrologic Modeling System
IPCC	-	Intergovernmental Panel on Climate Change
LULC	-	Land-use Landcover
MIT	-	Minimum Inter-event Time
NEM	-	North East Monsoon
NSE	-	Nash Sutcliffe Efficiency
PBIAS	-	Percentage Bias
POT	-	Peak Over Threshold
PVE	-	Percentage Streamflow Volume Error
R10	-	Heavy precipitation days

R20	-	Very heavy precipitation days
RAS	-	River Analysis System
RMSE	-	Root Mean Square Error
RMSE std dev	-	RMSE Observed Standard Deviation Ratio
RX1 day	-	Max 1-day precipitation
RX2 day	-	Max 2-day precipitation
RX5 day	-	Max 5-day precipitation
SCS	-	Soil conservation service
SIM	-	Second Inter Monsoon
SM	-	Soil Moisture
SMA	-	Soil Moisture Accounting
SMAP	-	Soil Moisture Active Passive
SPI	-	Standardized Precipitation Index
SSI	-	Standardized Streamflow Index
SSM	-	Satellite Soil Moisture
SWAT	-	Soil and Water Assessment Tool
SWM	-	Southwest Monsoon
SX1 day	-	Max 1-day flow
SX2 day	-	Max 2-Day Flow
SX5 day	-	Max 5-Day Flow

CHAPTER 1

1 INTRODUCTION

Streamflow variability is important in basin water resources management to analyze present hazards and vulnerabilities induced due to flood and drought affecting the effective water management in basins. Hydrologic processes that attribute to the streamflow generation largely depend on the spatial and temporal distribution of water in the catchment (McMillan & Srinivasan, 2015). Atmospheric variations along with land surface changes bring gradual changes to the streamflow over a long period. However, the accelerated anthropogenic intervention on the natural environment has induced climate change exacerbating the climatic conditions thereby affecting the streamflow variability in a short span of time (Gleick & Adams, 2000).

Climate change is a serious global problem, a concern for all stakeholders, and an important factor influencing hydrological cycles, resulting in changes in river flows. Intergovernmental Panel on Climate Change (IPCC) Sixth Assessment Report (AR6) has pointed out that in South Asia during the 21st century, both annual and summer monsoon precipitation will increase along with enhanced increased interannual variability (Zhai et al., 2021). Extreme weather events such as floods and droughts have become more common and severe as a result of these changes, posing a substantial threat to water resources and their proper management. However, the lack of hydrometeorological data with sufficient spatial and/or temporal resolution in many watersheds around the world is a major impediment to effective water resources management (Johnston & Smakhtin, 2014).

A principal variable in the hydrological modeling is soil moisture (SM) which largely influences the partition of rain between runoff and infiltration and therefore regulates outflow from the watersheds (Aubert et al., 2003). Accurate SM information is very important for real-time flood forecasting (Zhuo & Han, 2017). The availability of remote sensing data has increased over the past few decades. Indirect measurements

can be used to remotely estimate many hydrological variables and water fluxes like SM. Satellite remote sensing furnishes serviceable data for the calibration and validation of hydrologic models (Milzow et al., 2011). The SM information obtained from satellite data sets can be used to model the ungauged basins making it easier to conduct river hydrology-related studies in developing countries with limited data sets.

The Asian region exhibits ten of the world's biggest rivers that provide water, energy, and food to the billions of people living in the region. Yet there is a lack of integrated understanding of spatiotemporal streamflow variability in the region (Nguyen et al., 2020). Sri Lanka, an island nation in South Asia, has around 103 river basins that cater to the need of the people living in dry and wet zones. Lack of hydrometeorological data and economic constraints make it difficult to manage water resources properly in those basins. Streamflow variability study in a few major basins has demonstrated the hastened changes in the streamflow which are attributed to climate change and direct human intervention on the basins (Dissanayaka & Rajapakse, 2018; Shelton & Lin, 2019). The authors also pointed out that the streamflow variability study is important to scientifically manage water resources in the basin and to provide effective decisions in the process and further study needs to be carried out incorporating direct and indirect human influences, soil moisture, land-use changes, and irrigation practices.

Floods during 2003, 2008, 2016, and 2017 in Kalu Ganga (Ministry of Disaster Management, 2017) and droughts during 2004, 2012, 2014, and 2016 in Kirindi Oya (Chandrasekara et al., 2021) represent streamflow variabilities in different time scales that have affected people in the basins along with various agricultural and economic activities. Thus, there is a dire need for a deeper understanding of the variability of streamflow.

This study examines the climate extremes and precipitation trends assimilating them with the soil water moisture to model streamflow in a dry basin (Kirindi Oya) and wet basin (Kalu Ganga) of Sri Lanka using the commonly employed Hydrologic Engineering Centre's system known as Hydrologic Modelling System (HEC-HMS). The model developed is employed for the simulation of variability in streamflow at different time scales and is calibrated and validated using the streamflow measurements at the outlet section of the river basin. The results obtained from the

model are compared with model results forced with satellite soil moisture data to assess the impact of SM on watershed hydrology and analyze the practicality of incorporating satellite soil moisture (SSM) data sets. The findings can be used to provide recommendations for basin-wide water resource management which is both effective and sustainable.

1.1 Problem Identification

It is evident that climate change is affecting the hydrological cycle distressing water resources and a deeper understanding of the process through distributed modeling is required for efficient water resources management. Most of the modelers avoid modeling streamflow variability in diverse saturation scenarios as the models demand comprehensive parameters. In-situ SM data is barely available in most parts of the world owing to the complexities and expenses incurred for obtaining data. The widespread availability and increasing accuracy of SSMs allow modelers to investigate the value of SMs in hydrological models. Yet, there is a substantial gap in the application of SSM in hydrological models to accurately simulate streamflow in varying saturation scenarios.

The wet and dry zone river basins, experiencing heavy flooding during the rainy season and conversely experiencing severe drought during the dry periods making it hard for water managers to cater to multiple water demands in the basins, are considered as pilot study areas for this research. Proper recommendations can be given through this study to sustainably manage water resources in the basin.

1.2 Problem Statement

The effect of climate change can be well observed in dry and wet zone rivers of Sri Lanka generating frequent streamflow variabilities such as increased drought and flooding. This is attributed to land-use changes which reduce effective soil moisture capture area leading to instant saturation of the soil during intense precipitation and rapid drying during dry periods. The runoff and water storage in the basin is influenced by soil moisture but very few give regard to its role in the modeling process. There is always a big challenge in developing a model with different layers of soil that would

store water simultaneously and release it to the basin like a natural system. Very few models have been developed in the Asian region that would precisely simulate both wet and dry flow conditions with high accuracy incorporating SSM data made available in the recent past.

1.3 Objectives

1.3.1 Main Objective

The principal objective of this study is to evaluate the impact of soil moisture on streamflow variability in two selected dry and wet zone river basins in Sri Lanka by considering different soil saturation scenarios and incorporating the findings in improving model accuracy.

1.3.2 Specific Objectives

The specific objectives of the study are as listed below.

a) To identify the natural precipitation and streamflow extremes and trends analyzing data of historical periods in the basin and their impact on soil moisture and streamflow.

b) To identify an appropriate model and estimate the streamflow variability considering different saturation scenarios.

c) To develop, calibrate and validate the model and evaluate model performance with the available past data sets.

d) To develop a relationship between soil moisture and streamflow variability under different saturation scenarios.

e) To verify the use of satellite soil moisture data in the region and derive conclusions/recommendations for basin water resources management.

CHAPTER 2

2 LITERATURE REVIEW

2.1 General

The ability to predict river temporal and spatial changes at the catchment level is essential to understanding the potential impact of anthropogenic climate change on humans and ecosystems (Chien et al., 2013). However, due to the sheer volume of data required for advanced hydrological models, it is tedious to accurately evaluate the influence of streamflow variability. Thus, there is a substantial gap in modeling, where a simple model would consider optimum parameters available to provide output comparable to highly sophisticated distributed models. To start with this, a systematic literature survey is conducted to find the potential gaps and research needs in the study area and develop a scientific approach to get near to the solution.

Under the literature review, investigations have been conducted to identify a suitable hydrological model with minimal parameters competent in simulating both wet and dry period flows in the basin. Since the main motive of this study is to assess the importance of satellite soil moisture (SSM) in producing runoff, various models which are capable of accommodating SM as input were studied. The application of these models in water resources management was also explored during the literature review process. Input data (precipitation, land use, and soil data) along with their resolution and source, parameters coupled with the model, ways to develop parameters, and data associated with those parameters were also investigated during the literature review process. Different sources of SSM data, their temporal and spatial resolution, usefulness, and accuracy compared to in-situ SM were also assessed to select an appropriate SSM data set. Data collected should be checked for inconsistencies, missing values, and a literature review on this was also performed for handling missing data and checking for consistency.

In addition, systematic studies were conducted to investigate how events have been identified during wet and dry conditions. In this study, various objective functions were studied to explain the model outputs and analyze the goodness of fit of simulated results with the observed records. Also studied about the calibration procedures and validation of the model results with the available data sets along with the ways of performing sensitivity analysis. The entire literature review process mentioned above proceeds in the order of global application at first, then the regional application and application in the Sri Lankan region.

2.2 Soil Moisture and Hydrology

Land surface hydrology is largely controlled by soil moisture which acts as a critical atmospheric boundary condition thereby, regulating energy and water interchanges between the atmosphere and land through the regulation of the evapotranspiration fluxes (Lettenmaier et al., 2015). The SM is broadly identified as an important parameter that maintains a balance between the surface and the atmosphere in terms of mass and energy, and the accurate estimation of SM in hydrology has a huge social and hydrological benefit. Technically, the amount of water contained (expressed in weight or volume) in the soil is defined as soil moisture. Here, soil moisture refers to the water stored in between the pores of the solid particles in the soil. Water enters into the soil mainly from precipitation and is removed from the soil by drainage, evaporation, or transpiration. During the whole process of water traveling in and out of the soil, water is trapped into the pores of the soil. Precipitation, temperature, and soil properties (size of solid particles and pores) all influence the amount of water retained in the soil.

In hydrology, soil moisture plays a key role in producing runoff and storing water for the use of plants and the ecosystem. Depending on the saturation level of the soil, the runoff from the precipitation is determined. If the soil is unsaturated or partially saturated, the precipitation falling into the soil surface will be first stored in the underlying soil layers depending on soil properties and intensity of precipitation and then produced as runoff once the soil is unable to store or pass water through it. The water stored will be useful for the plants or will contribute to the baseflow eventually

traveling through different soil layers. If the soil is fully saturated or precipitation can not pass water through it, a large proportion of precipitation is lost as a runoff leading to decreased storage, increased peak flows, and occurrences of flooding (Brocca et al., 2017; Nasimi, 2018; Parajka et al., 2006).

2.2.1 Estimation of Soil Moisture

The SM estimates can be obtained through in-situ observations, remote sensing, and land surface models. Point in-situ measurement of SM is the most accurate technique compared to the other two methods. Yet the method only represents moisture of a point and is unable to represent on a large area. Recent development in remote sensing and computation power has improved the accuracy of satellite soil moisture datasets making them usable in many fields of applications (Ahmad et al., 2021; Brocca et al., 2017; Vereecken et al., 2008). Techniques like assimilation of SSM data with the land surface models provide near-accurate SM estimates increasing the overall accuracy of datasets (Ahmad et al., 2021; Enrekhabi et al., 2014).

2.2.2 Application of Soil Moisture Data

SM data sets can be employed in various fields for the application of runoff modeling and flood forecasting, drought monitoring, numerical weather prediction, climate models assessment, crop yield forecast, land surface and agricultural monitoring, and wildfire risk assessment (Brocca et al., 2017). The author further discussed the emerging applications of SM in the field of erosion and landslide prediction, rainfall estimation, epidemic risk monitoring, and irrigation management.

Several studies in the different parts of the world employed SM estimates for the enhancement of the flood simulation through data simulation approach, estimation of initial conditions in flood modeling, estimating basin-wide water budget, and calibration of hydrologic models (Alvarez-Garreton et al., 2016; Aubert et al., 2003; Bennett & Peters, 2004; Bhuiyan et al., 2017; Brocca et al., 2012; López et al., 2016; Parajka et al., 2006; Tavakol et al., 2019; Vrugt et al., 2006). Although the importance of SM in runoff modeling is unclear (Brocca et al., 2017), some authors observed moderate to significant improvements in model performance after assimilating SM in the model (Brocca et al., 2012, 2010; Cenci et al., 2016), while some authors witnessed

a decline in the model performance (Alvarez-Garreton et al., 2015). Hence, depending upon the scope of the work, adequate care should be given for the assessment of data before its use in the model.

Soil Moisture has been widely used in various fields of application such as drought assessment, flood modeling, and others related to hydrology in the South Asian region. Ahmad et al. (2021) assimilated SMAP retrievals with a land surface model and obtained improved SM estimation across the South Asian region highlighting the importance of satellite data in data-scarce regions. Sheffield and Wood (2007) used soil moisture data from land surface model simulations to analyze the spatial and temporal characteristics of global droughts in the second half of the 20th century. The results showed general agreement for major events in the world at global scales but diverge noticeably in cooler seasons and regions in latter years. Thus, the SM data sets can be used in the application of hydrological related modeling in the data-scarce regions.

2.3 Hydrological Modelling

A hydrological model defined by Chow et al. (1988) is an approximation of the actual system. Models are primarily used to predict system behavior and understand different hydrological processes and their properties are defined by several parameters. For environment and water resources management, hydrological models these days are considered an essential tool (Devia et al., 2015). The author pointed out that the best model is the one that provides near-realistic results with the use of fewer parameters and less model complexity.

Chow et al. (1988) defined hydrological models into namely two (2) categories: a physical model and an abstract model. A physical model is a scalar representation of a system. An abstract model represents a system as a set of equations connecting input and output variables which are functions of space and time. A simple runoff model is an abstract model defined as a set of equations that help to estimate runoff as a function of various input parameters (mainly precipitation and discharge area) used to characterize catchments. It also considers catchment characteristics such as soil

characteristics, vegetation cover, catchment topography, SM content, and characteristics of groundwater aquifers.

2.3.1 Types of Models

Based on model parameters and the input provided and the range of physical principles employed in the model, rainfall-runoff models can be classified into different categories. The distributed and lumped model are two different types of models defined based on the model parameters applied as a function of time and space. In the lumped model, the watershed is regarded as a single point in space (spatially averaged) without dimensions. In a distributed model, hydrological processes at diverse points in space are considered and the space dimensions are used to define the model variables. A single set of input values will provide the same output in a deterministic model whereas, outputs are at least partially random in stochastic models (Chow et al., 1988). Based on temporal consideration, the models are classified as static and dynamic models. Time is excluded in a static model whereas time is incorporated in the dynamic model. The event-based model and continuous model are two types classified by Wheater et al. (2008) where the event-based produces output for the specific periods only while the latter one produces an output for a continuous period.

The models can be categorized as empirical, conceptual, or completely physical. An empirical model does not include a physical transformation function that connects inputs and outputs. This is because these models typically build relationships between inputs and outputs based on hydrometeorological data (Sarkar et al., 2012). Ondieki (1997) investigated four catchments with non-perennial rivers located in different arid conditions to analyze the water resource potential and identified the existence of some relationship between rainfall and runoff along with suspended sediment load. But a study by Costa et al. (2003) identified that the variation in runoff can not be explained by rainfall alone. The author concluded that other factors such as rainfall intensity, antecedent moisture content, and various physical characteristics of the catchment (e.g., soil, land use, geology, slope, and land-use conditions) too affect the generation of runoff.

Jackson et al. (2011) defined conceptual models based on two criteria, i.e., a model structure defined prior to simulation, and all model parameters cannot be interpreted physically and need to be estimated using observed data through calibration. A study on SM dynamics carried out by Parajka et al. (2006) revealed that a conceptual semi-distributed model employed with scatter meter data had a substantial impact on hydrological processes. Valent et al. (2013) developed a lumped conceptual model that would predict the runoff and test the calibration procedure and concluded that uncertainties would arise in the runoff generation due to the conceptualization and the quality of input fed to the model.

St. Venant equations, Green–Ampt equations, and other basic mathematical equations can be employed to relate parameters in a physics-based model. The physics-based models can well reflect spatial variations in critical land surface properties such as slope, vegetation, and aspect, as well as climatic parameters such as precipitation, temperature, and evapotranspiration (ET) distribution. (Akbari & Singh, 2012).

2.3.2 Model Selection

Among various types of models mentioned above, there are many hydrological models developed based on the various approaches to simulate discharge at the outlet. There are models such as HEC-HMS (semi-distributed), ABCD model, SWAT (distributed), MIKE II, MIKE-SHE, RRI model and so on that can simulate discharge with the input of precipitation and other basin parameters. Some models have their standalone program interface while some need to be developed using other applications/systems (Excel, python, etc.). Few models are discussed below with their advantages and disadvantages as portrayed in Table 2-1.

The HEC-HMS is a semi-distributed, physically-based model developed by the U.S. Army Corps of Engineers HEC which can be used in a dendritic watershed for the reproduction of runoff processes. The model is applied in the simulation of the individual fluxes associated with the hydrologic cycle such as infiltration, base flow, snow-melt, evapotranspiration, and channel routing. The model is relevant to several analyses such as streamflow forecasting, flood studies, water quality, erosion, reservoir spillway design, urban drainage, and sediment transport.

The Soil and Water Assessment Tool (SWAT) is a model relevant for any size basin (small to large basin) developed and supported by the Agricultural Research Service (ARS) of the United States Department of Agriculture (USDA), which is used to simulate both quantity and quality of groundwater and surface water and assess the effect of land management practices, land use, and climate change on the environment. The model divides the entire catchment into hydrologic response units (HRU) considering land use, soil characteristics, and vegetation. The various inputs employed by the model are rainfall data, solar radiation, minimum and maximum air temperature, wind speed, and relative air humidity which are used to illustrate sediment and water circulation and nutrients circulation. Watershed management, assessment of soil erosion, and pollution source identification and control are the wide areas of application of SWAT (Devia et al., 2015).

Système Hydrologique Europeèn (MIKE-SHE) model developed in 1990 by Danish Hydraulic Institute (DHI) is a physical-based model which involves extensive ranges of physical parameters for the simulation of runoff. Different processes associated with the hydrological cycle such as river flow, precipitation, interception, evapotranspiration, unsaturated and saturated groundwater flow, etc are accounted for in the model. The model can be employed in the simulation of groundwater and surface water movement, their interactions, nutrient, sediment, and pesticide transfer in the watershed, and water quality assessments which can be exercised for large watersheds (Devia et al., 2015).

Upon studying various types of available models, HEC-HMS was adopted as a suitable model for this study. The model was selected based on data availability, the requirement of fewer parameters for generating highly accurate results, and ease of development and use of the model.

Table 2-1: Advantages and disadvantages of different hydrological models

Advantages	Disadvantages
Hydrologic Modeling System (HMS)	
• Requires less parameter input than fully distributed models making it easier to use. • Freely available and widely used throughout the world. • Detailed technical report and user's manual.	• Cannot model branching or looping and backwater in stream networks. • Parameters relating to soil and others require initial conditions only which may not fully justify the actual condition of the watershed. • Simplified model formulation, and simplified flow representation
Soil and Water Assessment Tool (SWAT)	
• Numerous parameters to describe watershed physical conditions to obtain results of higher accuracy. • Freely available in the public domain and open source. • Simulates sediment, pollutant loading, and downstream impacts	• Spatial representation of HRUs ignores pollutant routing within a sub-watershed. • Model formulas are empirical. • Not applicable for 2D or 3D hydraulics applications
MIKE-SHE (Systeme Hydrologique European)	
• Advanced, integrated modeling system for simulating hydrological processes in linked surface and groundwater systems. • Simulates sediment and water quality changes	• Not available freely. • Highly parsimonious making it difficult to use for general modelers.

2.4 Hydrologic Modeling System (HMS)

The HEC-HMS is a hydrological model developed in 1998 by the US Army Corps of Engineers. The HEC-HMS is devised to simulate the hydrologic processes (rainfall-runoff simulation) of a dendritic watershed system (Schaffenberg & Fleming, 2013). It can be used for flood analysis, reservoir, and spillway analysis (USACE, 2008). The model can be implied for both event-based and continuous modeling. Feldman (2000) signified that the procedures involved in HEC-HMS are mostly empirical. The model mainly uses Muskingum's wave method and kinematic wave method for routing of flow in the channel. In terms of hydraulic modeling, HEC has another model known as HEC-RAS where the HEC-HMS output is deployed as input data for river analysis. Several studies have been conducted combining both HMS and RAS for hydrological and hydraulic analysis of the river basin.

The HEC-HMS model allows input for both point and grid precipitation and discharges data for hydrological analysis of the catchment. The model has reasonable physical data requirements such as digital elevation models (DEMs) or contours for slope, elevation and flow path, soil map, and land use map (Baumbach et al., 2015). The HEC (USACE) has made available both the technical reference and user manual for easy usage of the model. Halwatura and Najim (2013) indicated that the model has an enhanced system interface and uses an interactive elemental system for managing and storing data along with well-demonstrated hydrologic components. There is an inherent automatic optimization option for the user to optimize model results (Kamali et al., 2013).

2.4.1 Model Structure

The HEC-HMS processes runoff volume by withdrawing the total amount of losses in the catchment system (infiltration, interception, storage, evaporation, and transpiration) from precipitation (Feldman, 2000). There are three (3) basic components in the model which are the precipitation loss model, basin model, and control specification. The Basin model transforms input atmospheric conditions into runoff at a specific point considered as an outlet of the watershed. Meteorological data is fed into the precipitation model to simulate the hydrologic processes. The specific

period of starting and ending of the simulation along with the simulation time interval is specified in the control specification. The physical components of the basin model (precipitation loss model, baseflow model, transform model, and routing model) are the inherent components of the basin model. The model offers different methods for the simulation of each cycle of components/segments in the model. The cons and pros of each method are clearly described in Schaffenberg and Fleming (2013).

2.4.2 Precipitation Loss Model

The HEC-HMS offers nine (9) different precipitation loss methods for simulation of streamflow where only two methods i.e., the SMA and Deficit and constant method can be employed best for continuous simulation (Schaffenberg & Fleming, 2013). The deficit and constant method is comparable to the initial/constant loss method which considers total losses in the model to equate an initial value. The input parameters for simulating precipitation loss are maximum deficit, initial deficit, impervious area, and constant loss rate.

Initial deficit specifies the water necessary for the soil layer to get saturated at its maximum storage capacity. Maximum storage represents the upper limit of the amount of water (expressed in terms of depth) possible to store in the soil layer. The parameter does not have any specific value ranges, but it is analogous to potential retention (maximum) defined by the soil conservation service (SCS) curve number which can be estimated referring to SCS (Chow et al., 1988). The constant rate is indicated by the rate of percolation in saturated soil. The initial loss can regain after a dry period of longer duration in this method which makes it unique compared to the initial/constant loss model.

The dynamic transfer of water into the soil can be simulated using the SMA method considering five different soil layers i.e., canopy interception storage layer, surface depression storage layer, soil layer, upper groundwater, and lower groundwater layers. Unlike the SCS curve number loss model that ignores soil profile considering difficulties in parameter estimation and focuses only on the surface processes, SMA considers those layers with a variety of parameters defining the soil layers (Tramblay et al., 2010). All of these layers require initial water storage expressed in percentage

as an input. Maximum infiltration rate represents the amount of water (depth) that can travel from the surface to the underlying soil layer and the initial estimation is carried out using hydraulic conductivity rates of different soil types. The surface which restricts transmission of water into the underlying soil layers is represented as the impervious area in the model. Soil storage is the maximum amount of water (depth) possible to store in the top layer of soil and can be withdrawn by both percolation and evapotranspiration. The amount of water stored in the pores of the soil layer is expressed as tension storage and it can only be removed by evaporation. The rate of movement of water from the top layer of soil to the groundwater layers is specified as percolation rate which can be adopted referring to the literature. Groundwater storage (GW1 and GW2) and percolation rate are analogous to the soil layer while groundwater coefficient expressed in time is the maximum period of retention of water in the respective groundwater layers (Schaffenberg & Fleming, 2013). Singh and Jain (2015) in their study identified soil percolation and soil storage as highly sensitive parameters of this model.

It is very important to select an appropriate loss method for obtaining higher accuracy in the estimation of runoff. Loss methods available in HEC-HMS were compared regarding different objective functions and were ranked high to low by Rostami and Khalighi (2016) in Iran. Green Ampt method was identified as the most suitable loss method considering event-based simulation by the authors. Moreover, Razmkhah (2016) compared different loss methods, and based on the findings of event-based modeling, SMA was ranked as the best method.

2.4.2.1 Soil Moisture Accounting Method

There are five (5) layers in the soil moisture accounting (SMA) method to store the water in the leaves (canopy storage), in surface (surface storage), in the upper soil profile (soil storage), and two (2) ground layers (Groundwater 1 and Groundwater 2). When rain falls, the initial loss is the water stored in leaves in the form of canopy storage. The water stored on the depression in the surface, which is not infiltrated, credits to surface storage. Precipitation exceeding canopy and surface storage is deducted with infiltration to obtain direct runoff/surface flow. Evaporation is the only process to remove water from the canopy whereas evaporation and infiltration are the

processes involved in removing water from the surface storage. The impervious parts of the basin do not allow deep storage and infiltration losses. The shallow surface storage and deep aquifer are hydraulically linked to streamflow by the two (2) groundwater layers. The base flow arises as a lateral flow from groundwater layers. The weather condition, water stored in the canopy, surface depression and soil profile, and canopy vegetation type are the factors influencing evaporation. The monthly evapotranspiration (ET) values can be provided as a direct input in the model, or the model can calculate potential ET from temperature and net radiation data using the Priestly-Taylor method (Schaffenberg & Fleming, 2013).

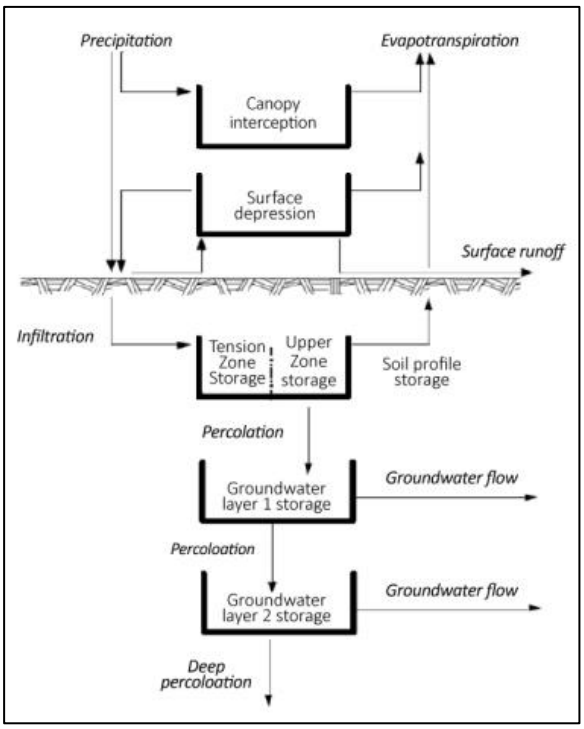

Figure 2-1: Schematic diagram of HEC-HMS soil-moisture accounting module

Source: Schaffenberg and Fleming, (2013)

2.4.2.2 Antecedent Moisture Condition

Antecedent Moisture Condition (AMC) is the moisture content of the pervious surfaces before the start of any rainfall event. The AMC, also known as Antecedent Runoff Condition (ARC) is an important factor in the runoff process because it reflects the relative saturation of the soil, which influences the infiltration process. The lower moisture content due to little preceding rainfall characterizes low AMC condition

whereas higher moisture content (saturated soil) due to higher preceding rainfall is considered as high AMC (Schaffenberg & Fleming, 2013).

For purpose of practical application, SCS suggests three levels of AMC as follows:

a) AMC-I: Relatively dry soils with less saturated soil and less rainfall
b) AMC-II: Medium saturation levels in the soil
c) AMC-III: Highly saturated soil with sufficient rainfall within the immediate past 5 days

Compared to total water availability on earth, a minimal part of the water is stored in the soil, but it is undoubtedly one of the most elemental factors influencing runoff generation and its understanding allows flood forecasting as the runoff is directly affected by soil saturation (Dorji, 2018). Various researchers have incorporated AMC in hydrologic modeling in Sri Lanka using HEC-HMS where the model performed significantly better in AMC III compared to traditional models which do not consider the wetness of the soil (Dorji, 2018; Kamran & Rajapakse, 2018).

2.4.3 Transform Model

There are seven (7) transform methods available in HEC-HMS for the transformation of excess precipitation to runoff. They are Snyder unit hydrograph, user-specified unit hydrograph, Clark unit hydrograph, Soil conservation service (SCS) unit hydrograph, Kinematic wave model, and ModClark Model. The SCS unit hydrograph is the simplest of all and generates accurate results with a single parameter as an input. Here, a portion of the unit flow generated before the peak flow is analyzed to define a curvilinear unit hydrograph (Schaffenberg & Fleming, 2013). Lag time is required to be provided as an input in the SCS unit hydrograph model which is calculated using the Kirpich equation explained in Chow et al. (1988). A comparative study of different available transform methods carried out by Halwatura and Najim (2013) in Attanagalu Oya basin, Sri Lanka demonstrated that Snyder unit hydrograph is more efficient in simulating streamflow than Clark unit hydrograph. A study carried out by De Silva et al. (2014) considered Clark unit hydrograph for the transformation accounting for a small storage unit located upstream of the catchment. The Clark unit hydrograph represents attenuations considering storage like reservoirs in the sub-basins along with

the translation of excessive rainfall. Time of concentration and the Storage coefficient are two (2) input parameters essential for this method.

2.4.4 Baseflow Model

There are different approaches to modeling baseflow i.e., conceptual and process-based among which HEC-HMS uses conceptual methods for modeling baseflow with each one having its pros and cons. The models available in HEC-HMS are bounded recession, linear reservoir, constant monthly, recession, and non-linear Boussinesq.

The recession method is primarily designed for simulation of events simulation but maintains an ability to reset to normal after simulation of each storm event and thereafter be employed for continuous simulation (Schaffenberg & Fleming, 2013). Recession constant, initial discharge, and ratio to peak are three (3) input parameters involved in this method. The flow condition at the beginning of the simulation is specified as the initial flow. The recession constant characterizes the rapid/slow fall in the baseflow. A ratio to peak denotes the abrupt or slow transition of peak to the baseflow.

The linear reservoir model is suited best for simulating base flow in linking with the SMA model. It simulates the movement and storage of sub-surface flow by considering storage and also simulates the movement of water through reservoirs. The Clark unit hydrograph represents runoff of watershed mathematically similar to SMA (Schaffenberg & Fleming, 2013). In an undisturbed catchment, the baseflow can be efficiently simulated using a linear reservoir model due to smooth fall in baseflow as the baseflow recedes 40% faster in a disturbed catchment (Buytaert et al., 2004). Groundwater coefficient, Initial discharge, and the number of reservoirs are the input parameters required for this model.

2.4.5 Routing Model

There are different approaches to route or model a flow through the channel in HEC-HMS. They are lag, Muskingum, Muskingum-Cunge, modified puls, and kinematic wave models. Each of these models takes the upstream hydrograph as the boundary condition and computes the downstream hydrograph. Everyone does this by solving

the equations of continuity and momentum (Feldman, 2000). Some models provide lag only whereas some models perform both lag and flow attenuation at the same time. The HEC-HMS technical manual provides a detailed explanation of each of these models mentioned above and guidelines on how to select them. Few models are compared for the purpose of our study.

Table 2-2: Advantages and disadvantages of routing models available on HEC-HMS

Model	Advantages
Lag Routing	*Advantages* • Simple to set up and use • The method is parsimonious (uses one parameter only) *Disadvantages* • No attenuation simulated by this method, only translation • Parameters cannot be estimated using measurable channel characteristics • Cannot simulate backwater effects or impacts of hydraulic structures
Muskingum Routing	*Advantages* • Easy to set up and use • The method is parsimonious (uses few parameters) • Successfully used in many studies *Disadvantages* • Only appropriate for use in moderately steep streams • Cannot simulate variable translation and attenuation • Cannot simulate backwater effects or impacts of hydraulic structures
Muskingum Cunge Routing	*Advantages* • Predicted values are in accordance with open channel flow theory • Parameters can be calculated using measurable channel characteristics • Suitable for ungagged reaches *Disadvantages* • Requires many parameters to be defined • Only appropriate for use in moderately steep streams • Cannot simulate backwater effects or impacts of hydraulic structures

2.5 Satellite Soil Moisture

Soil moisture data exhibits large spatiotemporal variation making it difficult to model and measure. Since the development of satellite applications, various earth fluxes of spatial and temporal variability can be easily obtained with higher accuracy. Researchers have been using satellite data to study the behavior of water from the onset of satellite applications in the wider field of science. Distant observation of soil has allowed researchers to explore a wide horizon of soil properties and the interaction of soil and water in the atmosphere.

Increased availability of soil moisture estimations from satellite sensors currently imparts a significant opportunity in improving real-time flood simulation through assimilation of data (Brocca et al., 2012). The SSM is captured through a concept of analyzing changes in the microwave frequency's backscattering properties and surface emissivity that can show changes in surface soil moisture. The passive satellite sensors measure the brightness temperature of the emitting surface to detect soil moisture variations (Njoku & Kong, 1977). Similarly, the backscattered radar signal returned to a satellite sensor helps to detect the soil moisture variations (Dobson et al., 1985). Since the inception of the measurement of SSM, passive sensors have been used widely used to capture SM properties (Lettenmaier et al., 2015). The author also pointed out that recent development in science and technology has allowed researchers to use active and passive sensors together to estimate SM of higher accuracy.

2.5.1 Comparison of Satellite Soil Moisture Data

A comparison of different satellite sensors implied to estimate SM was carried out by Lettenmaier et al. (2015) and the author denoted that recent satellite sensors have higher accuracy when compared to previous satellite sensors in estimating SM. An extract of the author's study is presented in Table 2-3 where the satellite sensors and platforms, radiation frequency/channel, data resolution, revisit time, and data availability period are compared. It can be observed that the spatial resolution of the SSM has significantly increased throughout the period. Considering the spatial resolution, and higher accuracy compared to in-situ SM, SMAP was selected as the SSM data for this study.

Table 2-3: Summary of all available satellite sensors estimating SSM

(*Extracted from* Lettenmaier et al. (2015))

Sensor and Platform	Channel	Resolution	Revisit	Period
Scanning multichannel microwave radiometer (SMMR), Nimbus-7	Multiple, from 6.6 GHz	140 km	Daily	1978-1987
Microwave Imager/Sounder (MIS), WindSat	Multiple, from 6.8 GHz	25 km	Daily	2003-present
TRMM Microwave imager (TMI), TRMM	Multiple, from 10.7 GHz	25 km	Daily	1997-present
Special sensor microwave imager (SSM/I), DSMP	Multiple, from 19.4 GHz	25 km	Daily	1987-present
Advanced microwave scanning radiometer (AMSR-E). EOS-Aqua	Multiple, from 6.6 GHz	25 km	Daily	2002-2011
Scatterometer (SCAT), ERS	5.3 GHz	~ 50 km	3-4 days	1992-present
Advanced Scatterometer (ASCAT), MetOp	5.3 GHz	25 km	1-2 days	2006-present
Soil Moisture and Ocean Salinity (SMOS), SMOS	1.4 GHz	~ 35 km	2-3 days	2009-present
Advanced Microwave Scanning Radiometer 2 (AMSR-2), GCOM-W	Multiple, from 6.9 GHz	25 km	Daily	2012-present
Soil Moisture Active Passive (SMAP), SMAP	1.4 GHz	3, 9, 36 km	2-3 days	2015-present

2.5.2 SMAP Soil Moisture Data

The satellite mission Soil Moisture Active Passive (SMAP) was commenced with its launch in January 2015, and measures the amount of water in the surface soil everywhere on Earth, every 2-3 days. The SMAP produces global maps of soil moisture which can be used to better understand how carbon fluxes, energy, and water keep our climate and environment in balance (Reichle et al., 2020). A total of 24 data products has been produced by the mission that constitutes four layers of data processing, each of which provides different soil moisture-related data. Using NASA's Catchment Land Surface Model and brightness temperatures acquired by SMAP, the SMAP level 4 soil moisture (L4 SM) data were produced. (Reichle et al., 2018). Furthermore, the SMAP L4 SM product offers observations and analysis update data covering key geophysical domains reported as 3-hourly time averages across a smaller 9-km grid. (Reichle et al., 2020).

The level 4 data consists of geophysical parameters derived by assimilating level 1, 2, and 3 data into a land surface model. The SMAP L4 SM can be used in various fields of study because of its accuracy in estimating the soil moisture data (Reichle, de Lannoy, Liu, Ardizzone, et al., 2017; Reichle, de Lannoy, Liu, Koster, et al., 2017; Stillman & Zeng, 2018; Suman et al., 2020; Tavakol et al., 2019). Daily analysis of SM at a total of 156 SM monitoring stations in the United States with SMAP L4 SM and AMSR2 SM data significantly suggests that SMAP SM retrievals are better than AMSR2 SM data (Zhang et al., 2017). On comparison of the SMAP L4 SM data with the in-situ SM data measurements at 17 different core sites in the world illustrates that the level of accuracy required can be obtained with scanter bias (Reichle, de Lannoy, Liu, Ardizzone, et al., 2017).

2.6 Event Selection

2.6.1 Conceptualization

The development of event-based models helps hydrologists to better understand basin response to the extreme high and low rainfall periods thereby allowing planners to manage water properly in the basin. Identification of independent events for the modeling purpose remains a major challenge as continuous rainfall data requires

various criteria of rainfall threshold value able to produce required runoff and inter-event period. A minimum event depth (threshold values) is frequently used as criteria to identify rain events. An event may be separated by a period of rainfall producing enough runoff independent of other rainfall separated by a valid minimum inter-event time. The extreme events are identified incorporating both minimum event depth and time with a specific discharge value (annual maximum or threshold approach) considered to identify the events.

2.6.2 Approaches for Identifying Events

Hydrologic study of extreme nature and flood frequency analysis require extreme events that are separated mainly by two (2) approaches, annual maximum (AM) and peat over threshold (POT). The extreme discharge events of each year are considered in AM approach whereas the POT approach considers events with peak discharge above a threshold value. Different approaches for the selection of events have been applied by researchers from the past. Although the POT approach is widely used and considers the events that are extreme in nature, the identification of events solely depends on the threshold value considered. Hossain et al. (2019) identified events considering the threshold to be five times higher than the mean annual flow for event-based modeling in southern Australia. Various authors have used fixed quantile ranges to identify events for the purpose of modeling (Jeong et al., 2014; Solari & Losada, 2012), mean exceedance above the threshold (Davison & Smith, 1990; Lang et al., 1999), and automated threshold selection considering various criteria of discharge and rainfall (Liang et al., 2019; Solari & Losada, 2012).

2.6.3 Minimum Inter-Event Time

A minimum inter-event time (MIT) is defined as a rainless period that must be met or exceeded before and after each event in order for two events to be considered independent of one another (Nojumuddin et al., 2018). Various MIT values mostly on a sub-daily scale ranging from 1, 2, 4, 6, 9, 12, 18, 24 hrs. and so on have been used by researchers in a wide range of study areas to delineate the events from continuous rainfall data and analyze the obtained events (Gabriel-Martin et al., 2019; Hvitved-Jacobsen & Yousef, 1988; Medina-Cobo et al., 2016; Molina-Sanchis et al., 2016;

Nojumuddin et al., 2018; Xuereb & Green, 2012). The MIT had a significant impact on the number of events selected as the increasing MIT resulted in the decrease in the number of events but an increase in mean event duration and depth thereby signifying the importance of identification of suitable MIT value (Nojumuddin et al., 2018).

Dunkerley (2008a, 2008b) evaluated various criteria for the selection of events and stated that the applied MIT varies from 3 minutes to 24 hours while the minimum event depth values range from a measurable amount of 0.2 mm to 13.0 mm. Molina-Sanchis et al. (2016) in a study in the southeast of Spain considered rainfall > 0. 71 mm for the selection of events as rainfall below 0.71 mm would not be able to affect antecedent soil moisture and the receding event. Haile et al. (2011) considered a minimum event depth of 1.0 mm for a study in the source of the Blue Nile River that would produce independent events when duly separated by an MIT of 30 min. Considering the importance of minimum event depth in the identification of events, a minimum event depth needs to be considered for the calculation of MIT.

Restrepo-Posada and Eagleson (1982) devised an exponential approach for calculating MIT, in which the storm arrival time and the interval between two storms are considered to follow an exponential distribution. As a result, the length of dry spells may be estimated using an exponential distribution with a mean equal to the standard deviation, and the coefficient of variation (CV) is one. The CV for different dry-period lengths was determined utilizing Equation [2-1] to acquire the MIT value;

$$CV_k = \frac{std(dp_k)}{\overline{dp_k}} \qquad [2\text{-}1]$$

where k is the dry-period duration (1 h, 2 h, . . .), $\overline{dp_k}$ is the average of dry-period durations longer than the duration of k_{th}, and $std(dp_k)$ is its standard deviation. The MIT value is determined by the value of k, where CV_k approximates one (1).

2.7 Objective Functions

The objective functions are indications that are used to determine how well a solution accomplishes a specific goal (Dorji, 2018). Objectives functions are applied to reflect the model outcomes to reality (Dissanayaka & Rajapakse, 2018) and indicate how

much each variable contributes to the value to be optimized in the problem. Modelers divide the modeling work into calibration and validation parts. Parameters are optimized for the calibration set obtaining objective functions after calibration. Same optimized parameters are applied in the validation data set and then the results are compared in terms of objective functions after validation. The use of objective functions depends on the purpose of study and condition of modeling (i.e., high flow studies, low flow studies, event-based modeling, continuous modeling, and so on). Yet the same objective function can be used for different modeling purposes as they can capture overall changes in the result rather than a part of the result.

There are objective functions in the HEC-HMS that indicates how much each variable contributes to the value to be optimized in the problem (Schaffenberg & Fleming, 2013). The objective functions whose values are calculated within the HEC-HMS are Root mean square standard deviation (RMSE std dev), percent bias (PBIAS) or percentage streamflow volume error (PVE), and Nash Sutcliffe efficiency (NSE). Referring to Dissanayaka and Rajapakse (2018); Green and Stephenson (2009); Nasimi (2018); Xuefeng and Alan (2009), these three (3) objective functions are used in this study considering the HEC-HMS model, SMA loss method, and event-based modeling. Furthermore, an objective function called the coefficient of determination (R^2) is also selected referring to the above-mentioned authors.

2.7.1 Nash Sutcliffe Efficiency (NSE)

Nash and Sutcliffe (1970) derived a normalized statistic to quantify the level of residual variance contrasted to the observed variation. It is one (1) minus the sum of absolute squared differences between predicted and observed values across the study period, normalized by the variance of observed values (Krause et al., 2005). The calculation is performed using Equation [2-2] shown below;

$$NSE = 1 - \frac{\sum(Q_{obs} - Q_{sim})^2}{\sum(Q_{obs} - Q_{mean})^2} \quad [2\text{-}2]$$

where Q_{obs} is the observed value of discharge, Q_{sim} is the simulated value and Q_{mean} is the mean of observed data. The NSE coefficient spans from infinity (-∞) to

one (1), with the optimum fit being closer to one (1). Because the NSE is the error obtained from the initial variance, which is reliant on the mean of the observed data, it is impractical to compare two different catchments (Dorji, 2018).

2.7.2 RMSE Observed Standard Deviation Ratio (RMSE std dev)

Root mean square error (RMSE) is a commonly used error-index statistic which is the square root of the mean of the squared discrepancies between relevant elements of the estimates and observation (Barnston, 1992). The mathematical expression for the calculation of RMSE is as shown in Equation [2-3];

$$RMSE = \sqrt{\frac{\sum_{i=1}^{n}(Q_{obs} - Q_{sim})^2}{n}} \quad [2\text{-}3]$$

where Q_{obs} is the observed value of discharge, Q_{sim} is the simulated value, and n is the number of observations. The RMSE value near 0 indicates that the model can predict the data accurately.

The RMSE std dev is the ratio of RMSE and standard deviation (σ) where the standard deviation is calculated as shown in Equation [2-4].

$$\sigma = \sqrt{\frac{\sum_{i=1}^{n}(Q_{obs} - Q_{mean})^2}{n}} \quad [2\text{-}4]$$

The RMSE std dev as a ratio explained by Moriasi et al. (1983) is calculated as shown in Equation [2-5] below.

$$RMSE\ std\ dev = \frac{\sqrt{\sum_{i=1}^{n}(Q_{obs} - Q_{sim})^2}}{\sqrt{\sum_{i=1}^{n}(Q_{obs} - Q_{mean})^2}} \quad [2\text{-}5]$$

The RMSE std dev combines the merits of error index statistics with a scaling/normalization factor that enables the statistics and reported values to be employed to other components. The value ranges from 0 to a large positive value where 0 value represents an ideal simulation. The RMSE and model simulation

performance are both improved when the RMSE std dev value is low (near to zero) (Moriasi et al., 1983).

2.7.3 Coefficient of Determination (R^2)

The coefficient of determination (commonly abbreviated as R^2) is a concept in the assessment of variance and regression analysis. It is a metric for how much of the data's perceived variance is present. It's also known as the correlation coefficient's squared value (Krause et al., 2005). According to Nash and Sutcliffe (1970), it is defined as the ratio of the original variance perceived by this model. The value of R^2 is estimated as shown in Equation [2-6].

$$R^2 = 1 - \frac{\sum_{i=1}^{n}(y_i - \hat{y}_i)^2}{\sum_{i=1}^{n}(y_i - \bar{y})^2} \quad [2\text{-}6]$$

Here, the average of the obtained observations is denoted by $\bar{y}$, and the forecast of y_i using the fitted model is denoted by $\hat{y}_i$. If there is no relationship between the response variable and the predictor variable(s), then the best 'model' to explain the data is $\bar{y}$. As a result, $y_i - \bar{y}$ represents deviations when the predictor variable(s) and the response variable have no relationship at all. The range of values of R^2 values varies depending on the type of model being fitted; in most circumstances, such as linear least-squares regression models, they fall between zero (0) and one (1). A value of zero (0) indicates that there is no connection at all, whereas a value of one (1) indicates that the prediction's dispersion is equal to the observation's (Nasimi, 2018). Therefore, the higher the R^2 value, the better the model describes the data (Di Bucchianico, 2008).

2.7.4 Percent Bias (PBIAS)

The average propensity of simulated data to be greater or smaller than observed data is measured by percent bias (PBIAS) or percent flow error (PVE) (H. V. Gupta et al., 1999). The PBIAS is used as the primary measure of the objective function in most hydrological models (Kumar, 2011) and shows overall agreement between simulated and observed flows over a specified period (Samady, 2017). PBIAS is calculated as shown in Equation [2-7].

$$PBIAS = 1 - \frac{\sum_{i=1}^{n}(Q_{obs} - Q_{sim}) * 100}{\sum_{i=1}^{n} Q_{obs}} \quad [2\text{-}7]$$

The optimal value of PBIAS is 0.0, with low magnitude values indicating an accurate simulation of the model. A positive value indicates a bias that underestimates the model and a negative value indicates a bias that overestimates the model.

2.7.5 Selection of Objective Functions

There are various metrics such as NSE, RMSE std dev, R^2, and PBIAS which are widely used by the researcher to assess the performance of the event and continuous based hydrological models (De Silva et al., 2014; H. V. Gupta et al., 2009; Nasimi, 2018; Westerberg et al., 2011; Wöhling et al., 2013). In hydrological modeling, the R^2 coefficient is used to analyze the collinearity between observed discharge and simulated discharge, while metrics for instance RMSE evaluate the average error between observed discharge and simulated discharge. The NSE considers the average of all observed streamflow to assess the overall performance of a hydrological model. The NSE is more inclined to predict the simulation of peak flow whereas the logarithmic form of NSE (LNNSE) highlights the simulation of the low flow (Huo & Liu, 2020).

The coefficient R^2 is most frequently employed to assess the extent of linear closeness and dispersal between simulated and observed datasets. The RMSE std dev is used to assess the overestimation and underestimation of streamflow by the hydrological models (Ferreira et al., 2020). The PBIAS is used to assess the mean error between the simulated and the observed discharge and also the analysis of water balance errors (Rientjes et al., 2013; Rwetabula et al., 2012). Hence, these four (4) objective functions are considered to analyze the high flows, low flows, and the overall performance of the model in simulating the discharge at the outlet of the basin.

2.8 Application of Study

Although the SSM has a possibility of significantly increasing the model performance for simulation of streamflow, it requires lots of other data and processing to develop huge distributed hydrological models that incorporate real-time SSMs. The HEC-HMS

has been employed successfully by several researchers to model flood events (Du et al., 2012; Knebl et al., 2005). Among several loss methods available, SMA has been successfully applied in a continuous flow simulation of the watershed under study (Gebre, 2015). Bhuiyan et al. (2017) employed RADARSAT-2 soil moisture to initialize the HEC-HMS model in a cold zone watershed where the simulated discharge was comparable to the observed discharges.

A distributed hydrological model was applied in humid regions by utilizing SSM data from the SMAP satellite data and that produced streamflow of higher accuracy when SSM data was assimilated with the model (Yang et al., 2019). Assimilation of SSM improved streamflow prediction in data-scarce catchments and these results of the enhanced model are comparable to those of a local model forced using local meteorological data (Alvarez-Garreton et al., 2016; López et al., 2016). In a data-scarce scenario, a paper investigates the use of active and passive microwave SSM products for enhancing streamflow prediction inside of semiarid catchments in Australia, intending to adjust two key critical factors in streamflow generation: catchment wetness condition and rainfall forcing data (Alvarez-Garreton et al., 2016). These findings are significant in light of current efforts to transition to global hyper-resolution modeling and can aid in the advancement of this study. Thus, the study aims to capture the potential of remotely sensed SSM in assimilation with the rainfall data to produce streamflow of a higher degree of accuracy for proper planning of water resources in a data-scarce situation using the HEC-HMS software.

CHAPTER 3

3 METHODOLOGY

3.1 Study Area

For this study, one dry basin (Kirindi Oya) and another wet basin (Kalu Ganga) of Sri Lanka are considered as they would represent streamflow variability with both flooding and drought conditions along with their varying soil moisture state in different periods. The Kirindi Oya located in the dry zone characterizes a basin with relatively dry soil attributes whereas Kalu Ganga represents a basin with wet soil for a longer period in any year. Data required for the study were also available for both the basins.

3.1.1 Dry Zone Basin: Kirindi Oya Basin

The Kirindi Oya river basin (Figure 3-1) flows from Sri Lanka's medium-range highlands to the Indian Ocean in the south-eastern part of the dry zone (Molden et al., 2001). The 118 km long river originates in Bandarawela and empties into the Indian Ocean at Bundala, with a catchment area of 1,203 km² (Hendawitharana et al., 2020; Sirisena, 2008). The river basin falls within two (2) provinces covering three (3) districts and seven (7) DS divisions where the higher hills of the catchment fall in the Uva province and the lower flat plains lie in Southern Province. The average annual rainfall is approximately 1,000 mm, with almost 75 % pouring during the Maha season (October to April) and 25 % falling during the Yala season (April to October) (Meinzen-Dick & Bakker, 2000). Evaporation is higher during the months from June to September, with an average annual of approximately 2,100 mm (Bakker et al., 1999). The basin is regarded to be closing because there are only a few outflows to the Indian Ocean during certain times of the year. There is abundant outflow to the Indian Ocean through drains during the rainy seasons, and the river encounters an excess of environmental requirements (Molden et al., 2001).

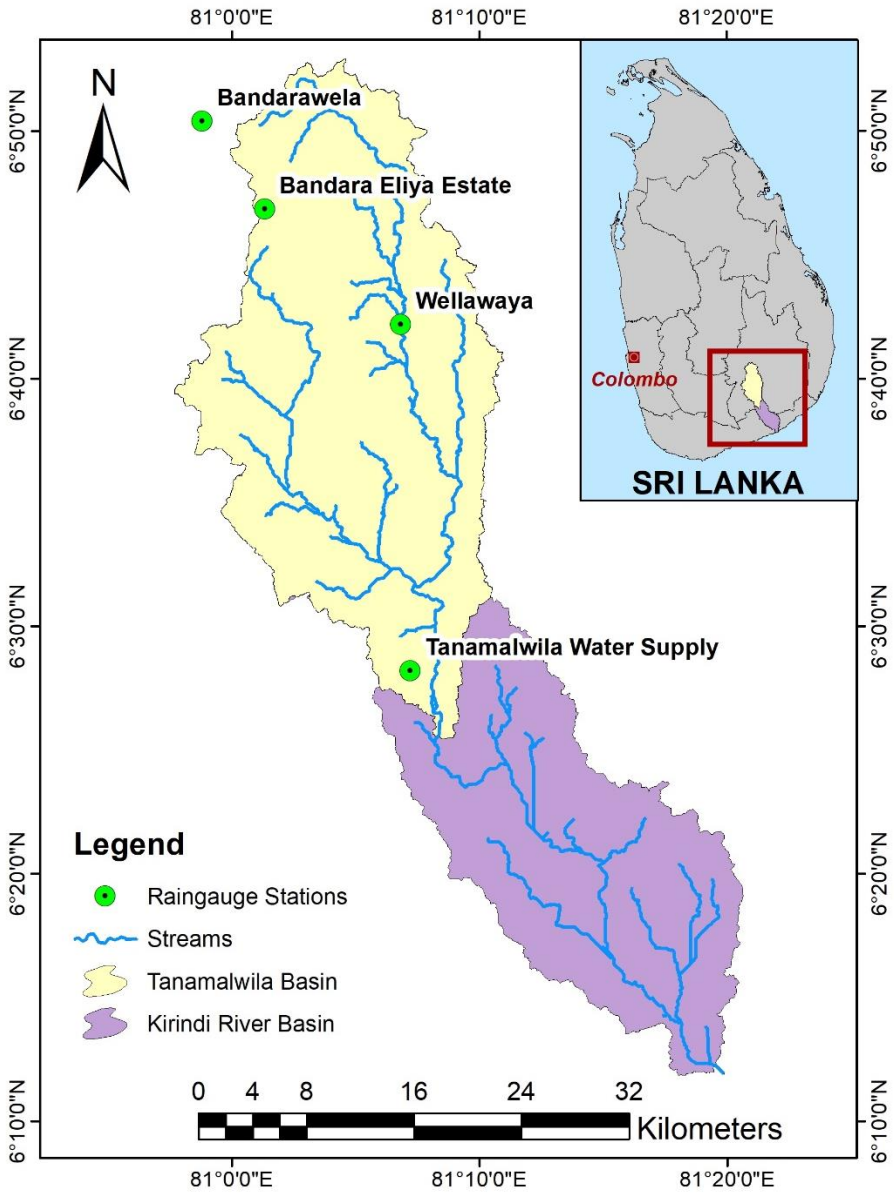

Figure 3-1: Kirindi Oya basin with Tanamalwila watershed, rain/stream gauge stations

The dry conditions in the area are portrayed by minimal rainfall, high temperatures, and low relative humidity. This incites considerable evaporation, which in most months of the year exceeds rainfall. As a result, the issue of water scarcity has become a serious impediment to the farming practices used in this region. (Abeysingha et al., 2017). Water resources in the basin have supported agriculture since ancient times (Molden et al., 2001). Tanks situated downstream of the basin such as Lunugamwehera Reservoir (with an irrigable extent of 5,362 ha), Yoda Wewa (1,322 ha), Badagiriya Tank (668 ha), and Debara Wewa (382 ha) utilize the upstream water of the basin for

fulfilling irrigation requirements and other uses. The outlet at Thanamalwila is considered where the catchment area is 716 km^2. The basin map with Tanamalwila catchment and gauging stations is shown in Figure 3-1.

3.1.2 Wet Zone Basin: Kalu Ganga Basin

Kalu Ganga, a 129-kilometer-long river that flows from Sri Padhaya (Adams Peak) to the sea at Kalutara, is one of Sri Lanka's major rivers. The basin receives heavy rainfall and yields high discharges. The river flows through Sri Lanka's wet zone, and the lower floodplain is subject to regular flooding as a result of its hydrological and topographical qualities, which has a significant impact on the country's socioeconomic profile.

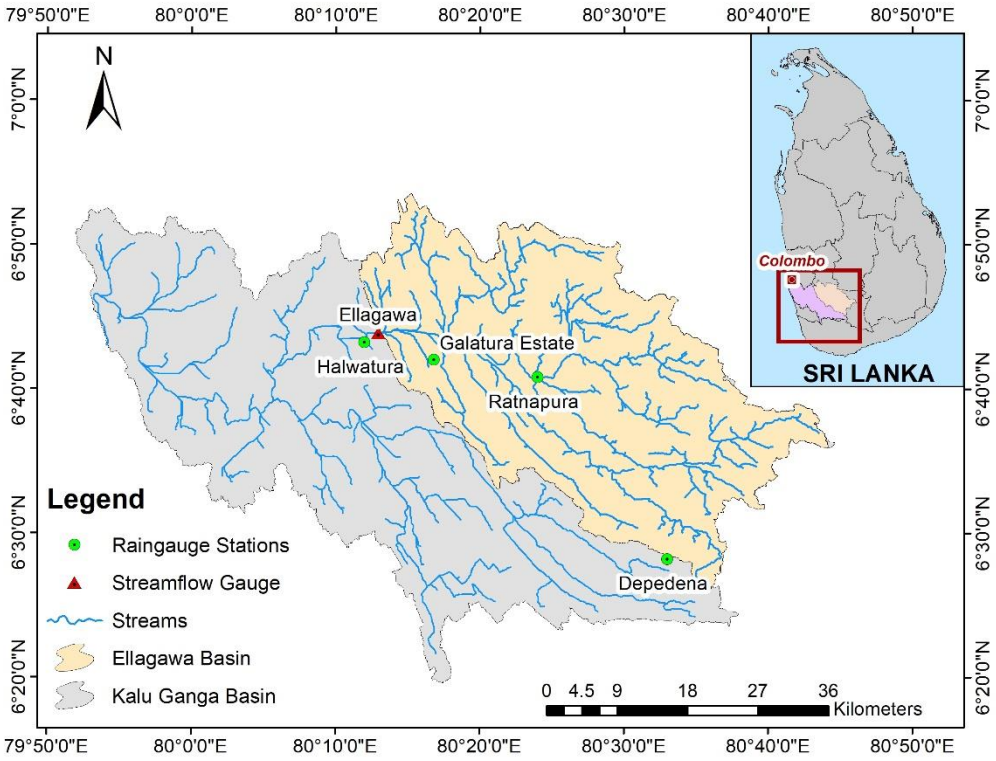

Figure 3-2: Ellagawa Watershed at Kalu Ganga basin with rain gauge and streamflow gauging stations

Many researchers have explored climatic changes in the country's major river basins in recent years, but no studies focused on climatic changes along with influence from soil moisture in the Kalu Ganga basin have been conducted. The study area is selected as the Kalu Ganga basin since this basin gets affected by frequent flooding during the

rainfall in the area. The outlet at Ellagawa is considered where the catchment area is about 1,409 km^2. The upstream area consists of slopes of high elevation with the elevation gradually decreasing towards the outlet considered. A stream network along with the catchment boundary is shown in Figure 3-2.

3.2 Overall Methodology

The methodology adopted for this research is as shown in Figure 3-3. In the present study, the importance of incorporating soil moisture data was recognized and an HEC-HMS hydrological model was developed with soil moisture accounting (SMA) as the loss method to simulate flow during dry and wet events for two selected pilot basins. The developed model was then compared with the model simulated using satellite soil moisture (SSM) data to assess streamflow variability under different saturation scenarios in the basin. The detailed methodology is further explained as follows.

Initially, the study area was identified, and objectives were set to analyze streamflow variability incorporating soil moisture (SM) in the basin. Based on the basin identified and objectives of the study, a comprehensive analysis of the literature was conducted regarding the prevalent approaches to provide the solution. Different models/tools applied for these kinds of studies, and data required to develop those models were analyzed and HEC-HMS was decided as an appropriate model for this research. HEC-HMS was carefully chosen as the best fit model for the study considering data availability, ease of use, and accuracy of the results from the model. The SMA was identifed as the suitable loss method in the model because of its capacity to simulate both low flow and high flows accurately and the parameters required were selected.

Rainfall data and evaporation data were gathered from the Meteorological Department and discharge data were obtained from the Irrigation Department. A land-use map of the basin was acquired from Environmental Systems Research Institute (ESRI's) 10-m meter land cover map of 2020 (Karra et al., 2021) along with a soil type map was obtained from the Survey Department. The SSM data was obtained from the Earthdata Portal (Reichle et al., 2020). The obtained data were rigorously checked for general hydrological statistics, missing values, homogeneity, and inconsistencies through the use of graphical and statistical techniques. The missing values were filled using the

linear regression technique. Statistical analysis of the hydrometeorological data was performed to compute the average recurrence interval (ARI) and to select the extremely dry and wet events for the modeling purpose. Similarly, the best parameters for the model obtained through the literature survey were fed into the model along with selected events for simulation.

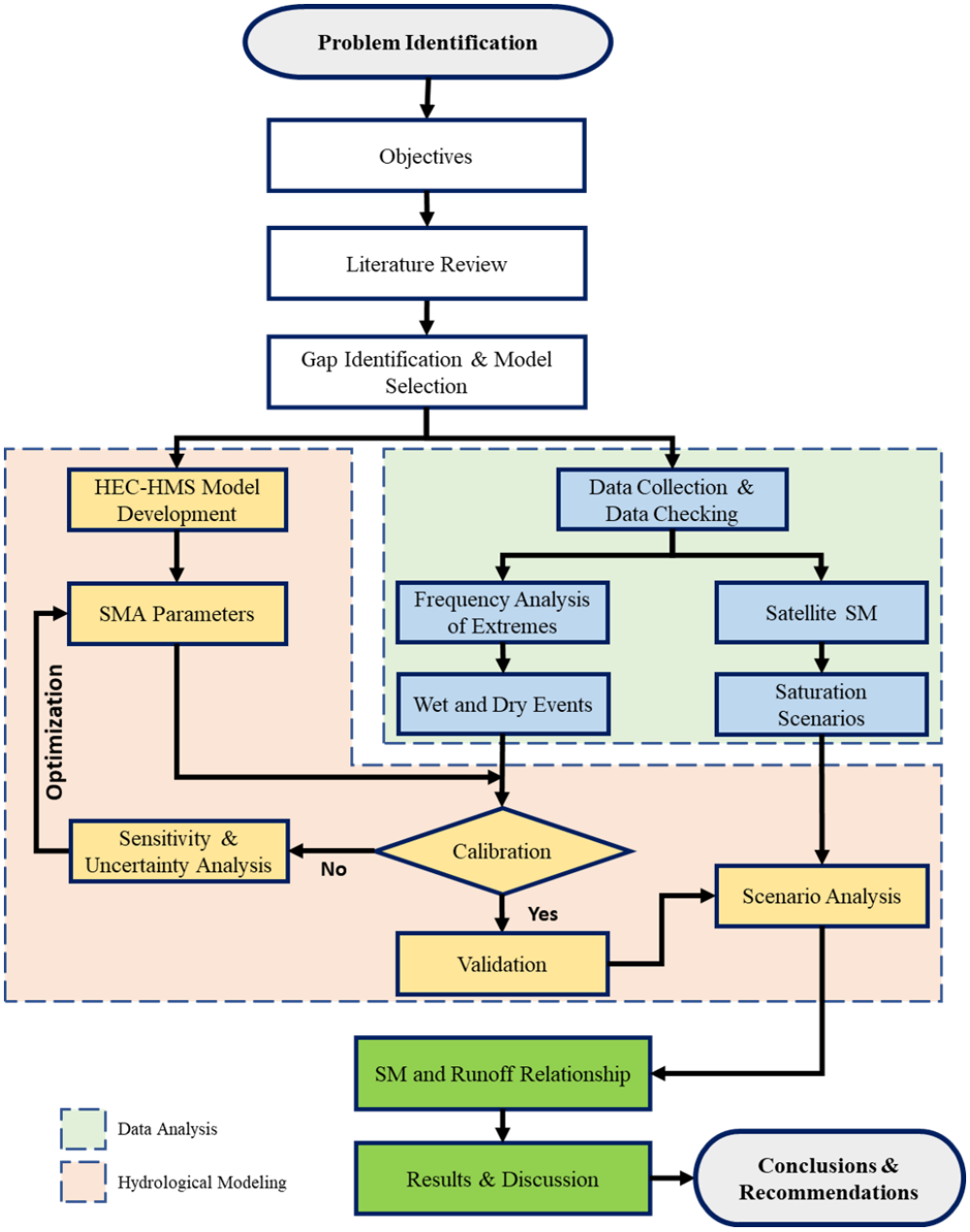

Figure 3-3: Methodology flowchart for the study

Calibration of the model was carried out using the events identified for the period before 2013/14 (5 events for Kirindi Oya basin and 2 events for Kalu Ganga basin) to

optimize the parameters associated with the model along with sensitivity and uncertainty analysis. The optimized parameters for the model were then used to validate the model performance considering the data period after 2014/15 (4 events for Kirindi Oya basin and 2 events for Kalu Ganga basin).

A scenario analysis was carried out to compare and contrast the variability of streamflow in diverse saturation conditions obtained using SSM data. The overall enhancement in the model performance employing soil moisture data was also evaluated. Results from the study were provided and the discussions from the findings were also specified. Finally, conclusions and recommendations from the study were furnished which can be applied for sustainable water management in the basin.

3.3 Climatic Trends and Extremes

Climate trends and extremes in the basin were studied with the help of various indices defined by IPCC and various other researchers (Dissanayaka & Rajapakse, 2018; Hu et al., 2017; IPCC, 2007). Historical streamflow and precipitation data were analyzed and then trends along with extremes were computed with predefined extreme indices which are listed in Table 3-1 and Table 3-2.

Table 3-1: Extreme indices used for the analysis of streamflow in this study

Indicator Name	Code	Description
Consecutive low-flow days	CDS	Annual maximum number of consecutive days with daily streamflow <10th percentile of streamflow data (Hu et al., 2017)
Consecutive high-flow days	CWS	Annual maximum number of consecutive days with daily streamflow >90th percentile of streamflow data (IPCC, 2007)
Max 1-day flow	SX1 day	Annual highest daily streamflow (Hu et al., 2017)
Max 2-day flow	SX2 day	Annual highest average streamflow in consecutive 2 days (IPCC, 2007)
Max 5-day flow	SX5 day	Annual highest average streamflow in consecutive 5 days (Hu et al., 2017)

In Kirindi Oya Basin, streamflow analysis is performed for the Tanamalwila station at the outlet of the basin whereas precipitation analysis is conducted for all four (4) precipitation gauging stations (Bandarawela, Bandaraeliya, Wellawaya, and Tanamalwila). Furthermore, in Kalu Ganga, streamflow analysis is performed for the Ellagawa station, and precipitation analysis is conducted for all four (4) gauging stations as mentioned above.

Table 3-2: Extreme indices used for the analysis of precipitation in this study

Indicator Name	Code	Description
Consecutive dry days	CDD	Annual maximum number of consecutive days with daily precipitation < 1 mm (IPCC, 2007)
Consecutive wet days	CWD	Annual maximum number of consecutive days with daily precipitation ≥ 1 mm (IPCC, 2007)
Heavy precipitation days	R10	Annual count of days when precipitation ≥ 10 mm (IPCC, 2007)
Very heavy precipitation days	R20	Annual count of days when precipitation ≥ 20 mm (IPCC, 2007)
Max 1-day precipitation	RX1 day	Annual maximum 1-day precipitation (IPCC, 2007)
Max 2-day precipitation	RX2 day	Annual maximum consecutive 2-day precipitation (IPCC, 2007)
Max 5-day precipitation	RX5 day	Annual maximum consecutive 5-day precipitation (IPCC, 2007)

Further, streamflow data at Tanamalwila from 1987/88 to 2019/2020 was used to compute standardized streamflow index (SSI) using the standardized precipitation index (SPI) technique developed by Mckee et al. (1993, 1995) which is widely used as a measure of drought. A similar procedure was followed for the streamflow data at

Ellagawa from 1994/95 to 2019/20 to compute SSI. There are various categories of precipitation regimes (from dry to wet) depending on the value of SSI obtained (Chandrasekara et al., 2021). The categories of precipitation regimes are presented in Table 3-3.

Table 3-3: General classification categories of SSI

SSI	Category
> 2.00	Extremely wet
1.50 - 1.99	Severely wet
1.00 - 1.49	Moderately wet
0.00 - 0.99	Mildly wet
-0.99 – 0.00	Mild drought
-1.49 - 1.00	Moderate drought
-1.99 - 1.50	Severe drought
<-2.00	Extreme drought

The SPI is calculated on different time scales depending on the nature of the study, such as drought assessment, reservoir study, and groundwater recharge. When the SPI is calculated for shorter accumulation periods (e.g. 1-3 months), it can be employed to indicate immediate impacts such as snow cover changes, soil moisture loss, and runoff from small streams. It can be used as an indicator to reduce runoff and build-up in a reservoir when calculating the SPI for an average accumulation period (e.g. 3 to 12 months). When SPI is calculated for longer accumulation periods (e.g. 12 to 48 months), it can be employed to indicate a reduction in the refilling of reservoirs and groundwater (Mckee et al., 1993, 1995). For the present study, SSI is calculated for 9 months and 12 months periods to analyze the drought in the study area.

3.4 Event Identification

After an extensive literature review on events identification, a minimum event depth of 1.0 mm was adopted for the present study considering that rainfall below this value will not produce sufficient runoff and will not affect the antecedent moisture condition. Then minimum inter-event time (MIT) was calculated using an exponential method developed by Restrepo-Posada and Eagleson (1982) which is shown in Equation [2-1] With minimum event depth and MIT known, now the Thiessen average rainfall calculated referring to Chow et al. (1988) was analyzed considering minimum event depth. An event is said to be started when daily precipitation equals or exceeds minimum event depth and only ends when the precipitation is below the minimum event depth. To isolate the events, there should be a gap of MIT (days); which means there should be no minimum event depth precipitation for a period equal to or greater than MIT.

A large number of events will be obtained through this process and representative events for the modeling purpose need to be selected based on criteria of maximum precipitation, 2-day maximum precipitation, and peak discharge of the event. Only one criterion is adopted for the selection of representative events upon analyzing all three (3) criteria after all the events during the study period have been obtained.

3.5 Hydrological Modeling

The HEC-HMS was selected as the suitable model for this study and different methods/models used in it were selected through an extensive literature review as explained in Sections 2.3 and 2.4. Simple surface and simple canopy were adopted to model canopy losses and surface storage losses, respectively. Since Soil moisture accounting is practical in modeling dynamic situations of high and low flow, it was selected as the suitable loss method for the study which requires modeling both dry and wet period flow. The soil conservation

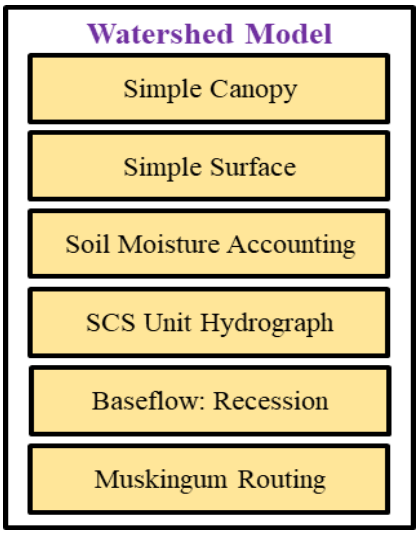

Figure 3-4: HEC-HMS model structure

service (SCS) unit hydrograph was selected as the suitable transform method in the model. For the baseflow and routing, recession baseflow and Muskingum routing were adopted due to their flexibility in modeling diverse scenarios and ease of parametrization.

3.6 Performance Rating

Many authors have described the model results through objective functions by developing performance metrics range which would indicate the model results in terms of good or unsatisfactory (Moriasi et al., 1983; Nasimi, 2018). The recommended performance rating for the present study with reference to the literature review from Section 0 is as indicated in Table 3-4.

Table 3-4: General performance rating for the model results

Performance Rating	RMSE std dev	R^2	PBIAS/PVE	NSE
Very good	$0.00 < \text{RMSE std dev} \leq 0.25$	$0.75 < R^2 \leq 1.00$	$\text{PBIAS} \leq \pm 10$	$0.75 < \text{NSE} \leq 1.00$
Good	$0.25 < \text{RMSE std dev} \leq 0.50$	$0.65 < R^2 \leq 0.75$	$\pm 10 \leq \text{PBIAS} < \pm 15$	$0.65 < \text{NSE} \leq 0.75$
Satisfactory	$0.50 < \text{RMSE std dev} \leq 0.70$	$0.50 < R^2 \leq 0.65$	$\pm 15 \leq \text{PBIAS} < \pm 25$	$0.50 < \text{NSE} \leq 0.65$
Unsatisfactory	RMSE std dev > 0.70	$R^2 \leq 0.50$	$\text{PBIAS} \geq \pm 25$	$\text{NSE} \leq 0.50$

CHAPTER 4

4 DATA CHECKING AND ANALYSIS

4.1 Kirindi Oya River Basin

4.1.1 Data

4.1.1.1 Data Sources and Resolution

Data required for this study are precipitation, streamflow, evaporation, SMAP geophysical data, soil properties, and land-use map of the study area. The details regarding the above-mentioned data and their source are listed in Table 4-1. Gridded satellite data which is available for the whole world was then processed at catchment level and required soil moisture was computed.

Table 4-1: Data required for the study with their resolution and source

S. N	Data Description	Resolution	Source
1	SMAP L4 Global 3-hourly 9 km EASE-Grid Surface and Root Zone Soil Moisture Geophysical Data (SPL4SMGP) (Reichle et al, 2018),	9 km grid	https://nsidc.org/data/SPL4SMAU/versions/5
2	Rainfall data from gauge stations in Kirindi Oya	Daily (2002 to 2020)	Meteorology Department
3	Streamflow data of Tanamalwila Station	Daily (1987 to 2020)	Irrigation Department
4	Evaporation Data of Lunugamawehera station	Daily (2002 to 2020)	Meteorology Department
5	Soil Type Map	1:50,000	Survey Department
6	Landuse Map	10 m	ESRI (Karra et al., 2021)

4.1.1.2 Hydrometeorological Data

Rainfall data were collected for various rain gauge stations from the Meteorological Department and while streamflow at Tanamalwila station was collected from the Irrigation Department. Streamflow data of more than 30 years period is collected to quantify return period discharge in the basin. Different data collected for various stations and periods of data obtained are mentioned in Table 4-2.

Table 4-2: Data collected for the analysis

Name of the Station	Latitude (°N)	Longitude (°E)	Period of Record	
			From	To
Streamflow				
Tanamalwila	6.4449	81.1375	Oct-1987	Dec-2020
Rainfall				
Bandaraeliya	6.7808	81.0220	Jan-2002	Dec-2020
Bandarawela	6.8400	80.9800	Jan-2002	Dec-2020
Wellawaya	6.7033	81.1137	Jan-2002	Dec-2020
Tanamalwila	6.4700	81.1200	Jan-2002	Dec-2020

4.1.1.3 Other Data

Root zone (0-100 cm) soil moisture (SM) data (m^3/m^3) for the period of 2015-03-31 to 2020-12-31 was obtained from the Earthdata portal and then extracted for use in the study. On visual comparison with the rainfall and climatic zones (Dry/Wet Zones) of Sri Lanka, the data showed a greater resemblance. Figure 4-1 shows the root zone soil moisture of date 2020-09-15 at 19:30 UTC for the whole Sri Lankan region and this was compared with the dry and wet climatic zones as an initial checking of the data set.

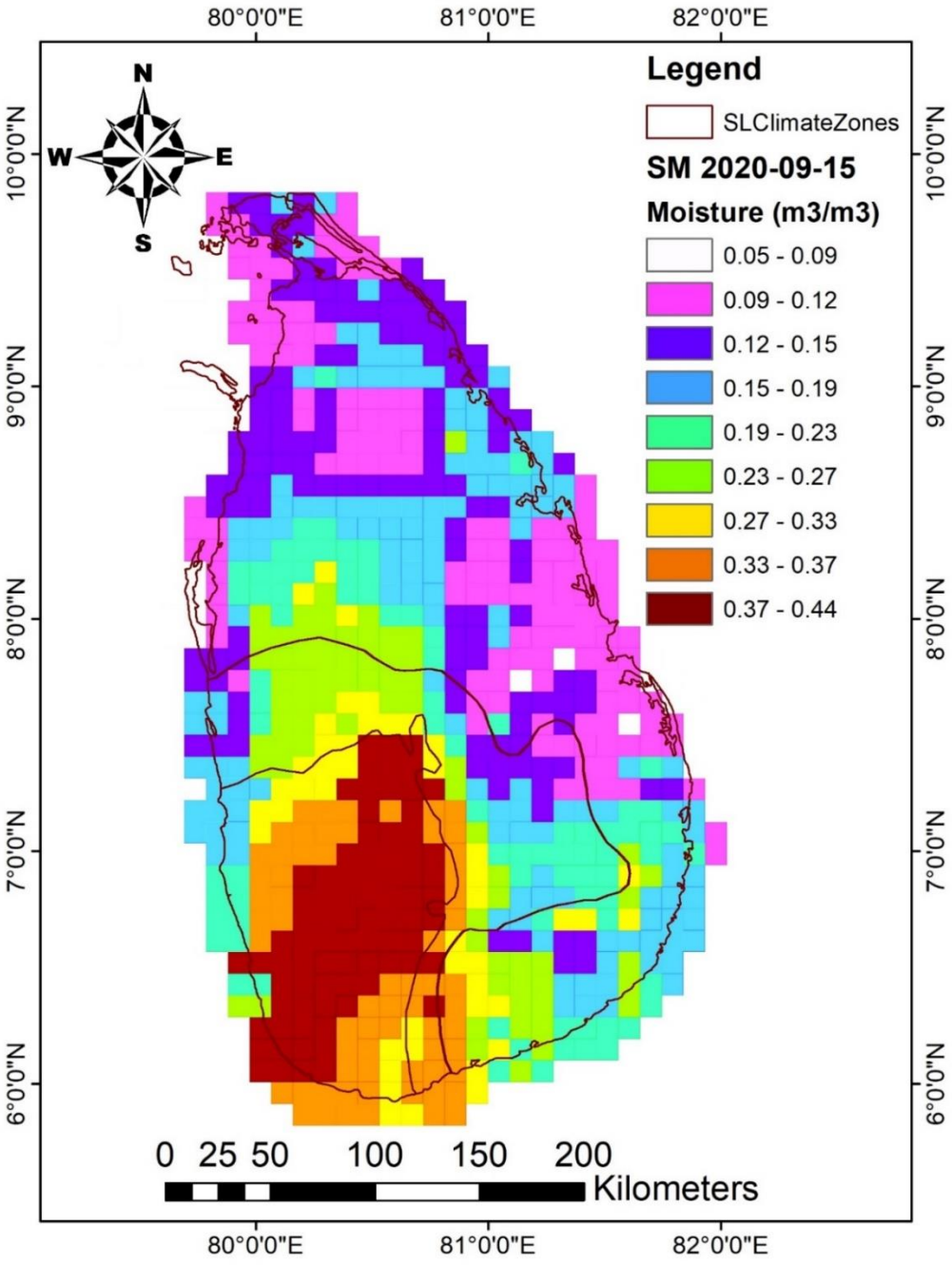

Figure 4-1: Soil Moisture data (2020-09-15) obtained from SMAP L4 V5 dataset

For the study area, a soil Map was obtained from the Survey Department of Sri Lanka. As shown in Figure 4-2, Reddish-brown earth and low humic gley soil were dominantly found in the study area followed by the presence of Reddish-brown earth and immature brown loams; rolling and hilly soil (Source: Survey Department, Sri

Lanka). The distribution of various soil types in the basin is represented in a pie-chart shown in Figure 4-2.

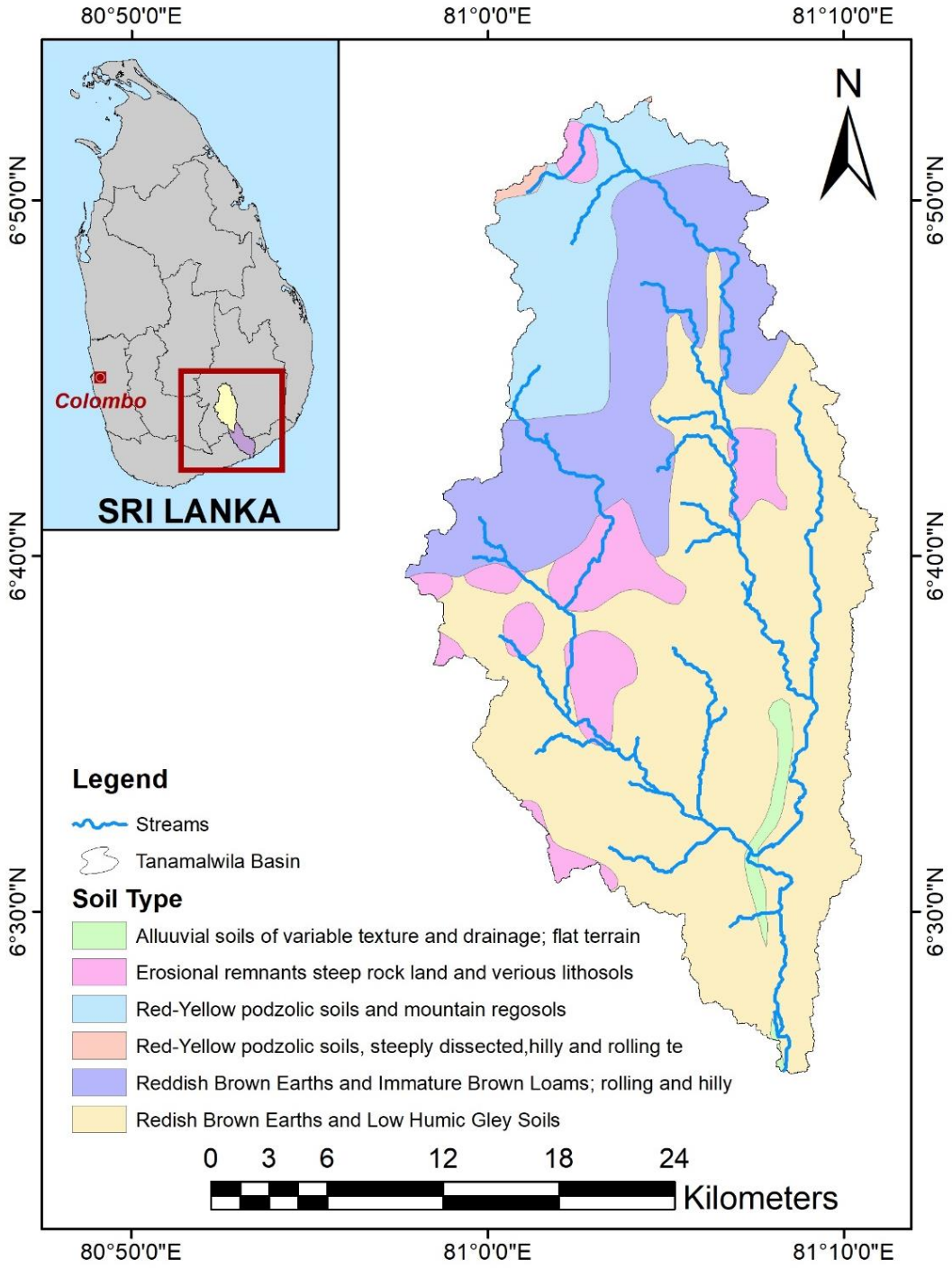

Figure 4-2: Soil map of Tanamalwila basin obtained from the Survey Department of Sri Lanka

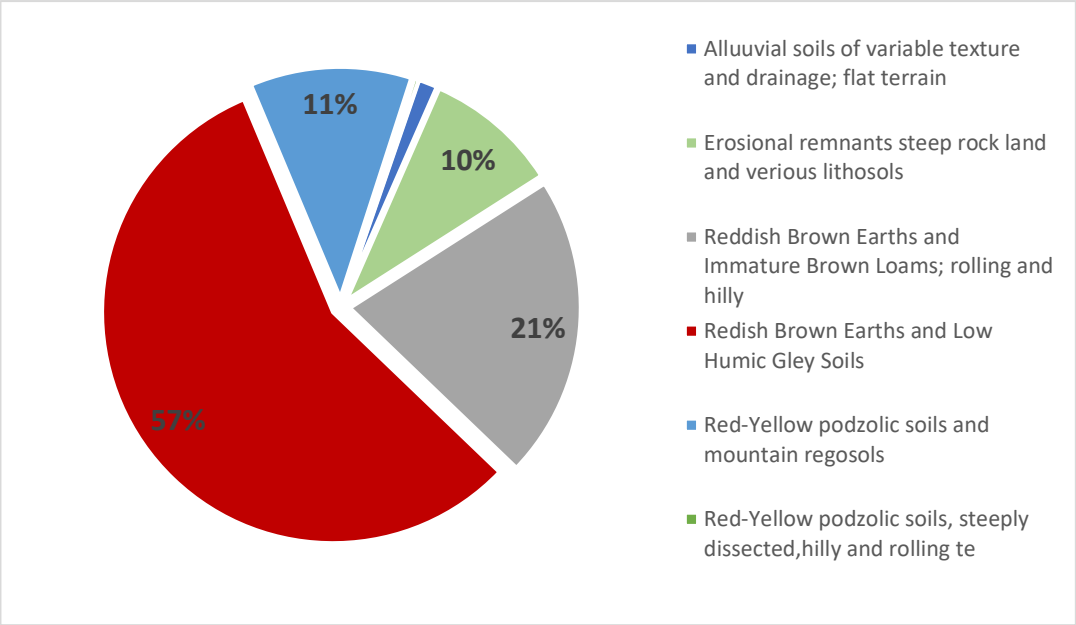

Figure 4-3: Distribution of various soil types in Tanamalwila basin

The Land-use map was obtained from the Environmental Systems Research Institute (ESRI's) land cover map of 2020 (Karra et al., 2021). The map was acquired from European Space Agency (ESA) Sentinel-2 imagery at 10 m resolution. To create a representative snapshot of 2020, the map is a composite of land-use landcover (LULC) estimates for ten classes over the course of a year. The pie chart below in Figure 4-4 shows the distribution of land use in the study area.

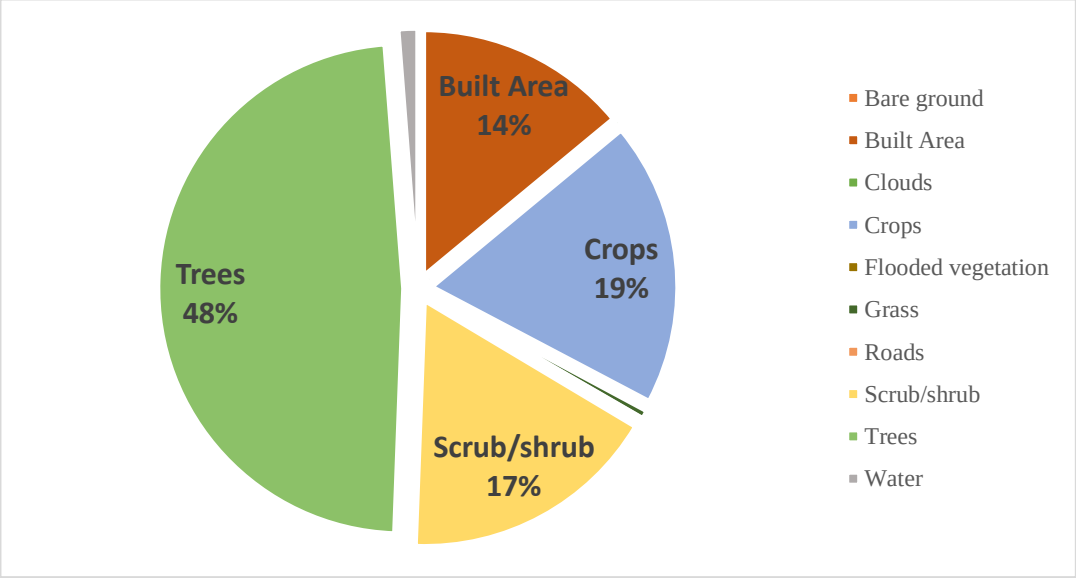

Figure 4-4: Pie chart showing the distribution of land use in the study area

The maximum part of the area is covered by forests followed by crop cultivations. All associated land-use with the area coverage and percentage coverage of the area is as shown in Table 4-3 below.

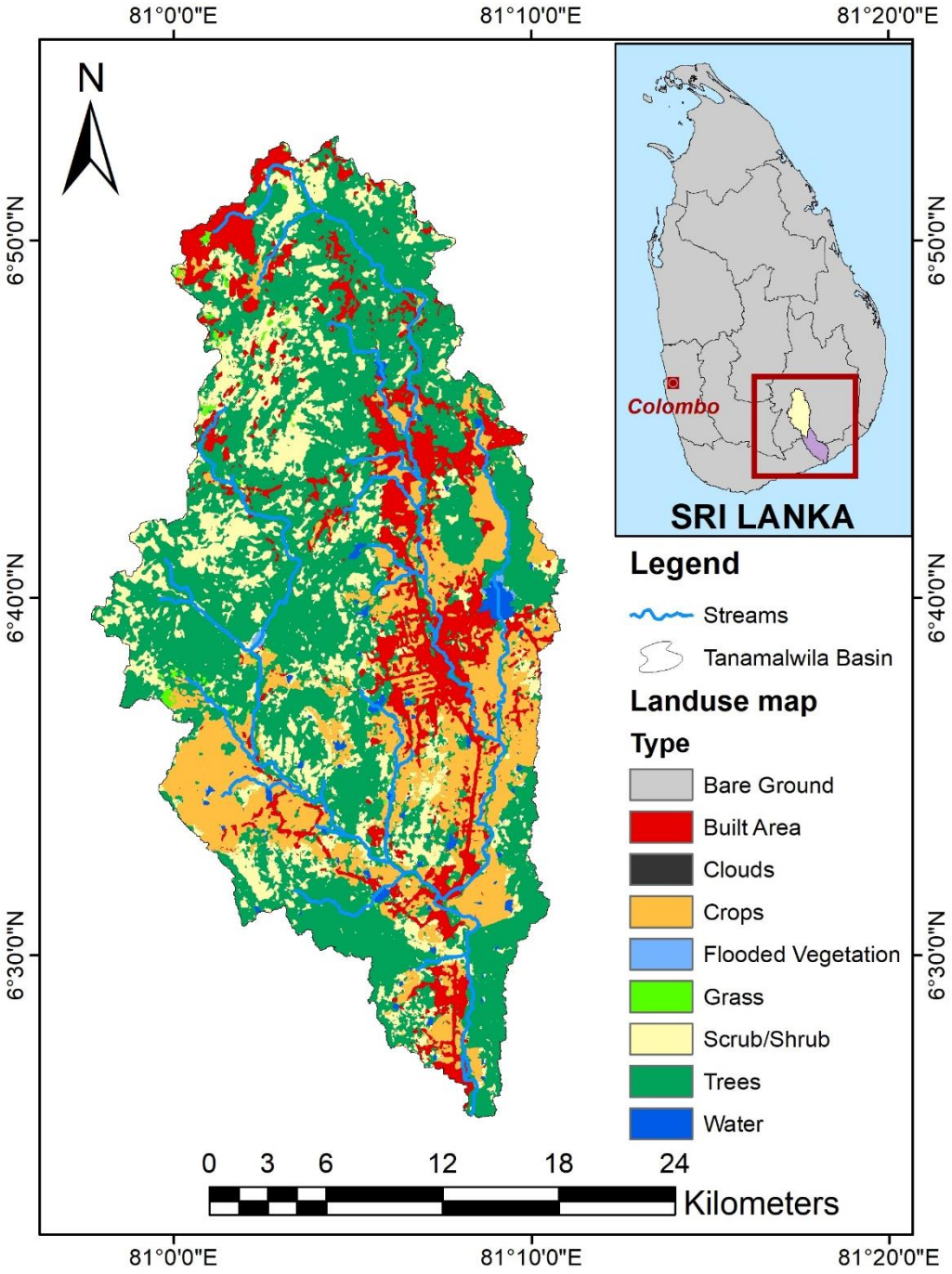

Figure 4-5: Distribution of various types of land use in Tanamalwila Watershed

Source: ESRI's 10-m land cover map of 2020 (Karra et al., 2021)

Table 4-3: Different land-use in the study area with their area and percentage coverage

Landuse Type	Area (sq km)	Percentage (%)
Bare ground	0.01	0.00%
Built Area	100.19	13.99%
Clouds	0.00	0.00%
Crops	134.13	18.73%
Flooded vegetation	0.87	0.12%
Grass	3.60	0.50%
Roads	1.65	0.23%
Scrub/shrub	121.89	17.02%
Trees	345.13	48.19%
Water	8.77	1.22%
Total	**716.23**	**100.00%**

4.1.2 Data Checking

First of all, collected data is checked visually using popular tools in excel like conditional formatting, charts, and graphs. Then computational checks and other checks are carried out through average and seasonal values.

4.1.2.1 Visual Data Checking

Daily Analysis

Rainfall data is arranged in chronological order with every station data in columns for easy comparison. Missing values are identified by negative values and blank cells as shown in Figure 4-6. Here, we can observe that the cells in pink colors have missing values. The precipitation data was also visually compared with the streamflow data using data bars to analyze the response of a catchment to the rainfall.

	Rainfall (mm)				Streamflow(Cumecs)
Time Period	1976 - 2015	1985 - 2015	1983 - 2015	2015 - 2020	1987-2015
Station Code	01BD0034	143476	01MG540A	01MG488A	
Date	Bandaraeliya	Bandarawela	Wellawaya	Tanamalwila	Thanamalwila
28-Apr-2016	0	0	0	0	2.39
29-Apr-2016	0	0	0	0	2.15
30-Apr-2016	6	2.5	35	23.9	1.77
1-May-2016	6	1.2	65.5		2.51
2-May-2016	7	0	18.5		7.38
3-May-2016	6	0.9	12.5		8.50
4-May-2016	8.5	0	71.5		16.32
5-May-2016	0	0	3		18.68
6-May-2016	12	5	70		8.52
7-May-2016	22	4.6	78.2		20.68
8-May-2016	109	53.4	91.1		39.14
9-May-2016	23	8.1	0.3		47.45
10-May-2016	0	2	0.2		23.32
11-May-2016	33	31.1	15.5		15.03
12-May-2016	1.5	0	0.2		24.79
13-May-2016	66	33	42.6		29.01
14-May-2016	40	47.6	85.2		40.92
15-May-2016	100	62.1	44.1		67.81
16-May-2016	3	0.4	0.4		63.55
17-May-2016	28	15.9	19.6		33.06
18-May-2016	4	0.2	0		31.37
19-May-2016	0	2.2	3.3		23.97
20-May-2016	0	0	0		20.28
21-May-2016	0	0	0		16.09

Figure 4-6: Hydro-meteorological data in the chronological order to identify missing data

Graphically the missing data were identified when plotted in a daily time series scale as shown in Figure 4-7 below. When plotted on an annual scale, the trend of the data can be observed by adding the trendline in the chart. Missing data can also be observed when a cumulative plot shows a long (horizontal) straight line deviating from the trendline.

Annual precipitation in the Bandaraeliya station demonstrated decreasing trend throughout the study period as shown in Figure 4-8 below. A single mass curve is drawn for all the rain gauge stations in Kirindi Oya that presents cumulative precipitation in each station over the study period. A single mass curve analysis is useful in identifying the inconsistencies in the data set over a long period as the break in the cumulative precipitation would indicate the inconsistencies or missing data

(Chow et al., 1988). The Bandaraeliya station has the highest accumulated precipitation in the basin as it is located at the highest point of the basin near the wet zone. The Tanamalwila station has the lowest accumulated precipitation in the basin as presented in Figure 4-9.

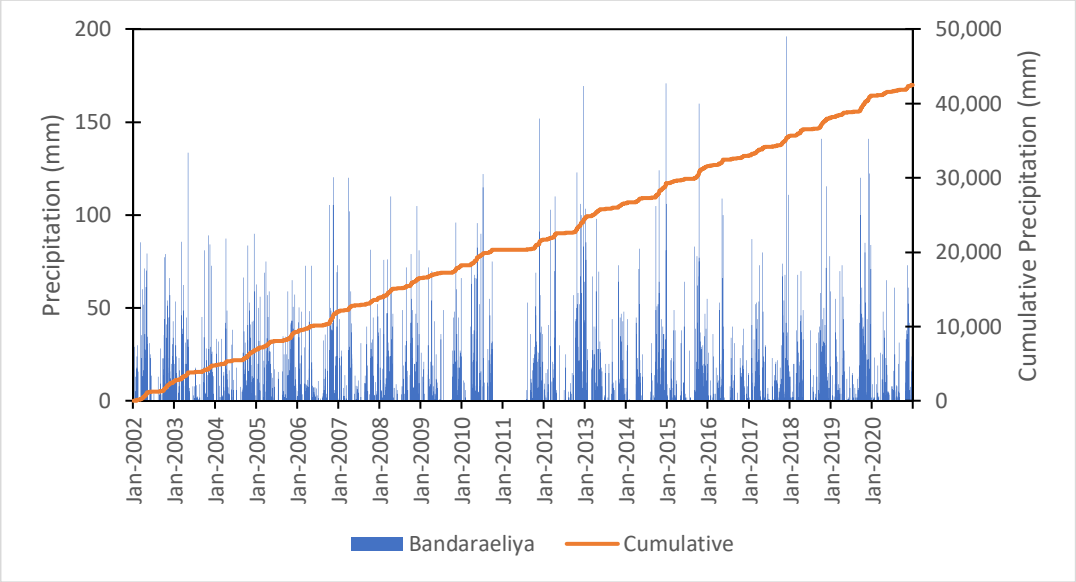

Figure 4-7: Daily precipitation and cumulative precipitation plot of Bandaraeliya Station

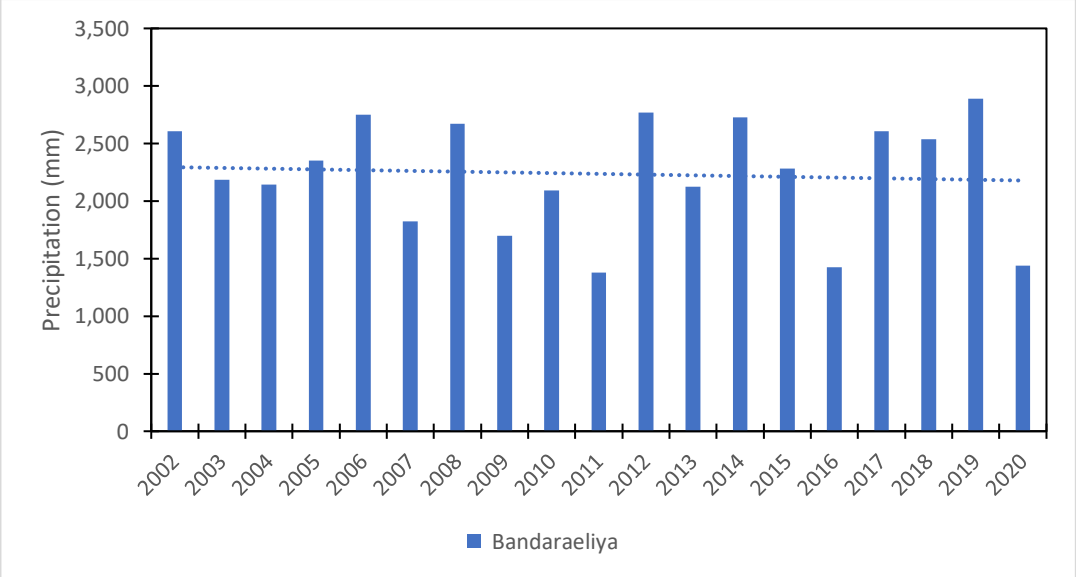

Figure 4-8: Annual precipitation in Bandaraeliya station from 2002 to 2020

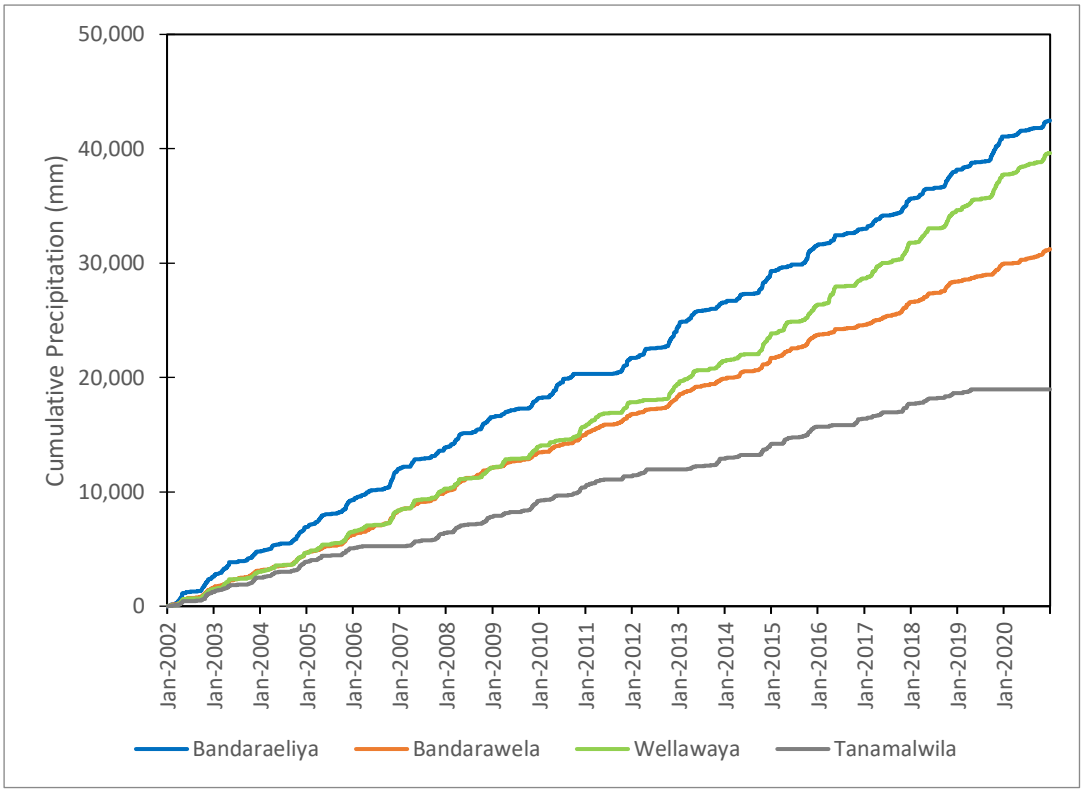

Figure 4-9: Cumulative precipitation in the various stations in the basin

Monthly, Seasonal and Annual Analysis

The missing values were also identified using the conditional formatting tools in Excel spreadsheets by visually observing the data sets even in monthly arrangements as shown in Figure 4-10. It can be observed that during October and November 2010, there is no precipitation at all (red color). But the precipitation is high during other years as indicated by the green color, which suggested that there are missing data and detailed checking needs to be further explored at daily scale. Further, the missing data set can also be analyzed from the annual sum, where data bars are indicating lower annual totals during the year 2011 where data sets of many months are missing. The above-mentioned attributes can be observed in Figure 4-10.

Year	Bandaraeliya												
	Oct	Nov	Dec	Jan	Feb	Mar	Apr	May	Jun	Jul	Aug	Sep	Sum
2002	612.8	343.0	227.6	92.7	85.7	276.7	545.4	195.2	62.6	4.0	72.3	86.3	2604.3
2003	188.3	384.4	53.1	233.7	59.3	412.6	299.3	239.0	20.2	63.7	11.0	218.2	2182.8
2004	468.7	313.0	313.2	110.5	68.7	87.3	300.1	96.5	17.3	26.0	12.6	330.9	2144.8
2005	231.2	672.2	135.5	182.4	90.6	216.2	440.0	164.0	24.5	30.8	66.4	95.9	2349.7
2006	604.1	716.4	325.6	216.6	79.3	181.6	213.4	161.0	23.8	13.5	62.0	154.6	2751.9
2007	306.6	178.9	257.5	149.3	27.7	130.0	488.5	17.7	54.9	33.2	52.7	127.0	1824.0
2008	517.0	328.2	208.5	112.9	229.1	416.7	491.5	18.0	10.0	60.5	236.4	40.3	2669.1
2009	198.0	405.0	351.0	87.0	4.0	182.2	213.0	137.5	37.0	82.0	0.0	0.0	1696.7
2010	0.0	0.0	0.0	21.0	8.0	192.0	419.0	499.8	222.0	297.0	68.0	365.0	2091.8
2011	491.6	474.9	233.2	0.0	0.0	0.0	0.0	0.0	0.0	0.0	60.0	117.6	1377.3
2012	574.5	619.5	537.5	41.7	205.1	66.6	518.2	30.0	0.0	52.0	23.5	101.0	2769.6
2013	148.0	265.5	165.0	405.5	0.0	307.5	342.0	262.5	44.0	30.0	69.0	84.5	2123.5
2014	664.0	312.0	709.0	126.0	0.0	0.0	430.0	150.0	0.0	0.0	72.0	263.0	2726.0
2015	838.0	267.0	265.0	21.0	129.0	171.0	0.0	105.0	123.0	31.0	0.0	332.0	2282.0
2016	118.0	191.5	68.0	54.0	66.0	61.0	196.0	471.0	0.0	87.0	106.5	5.0	1424.0
2017	373.5	580.0	291.0	231.0	71.0	427.8	102.5	315.0	14.0	36.0	90.0	74.0	2605.8
2018	616.5	435.5	204.0	64.0	46.0	298.5	486.0	0.0	0.0	85.5	51.0	249.0	2536.0
2019	758.0	337.5	555.7	19.5	197.0	103.0	310.0	19.0	28.5	52.0	34.0	475.0	2889.2
2020	72.5	484.9	104.7	39.0	38.5	40.0	230.4	197.4	22.5	121.2	88.0	0.0	1439.1

Figure 4-10 Identification of missing values using conditional formatting

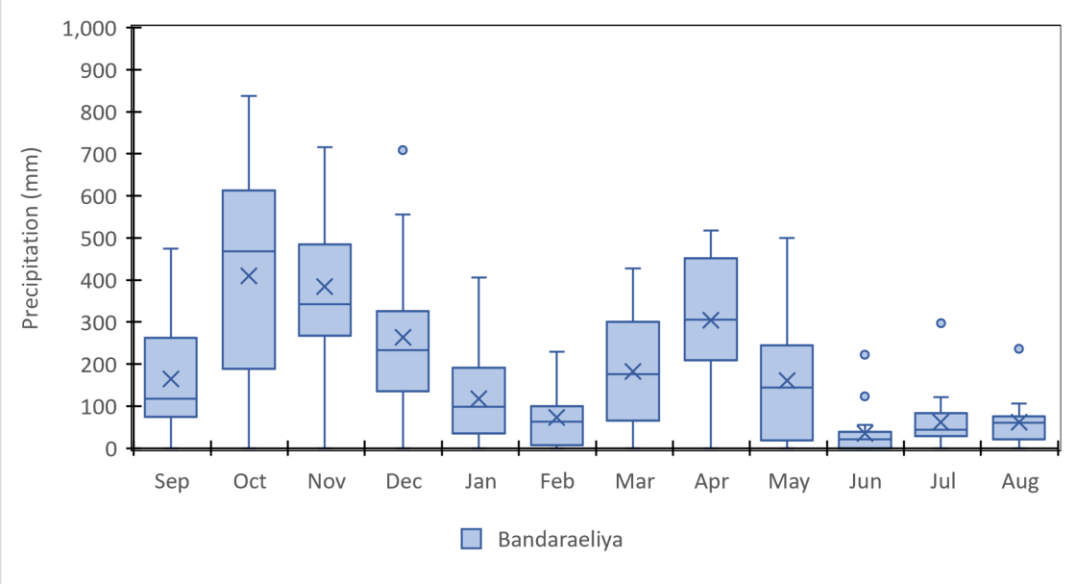

Figure 4-11: Box and whisker plot representing the monthly variation of rainfall in Bandaraeliya with top and bottom whiskers representing max and min, respectively

Box plot is developed to check the distribution of monthly values in each month of the series. Maximum and minimum analysis, extreme data, quartiles and mean values can be interpreted from the box and whisker plot (McGill et al., 1978). The top and bottom whiskers of the plot indicate the maximum and minimum values of a given variable. In addition, the lower and upper bounds of the box represent lower quartile (Q1) and

upper quartile (Q3) values with the median indicated by a solid line within the box. Further, the extremes/outliers can be identified as the individual points above or below the whiskers. A box plot for the Bandaraeliya station is as shown in Figure 4-11 which explains that higher precipitation can be observed from September to November and March to May. Further station-wise analysis was performed to compare one station with another as shown in Figure 4-12.

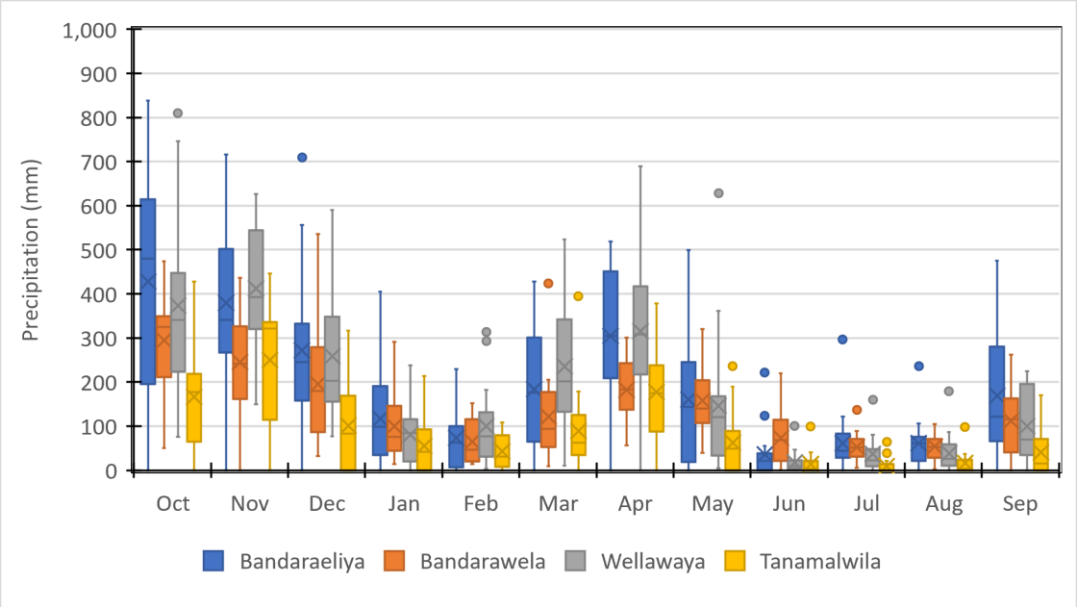

Figure 4-12: Monthly distribution of rainfall in various stations in the basin

There are four seasons in Sri Lanka influenced by variation in rainfall throughout the year. First inter monsoon (FIM) rainfall occurs during March and April which succeeds to southwest monsoon (SWM) rainfall from May till September. The October and November months experience second inter monsoon (SIM) rainfall succeeded by northeast monsoon (NEM) during December and ends in February. The seasonal distribution of rainfall in Bandaraeliya station is as shown in Figure 4-13 and it can be observed that more rainfall is contributed during the second inter monsoon followed by northeast monsoon rain in the Bandaraeliya station.

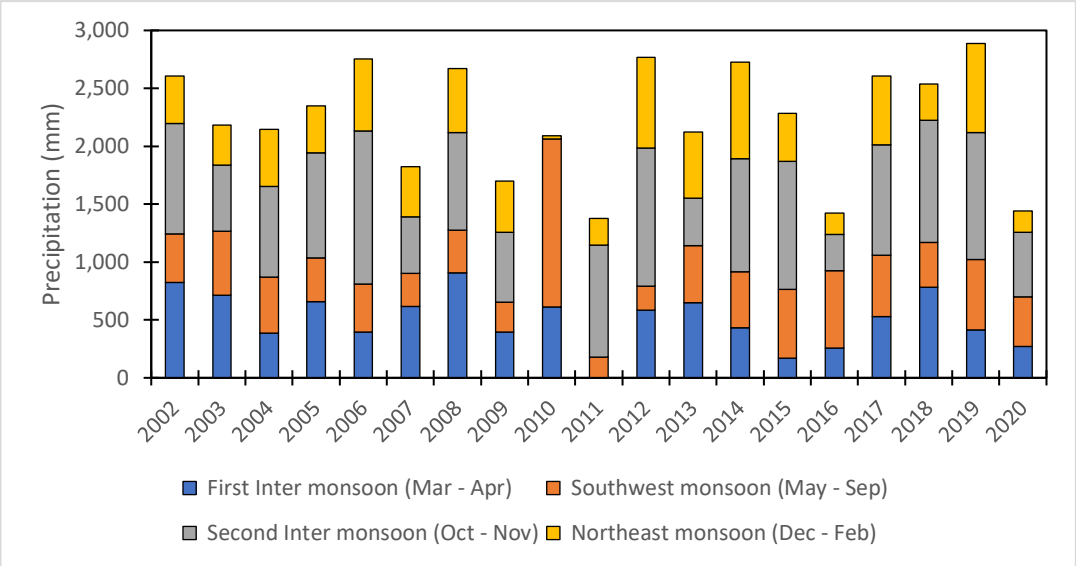

Figure 4-13: Seasonal distribution of rainfall in Bandaraeliya

Various stations are plotted on an annual scale where trends can be seen as shown in Figure 4-14. Precautions should be applied while identifying outliers and it should be verified whether it is an extreme event or an outlier from other secondary sources. The annual rainfall values at Bandaraeliya, Bandarawela, Wellawaya, and Tanamalwila stations are shown in Figure 4-14.

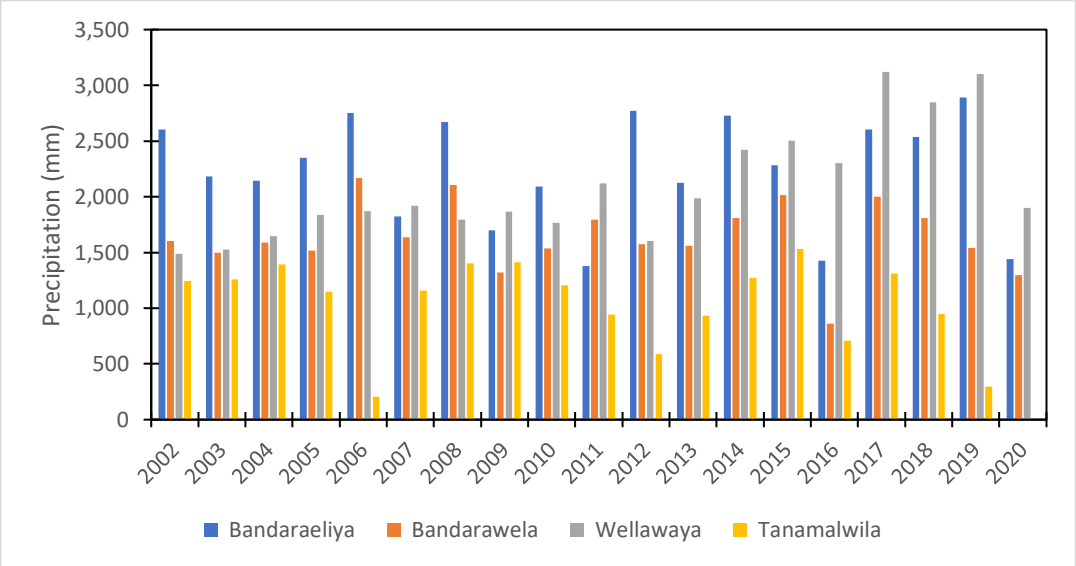

Figure 4-14: Annual rainfall in various stations in Kirindi Oya

Daily streamflow data in m^3/s from duration 1987 – 2020 is obtained and analysis is carried out using conditional formatting to see general trends in data. A conditional

formatting tool is used to analyze the streamflow data as shown in Figure 4-15. Further, the time series plot of daily streamflow is plotted in Figure 4-16 to observe the trends and extremes during the study period.

	Starting from 1997		Time Period	Streamflow(Cumecs)
				1987-2015
			Station Code	
Year	Month	Day	Date	Thanamalwila
1997	11	1	1-Nov-1997	99.76
1997	11	2	2-Nov-1997	107.54
1997	11	3	3-Nov-1997	94.52
1997	11	4	4-Nov-1997	117.63
1997	11	5	5-Nov-1997	97.81
1997	11	6	6-Nov-1997	40.06
1997	11	7	7-Nov-1997	90.08
1997	11	8	8-Nov-1997	56.76
1997	11	9	9-Nov-1997	33.16
1997	11	10	10-Nov-1997	34.55
1997	11	11	11-Nov-1997	92.80
1997	11	12	12-Nov-1997	72.38
1997	11	13	13-Nov-1997	65.54
1997	11	14	14-Nov-1997	93.68
1997	11	15	15-Nov-1997	98.44
1997	11	16	16-Nov-1997	62.63
1997	11	17	17-Nov-1997	44.06
1997	11	18	18-Nov-1997	66.21
1997	11	19	19-Nov-1997	177.27
1997	11	20	20-Nov-1997	166.67
1997	11	21	21-Nov-1997	112.67
1997	11	22	22-Nov-1997	65.44
1997	11	23	23-Nov-1997	55.58
1997	11	24	24-Nov-1997	57.43
1997	11	25	25-Nov-1997	86.84

Figure 4-15: Visual checking of Streamflow data where blue horizontal bars indicate the magnitude of the streamflow and dark green indicating higher magnitudes

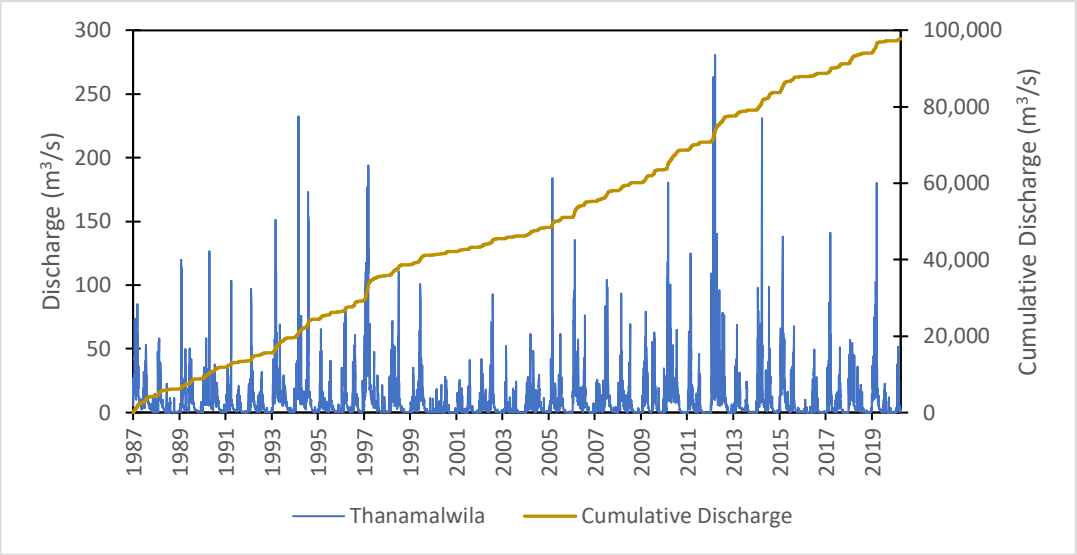

Figure 4-16: Daily discharge at the Tanamalwila station during the study period

From Figure 4-17, it can be seen clearly that the months June, July, August, and September months have low flow values compared to the other months and it can be verified from the rainfall pattern data above. The highest flow values are recorded in November, December, and April which can be observed visually in Figure 4-17.

Year	Tanamalwila												
	Oct	Nov	Dec	Jan	Feb	Mar	Apr	May	Jun	Jul	Aug	Sep	Sum
1987/88	24.6	20.0	26.8	7.8	4.3	9.8	25.7	12.3	4.2	3.0	1.8	2.0	142.4
1988/89	5.2	27.6	11.5	4.6	0.7	2.9	2.1	2.7	0.5	1.1	0.5	0.6	60.0
1989/90	7.1	20.2	3.2	8.5	4.2	17.7	15.3	7.8	2.0	0.9	0.6	1.9	89.4
1990/91	11.7	10.9	11.4	17.3	5.1	8.3	15.4	9.9	5.4	0.9	0.7	1.2	98.5
1991/92	3.0	13.3	12.6	6.7	2.2	1.1	5.3	5.2	0.9	0.3	0.2	1.3	52.0
1992/93	4.6	25.2	13.0	3.5	1.5	3.7	9.6	5.9	1.3	0.9	0.5	0.5	70.2
1993/94	9.1	25.8	29.5	12.7	17.8	8.2	15.6	8.3	2.0	1.1	0.9	3.1	134.1
1994/95	10.7	21.7	23.6	14.8	9.5	7.8	23.6	35.0	6.2	1.4	1.0	0.5	155.9
1995/96	2.7	20.0	6.1	4.3	3.2	1.7	18.2	3.2	1.5	0.6	1.1	0.8	63.3
1996/97	6.0	11.4	20.0	3.7	1.5	0.9	13.6	25.9	6.6	1.3	0.5	3.7	95.1
1997/98	30.2	78.8	50.7	17.7	8.7	8.6	3.7	10.4	0.9	2.3	2.2	0.6	214.7
1998/99	0.7	7.3	19.7	14.3	13.7	10.6	23.9	2.8	1.0	0.5	0.5	0.6	95.6
1999/0	2.2	10.8	5.2	3.1	15.9	25.4	13.4	4.5	1.1	0.5	1.3	1.2	84.5
2000/1	0.7	3.7	1.1	2.0	3.6	1.3	11.8	3.1	0.7	0.0	0.0	0.2	28.3
2001/2	3.1	9.5	3.6	1.1	0.6	0.5	9.8	8.6	1.1	0.0	0.1	0.1	38.2
2002/3	4.8	12.8	6.9	3.4	1.3	9.0	17.8	13.5	1.3	0.8	0.3	0.4	72.3
2003/4	0.4	8.0	4.2	1.4	0.7	2.3	4.6	3.8	0.2	0.0	0.0	0.7	26.3
2004/5	6.1	9.1	16.7	5.7	4.3	3.3	9.4	10.0	1.8	1.8	0.7	0.6	69.6
2005/6	2.0	27.1	19.6	5.3	2.5	8.6	17.5	5.1	0.7	0.1	0.0	0.3	88.8
2006/7	12.2	50.5	19.8	11.5	5.6	1.8	23.3	8.6	1.6	0.3	0.1	0.7	136.1
2007/8	2.7	10.8	6.4	4.1	5.8	18.6	31.1	8.7	2.8	0.8	1.0	0.4	93.2
2008/9	7.6	18.4	14.1	4.2	1.6	9.4	12.2	2.1	0.4	0.0	0.4	0.0	70.5
2009/10	2.4	15.7	28.6	9.9	1.5	6.1	17.8	22.2	2.7	1.9	0.3	1.4	110.4

Figure 4-17: Monthly average streamflow (m^3/s) in Tanamalwila station

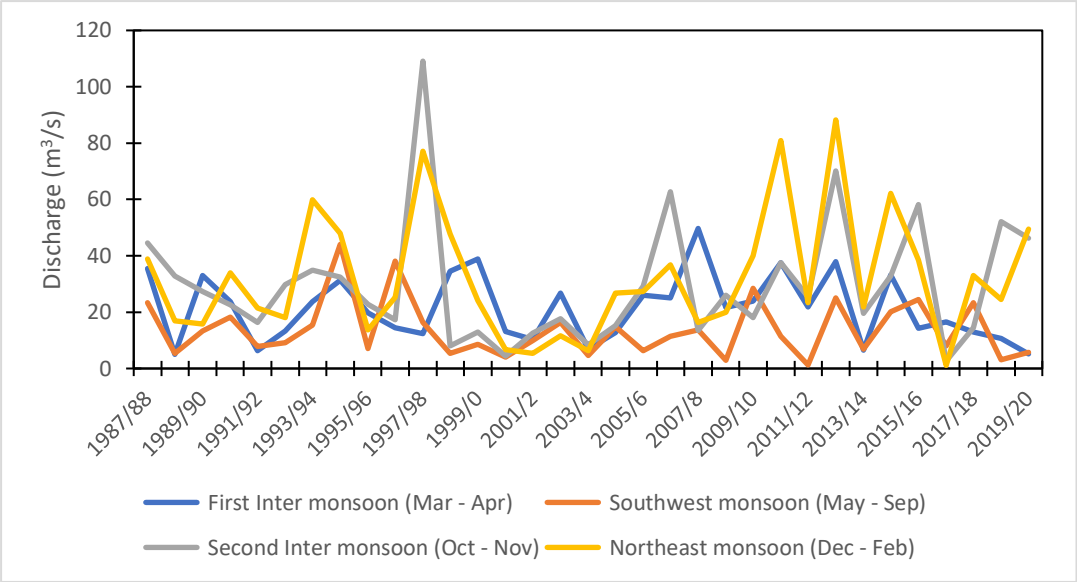

Figure 4-18: Seasonal distribution of streamflow in Tanamalwila basin

The seasonal distribution of flow for the study period is as shown in Figure 4-18. The Northeast monsoon period exhibits major discharge in the basin followed by the second intermonsoon period and first intermonsoon period. The southwest monsoon contributes the least to the total streamflow in the basin. The above-mentioned features can be well observed in Figure 4-19.

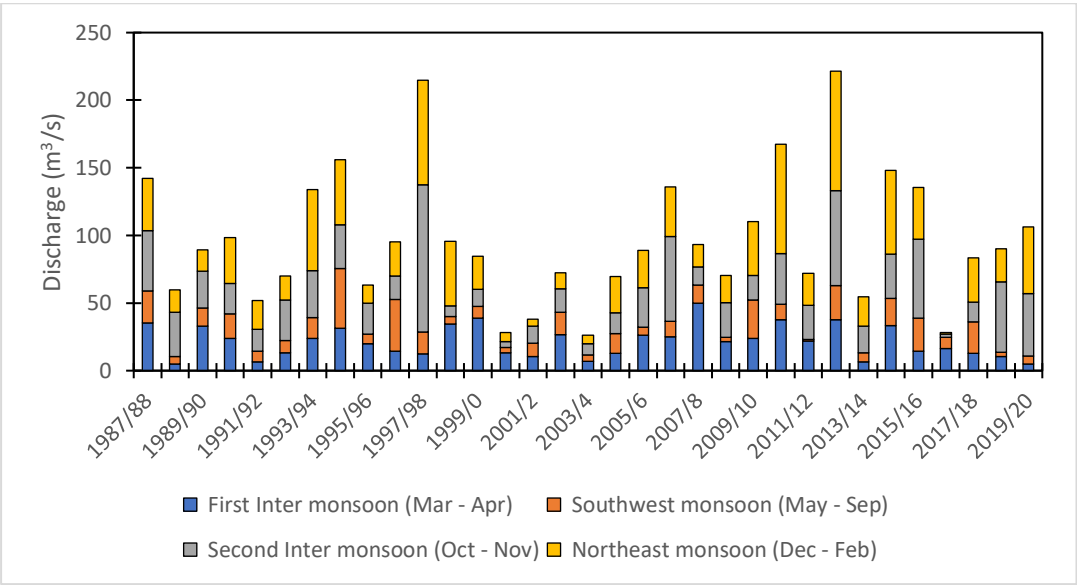

Figure 4-19: Contribution of seasonal flow in every water year during the study period

Missing data can be found from the rainfall vs streamflow graph where any of the parameters that usually do not follow the trend of other parameters indicate missing or outliers as shown in Figure 4-20 indicated by an orange box.

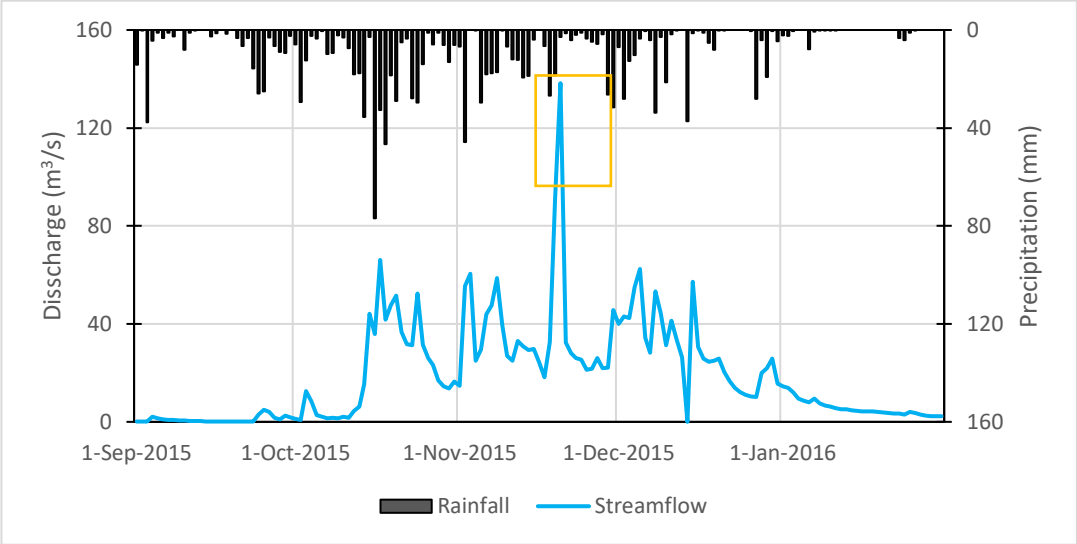

Figure 4-20: Rainfall vs Streamflow graph to observe missing data and irregularities

4.1.2.2 Consistency Test of the Record

Double-mass curve analysis is used to assess the consistency of a rainfall record. The cumulative yearly (alternatively seasonal or monthly) results of a station under consideration are compared to those of a reference station using this method. The reference station is usually the mean of several neighboring stations. This is based on a belief that when all of the data is collected from the same parent population, it will be consistent. Inconsistencies in observations can occur as a result of a rain gauge station moving, a station's neighborhood changing dramatically, changes in the ecosystem as a result of natural disasters, and observational and recording errors.

The cumulative annual precipitation of station X is plotted against the average annual rainfall of a set of base stations comprising a longer period arranged in reverse chronological order (i.e. most recent record as the initial entry and the ancient record as the final entry in the list). Any break in the plot indicates inconsistencies in the record and needs to be corrected referring to (Chow et al., 1988). All four (4) stations data showed consistent results and the double mass curve of Bandaraeliya and Bandarawela stations are as shown in Figure 4-21 and Figure 4-22, respectively.

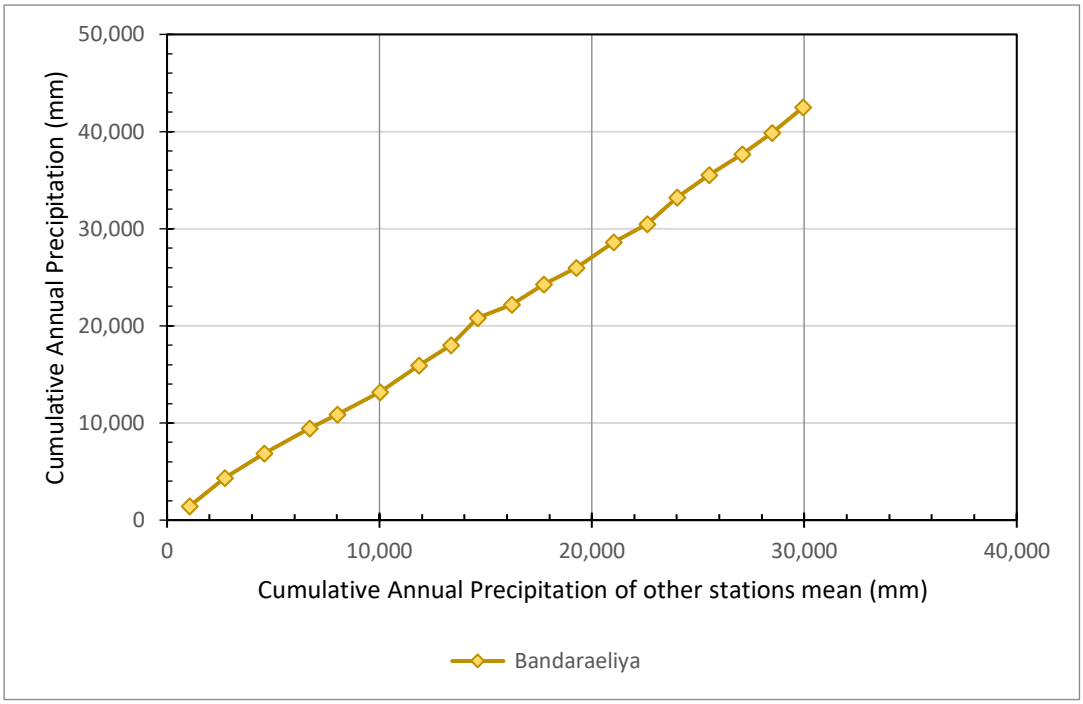

Figure 4-21: Double mass curve of Bandaraeliya station

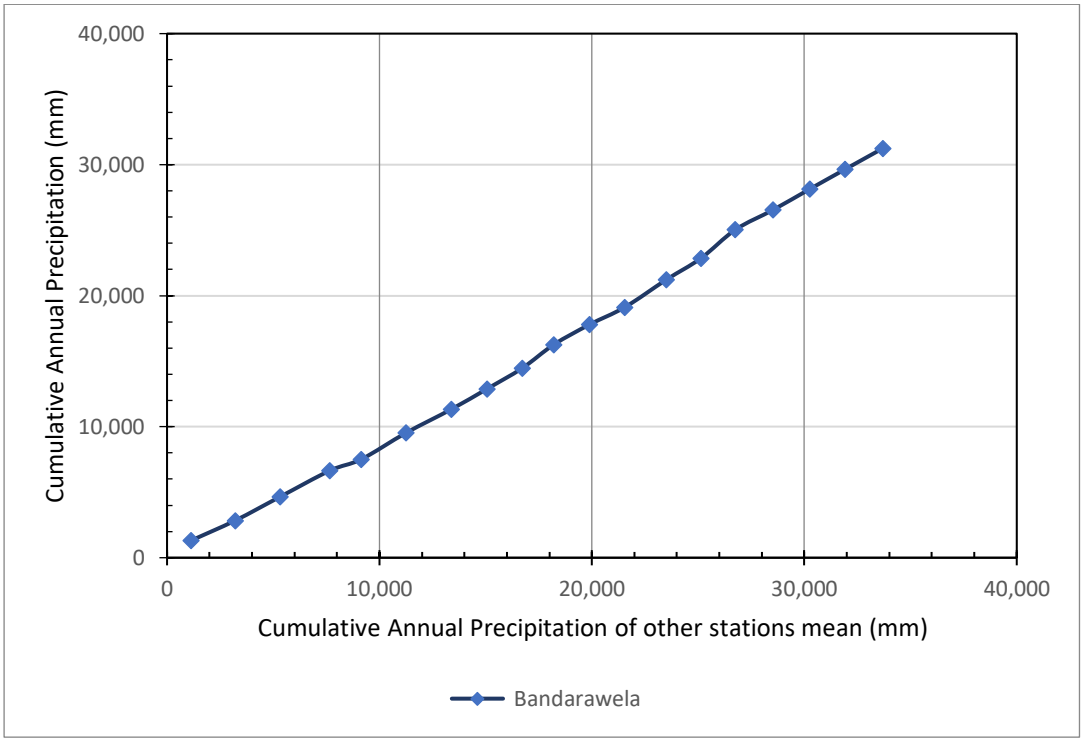

Figure 4-22: Double mass curve of Bandarawela station

4.1.3 Missing Data Filling

Every data set needs to be analyzed properly so that reliable results can be obtained overcoming uncertainties associated with the model. The missing data sets can be filled depending upon the percentage of missing and normal annual precipitation through the arithmetic average of nearby stations or weighted average as suggested by Chow et al. (1988). The number of days where data is missing is as listed in Table 4-4 and their respective percentages of missing data are too mentioned.

Table 4-4: Missing data in different stations in Kirindi basin

RF Station	Data Period	Missing days	Missing (%)
Bandaraeliya	2002 - 2020	604	9%
Bandarawela	2002 - 2020	35	1%
Wellawaya	2002 - 2020	213	3%
Tanamalwila	2002 - 2020	1,344	19%

The percentage of missing data is around 19 % in Tanamalwila station. Thus, missing data were filled in using regression analysis (Armanuos et al., 2020). A scatter plot was developed for every rainfall gauge station where rainfall at the station under consideration is plotted against average rainfall from all other stations. Equations developed from the scatter plot considering periods without missing data are used to fill the missing data for the station under consideration. The scatter plots for the rain gauge stations are as shown in Figure 4-23 and Figure 4-24. It can be observed that the trendline in Tanamalwila station is below the 45-degree line which is due to a large number of missing values in the recent period. Moreover, Tanamalwila station has the lowest R^2 value compared to other stations. New scatter plots after filling of data are developed and R^2 value thus computed is compared with R^2 before filling to assess the accuracy of filling of datasets.

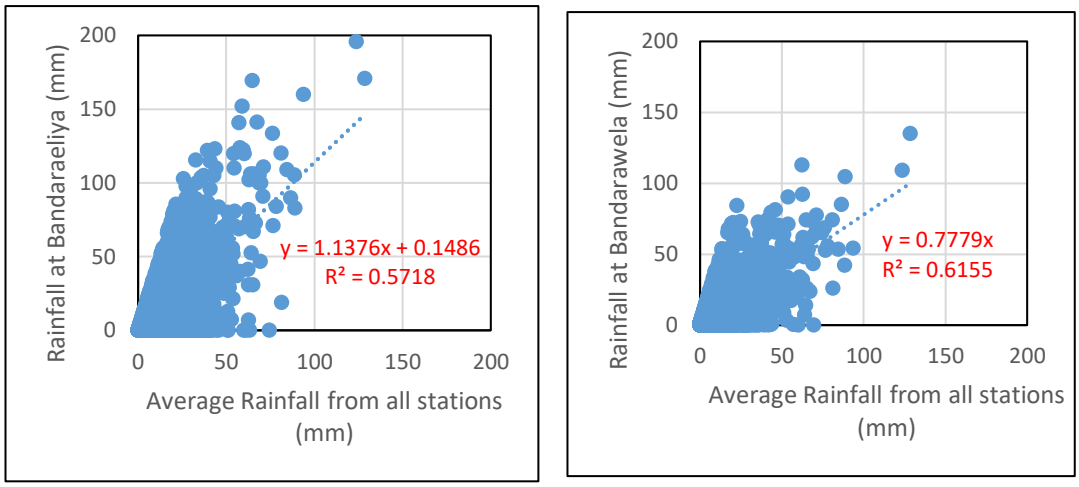

Figure 4-23: Scatter plot of rainfall in a) Bandaraeliya and b) Bandarawela Stations plotted against average rainfall in all stations

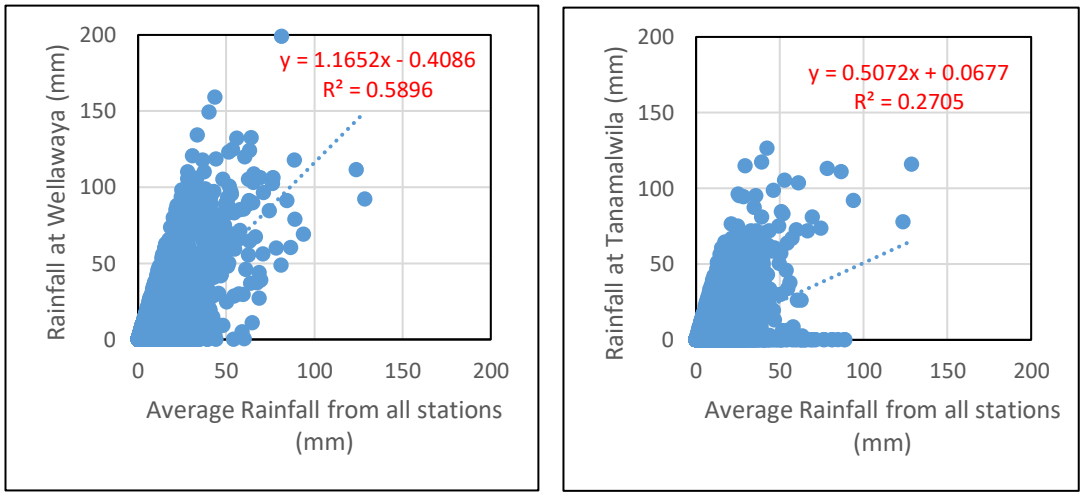

Figure 4-24: Scatter plot of rainfall in a) Wellawaya and b) Handapangala Stations plotted against average rainfall in all stations

4.1.4 Climate Trends and Extremes

As discussed in Chapter 3.3, various streamflow indices are calculated to observe trends and extremes in the basin.

4.1.4.1 Streamflow Indices

Various streamflow indices listed in Table 3-1 are calculated using streamflow data from the Tanamalwila gauging station in this section. The consecutive low-flow day (CDS) is defined as the annual maximum number of consecutive days with daily

streamflow less than the 10th percentile of streamflow data. The number of CDS days is showing a sharp increasing trend in the recent period.

The consecutive high-flow day (CWS) is defined as the annual maximum number of consecutive days with daily streamflow greater than the 90th percentile of streamflow data. The number of CWS days is also showing an increasing trend in the recent period.

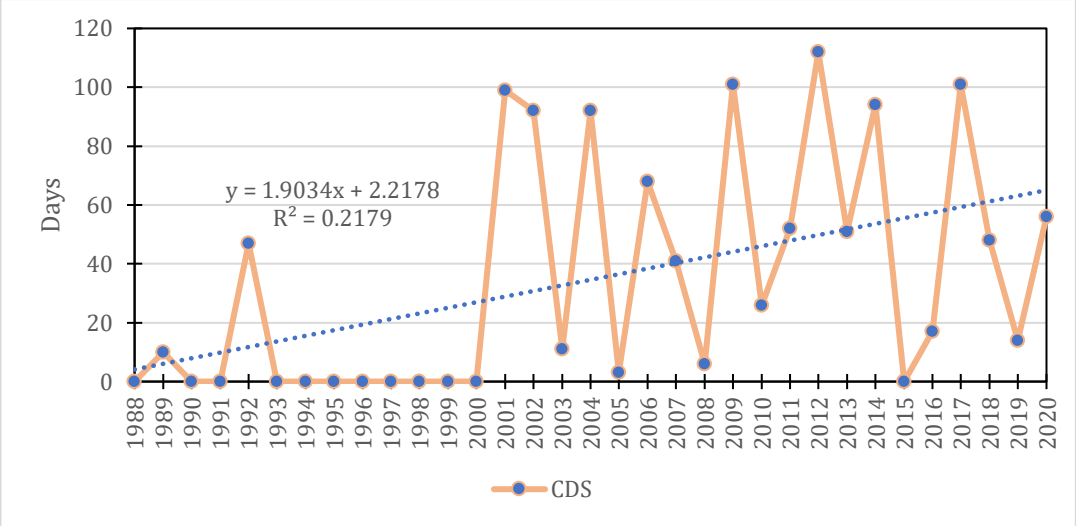

Figure 4-25: Consecutive low-flow days in Tanamalwila station

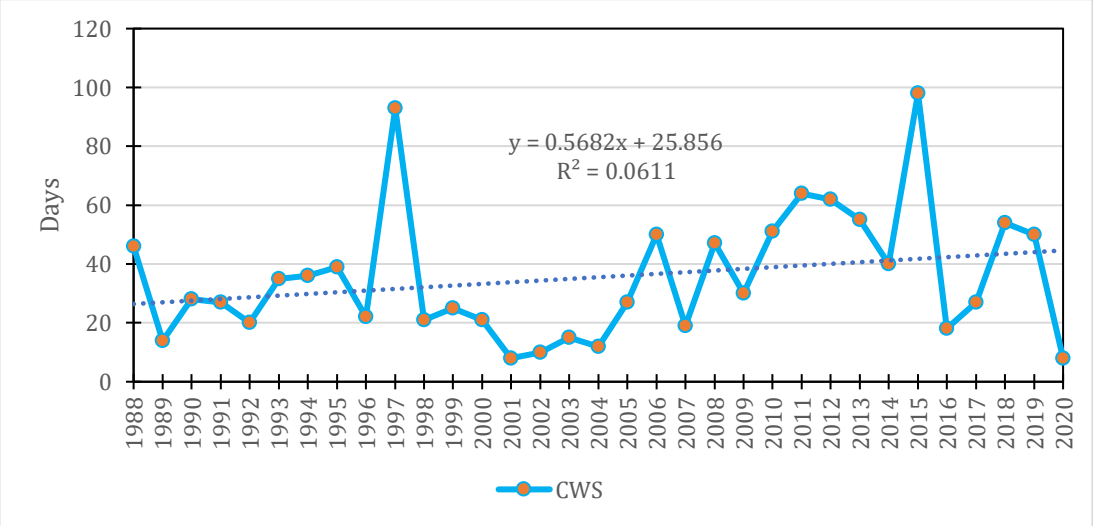

Figure 4-26: Consecutive high-flow days in Tanamalwila station

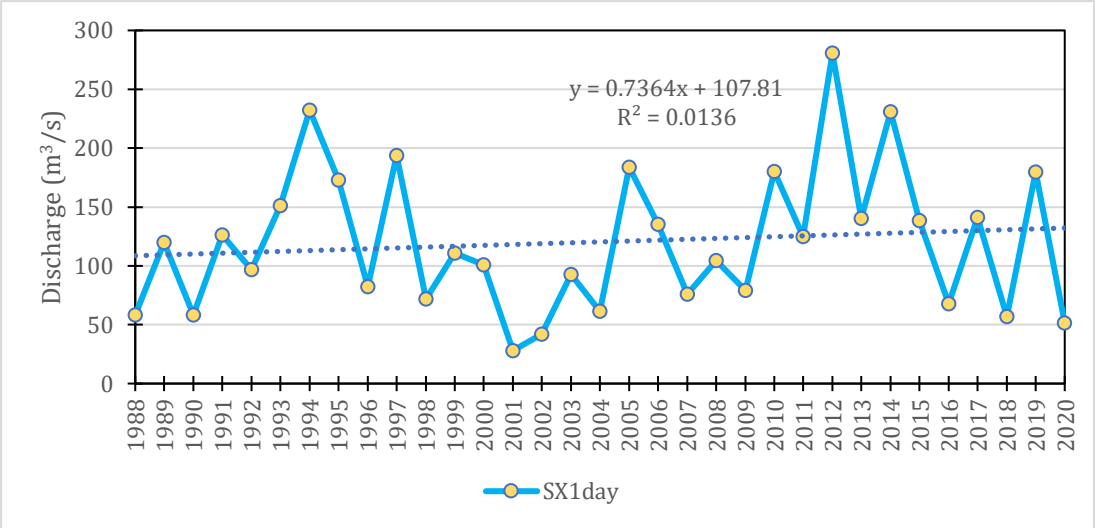

Figure 4-27: Annual highest daily streamflow in Tanamalwila station

The annual highest daily streamflow (SX1 day) is also showing an increasing trend in the recent period. The extreme high streamflow was observed in the year 2012 with a magnitude of 280.6 m^3/s whilst the basin experienced merely 28 m^3/s discharge as the maximum flow during the year 2001. This indicates that the basin is experiencing increased drought and flooding in the recent period.

Annual highest average streamflow in consecutive 2 days indexed as SX2 day and annual highest average streamflow in consecutive 5 days indexed as SX5 day is plotted as shown in Figure 4-28 below. The maximum streamflow in 1 day, an average of 2 consecutive days, and an average of 5 consecutive days showed an increasing trend. Although 1-day and 2-day averages are showing higher magnitudes, the 5-day average is slightly low in magnitude compared to the other two.

The SSI for Tanamalwila station for 12 months period was computed which is as shown in Figure 4-29 below. It can be observed that the frequency of drought is increasing in the recent period after 2006. Before the most severe drought from 2000 to 2005, intermittent drought was observed every 4 years. After 2006, droughts occurred frequently in 2-year intervals.

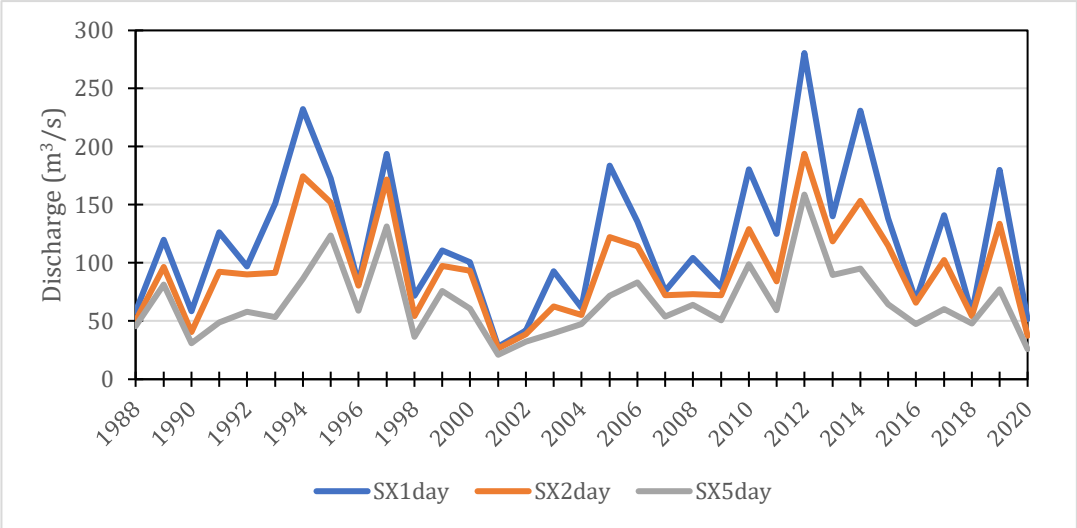

Figure 4-28: Annual highest streamflow in consecutive 1, 2, and 5 days in Tanamalwila station

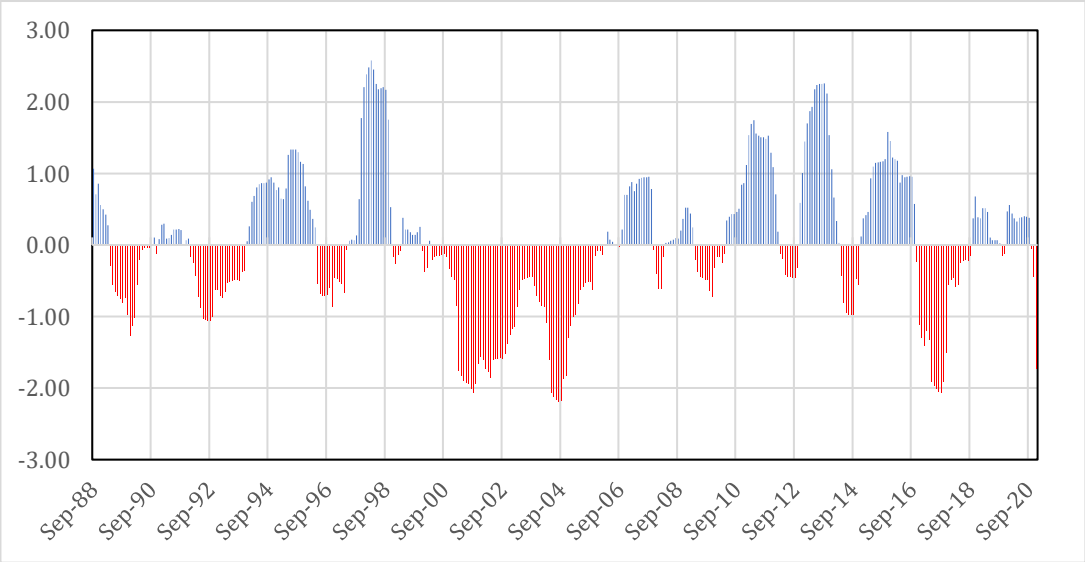

Figure 4-29: Standardized streamflow index for 12 month period in Tanamalwila station

4.1.4.2 Precipitation Indices

The precipitation indices listed in Table 3-2 are calculated using precipitation data from various gauging stations in this section. The Consecutive dry days (CDD) is defined as the annual maximum number of consecutive days with daily precipitation less than 1 mm. It was observed that CDD is showing a decreasing trend in the recent period which is shown in Figure 4-30.

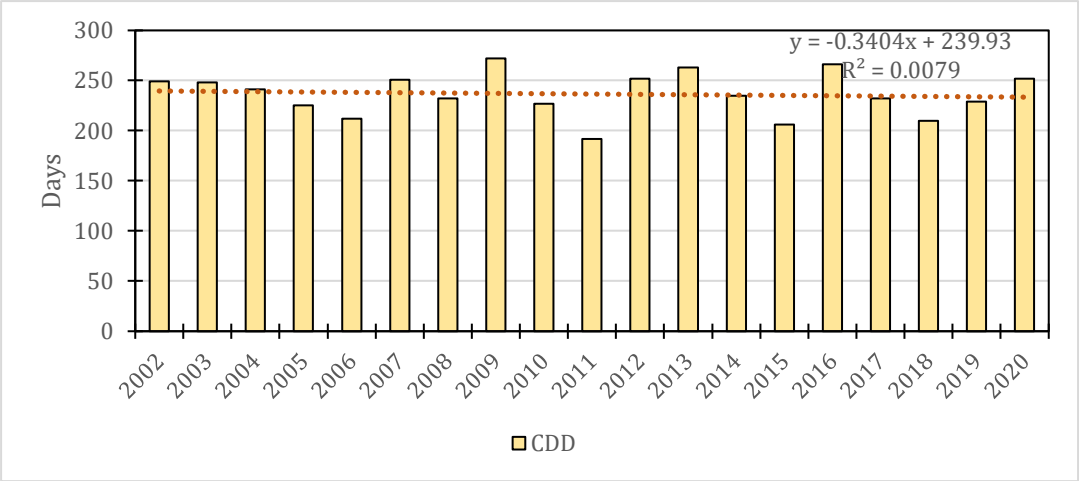

Figure 4-30: Consecutive dry days in Bandaraeliya station

The Consecutive wet days (CWD) is defined as the annual maximum number of consecutive days with daily precipitation greater than 1 mm. It can be observed that CWD is showing an increasing trend in the recent period in Bandaraeliya station as shown in Figure 4-31.

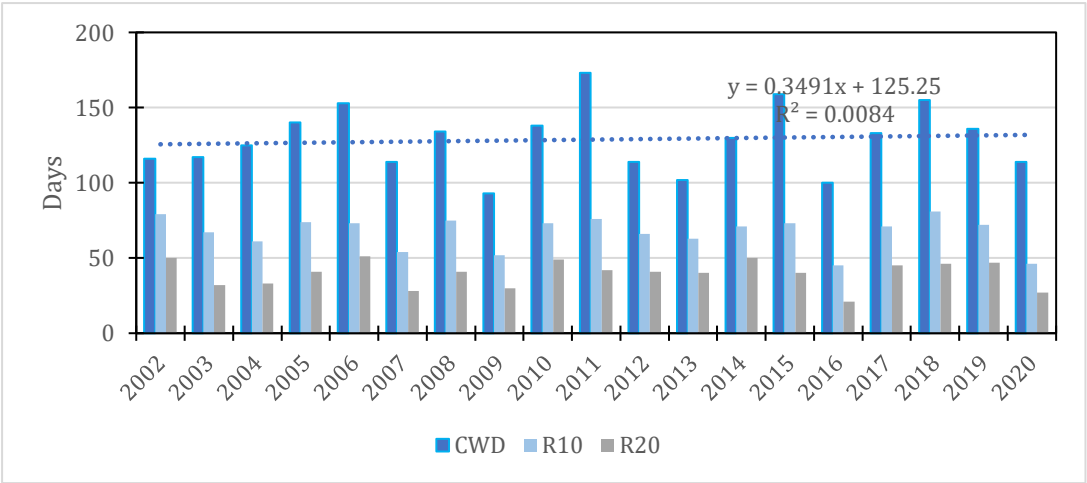

Figure 4-31: Consecutive wet days (CWD), heavy precipitation days (R10), and very heavy precipitation days (R20) in Bandaraeliya station

The annual precipitation extreme in Bandaraeliya station is showing an increasing trend along with higher magnitudes than previously observed in the station as shown in Figure 4-32.

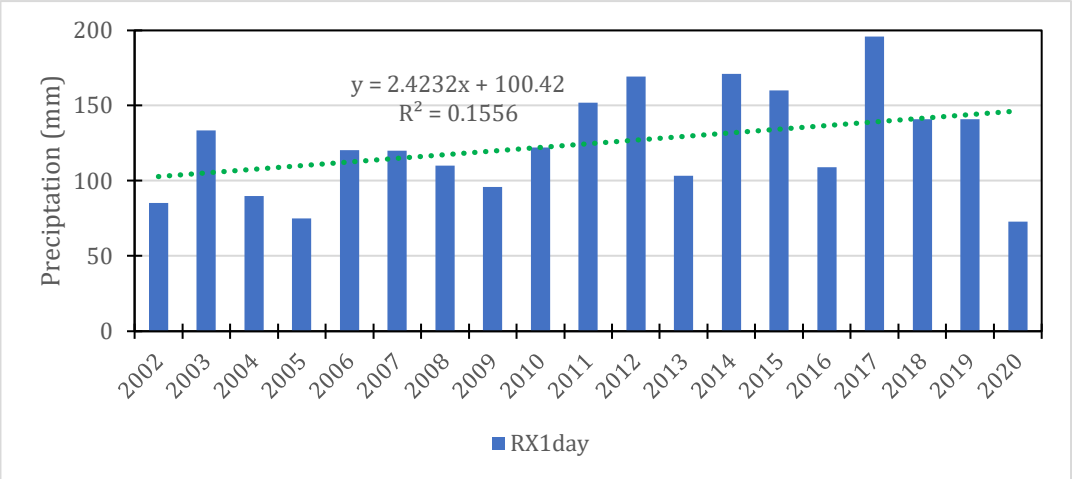

Figure 4-32: Annual precipitation extremes in Bandaraeliya station

Annual maximum 1-day precipitation along with 2-day consecutive precipitation and 5-day consecutive precipitation is presented in Figure 4-33. It can be observed that the precipitation trends in the above three (3) different time categories indices are increasing in the Bandaraeliya station.

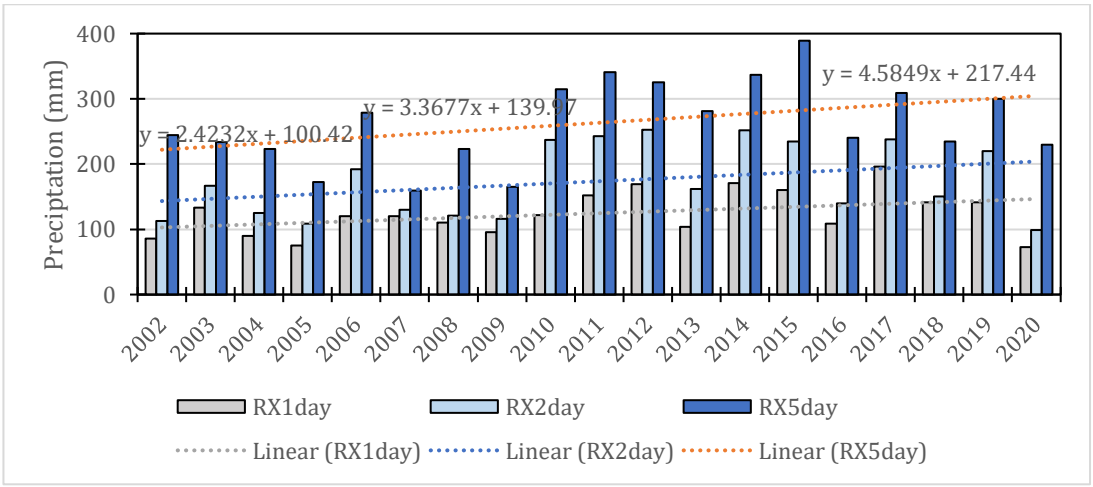

Figure 4-33: Annual maximum 1-day, 2-day, and 5-day precipitation in Bandaraeliya station

The annual distribution of wet and dry days in Bandaraeliya station as portrayed in Figure 4-34 depicts that the station experiences more dry days in a year. Although the dry days in a year is showing decreasing trend followed by an increase in wet days, there is still an increase in the frequency of occurrence of droughts.

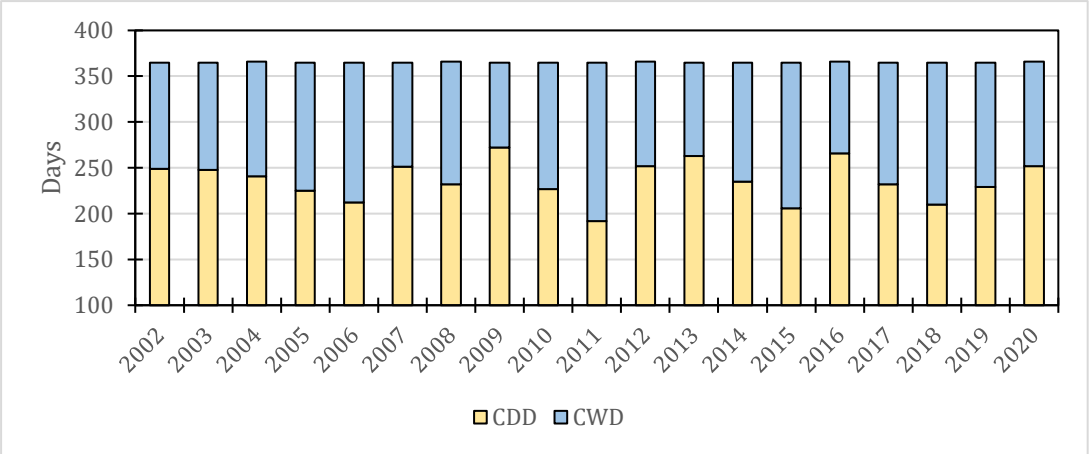

Figure 4-34: Annual distribution of wet and dry days in Bandaraeliya station

4.1.5 Precipitation Over an Area

Rain gauges only reflect a point measurement of a storm's areal distribution, but hydrological study necessitates the distribution of precipitation across a given area. There are many methods to distribute the point precipitation values at various stations over an area. The widely used methods are the Thiessen Polygon method (Chow et al., 1988). Inverse Distance Weightage (IDW) method (Golkhatmi et al., 2012), and Kriging Method (Karnieli, 1990).

Thiessen method assigns a weighting to rainfall reported at each station based on the area closest to the station by drawing polygons from the perpendicular bisectors on the line between stations over the area considered. Using a linearly weighted combination of a collection of sample points, inverse distance weighted (IDW) interpolation calculates cell values. The weight is inversely proportional to the distance. In this method, a weight is assigned at each point interpolating the distance to the reference point (Golkhatmi et al., 2012). When estimating values in an unknown domain, kriging applies a geostatistical interpolation approach that considers both the distance and degree of variation between known data points (Karnieli, 1990).

Zeinivand (2015) compared three interpolation methods (Thiessen polygon, IDW, and Kriging) for simulation of river discharge to study the impact of precipitation on runoff and discharge at the basin outlet. Considering the maximum discharges, Thiessen polygon showed better results compared to other methods. Considering the ease of use, the Thiessen polygon method is developed for the basin area.

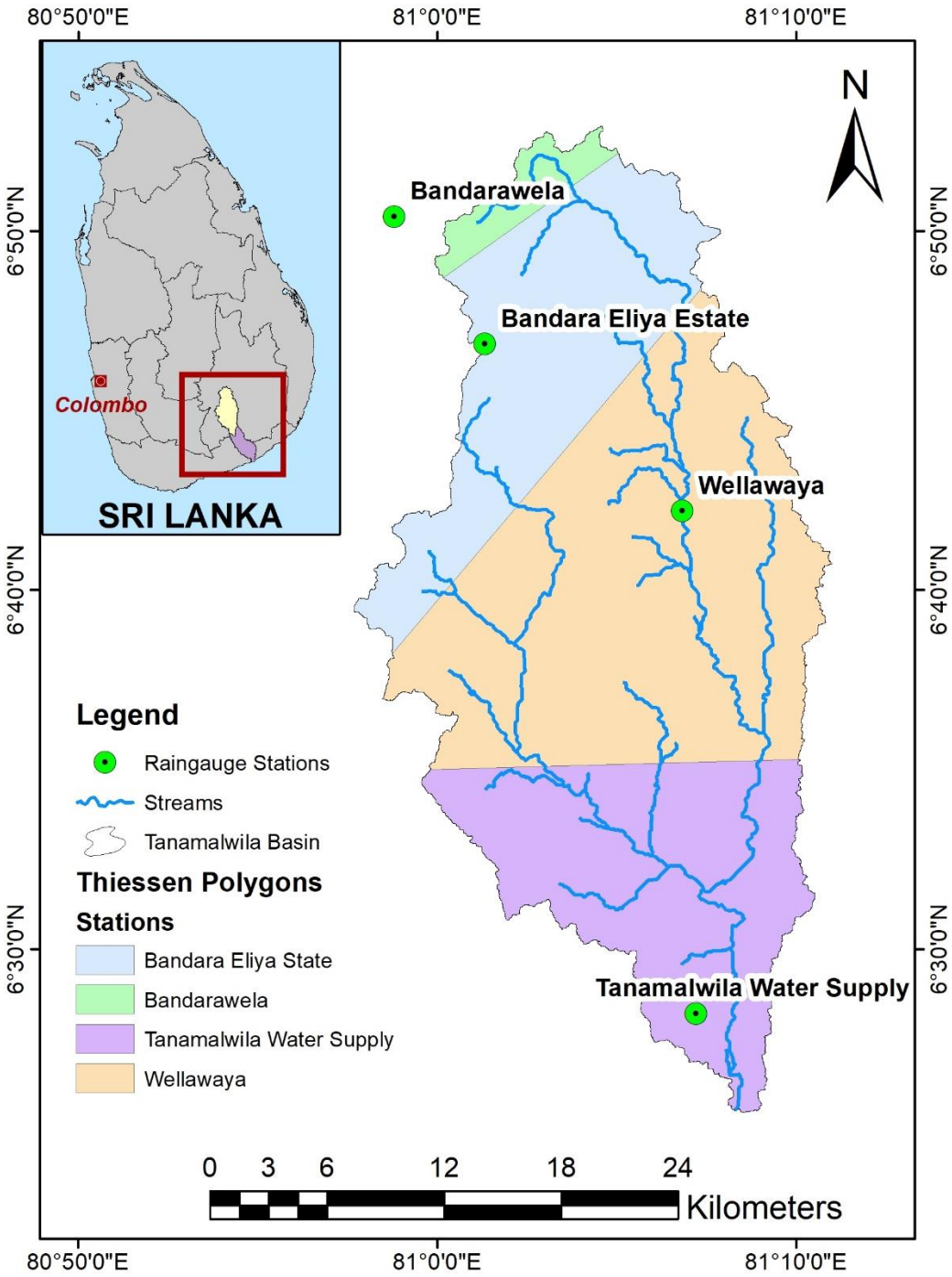

Figure 4-35: Thiessen polygon with weightage of individual stations

Thiessen polygon is drawn using ArcGIS 10.5 (ESRI, 2017) and the weightage for all stations is obtained as shown in Figure 4-35. Different values of weightage obtained for the rain gauge stations are mentioned in Table 4-5. The highest weightage is obtained for the Wellawaya station and the lowest weightage is obtained for the

Bandarawela station. Sub-basin wise Thiessen weightage is also calculated to provide input rainfall to the model.

Table 4-5: Thiessen weightage of rain gauge station in Kirindi Oya

Station Name	Longitude (° E)	Latitude (° N)	Area (km^2)	Weightage
Bandara Eliya Estate	81.0220	6.7808	167.15	0.23
Bandarawela	80.9800	6.8400	21.69	0.03
Wellawaya	81.1137	6.7033	336.00	0.47
Tanamalwila Water Supply	81.1200	6.4700	191.64	0.27
Total			**716.48**	**1.00**

4.1.6 Identification of Events

As discussed in Sections 2.6 and 3.4 earlier, a minimum event depth of 1 mm was adopted and events were separated for the whole study period considering Thiessen averaged rainfall and daily streamflow data at Tanamalwila station. A dry period in days before the occurrence of any event was noted along with the total wet period of the events, peak discharge during the event, cumulative rainfall of the event, and maximum 2-day accumulated rainfall. Then, MIT was calculated using Equation [2-1] and was obtained to be 1 day (24 hrs). Using the MIT value, now 3 different criteria are taken into consideration for the identification of events i.e. 1-day maximum rainfall, 2-day maximum rainfall, and return period discharge.

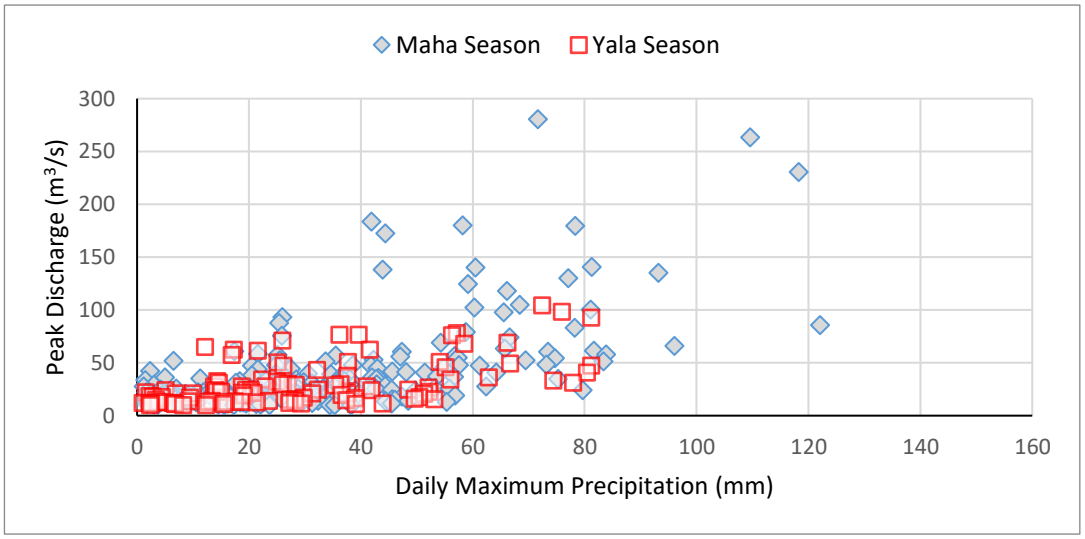

Figure 4-36: Daily maximum precipitation during events along with the event's peak discharge

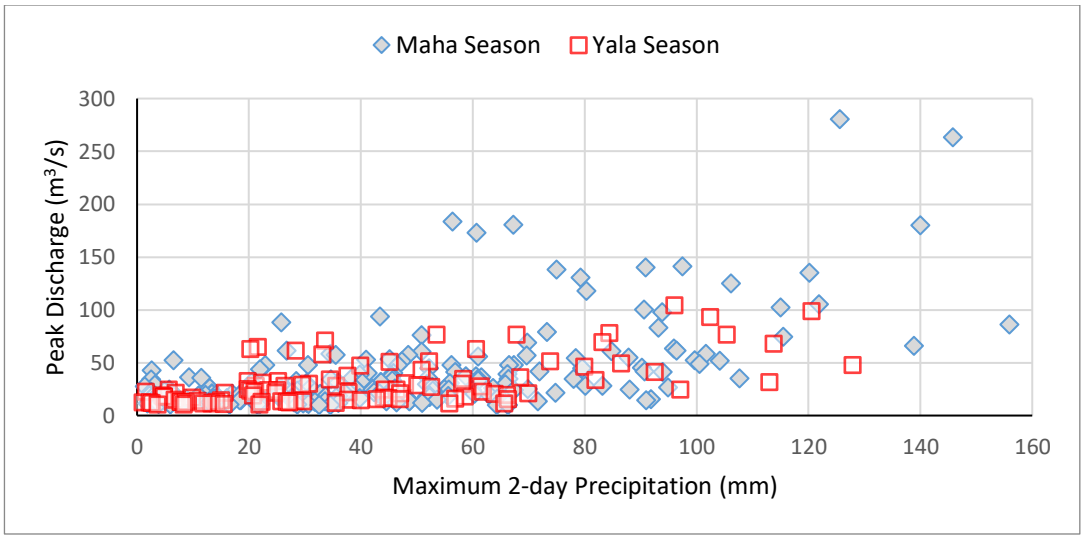

Figure 4-37: Maximum 2-day precipitation during events along with the event's peak discharge

Total 585 events were identified throughout the study period of 2002 to 2020. It can be well observed from Figure 4-36 and Figure 4-37 that the event peak rainfall is not solely responsible for producing peak discharge and the lower magnitude rainfall seems to produce high discharges in many cases. In the case of 2-day maximum rainfall, it can be observed that most of the peak discharge is associated with the 2-day peak rainfall. The events required for the modeling purpose are obtained capturing the

attributes of event peak discharge with the associated rainfall as presented in Figure 4-38.

The primary selection of events was carried out using three criteria.

a) Maximum daily rainfall in each identified event is divided into 10 percentile ranges (10^{th}, 20^{th}, 30^{th}, 40^{th}, 50^{th}, 60^{th}, 70^{th}, 80^{th}, 90^{th}, 100^{th}) and events selected according to those values obtained.
b) Maximum 2 days rainfall in each event divided into four quartiles and Maha and Yala events selected for each value obtained.
c) Maha and Yala events for 1, 2, 5, 10, 15, 25-year return period discharges

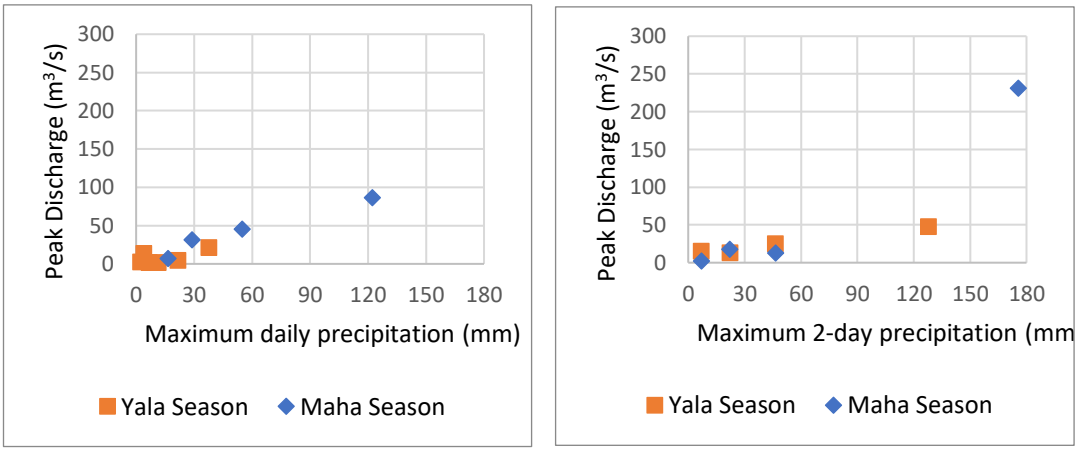

a) b)

Figure 4-38: Identified events a) considering percentile ranges of maximum daily rainfall, b) considering four quartile ranges of maximum 2-days rainfall

While considering 10 percentile ranges of maximum daily rainfall as mentioned in the first criteria above, 10 events are selected where most of the events are concentrated on lower discharge ranges as shown in Figure 4-38. Except for one (1) event, all of the events lie below the discharge of 50 m^3/s and daily maximum precipitation below 60 mm. Similarly, considering four (4) quartile ranges of maximum 2-days rainfall, 8 events are selected. These selected events also fall on the lower discharge range and lower precipitation range except for two (2) selected events as shown in Figure 4-38. Further, there is a substantial gap between extreme high flow events and low flow events considered in both of the cases.

The events for modeling were selected considering different year return period discharge. Return period discharge was calculated using Gumbel distribution and the 100 year return period discharge was obtained to be 338.69 m^3/s. Return period discharge for different durations calculated using Gumbel distribution are as shown in Figure 4-39. The computed return period discharge value follows the Gumbel distribution as shown in Figure 4-39.

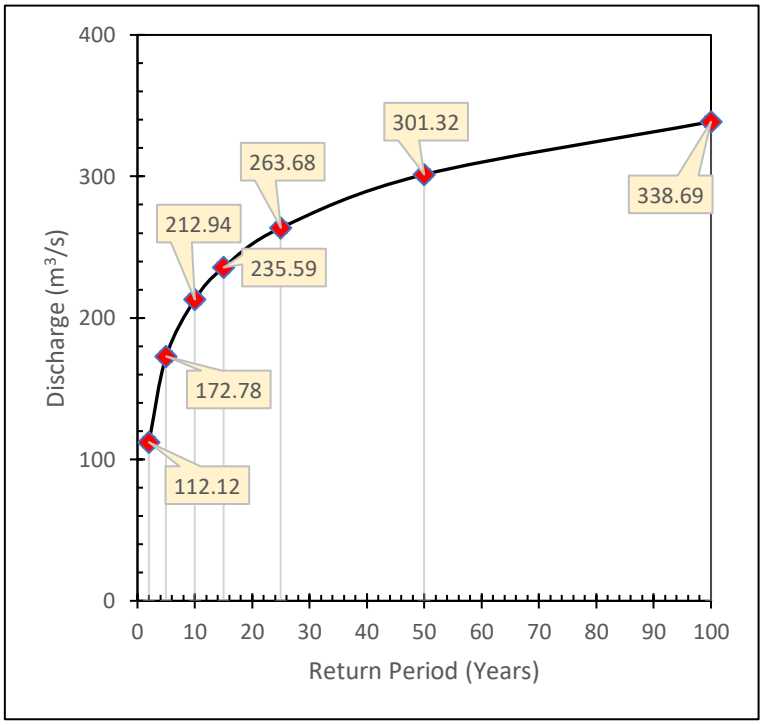

Return period (Years)	Discharge (m^3/s)
1	25.06
2	112.12
5	172.78
10	212.94
15	235.59
25	263.68
50	301.32
100	338.69

Figure 4-39: Different return period discharge in Tanamalwila basin

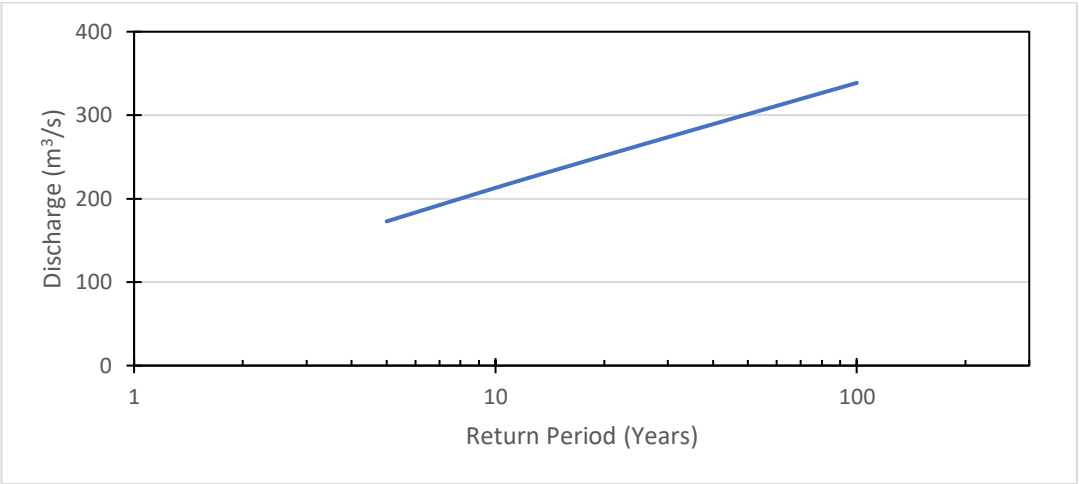

Figure 4-40: A straight line indicating a well-fitted curve in Gumbel distribution

The Gumbel distribution employed produces a curve when discharge is plotted against different return periods (normal scale) as shown in Figure 4-39. A check needs to be done whether the curve fits perfectly or not before applying the method in the study. For this, the curve is plotted such that the x-axis is adjusted in the log scale and the resultant curve obtained should follow a straight line. The Gumbel distribution curve obtained for the discharge data obtained from the Tanamalwila station generates a straight line which indicates that the curve is well fitted as shown in Figure 4-40.

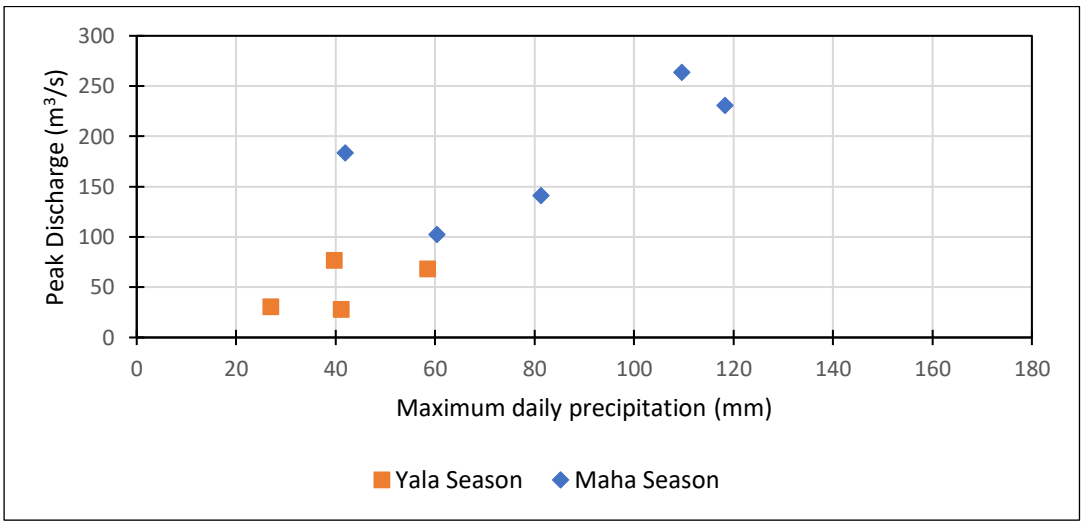

Figure 4-41: Identified events considering different return period discharge

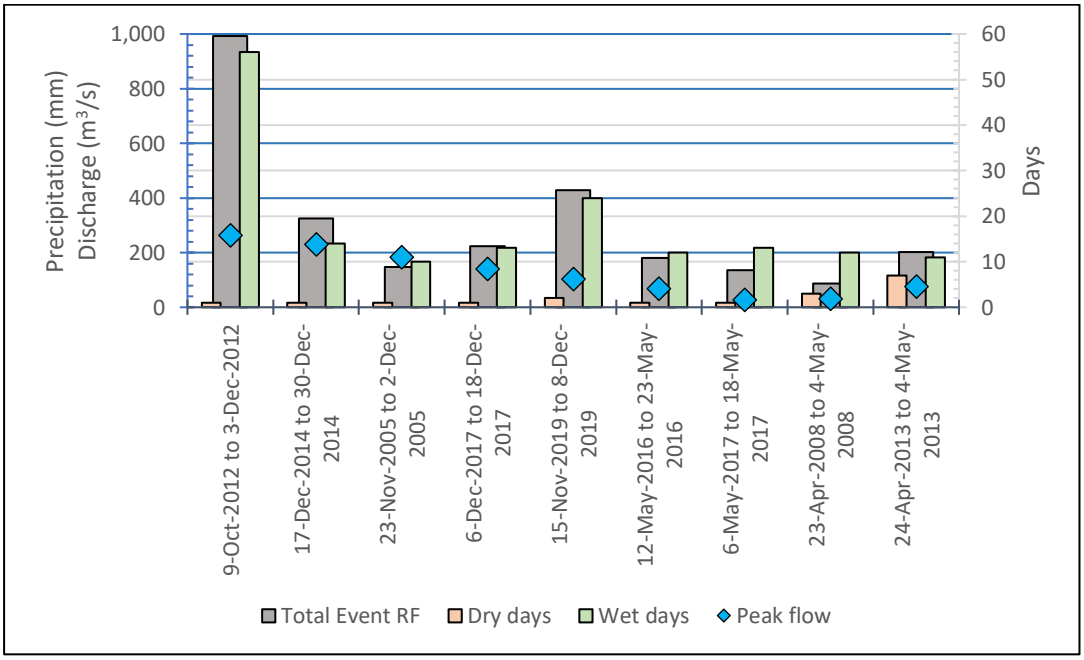

Figure 4-42: Events selected for the study

Events were selected considering 1, 2, 5, 10, 15, and 25-year return period discharge with Maha and Yala events identified for the modeling purpose. Total nine (9) events were selected with the discharge distributed in all ranges from high to low flow values. The distribution of flow and rainfall in events can be seen in Figure 4-41. The peak flow of the events ranges from 27 m^3/s to 263 m^3/s with all discharge values distributed in between this range and the peak daily rainfall during these events ranges from 20 mm to 120 mm.

The detailed information regarding events identified (such as dry period before the start of the event, total event RF, total event days, maximum RF, maximum 2-day RF, return period discharge, and so on) can be obtained from Table A - 6 attached in Annexure 3 of this document. The maximum total event rainfall identified was 991.80 mm with a wet period of 56 days whereas the minimum total event rainfall identified was 87.22 mm with a wet period of 12 days. The selected events which will be used for the event modeling purpose with their details are represented in Figure 4-43.

Table 4-6: Events of various return period discharge selected for calibration and validation in Kirindi Oya

ID	Dry days	Total Event RF (mm)	Wet days	Max RF (mm)	Peak flow (m^3/s)	Return Period (years)
1	1	991.8	56	109.58	263.41	25
2	1	324.3	14	118.29	230.95	15
3	1	148	10	41.89	183.79	5
4	1	223.6	13	81.25	141.05	5
5	2	428.8	24	60.34	102.49	2
6	1	180.3	12	58.56	67.81	1
7	1	136.1	13	41.1	27.51	1
8	3	87.22	12	26.98	30.36	1
9	7	201.2	11	39.7	76.34	1

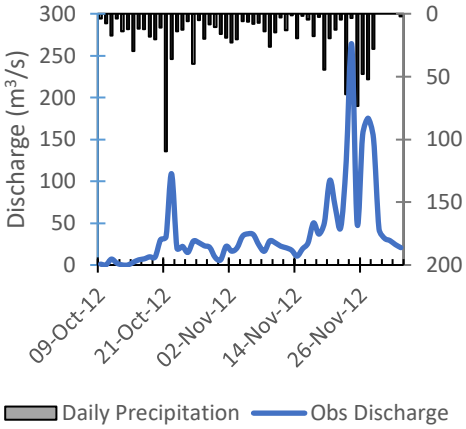

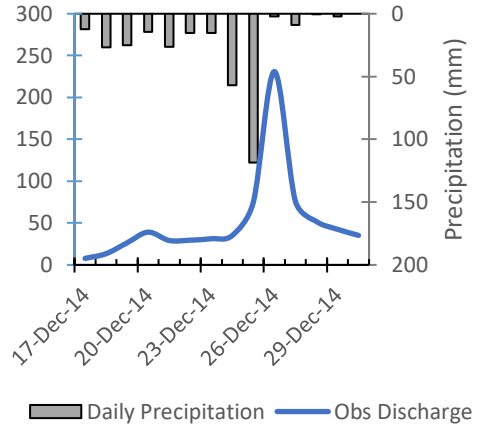

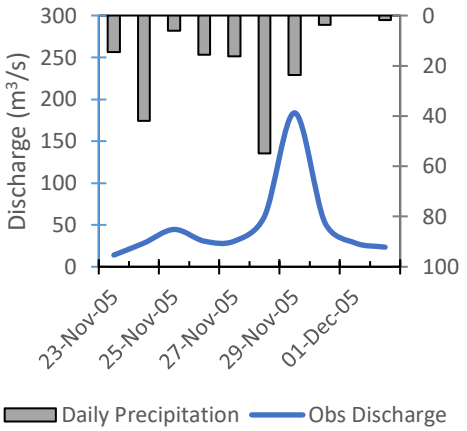

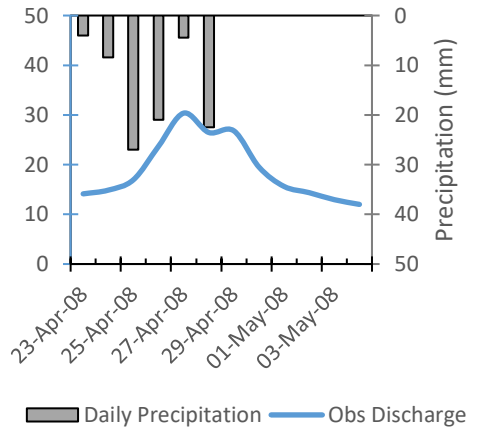

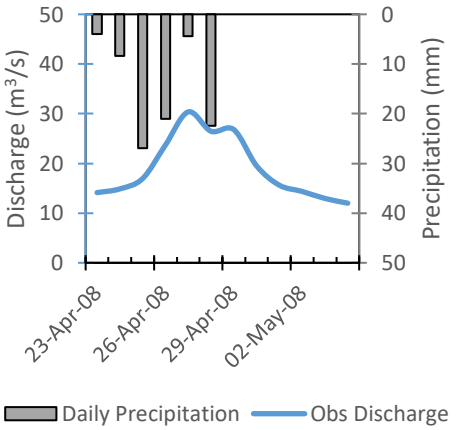

ID	Event Code
1	1D-56W-Oct/Dec12
2	1D-14W-Dec14
3	1D-10W-Nov/Dec05
8	3D-12W-Apr/May08
9	7D-11W-Apr/May13

Figure 4-43: Events selected for the calibration in Kirindi Oya basin

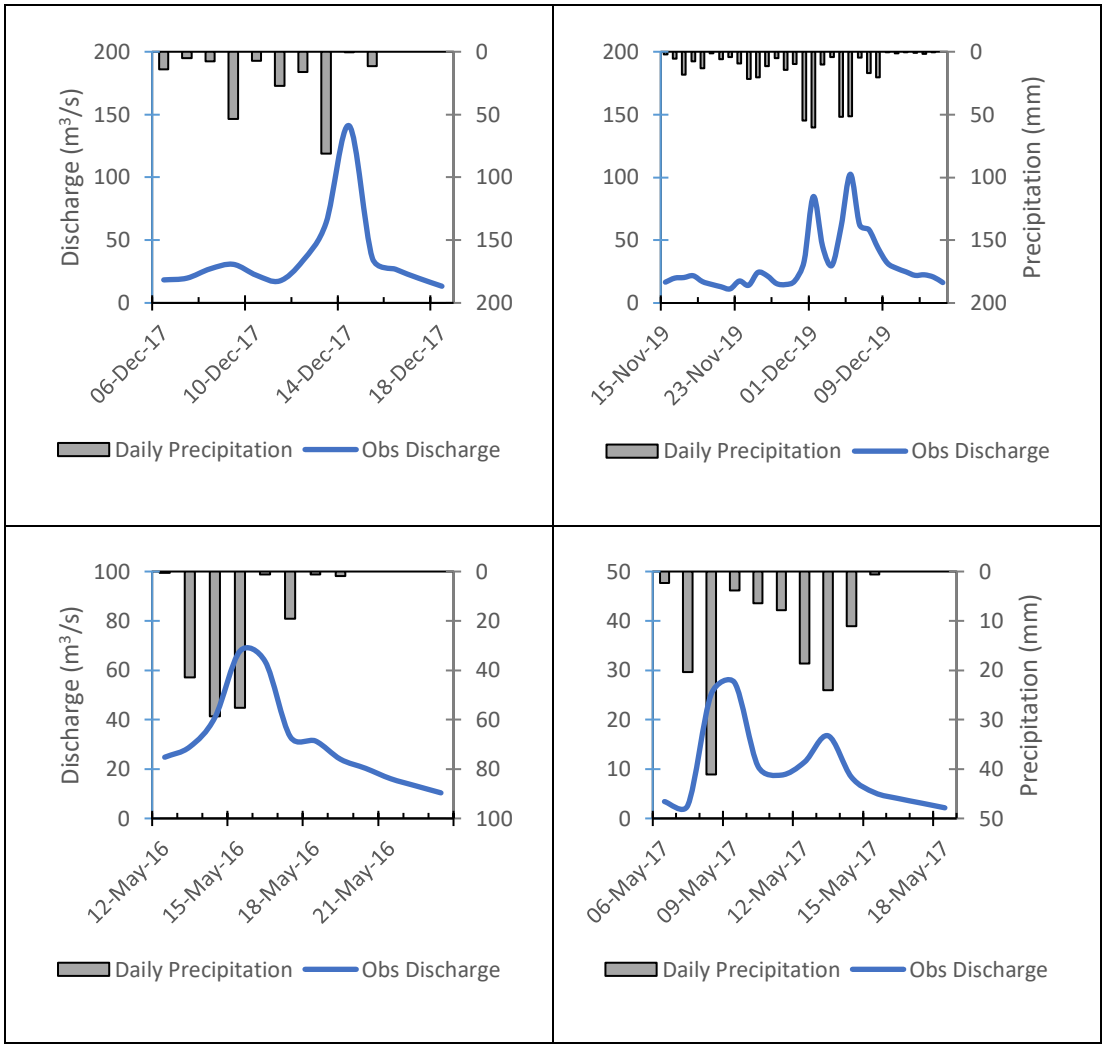

Figure 4-44: Events selected for the validation in Kirindi Oya

The events selected are of different magnitude in terms of discharge which is presented in Table 4-6. The peak discharge for a specific return period considering the 99 % confidence band is taken into account for the selection of events. The discharge considered for the selection of events are ranging from 1-year return period discharge to 25-year return period discharge.

4.1.7 Initial Soil Moisture for Validation of Events

The SMAP level 4 soil moisture data consists of many soil-related data sets that can be used in the modeling process. The raw data file with 3-hour time intervals and resolution of around 9 km was extracted using MATLAB software with the coordinates of the basin. Among various soil data available, root zone soil moisture

(0-100 cm) was extracted. The data extracted from different points were averaged throughout the basin to analyze and compare with the rainfall and streamflow data. The 3-hourly data was averaged to daily volumetric SM since the least period of data available was daily rainfall and streamflow.

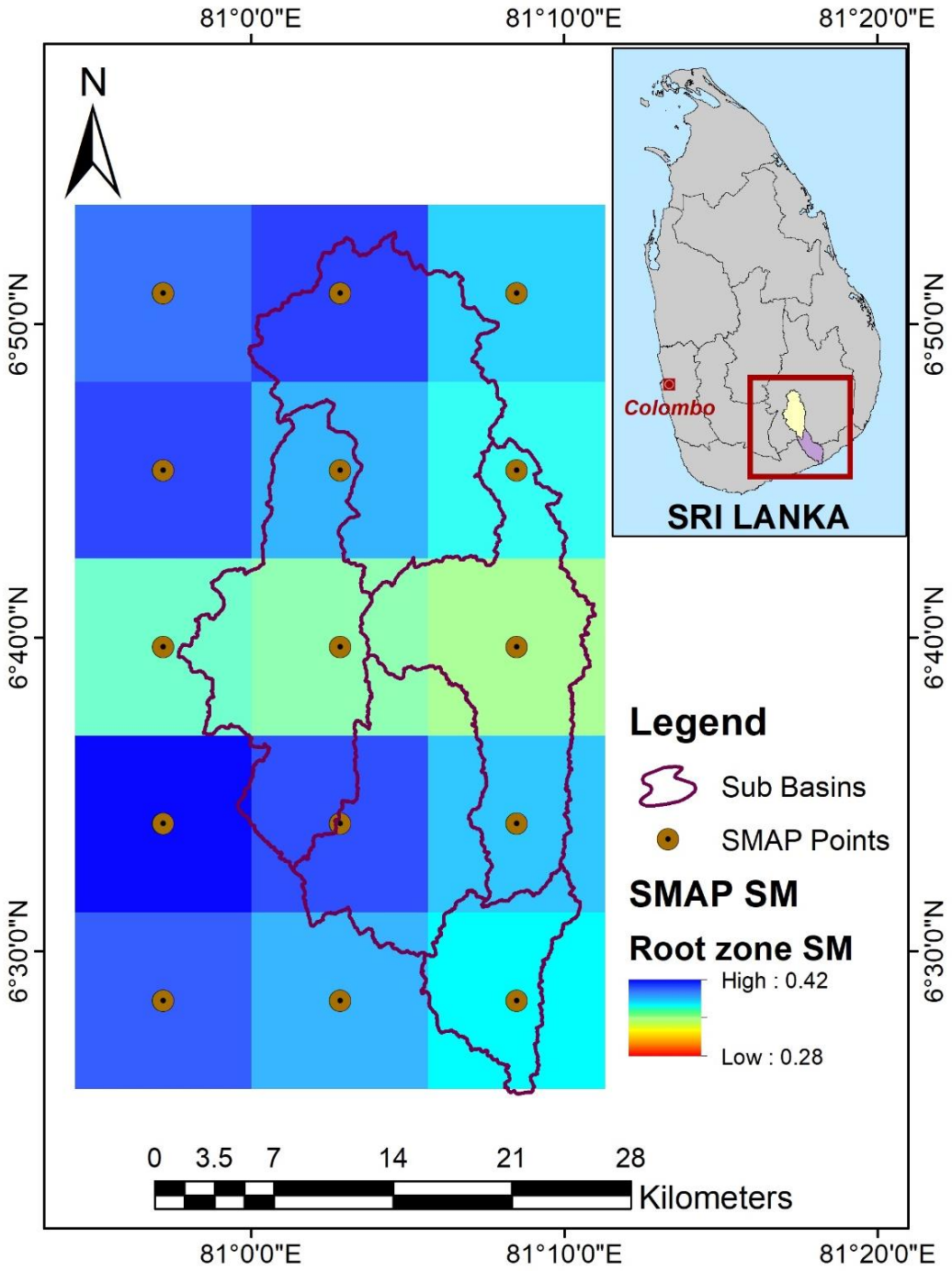

Figure 4-45: SMAP soil moisture grids and points in the study area over the sub-basin

For the input in the model, SSM data requires to be extracted using ArcGIS 10.5 (ESRI, 2017). First of all, the gridded data is converted to point data and then joined with each sub-basins in the Kirindi basin. Then, the dissolve operation is performed by averaging the soil moisture from each grid to obtain a final sub-basin-wise soil moisture value.

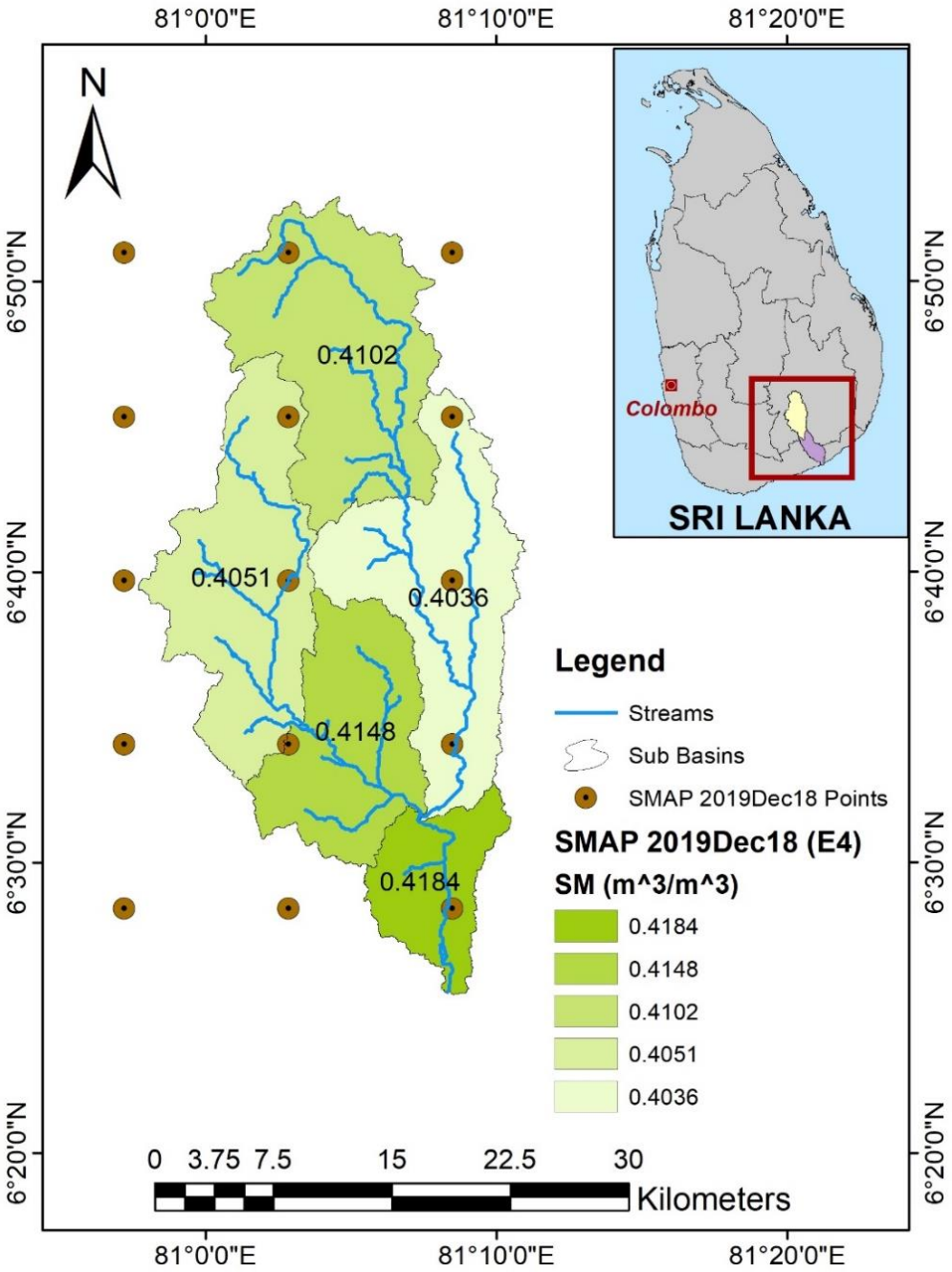

Figure 4-46: Sub-basin wise root zone SM dated 2019 Dec 18

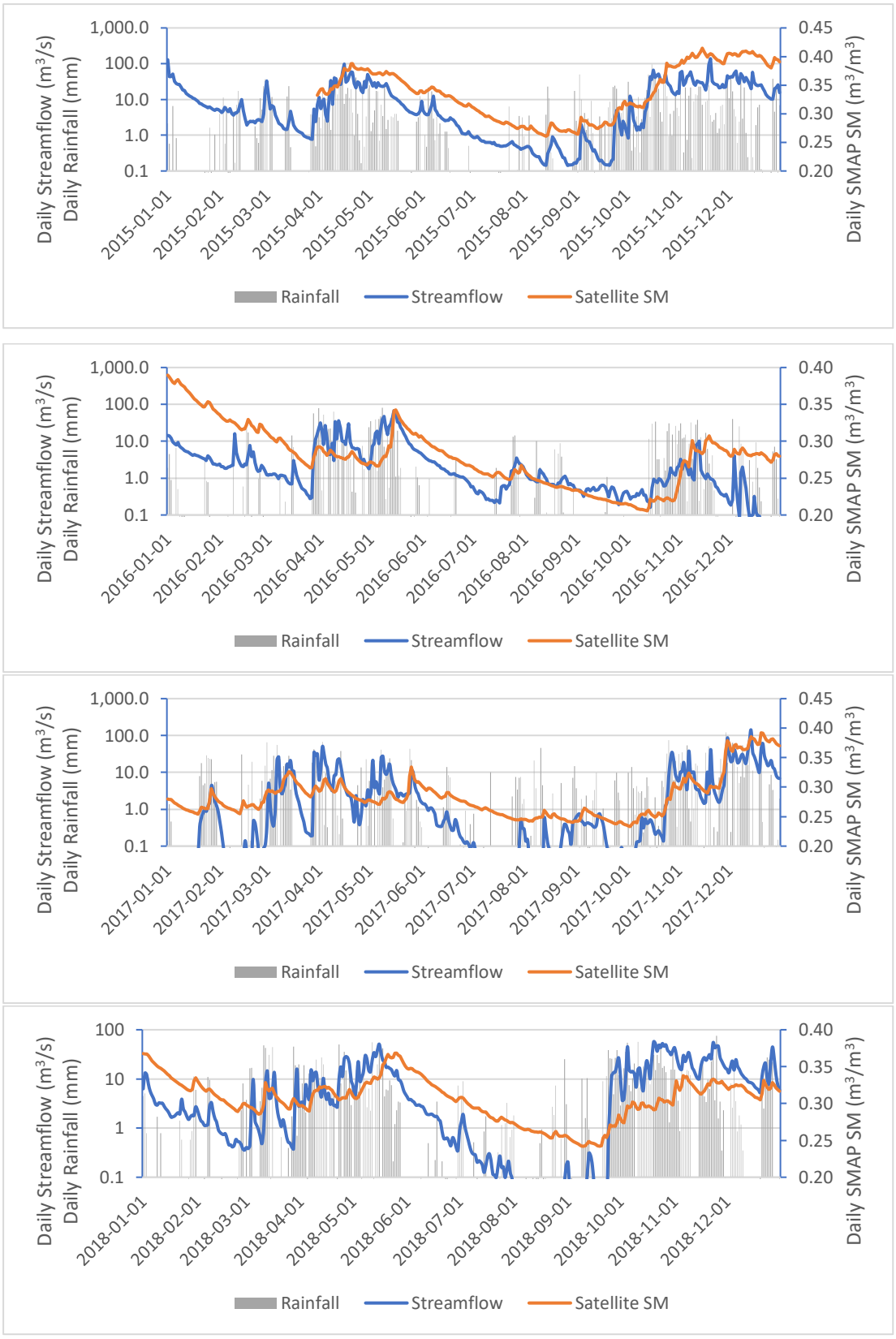

Figure 4-47: Daily root zone soil moisture (m^3/m^3) along with daily rainfall and streamflow from 2015 to 2018 in Kirindi Oya Basin

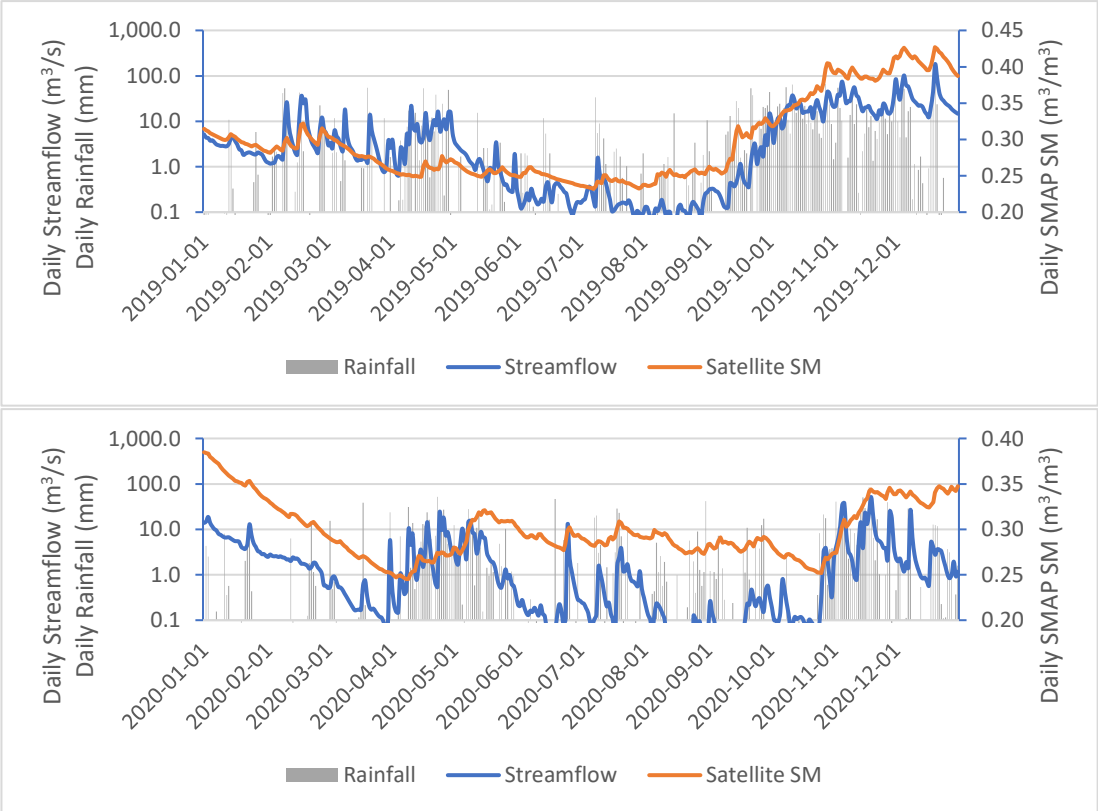

Figure 4-48: Daily root zone soil moisture (m^3/m^3) along with daily rainfall and streamflow from 2019 to 2020 in Kirindi Oya Basin

A representative sample of volumetric soil moisture in every sub-basin is as shown in Figure 4-46. Thus obtained SM values are compared with the daily streamflow and daily rainfall to observe the response of soil to the rainfall/streamflow in yearly order as shown in Figure 4-47. In most cases, the soil moisture has responded to the rainfall. Even though the values do not match in the order of magnitude, they seem to follow a similar trend, mostly following the rainfall trends.

The satellite soil moisture extractions are used in SMA to validate the results of the model and analyze the enhancement in the simulation capacity. HEC-HMS does not allow the user to input soil moisture directly into the model. Thus, the volumetric soil moisture extracted should be converted to the initial soil saturation percentage. This conversion is carried out referring to Bhuiyan et al. (2017) where the ratio of volumetric soil moisture to the soil porosity is related to the soil saturation level. Thus obtained saturation is converted to percentage saturation to provide input to the model;

$$S = \frac{\theta}{\Phi} * 100 \quad [4\text{-}1]$$

where, S = soil saturation percentage, θ is the volumetric soil moisture and Φ is the porosity of the soil. The sub-basin soil moisture storage as shown in Table 4-7 is now used with sub-basin porosity to calculate the initial soil moisture percentage which is expected to enhance the performance of the model.

Table 4-7: Initial soil moisture condition before the start of the event derived from SSM

Event	Event code	Initial Soil Moisture (%) in Sub Basin					Average
		1	2	3	4	5	
4	1D-13W-Dec17	89%	81%	85%	87%	82%	**84%**
5	2D-31W-Nov/Dec19	86%	84%	86%	93%	92%	**88%**
6	1D-12W-May16	72%	62%	72%	75%	70%	**70%**
7	1D-13W-May17	68%	57%	62%	71%	67%	**65%**

4.2 Kalu Ganga River Basin

4.2.1 Data

4.2.1.1 Data Sources and Resolution

Data required for this basin are similar to the data collected for the Kirindi Oya basin and most of the data can be used for this basin too. Only precipitation, streamflow, and evaporation data need to be collected specifically for the Kalu Ganga. The details regarding the above-mentioned data and their source are listed in Table 4-1.

4.2.1.2 Hydrometeorological Data

Rainfall data of various rain gauge stations (Halwatura, Galatura, Ratnapura, and Depedena) were collected from the Meteorological Department and Streamflow data of Ellagawa Station was obtained from the Irrigation Department. Different data collected for various stations and periods of data obtained are mentioned in Table 4-8.

Table 4-8: Data collected for the analysis for Kalu Ganga

Name of the Station	Latitude (° N)	Longitude (° E)	Period of Record	
			From	To
Streamflow				
Ellagawa	6.73° N	80.22° E	Jan-1995	Dec-2020
Rainfall				
Halwatura	6.72° N	80.20° E	Jan-2002	Dec-2020
Galatura	6.70° N	80.28° E	Jan-2002	Dec-2020
Rathanpura	6.68° N	80.40° E	Jan-2002	Dec-2020
Depedena	6.47° N	80.55° E	Jan-2002	Dec-2020

4.2.1.3 Other Data

Root zone (0-100 cm) SM data (m^3/m^3) obtained from the Earthdata portal as mentioned in Section 4.1.1.3 is used for this basin by using the coordinates of the Kalu Ganga basin for the extraction of the data. Soil Map for the study area was collected from the survey department of Sri Lanka as mentioned in Section 4.1.1.3 is also used for this basin by clipping the area with the basin boundary.

As shown in Figure 4-49, various types of red-yellow podzolic soils were dominantly found in the study area followed by the presence of various lithosols and bog and half-dog soil. The distribution of various soil types in the basin is represented in a pie-chart shown in Figure 4-50.

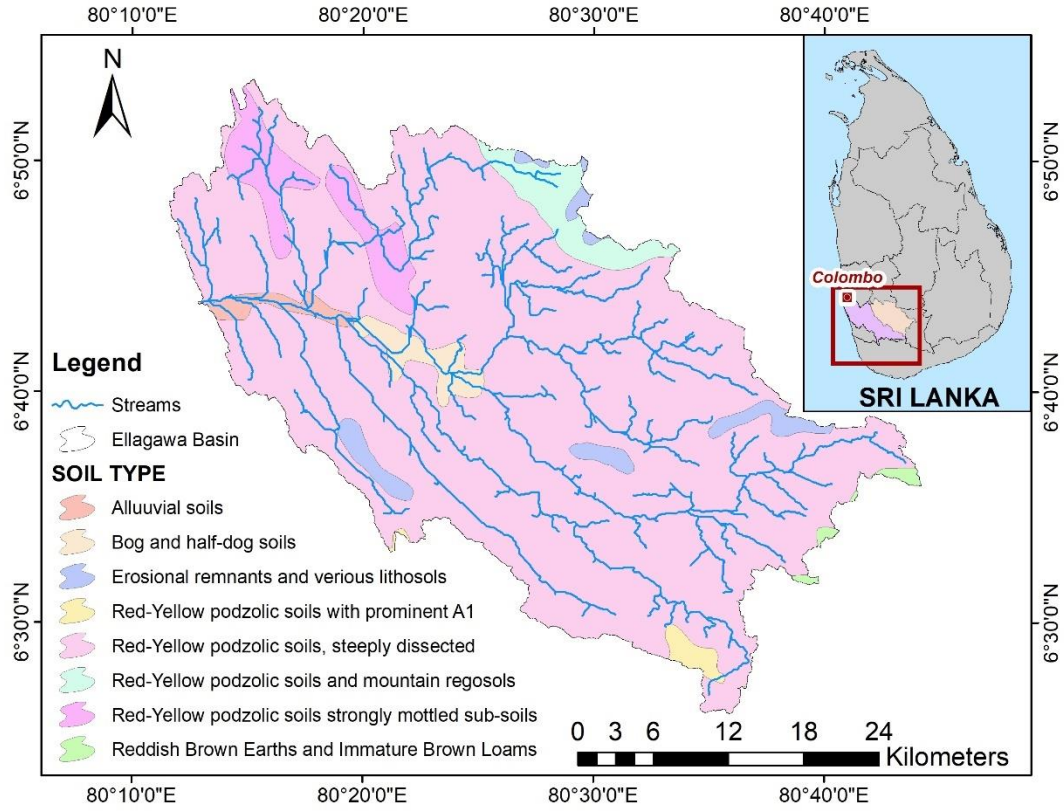

Figure 4-49: Soil map of Ellagawa basin

The land use map obtained from ESRI as mentioned in Section 4.1.1.3 is used for this basin too. The maximum part of the area is covered by trees/forests followed by built area and crop cultivations as shown in Figure 4-51. All associated land-use with the area coverage and percentage coverage of the area is as shown in Figure 4-52 below.

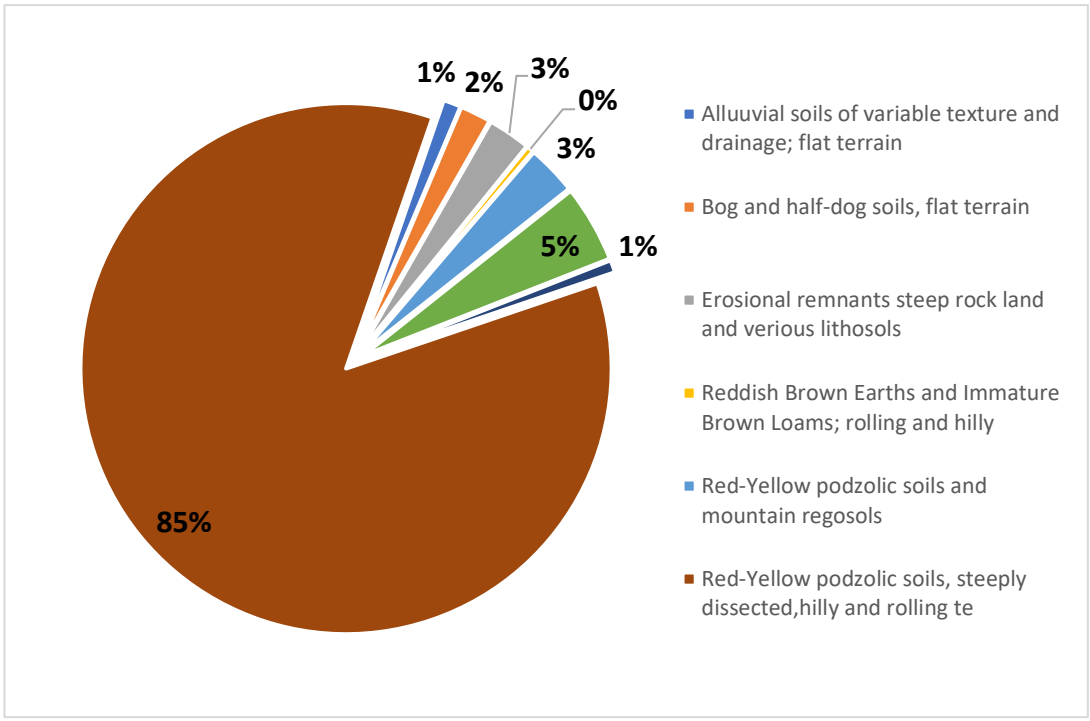

Figure 4-50: Distribution of various soil types in Ellagawa basin

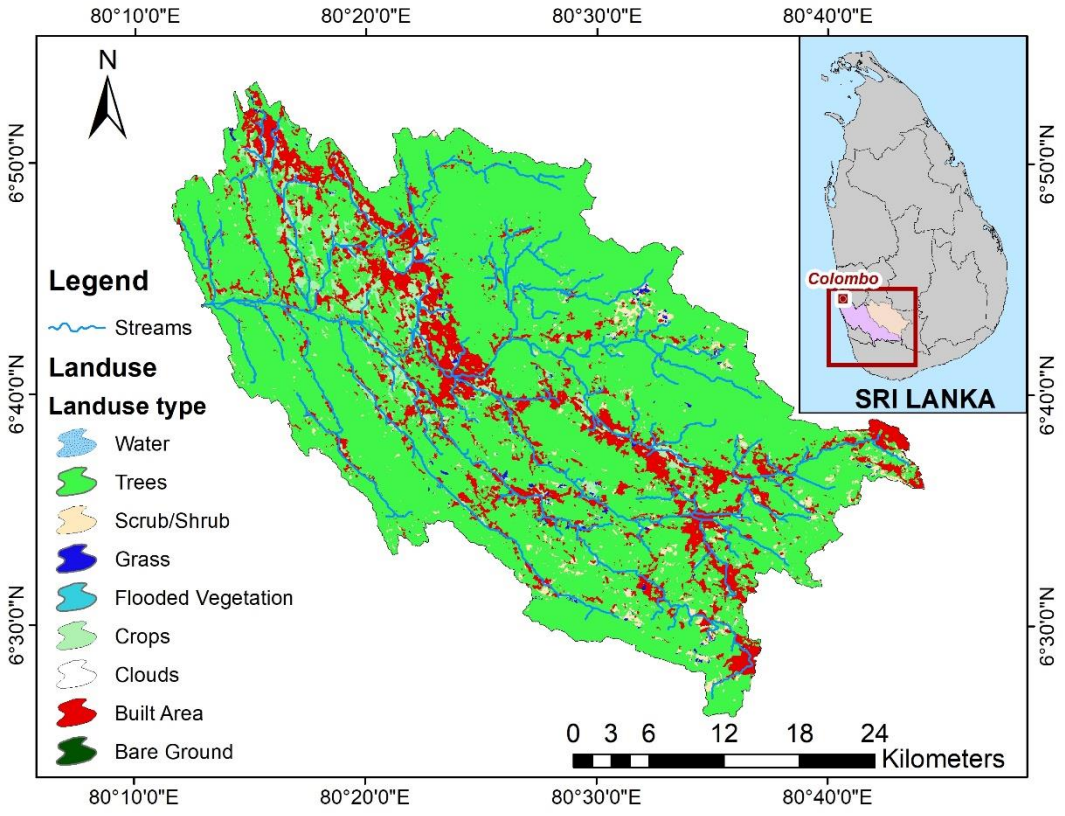

Figure 4-51: Landuse map of Ellagawa basin indicating various landuse types

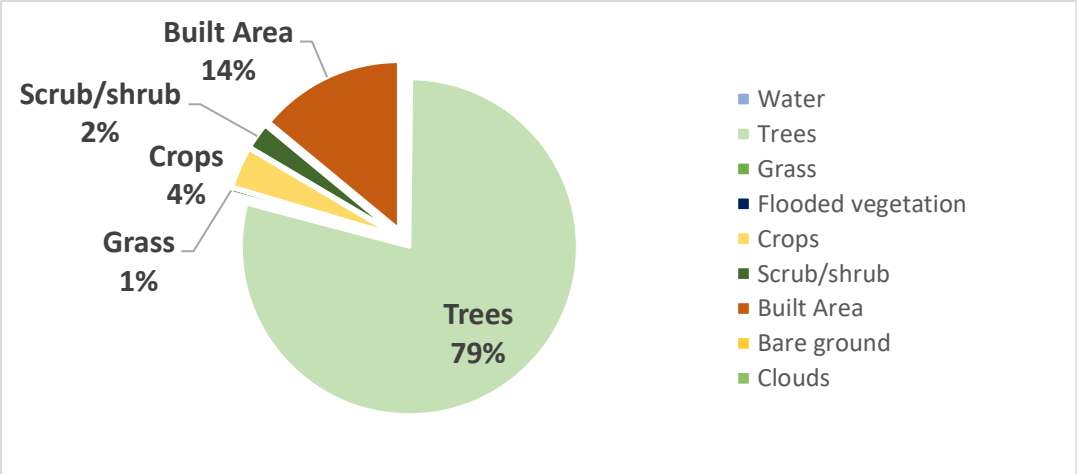

Figure 4-52: Pie chart showing the distribution of land use in the Ellagawa basin

Table 4-9: Different land-use in the study area with their area and percentage coverage

Land-use type	Area (km^2)	Percentage (%)
Bare ground	0.01	0.00%
Built area	100.19	13.99%
Clouds	0.00	0.00%
Crops	134.13	18.73%
Flooded vegetation	0.87	0.12%
Grass	3.60	0.50%
Roads	1.65	0.23%
Scrub/shrub	121.89	17.02%
Trees	345.13	48.19%
Water	8.77	1.22%
Total	**716.23**	**100.00%**

4.2.2 Data Checking

Data checking was carried out similarly to the process described in Section 4.1.2. Further, the additional description is followed in the sub-sections below.

4.2.2.1 Visual Data Checking

Daily Analysis

Rainfall data arranged chronologically is observed to check for missing data. The use of conditional formatting is explored to observe the trends of data on a monthly and annual scale. The precipitation data was also visually compared with the streamflow data using data bars to analyze the response of a catchment to the rainfall.

Graphically the missing data were identified when plotted in a daily time series scale as shown in Figure 4-53. When plotted on an annual scale, the trend of the data can be observed by adding the trendline in the chart. Missing data can also be observed when a cumulative plot shows a long straight line deviating from the trendline.

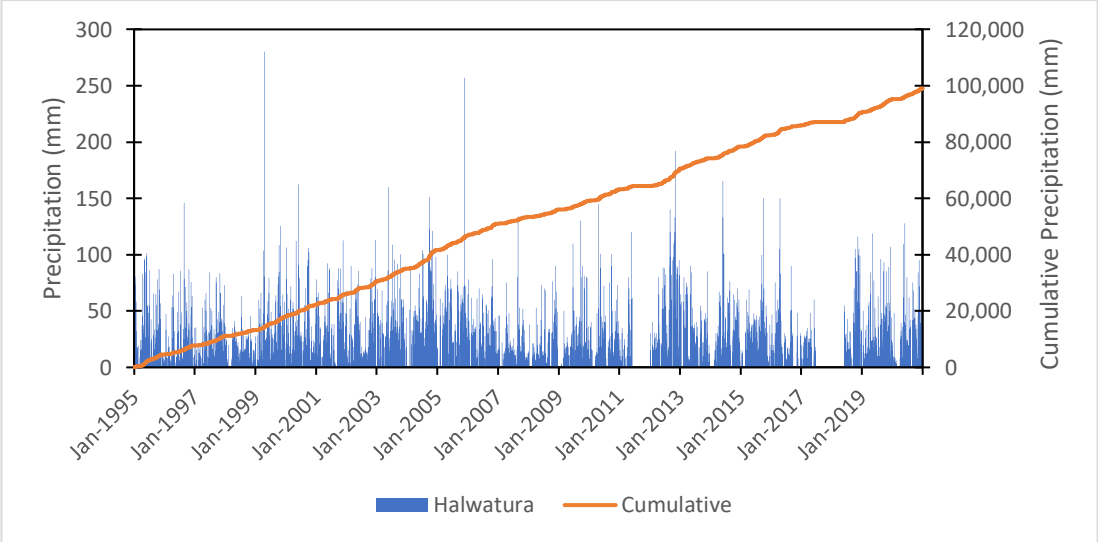

Figure 4-53: Daily precipitation and cumulative precipitation plot of Halwatura Station

Further, all station data is plotted in a single graph as a time series to see the correlation of stations with each other and the trends they are following throughout the study period as shown in Figure 4-55. This is also called the single mass curve analysis and is useful in identifying the inconsistencies in the data set over a long period as the break in the cumulative precipitation would indicate the inconsistencies or missing data (Chow et al., 1988).

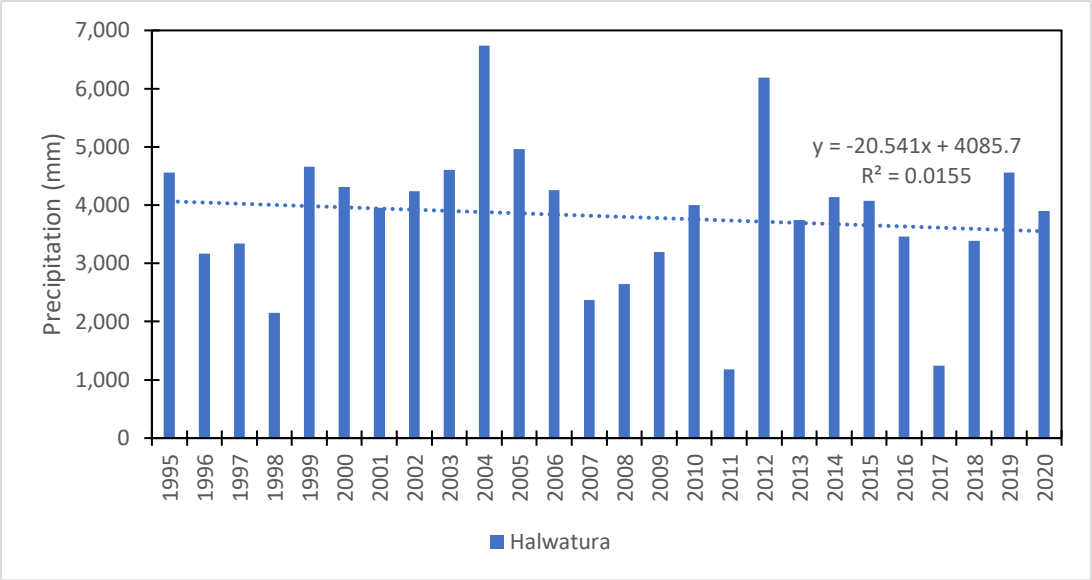

Figure 4-54: Annual precipitation in Halwatura station from 1995 to 2020

A single mass curve as explained in Section 4.1.2.1 is drawn for all the rain gauge stations in Kalu Ganga that present cumulative precipitation in each station over the study period. The Galatura station has the highest accumulated precipitation in the basin whereas the Depedena station has the lowest accumulated precipitation in the basin as presented in Figure 4-55.

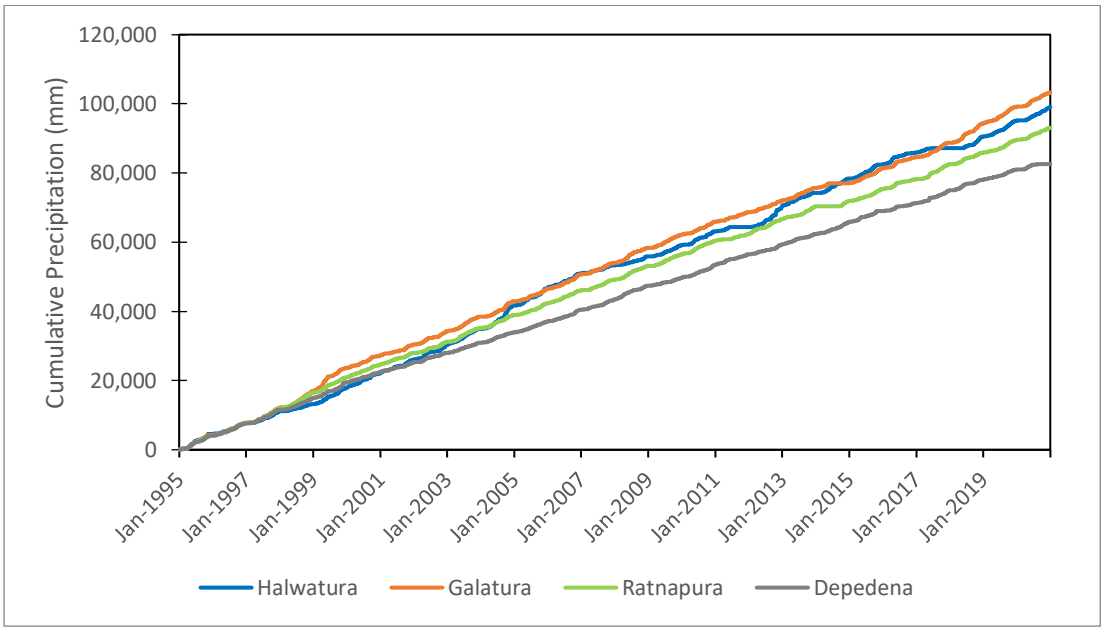

Figure 4-55: Cumulative precipitation in the various stations in the Ellagawa basin

Monthly, Seasonal and Annual Analysis

The missing value was also identified using the conditional formatting tools in excel and then visually analyzing the data sets even in monthly arrangements as explained in Section 4.1.2. A box plot for the Halwatura station is shown in Figure 4-56 which explains that higher precipitation can be observed from September to November and April to June. Further station-wise analysis was carried out to compare all stations as shown in Figure 4-57.

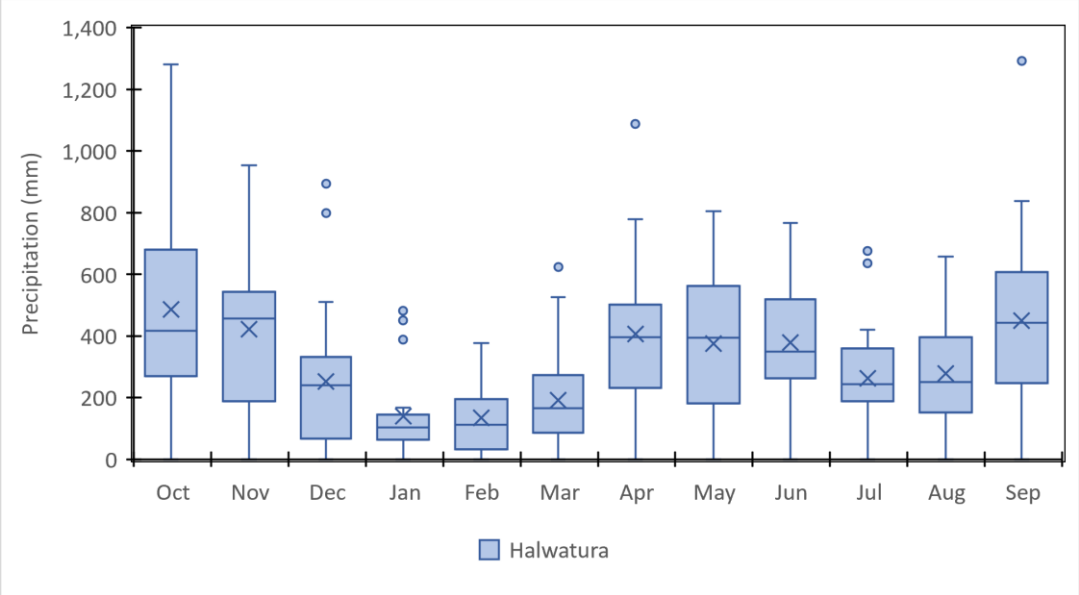

Figure 4-56: Box plot showing the monthly variation of rainfall in Halwatura

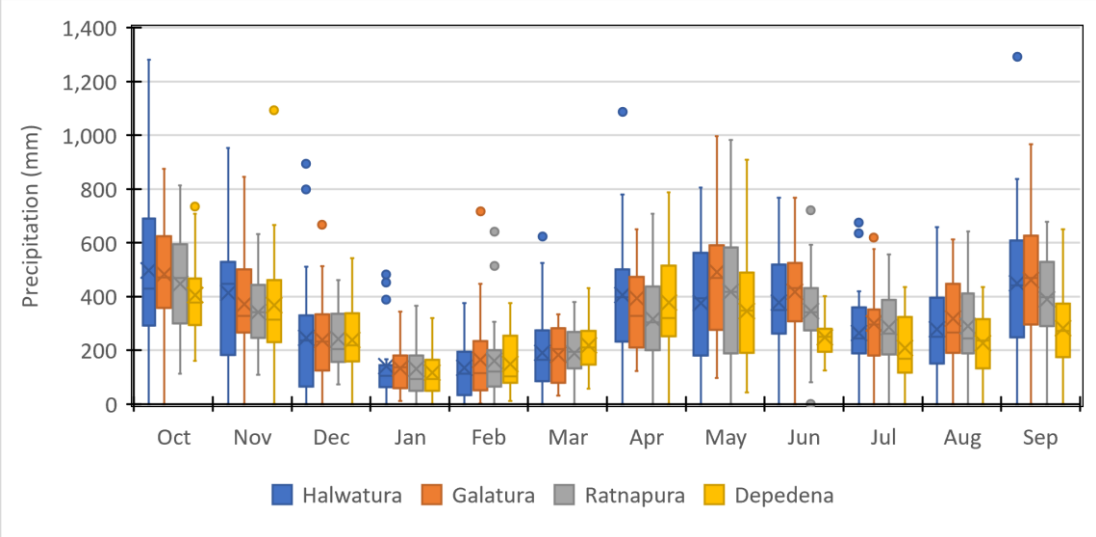

Figure 4-57: Monthly distribution of rainfall in various stations in the Kalu Ganga Basin

The seasonal distribution of rainfall in the Halwatura station is shown in Figure 4-58. From the figure, it can be seen that more rainfall is contributed during the southwest monsoon followed by second inter monsoon rain in the Halwatura station. Further, the missing data can be observed in many years (2017, 2018) where rainfall of a particular season is missing.

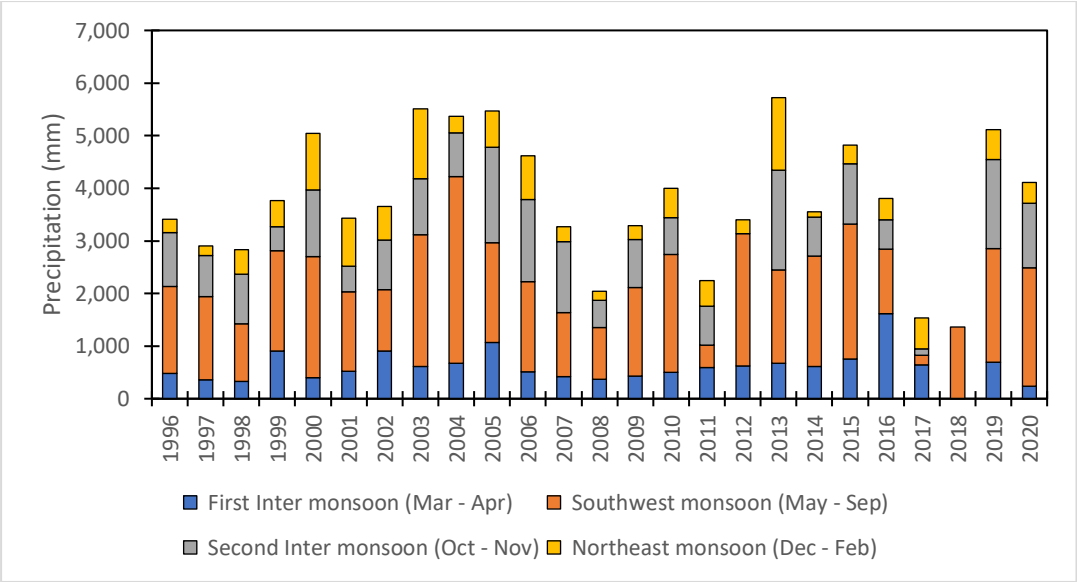

Figure 4-58: Seasonal distribution of rainfall in Halwatura station

The annual rainfall values at Halwatura, Galatura, Ratnapura, and Depedena stations are shown in Figure 4-59.

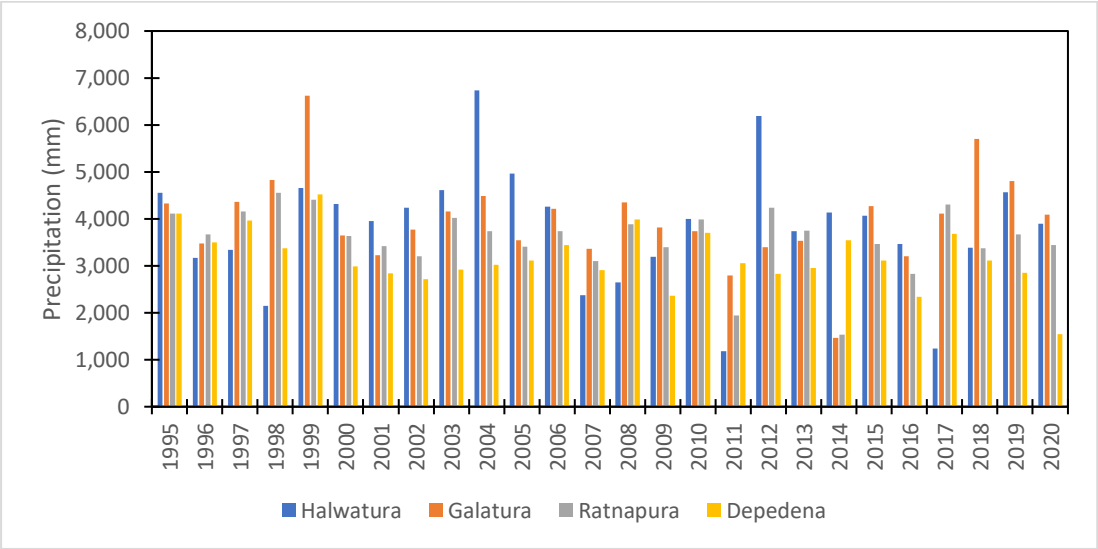

Figure 4-59: Annual rainfall in various stations in Kalu Ganga Basin

Daily streamflow data in cumecs of duration 1995 – 2020 is obtained and analysis is performed using conditional formatting to see general trends in data. A conditional formatting tool is used to analyze the streamflow. Moreover, the time series plot of daily streamflow is presented in Figure 4-60 to observe the trends and extremes during the study period.

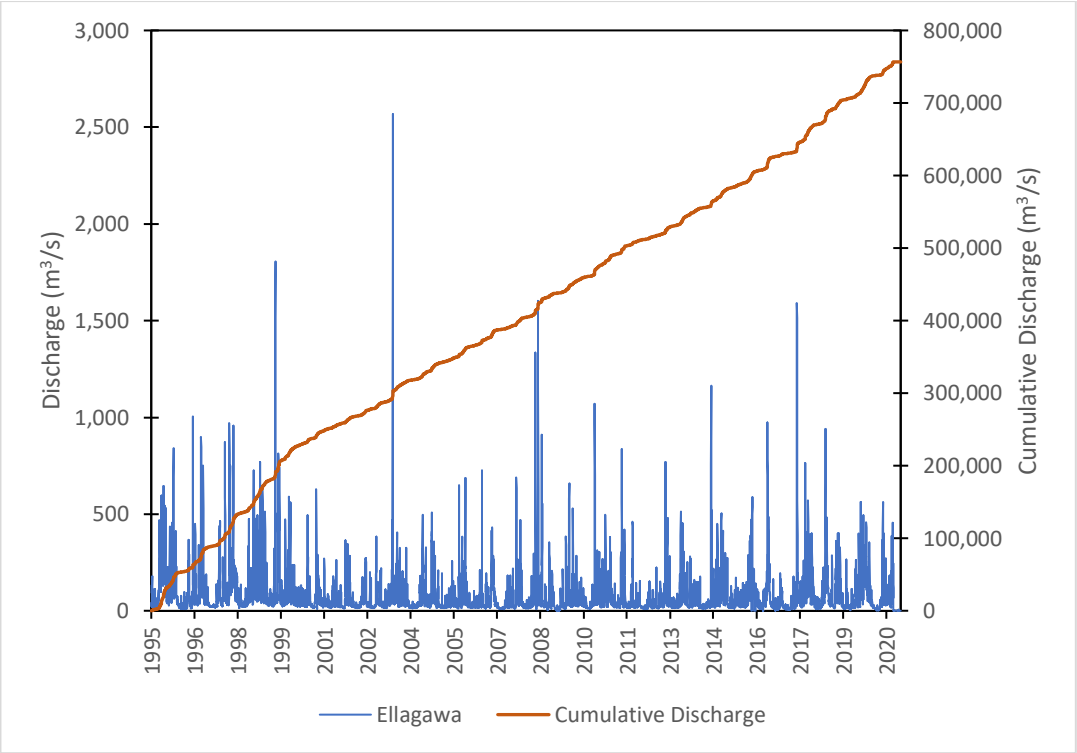

Figure 4-60: Daily discharge at the Ellagawa station during the study period

The seasonal distribution of flow for the study period is shown in Figure 4-61 below. The southwest monsoon period exhibits major discharge in the basin followed by the second intermonsoon period and northeast monsoon period. The first intermonsoon contributes the least to the total streamflow in the basin. The above-mentioned features can be well observed in Figure 4-62.

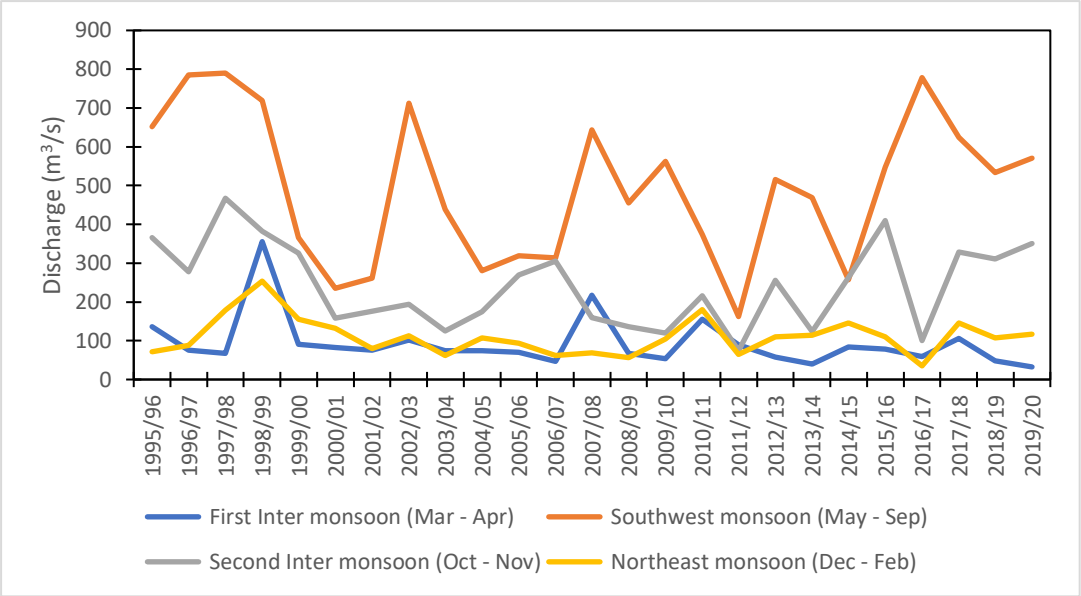

Figure 4-61: Seasonal distribution of streamflow in Ellagawa basin

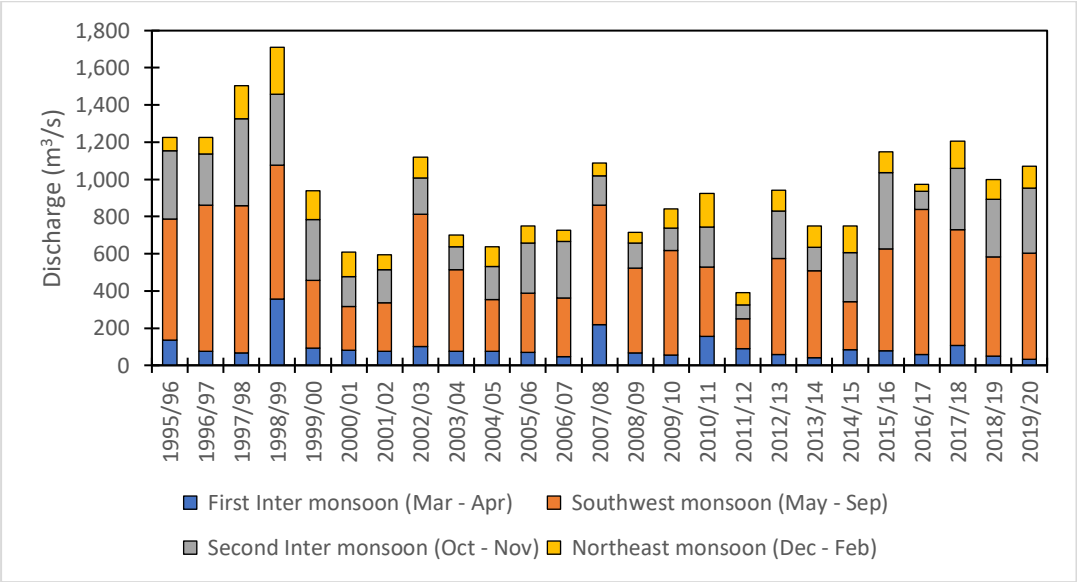

Figure 4-62: Contribution of seasonal flow in a year during the study period in Ellagawa

4.2.2.2 Consistency Test of the Record

The consistency of a rainfall record is tested with double-mass analysis as explained in Section 4.1.2.2. All of the four (4) stations data showed consistent results and the double mass curve of the Ratnapura station is as presented in Figure 4-63.

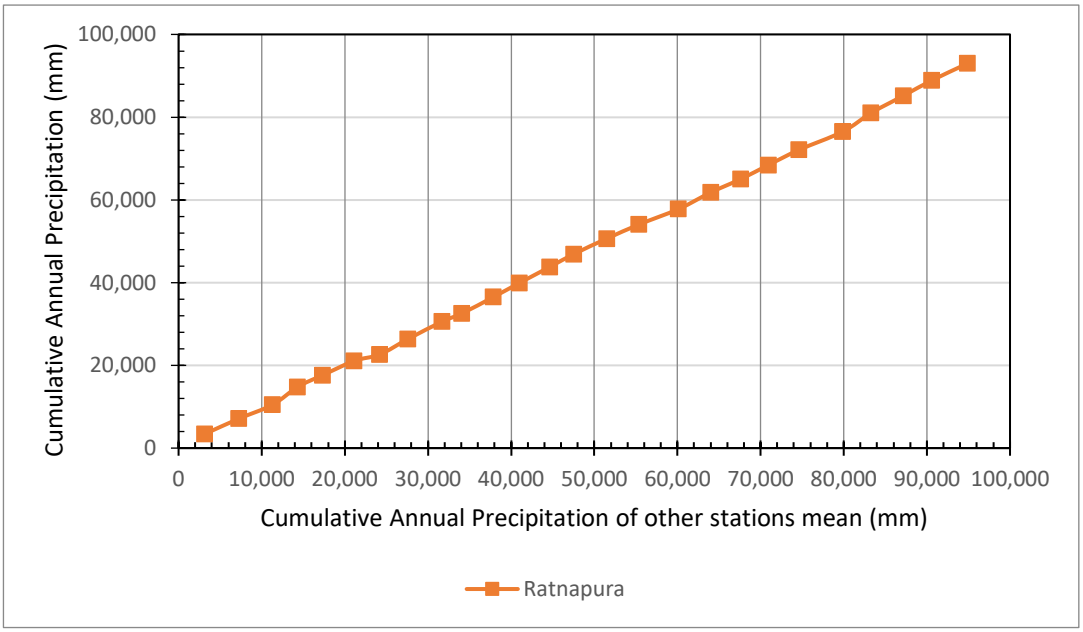

Figure 4-63: Double mass curve of Rathnapura station

4.2.3 Data Filling

The number of days where data is missing in the Kalu Ganga basin is as listed in Table 4-10 and their respective percentages of missing data are mentioned. The missing data is below 10% in all of the stations and there is no missing data in the Halwatura station. The missing data were filled using the linear regression technique as explained in Section 4.1.3.

Table 4-10: Missing data in different stations in Ellagawa basin

RF Station	Data Period	Missing days	Missing (%)
Halwatura	1995 - 2020	0	0%
Galatura	1995 - 2020	1	0%
Ratnapura	1995 - 2020	708	7%
Depedena	1995 - 2020	308	3%

4.2.4 Climate Trends and Extremes

As discussed in Chapter 3.3, various streamflow indices are calculated to observe trends and extremes in the basin.

4.2.4.1 Streamflow Indices

Various streamflow indices listed in Table 3-1 are calculated using streamflow data from the Ellagawa gauging station in this section. The number of consecutive low-flow (CDS) days is showing a sharp increasing trend in the recent period as shown in Figure 4-64. The number of consecutive high-flow (CWS) days is also showing a decreasing trend in the recent period as shown in Figure 4-65.

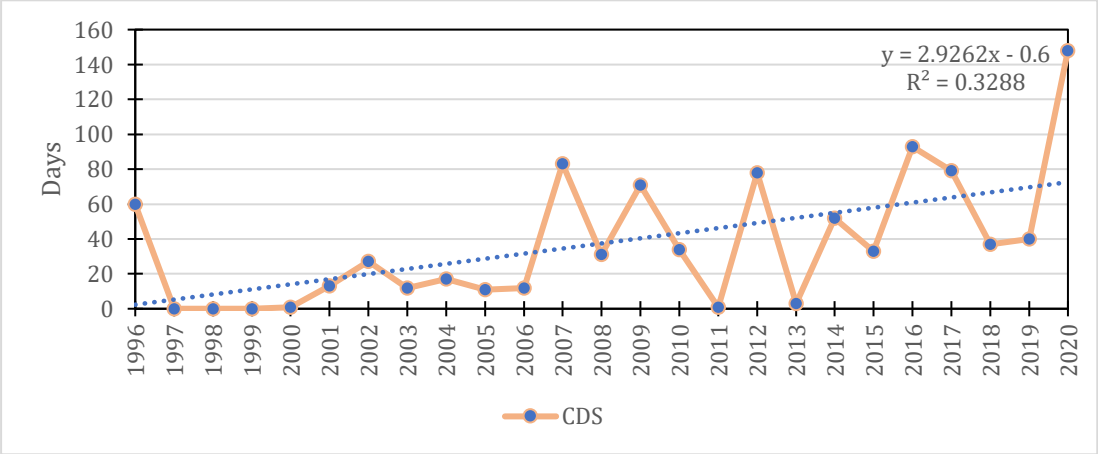

Figure 4-64: Consecutive low-flow days in Ellagawa station

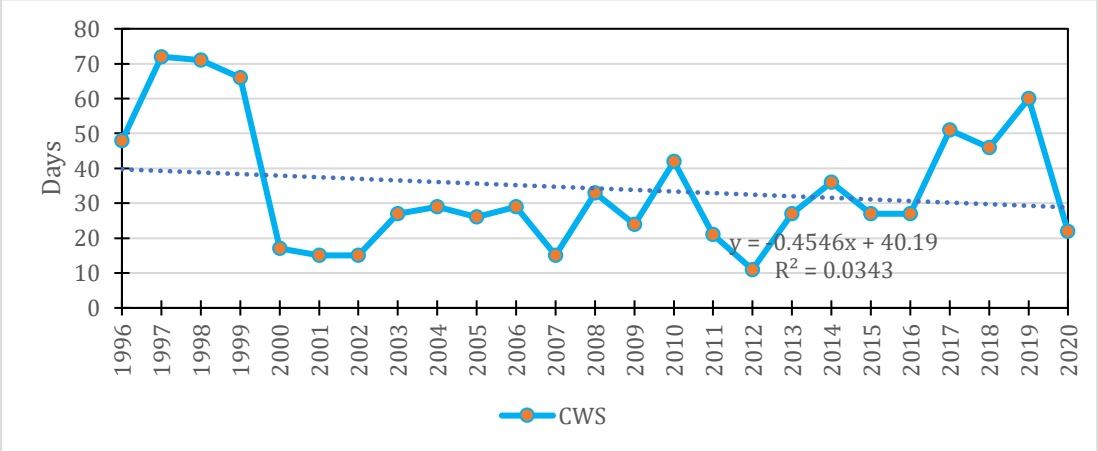

Figure 4-65: Consecutive high-flow days in Ellagawa station

The annual highest daily streamflow (SX1 day) is also showing a sharp decreasing trend in the recent period as shown in Figure 4-66. The extreme high streamflow was observed in the year 2003 with a magnitude of 2,568 m^3/s whilst the basin experienced merely 366 m^3/s discharge as the maximum flow during the year 2001. This indicates that the basin is experiencing a decreased streamflow in the recent period.

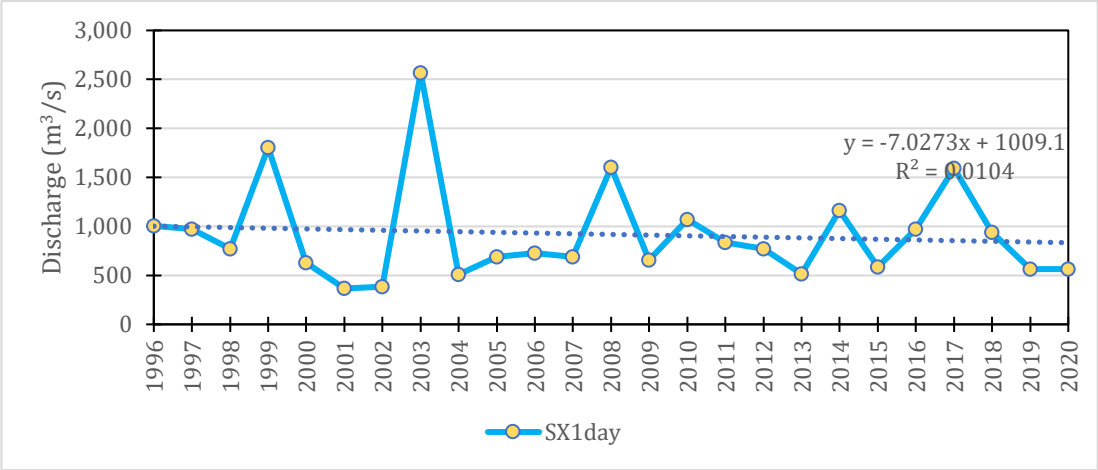

Figure 4-66: Annual highest daily streamflow in Ellagawa station

Figure 4-67 below contains the line graph of the maximum streamflow in 1-day, an average of 2 consecutive days, and an average of 5 consecutive days which showed a decreasing trend. Although 1-day and 2-day averages are showing higher magnitudes, the 5-day average is slightly low in magnitude compared to the other two.

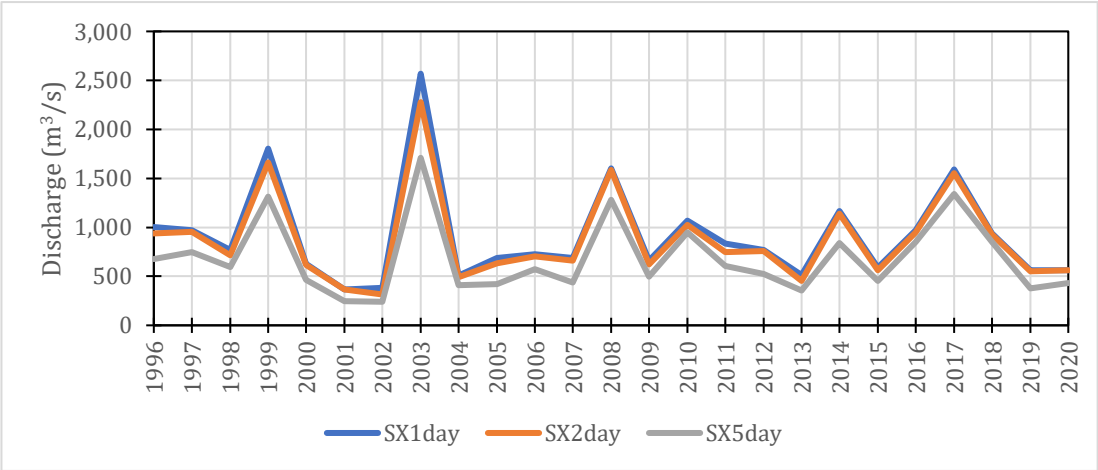

Figure 4-67: Annual highest streamflow in consecutive 1, 2, and 5 days in Tanamalwila station

The SSI for the Ellagawa station for 12 months period was computed which is as shown in Figure 4-68. It can be observed that the frequency of drought is increasing in the recent period after 2001. There was a prolonged drought from 2001 to 2008 in the basin between which the basin experienced a very high flood in 2003. It is also observed that the drought frequency is increasing in the recent period.

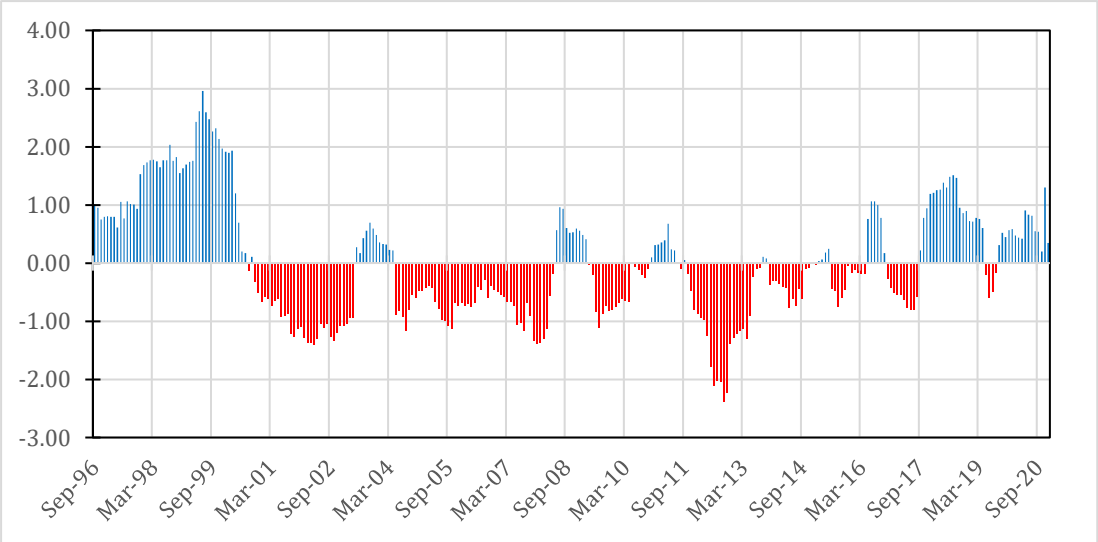

Figure 4-68: Standardized streamflow index (SSI) calculated for 12 month period in Ellagawa station

4.2.4.2 Precipitation Indices

The precipitation indices listed in Table 3-2 are calculated using precipitation data from various gauging stations in this section. It was observed that CDD is showing an increasing trend in the recent period as shown in Figure 4-69.

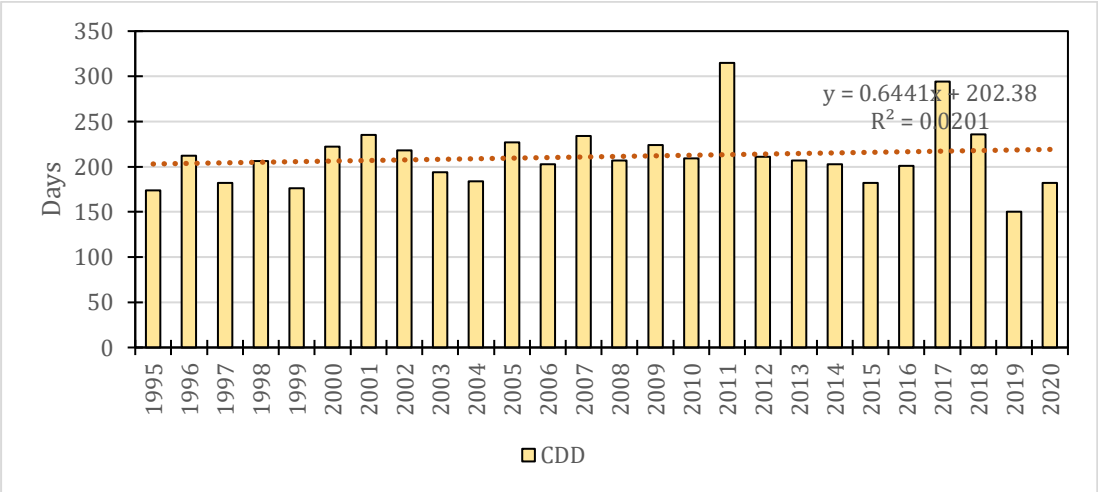

Figure 4-69: Consecutive dry days in Halwatura station

It can be observed that CWD is showing a decreasing trend in the recent period in Halwatura station as shown in Figure 4-70.

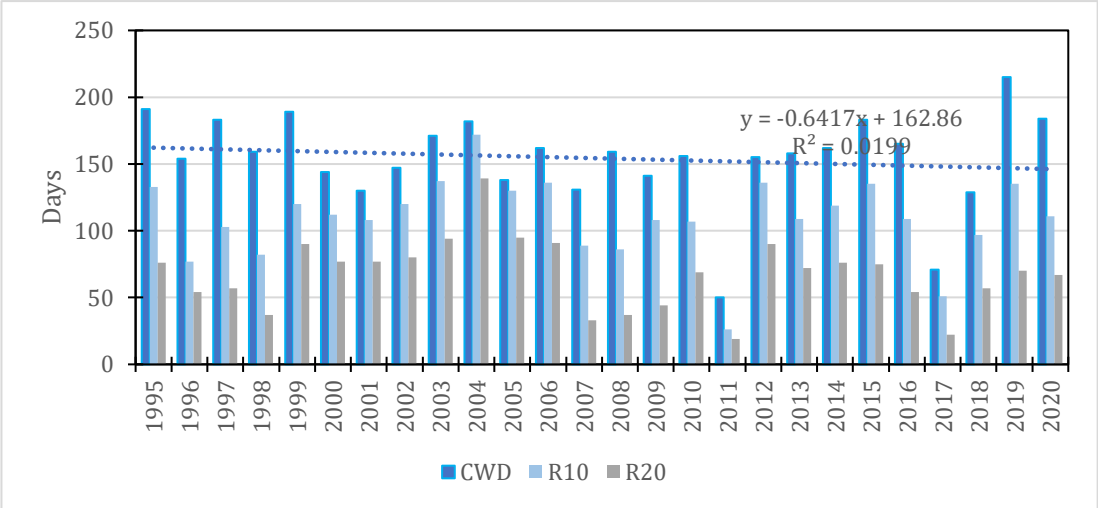

Figure 4-70: Consecutive wet days (CWD), heavy precipitation days (R10), and very heavy precipitation days (R20) in Halwatura station

The annual precipitation extremes in Halwatura station are showing a decreasing trend along with lower magnitudes than previously observed in the station.

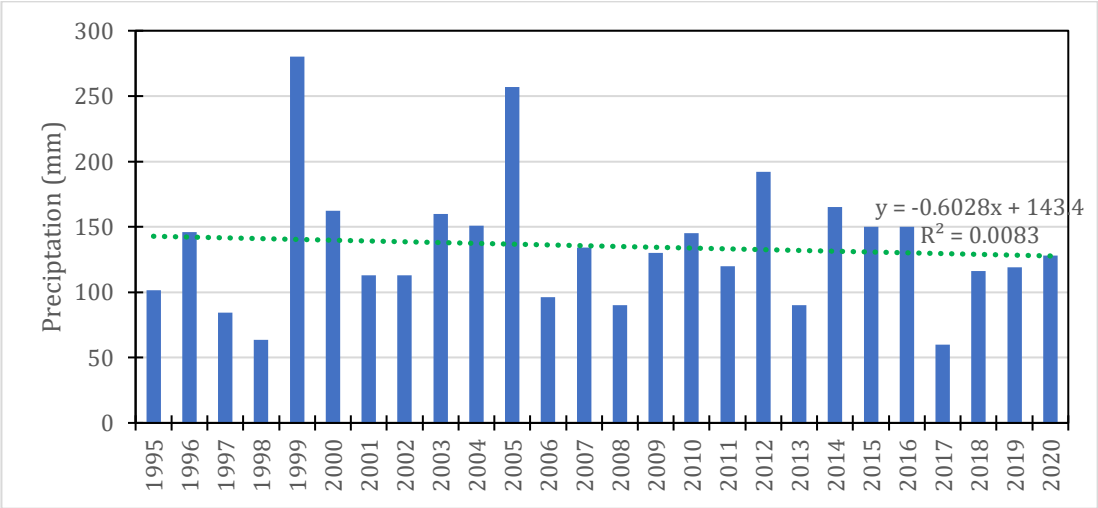

Figure 4-71: Annual precipitation extremes in Halwatura station

Annual maximum 1-day precipitation along with 2-day consecutive precipitation and 5-day consecutive precipitation are presented in Figure 4-72. It can be observed that the precipitation trends in 3 different indices are increasing in the Halwatura station.

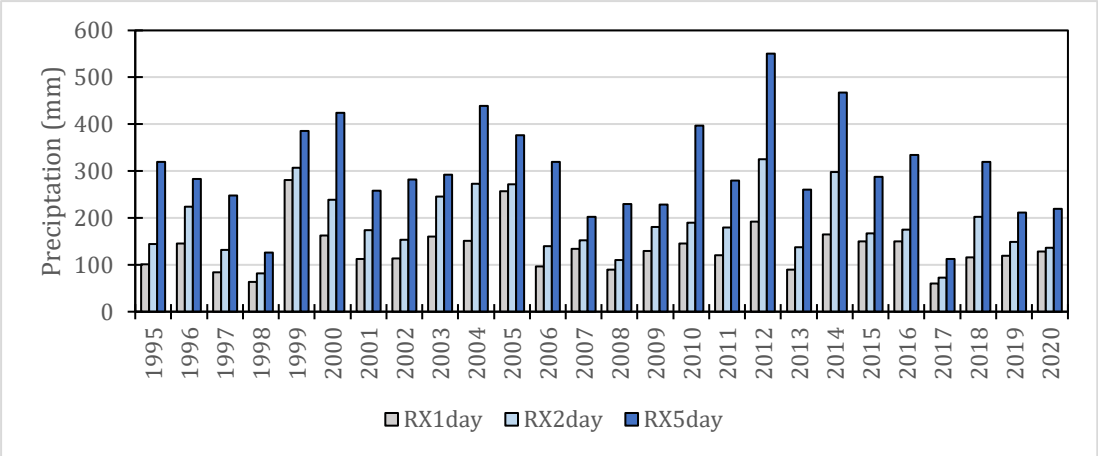

Figure 4-72: Annual maximum 1-day, 2-day, and 5-day precipitation in Halwatura station

The annual distribution of consecutive wet and dry days in Halwatura station as portrayed in Figure 4-73 which depicts that the station experiences more wet days in a year. The wet days in a year is showing decreasing trend followed by an increase in dry days in a recent period.

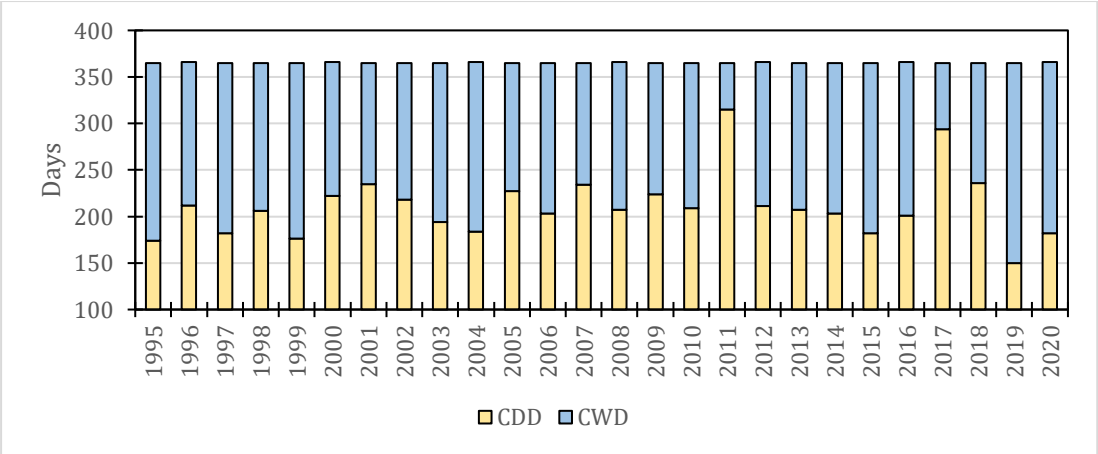

Figure 4-73: Annual distribution of wet and dry days in Halwatura station

4.2.5 Precipitation Over an Area

Thiessen polygon method is used to distribute point rainfall over an area as explained in Section 4.1.5. Thiessen polygons are drawn using ArcGIS 10.5 software and the weightage for all stations are obtained as shown in Figure 4-74. Different values of weightage obtained for the rain gauge stations are mentioned in Table 4-11. The highest weightage is obtained for the Ratnapura station and the lowest weightage is

obtained for the Halwatura station. Further, sub-basin wise Thiessen weightage is calculated to provide input rainfall to the model.

Table 4-11: Thiessen weightage of rain gauge stations in Kirindi Oya

Station Name	Latitude (° N)	Longitude (° E)	Area (km^2)	Weightage
Halwatura	6.72	80.20	91.65	0.07
Galatura	6.70	80.28	241.60	0.17
Ratnapura	6.68	80.40	684.54	0.49
Depedena	6.47	80.55	391.69	0.28
	Total		1,409.48	1.00

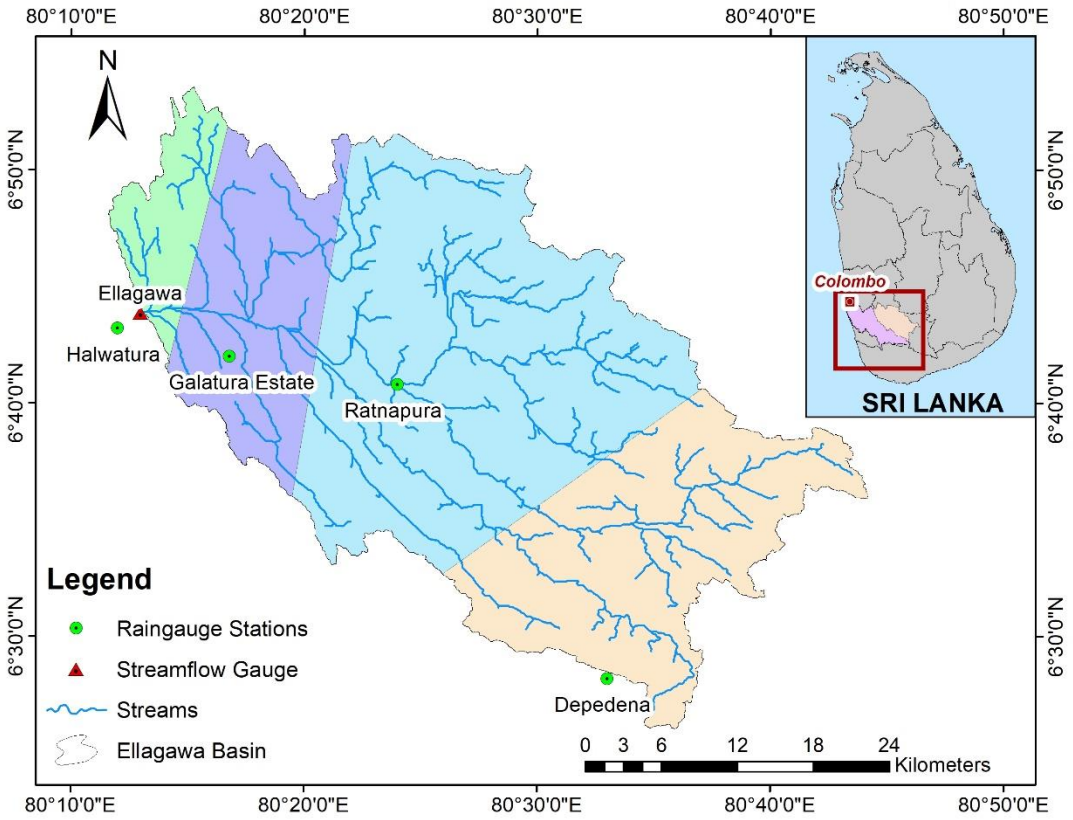

Figure 4-74: Thiessen polygons with weightage of individual stations in Ellagawa basin

4.2.6 Identification of Events

Events for the modeling purpose were selected considering the discussion in earlier Sections 2.6 and 3.4 and the procedure followed in Section 0. A minimum event depth of 1 mm and MIT of 1 day (24 hrs) was adopted which yielded 746 events in between the period of 1995 to 2020. It can be observed in Figure 4-75 and Figure 4-76 that extreme events happen in the basin in the Yala season and more extreme events were contributed by more than 1-day rainfall compared to daily rainfall.

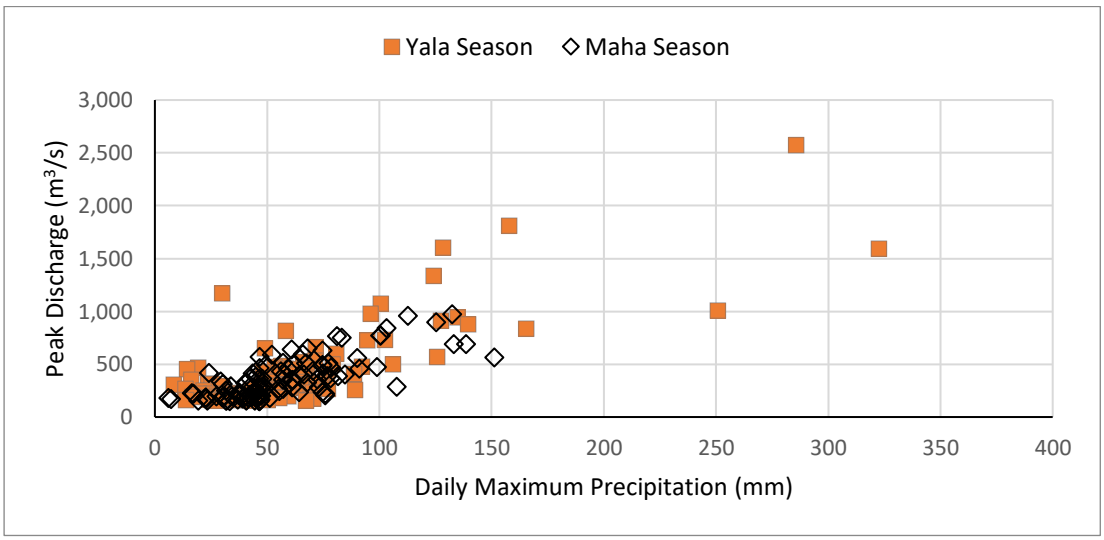

Figure 4-75: Daily maximum precipitation during events along with the event's peak discharge in Kalu Ganga

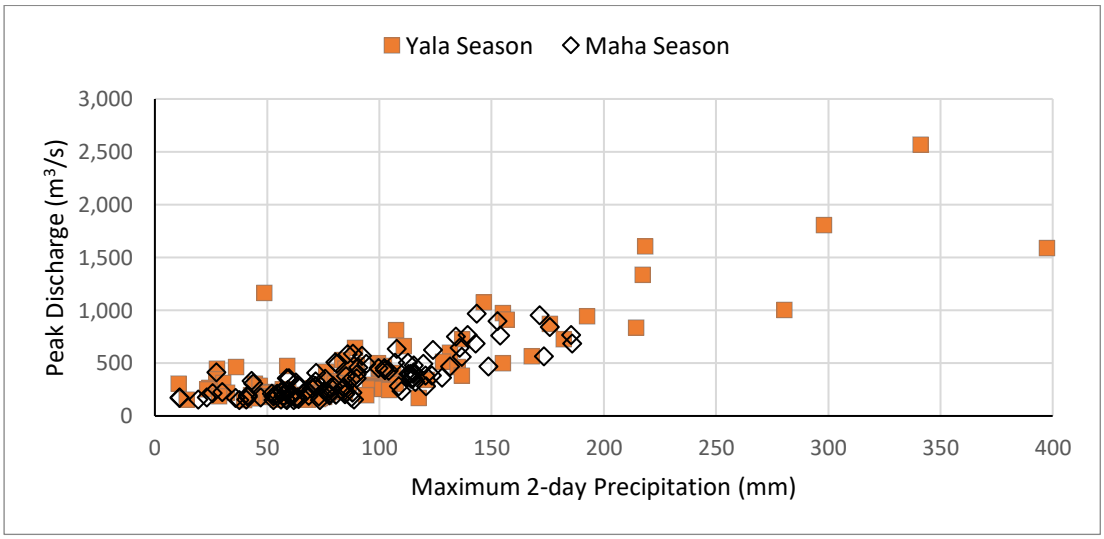

Figure 4-76: Maximum 2-day precipitation during events along with the event's peak discharge in Kalu Ganga

Among the events identified, the events for model calibration and validation were selected based on return period discharge. Return period discharge was calculated using Gumbel distribution and the 100 year return period discharge was obtained to be 2,727 m^3/s. Return period discharge for different durations calculated using Gumbel distribution are as shown in Figure 4-77. Considering the time availability to model the events, for the Kalu basin, only four (4) events were explored. The events were selected from 2, 5, and 15-year return period discharge.

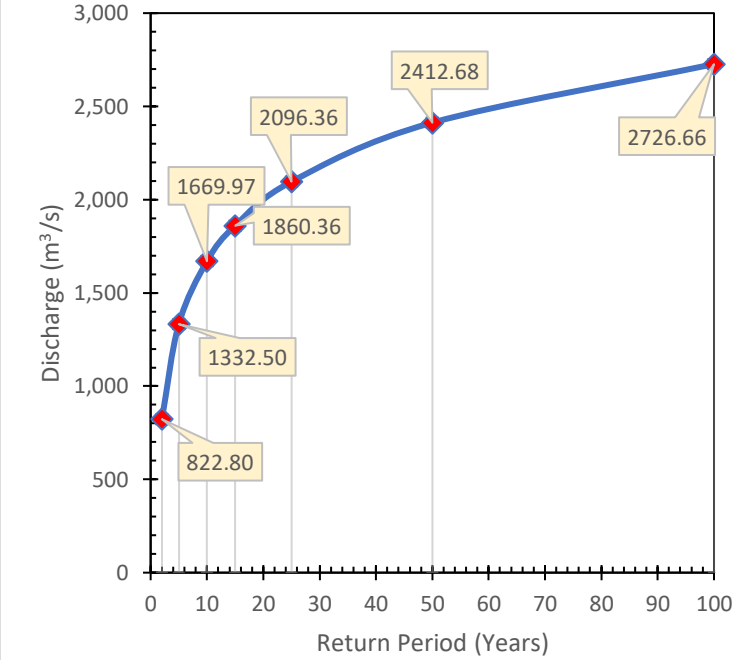

Return period (Years)	Discharge (m^3/s)
1	117
2	823
5	1,332
10	1,670
15	1,860
25	2,096
50	2,413
100	2,727

Figure 4-77: Different return period discharge in Kalu Ganga basin

The detailed information regarding events identified (such as dry period before the start of the event, total event RF, total event days, maximum RF, maximum 2-day RF, return period discharge, and so on) can be referred to Table A - 5 attached in Annexure 3 of this document. The maximum total event rainfall identified was 959 mm with a wet period of 51 days whereas the minimum total event rainfall identified was 477 mm with a wet period of 11 days.

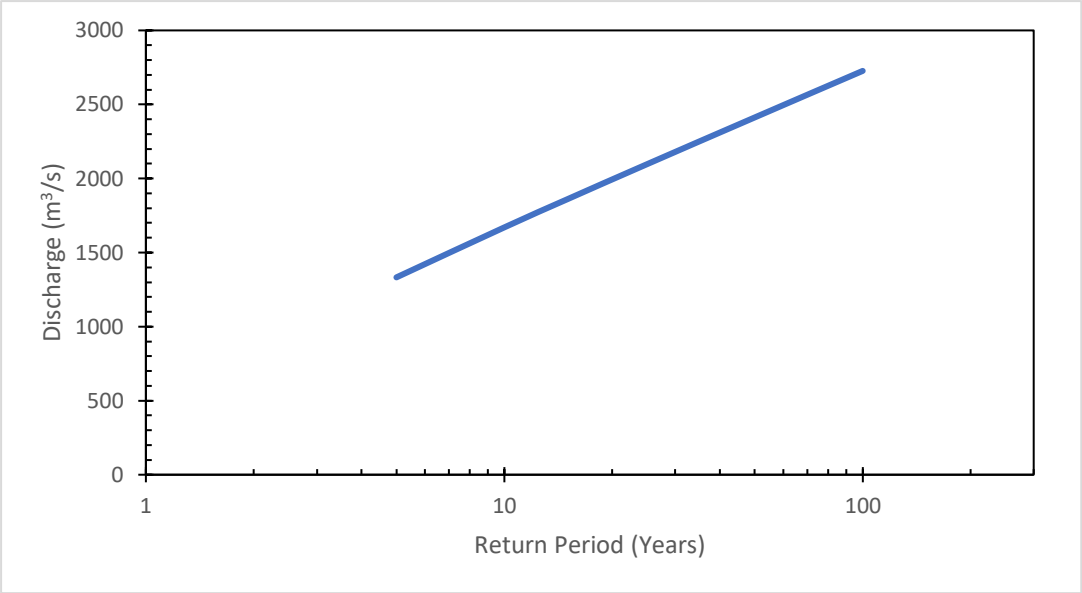

Figure 4-78: A straight line indicating a well-fitted curve in Gumbel distribution

The Gumbel distribution employed produces a curve when discharge is plotted against different return periods (normal scale) as shown in Figure 4-77. A check needs to be done whether the curve fits perfectly or not before applying the method in the study which is performed in Section 0. The Gumbel distribution curve (semi-log) obtained for the discharge data of the Ellagawa station generates a straight line which indicates that the curve is well fitted as shown in Figure 4-78.

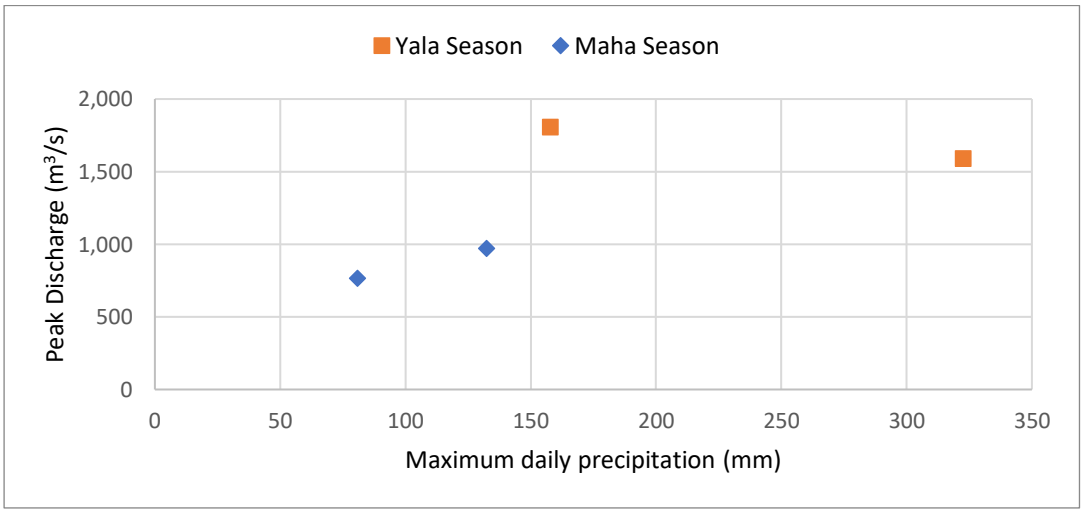

Figure 4-79: Identified events considering different return period discharge for Kalu Ganga

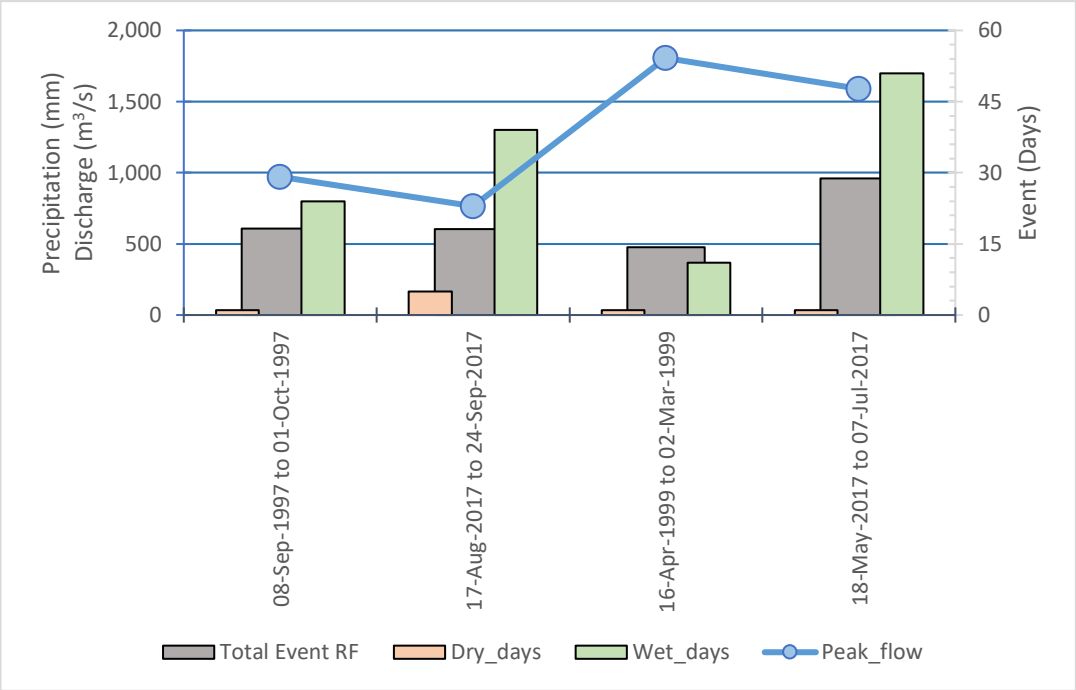

Figure 4-80: Events selected for the study in Kalu Ganga

The selected events which will be used for the event modeling purpose with their details are represented in Figure 4-80. The events selected are of different magnitude in terms of discharge which is presented in Table 4-12. The discharge considered for the selection of events are ranging from 2-year return period discharge to 15-year return period discharge.

Table 4-12: Events of various return period discharge selected for calibration and validation in Kalu Ganga

ID	Dry days	Total Event RF (mm)	Wet days	Max RF (mm)	Peak flow (m^3/s)	Return Period (years)
1	1	606.7	24	132.3	971.0	2
2	5	605.6	39	80.9	764.9	2
3	1	477.1	11	157.9	1806.0	15
4	1	959.8	51	322.6	1590.6	10

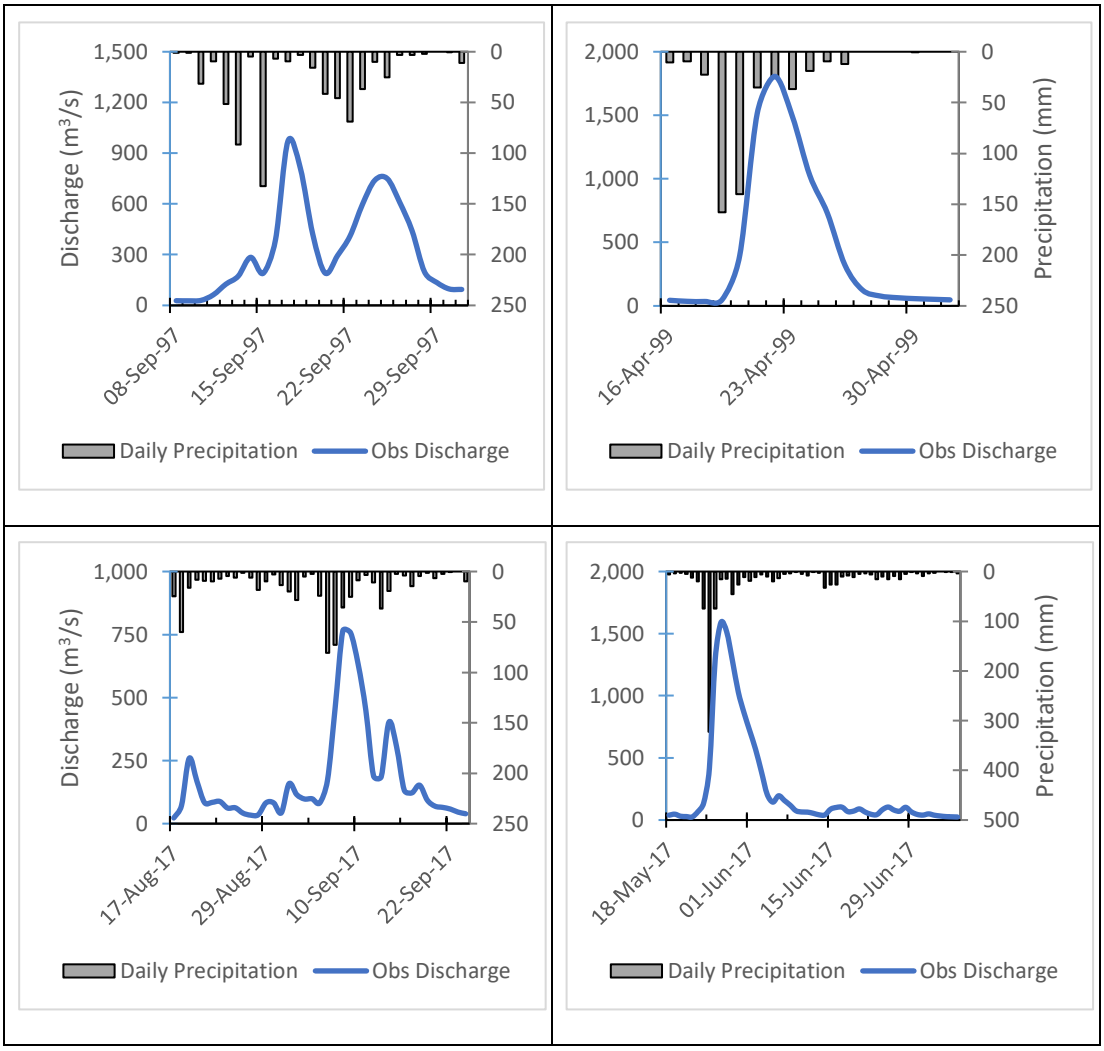

Figure 4-81: Events selected for the validation in Kalu Ganga

4.2.7 Initial Soil Moisture for Validation of Events

For the input in the model, SSM data was extracted using ArcGIS following the procedure explained in Section 4.1.7. Then, the volumetric soil moisture was converted to soil saturation percentage referring to Bhuiyan et al. (2017). The sub-basin soil moisture storage for a particular event date is as shown in Figure 4-82. The SM on date 2017 May 18 in Kalu Ganga shows wet upstream areas and slightly drier lower basin part. The SM value is now used with sub-basin porosity to calculate the initial soil moisture percentage which is expected to enhance the performance of the model.

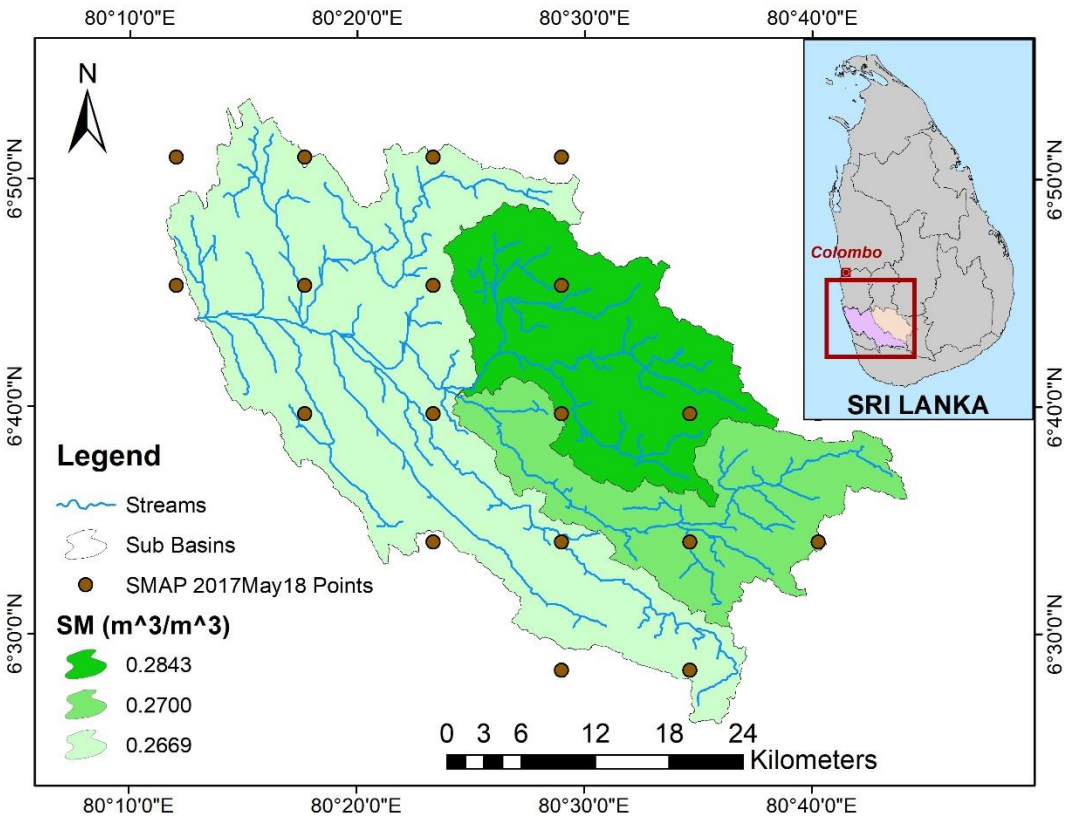

Figure 4-82: Sub-basin wise root zone SM dated 2017 May 18 in Kalu Ganga

The average daily soil moisture in the basin compared with daily precipitation and daily streamflow is attached in Annexure 4. The soil moisture values are higher during Event 2 (64 %) compared to Event 4 (59 %).

Table 4-13: Initial soil moisture condition before the start of the event derived from SSM

Event	Event code	Sub Basin			Average
		Sub Basin 1	Sub Basin 2	Sub Basin 3	
Event 2	5D-39W-Aug/Sep17	66%	66%	60%	**64%**
Event 4	1D-51W-May/Jul17	61%	58%	57%	**59%**

CHAPTER 5

5 MODEL DEVELOPMENT AND APPLICATIONS

5.1 HEC-HMS Model Development

The model development is carried out with reference to the methodology of model development as discussed earlier in Sections 3.2 and 3.5. There are various parameters associated with the model which need to be calculated with proper attention to obtaining the result of higher accuracy. Table A - 1 attached in Annexure 2 presents tables with different parameters required for the model to run and the ways of calculating those parameters. A summary of the list of the parameters is presented in Table 5-1.

Table 5-1: Different parameters required for model

S.N.	Parameters	S.N.	Parameters
1	Canopy max storage (mm)	10	Impervious (%)
2	Surface max storage (mm)	11	GW1 storage (mm)
3	Max infiltration rate (mm/hr)	12	GW1 max percolation rate (mm/hr)
4	Max soil storage (%)	13	GW1 storage coefficient (hr)
5	Groundwater 1 (%)	14	GW2 storage (mm)
6	Groundwater 2 (%)	15	GW2 max percolation rate (mm/hr)
7	Soil storage (mm)	16	GW2 storage coefficient (hr)
8	Soil percolation rate (mm/hr)	17	Time of concentration
9	Tension Storage (mm)		

5.2 Kirindi Oya Basin

First of all, terrain data is loaded into the HEC-HMS model and then a basin model is developed with five (5) sub-basins and three (3) reaches.

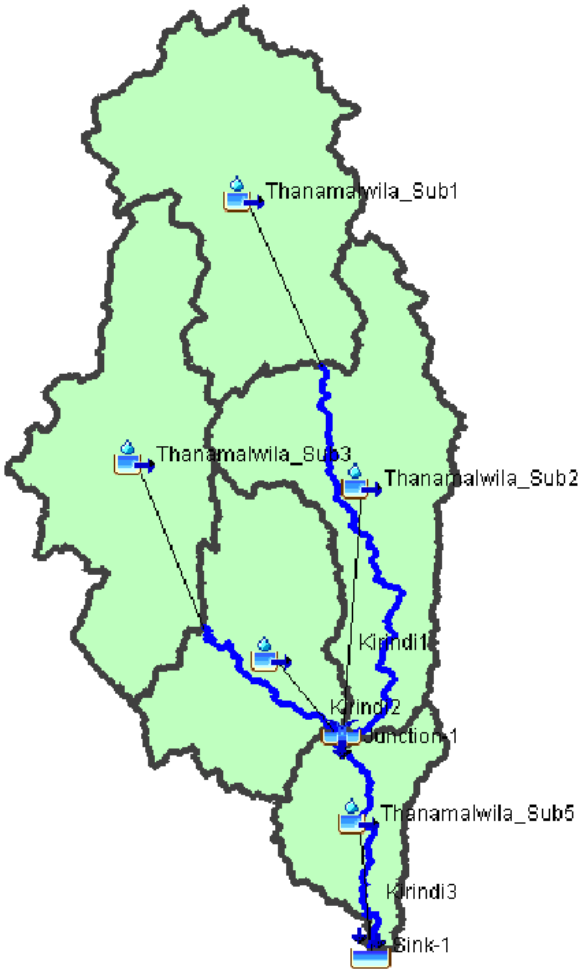

Figure 5-1: Kirindi Oya basin model with sub-basins developed in HEC-HMS

5.2.1 Canopy and Surface Storage

Canopy interception is the volume of precipitation intercepted by vegetation during the precipitation. During the rainfall, first, it falls to the canopy surface. After filling the canopy container, excess water drips to the surface. It is calculated using the land-use and land-cover map in ArcGIS. Different land uses are assigned with values of storage as mentioned in Table 5-2 below which is obtained from Bennett and Peters (2004). The developed canopy raster map for the Kirindi Oya basin is as shown in Figure 5-2 below.

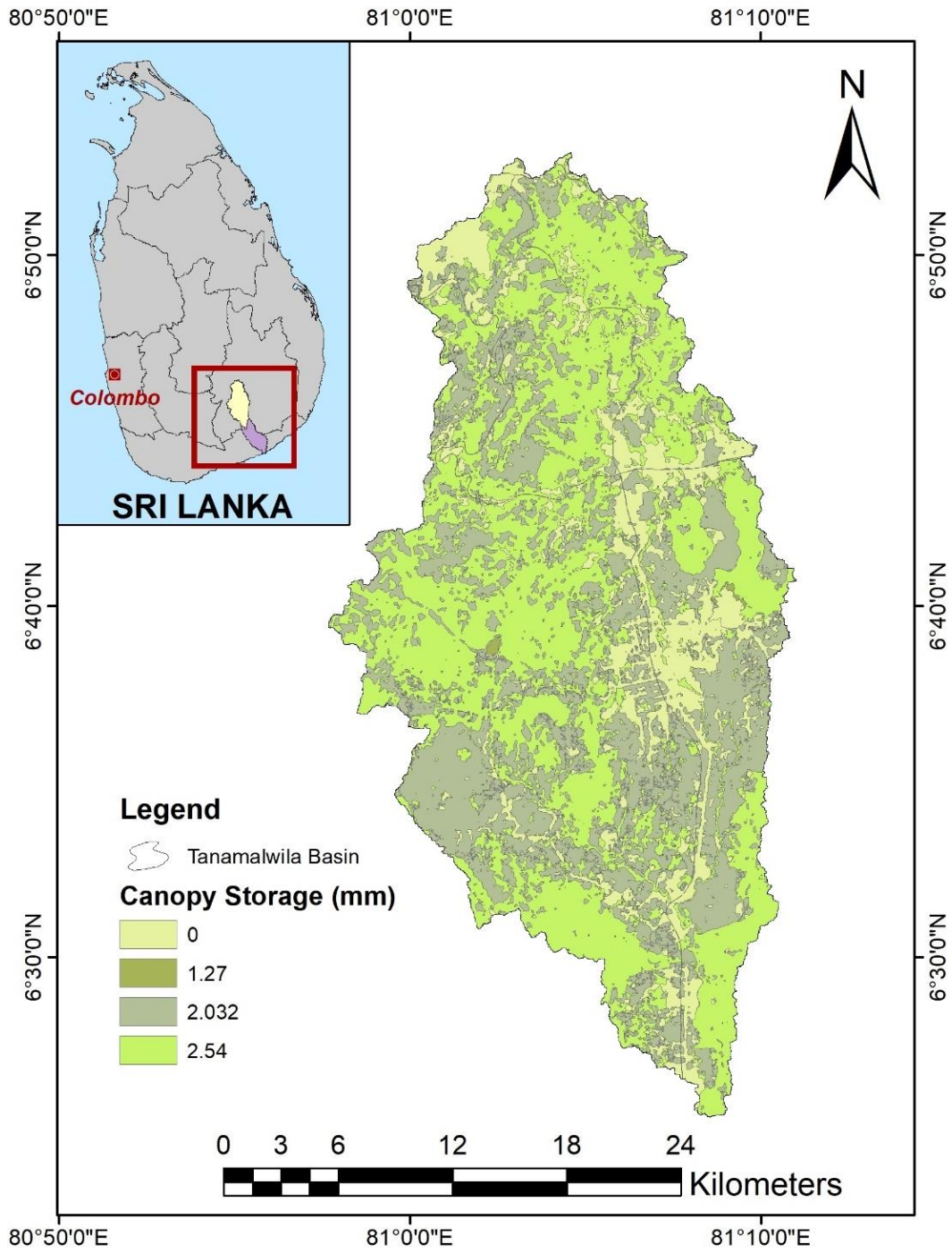

Figure 5-2: Canopy storage in the Kirindi Oya basin

The simple canopy model selected requires an input of maximum canopy storage (mm) and initial storage (%). Maximum canopy storage for the sub-basins was calculated using the canopy storage map obtained from GIS.

Table 5-2: Canopy storage values for different land-use types (Bennett & Peters, 2000)

Landuse Type	Canopy Interception	
	Inches	Millimetres
General Vegetation	0.05	1.270
Grasses and Deciduous Trees	0.08	2.032
Trees and Coniferous Trees	0.10	2.540

The water stored on the ground surface is referred to as surface depression storage. Rainfall that is not retained by the canopy falls to the ground or travels towards it. Some of it infiltrates or evaporates, whereas others accumulate on the surface. It is calculated using a terrain slope by assigning different slopes with surface storage values. Conceptually, steep slopes are considered to have low storage values as they contribute to the runoff of water to the downstream areas. Flat areas are considered to have relatively higher storage. Surface storage values for different slope conditions are as shown in Table 5-3.

Table 5-3: Surface storage values for different slopes (Fleming, 2002)

Description	Slope %	Surface Storage	
		Inches	Millimetres
Paved Impervious Areas	NA	0.125 – 0.25	3.18 – 6.35
Steep, Smooth Slopes	>30	0.04	1.02
Moderate to Gentle Slopes	5 – 30	0.25 – 0.50	6.35 – 12.70
Flat, Furrowed Land	0 – 5	2.00	50.80

The slope layer obtained by processing of digital elevation model (DEM) was reclassified with different slopes corresponding to specific surface storages and a layer of surface storage was obtained. The layer was combined with the layers of the road to obtain a map of surface storage. Maximum surface storage (mm) for sub-basins is computed in ArcGIS for the input in the model. The summary of canopy storage, surface storage, and impervious area (%) for sub-basins in Kirindi Oya used as input in the model is mentioned in Table 5-4.

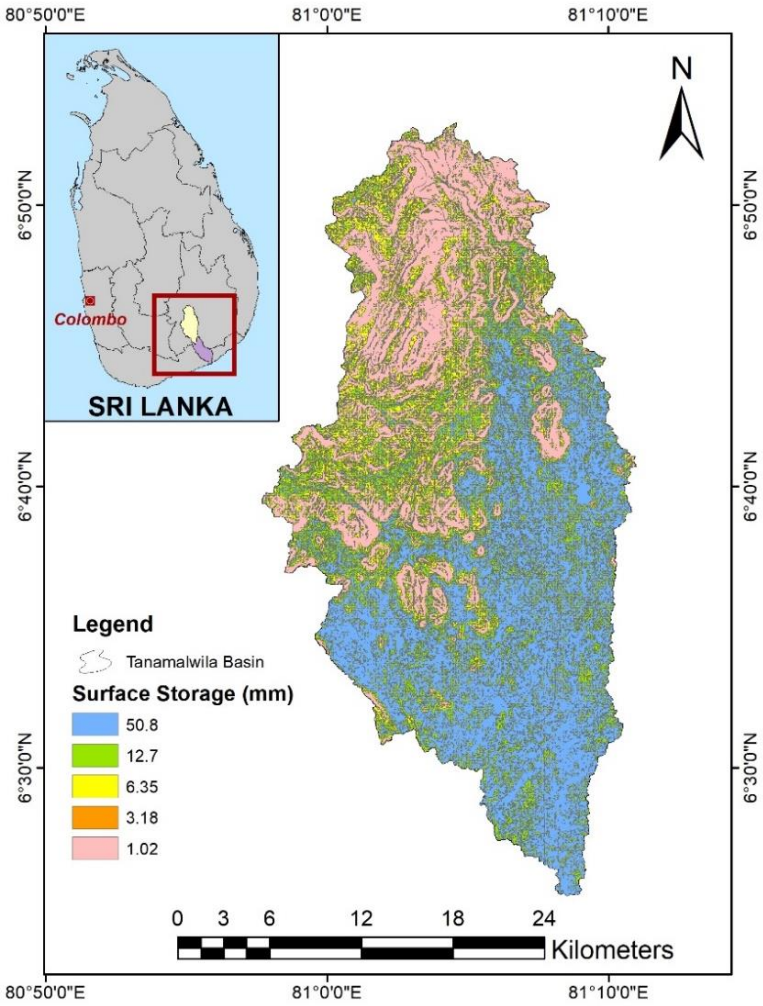

Figure 5-3: Surface storage in the Kirindi Oya basin

Table 5-4: Values of canopy storage and surface storage in Kirindi basin

Sub Basin	Canopy Storage (mm)	Surface Storage (mm)
Sub Basin 1	1.90	9.19
Sub Basin 2	1.69	33.85
Sub Basin 3	2.23	15.98
Sub Basin 4	2.04	34.08
Sub Basin 5	1.98	41.41

5.2.2 Soil Moisture Accounting Loss Method

Soil moisture accounting (SMA) was adopted as a suitable method for modeling the precipitation losses in the basin referring to the brief literature review in Section 2.4.2. There are 14 parameters associated with the SMA method among which many are physical parameters that can be estimated whereas some parameters are initial conditions that depend on the condition of modeling. Parameters associated with the topsoil layer are estimated using the soil properties of the basin. Parameters related to Groundwater 1 (GW1) and Groundwater 2 (GW2) are estimated by streamflow recession analysis of past streamflow data. The initialization is assumed during the modeling process and adjusted through optimization. The parameters that can be calculated through soil properties and streamflow recession analysis are explained in the Sub-Sections 5.2.2.1 and 5.2.2.2. Other remaining parameters mentioned in Annexure 2 are obtained during the calibration process.

5.2.2.1 Top Soil Layer

The calculated parameters for the topsoil layer are as presented in Table 5-5.

Table 5-5: Topsoil layer physical parameters for Kirindi Oya basin

Sub Basin	Maximum Infiltration (mm/hr)	Soil Storage (mm)	Impervious Area
Sub Basin 1	6.776	272.447	10.45%
Sub Basin 2	4.279	279.015	13.74%
Sub Basin 3	6.006	278.521	2.17%
Sub Basin 4	3.811	279.168	6.73%
Sub Basin 5	3.769	278.029	8.61%

The maximum infiltration (mm/hr) is calculated using the saturated hydraulic conductivity (K_{sat}) of the available soil types in the basin. The weighted average of K_{sat}

values of different soil found in the basin was performed to calculate the maximum infiltration parameters for the sub-basins. Similarly, the porosity of the soil is used to calculate the soil storage assuming a certain depth of soil layer in the basin. The percentage of impervious areas is calculated considering the land use that does not allow water to penetrate through it. Land use types like built-up areas, roads, and water are considered as the impervious part of the basin. In the case of built-up area, only 50% of the built-up area is considered as the impervious area as other areas may allow infiltration of water into it.

5.2.2.2 Groundwater 1 and Groundwater 2 Layers

The parameters associated with groundwater 1 and groundwater 2 layers are calculated using streamflow recession analysis as suggested by Bennett and Peters (2004). Isolated hydrographs from different periods where the streamflow rises rapidly and also recedes swiftly are considered to estimate the four (4) parameters of groundwater layers. The recession analysis is performed by breaking down the streamflow hydrograph into baseflow, runoff and interflow, and interflow as shown in Figure 5-4.

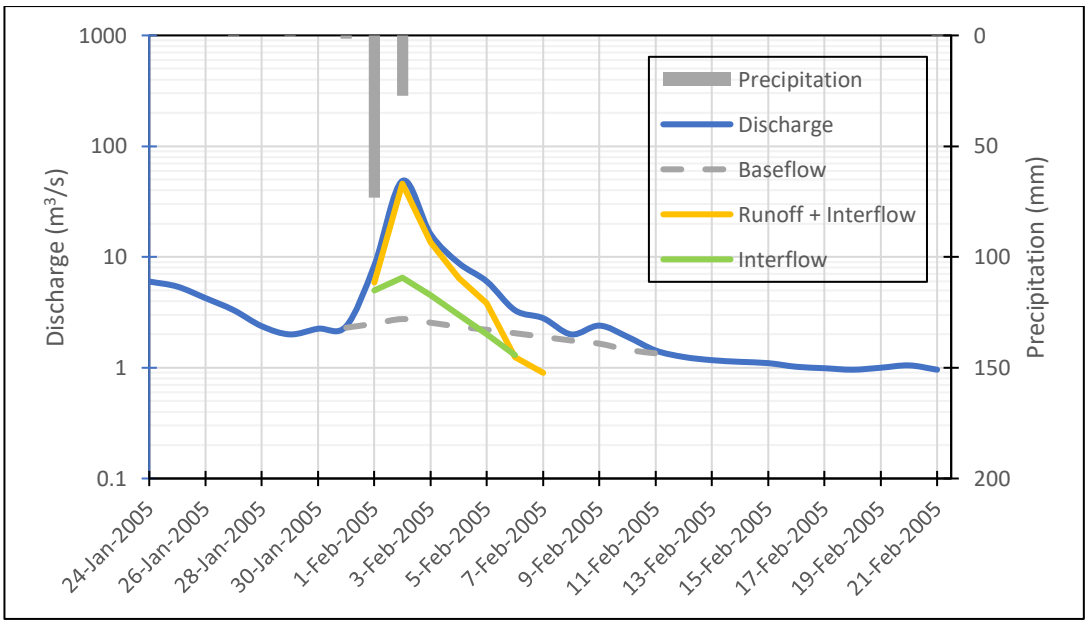

Figure 5-4: Streamflow recession analysis for the year 2005

In SMA, GW1 is represented by the interflow graph, and GW2 is represented by the baseflow graph. Streamflow recession analysis is carried out using the Equation [5-1]

to Equation [5-3]. The analysis is performed in a daily time step for every hydrograph considered. First of all, α is calculated using the Equation [5-1];

$$q_1 = q_o K_r = q_o * exp(-\alpha t) \quad [5\text{-}1]$$

where q_o is the initial streamflow, q_1 is the streamflow at a later time, t, K_r is a recession constant less than 1, and $\alpha = -ln(K_r)$. The recession coefficient is calculated using the Equation [5-2].

$$Recession\ Coefficient = 1/\alpha \quad [5\text{-}2]$$

The average values of α for the whole analysis period when inversed yield groundwater coefficient. The groundwater storage is calculated in daily steps as the ratio of discharge to α. Finally, all the storage values are averaged to get final groundwater storage computed using Equation [5-3].

$$S_t = q_1/\alpha \quad [5\text{-}3]$$

Table 5-6: Groundwater layers parameters obtained from streamflow recession analysis

S.N	Period		GW1 Storage (mm)	GW1 Constant (hr)	GW2 Storage (mm)	GW2 Constant (hr)
	From	To				
1	1/24/2005	2/21/2005	6.90	59.65	25.40	303.59
2	1/2/2007	2/26/2005	8.77	31.75	192.78	409.57
3	4/6/2009	4/28/2009	1.79	20.85	302.81	103.05
4	12/11/2012	12/25/2012	18.34	17.72	222.85	304.35
5	12/9/2019	1/21/2020	16.55	23.40	414.30	269.15
		Average	**10.47**	**30.67**	**231.63**	**277.94**

The above-interpreted steps are conducted for the baseflow hydrograph to calculate the GW2 storage and GW2 coefficient. The same steps are performed for interflow hydrograph to obtain GW1 storage and GW1 coefficient. The analysis is carried out for the different periods and possible different seasons to capture representative parameters.

5.2.3 SCS Unit Hydrograph Transform

Soil conservation service (SCS) unit hydrograph is considered as a transform method on the model. The model requires lag time in minutes to transform the flow at the outlet of each sub-basin. Time of concentration is calculated using the Kirpich equation shown in Equation [5-4];

$$t_c = 0.0195L^{0.770}S^{-0.385} \quad [5\text{-}4]$$

where t_c is time of concentration in minutes, L is Channel flow length in meters, and S = Main channel slope.

The lag time is calculated referring to Equation [5-5] mentioned below.

$$Basin\ lag = tc/1.67 \quad [5\text{-}5]$$

Required channel flow length and main channel slope were obtained from the sub-basin characteristics window of the HEC-HMS model. Time of concentration calculated from the Kirpich Equation is then relayed to the basin lag time by dividing t_c by 1.67. The time of concentration calculated for all sub-basins in the Kirindi Oya basin is shown in Table 5-7. Maximum lag time is 225 minutes in Sub-basin 2 and the minimum lag time is 118 min for Sub-basin 3.

Table 5-7: Basin physical properties and lag time

Subbasin	Area (sq. km)	Longest Flowpath Length (km)	Longest Flowpath Slope	Time of Concentration (min)	Basin Lag (min)
Sub Basin 1	184.71	38.6970	0.0371	236	141
Sub Basin 2	170.48	38.5018	0.0110	376	225
Sub Basin 3	170.08	34.9348	0.0488	196	118
Sub Basin 4	125.29	22.5423	0.0147	222	133
Sub Basin 5	65.93	19.5671	0.0033	357	214

5.2.4 Development of Baseflow Model

The recession model which has been successfully used to model the baseflow in and outside of Sri Lanka (Bhuiyan et al., 2017; Nasimi, 2018; Ud Din, 2018) was selected considering data availability and ease of use. The recession baseflow method models a hydrograph's recession curve using the following Equation [5-6];

$$Q_t = Q_o k^t \quad [5\text{-}6]$$

where Q_t is flow at time *t*, Q_o is flow at the beginning of the recession curve, and *k* is exponential decay constant (recession constant). The observed hydrograph is analyzed using the above equation to calculate parameters associated with the baseflow model.

The HEC-HMS requires initial discharge (either specified as rate or rate per area), recession constant, and threshold for starting the baseflow recession curve (specified as a flow threshold or as a ratio to peak) as input parameters to simulate baseflow. The initial type is selected as 'Discharge' which requires initial discharge as input. Initial discharge specifies the discharge prior to simulation interval which can be estimated by carefully observing the observed hydrograph (Nasimi, 2018; Ud Din, 2018). The initial estimation of this parameter was carried out by carefully analyzing the observed hydrograph of different periods.

Among two types of thresholds, i.e., threshold discharge and ratio to peak, the latter one was selected for the research. The ratio to peak is easier to apply across the basin model because it generally remains consistent across subbasins where a discharge threshold is dependent on subbasin size. A ratio to peak of 0.5 indicates the threshold would be half the peak flow indicating the slope of the falling limb of the hydrograph as shown in Figure 5-5. Recession analysis of the historical streamflow data provides the recession constant value of the streamflow. A recession constant closer to 1 results in a flatter recession curve and a constant closer to 0 results in a steeper recession curve as shown in Figure 5-5.

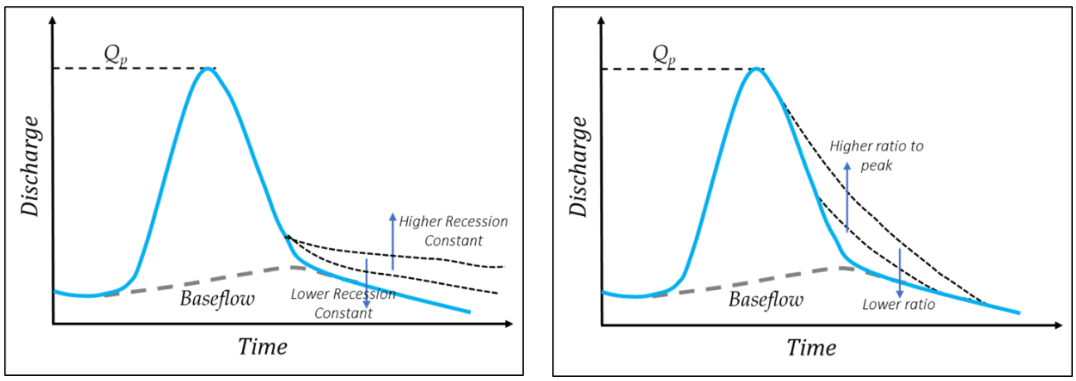

Figure 5-5: Hydrograph displaying different shapes of recession curves for values of recession constant (left) and shapes of falling limb for values of ratio to peak (right)

Table 5-8: Calculation of recession parameters through streamflow recession analysis

S.N.	Period		Recession constant (*k*)	Ratio to peak
	From	To		
1	6/17/2005	8/26/2005	0.9868	0.1670
2	6/26/2010	8/19/2010	0.9747	0.1000
3	12/26/2013	1/14/2014	0.9821	0.2190
4	11/22/2017	12/6/2017	1.0000	0.2300
	Average		**0.9859**	**0.1790**

5.2.5 Development of Routing Model

Among various approaches to modeling routing, Muskingum routing was selected as the appropriate routing model for the study as it would do both attenuation and lag at the same time with fewer parameters associated with the model. The parameters associated with the model are Muskingum *K* (hrs) and Muskingum *X*. The number of sub reaches is assumed to be 1 and adjusted during the calibration process. Muskingum *K* is calculated using the reach length which is divided by the velocity of a flood wave in the reach. In the case of Muskingum *X*, it is first assumed to be 0.25 and then adjusted further in the calibration process.

5.2.6 Model Warmup

Any model developed requires some period to adjust itself to reach an optimal state after which the model would respond naturally adhering to the parameters. This initial process of a model run is called a model warmup. The model warmup is performed for around three (3) month period and the model delivered a good response as shown in Figure 5-6. After the successful warmup of the model, the model is now ready for the simulation of the events selected earlier in Section 0.

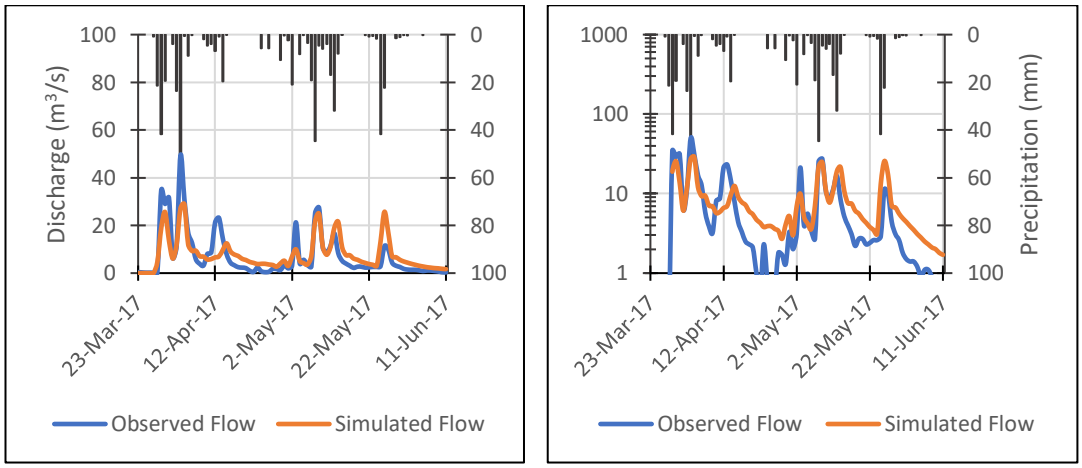

Figure 5-6: Simulated vs observed discharge a) normal plot, b) semi-log plot during the warmup period

5.2.7 Sensitivity Analysis

Sensitivity analysis involves measuring the effect of a parameter on the simulation process. The sensitivity analysis was performed while changing every parameter by

10 % and the lower and upper limit was ±50 %. While changing the parameters, simulated volume was noted and then compared with the simulated volume of the base parameters.

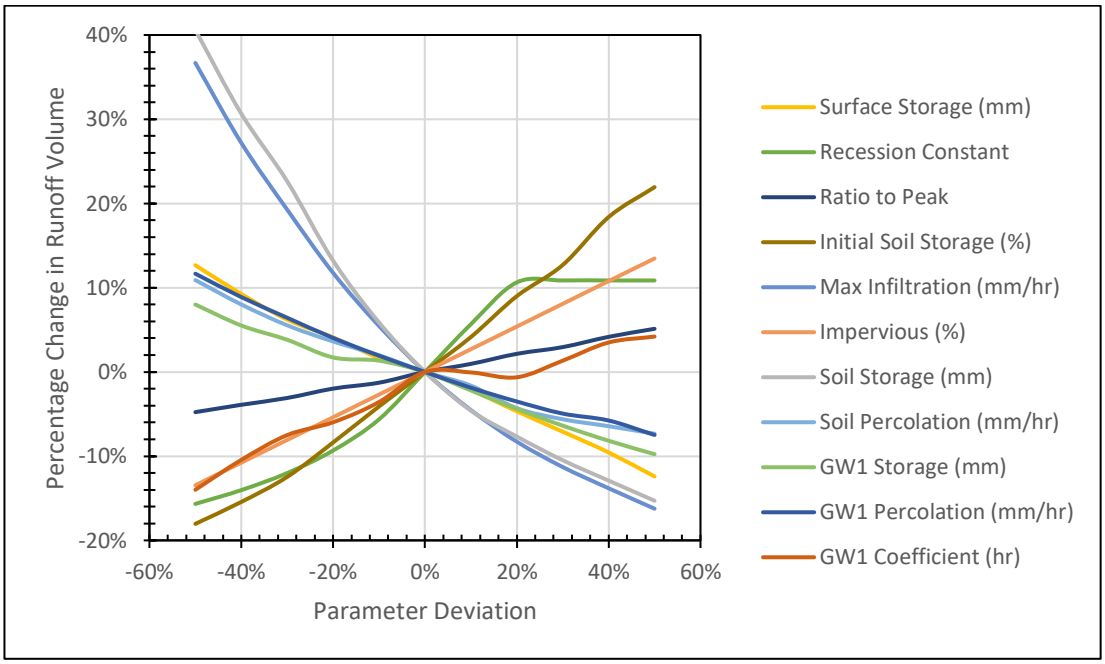

Figure 5-7: Sensitivity analysis of parameters in Kirindi Oya basin

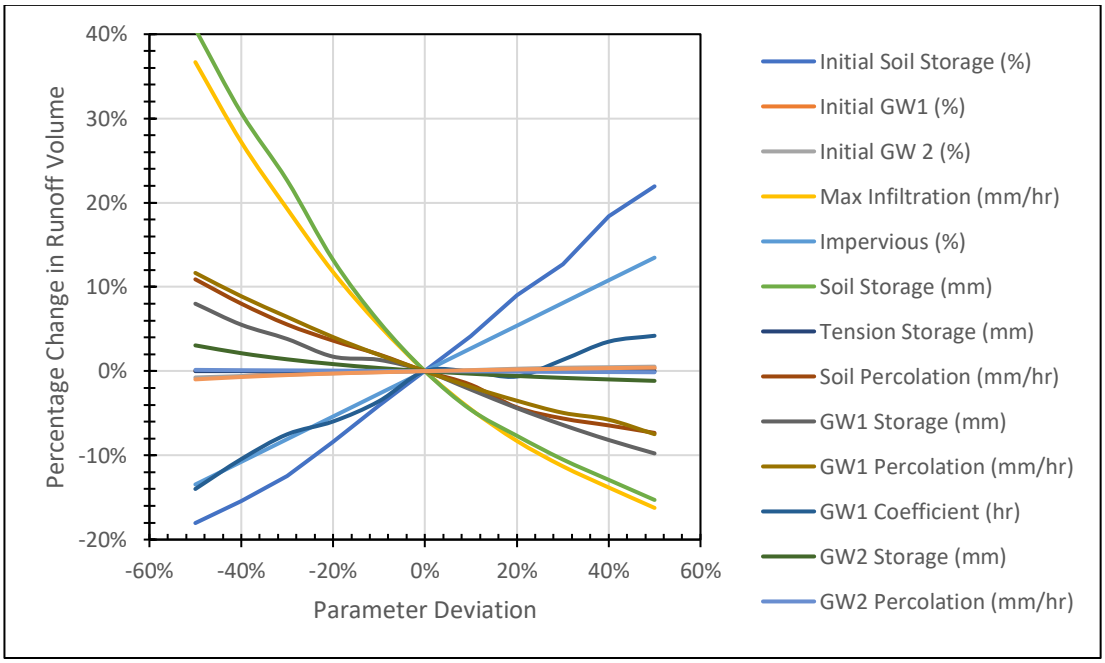

Figure 5-8: Sensitivity analysis of SMA parameters in Kirindi Oya

Table 5-9: Sensitivity ranking of model parameters in Kirindi Oya

Model	Parameters	Sensitivity Slope	Ranking
SMA	Soil Storage (mm)	56%	1
SMA	Max Infiltration (mm/hr)	53%	2
SMA	Initial Soil Storage (%)	40%	3
SMA	Impervious (%)	27%	4
Recession	Recession Constant	27%	5
Surface	Surface Storage (mm)	25%	6
SMA	GW1 Percolation (mm/hr)	19%	7
SMA	Soil Percolation (mm/hr)	18%	8
SMA	GW1 Coefficient (hr)	18%	9
SMA	GW1 Storage (mm)	18%	10
Recession	Ratio to Peak	10%	11
SMA	GW2 Storage (mm)	4%	12
Muskingum	Muskingum K (hr)	4%	13
Surface	Initial surface Storage (%)	2%	14
Canopy	Canopy Storage (mm)	2%	15
SMA	GW2 Coefficient (hr)	1%	16
SMA	Initial GW 2 (%)	1%	17
Canopy	Initial Canopy Storage (%)	1%	18
SMA	Initial GW1 (%)	0%	19
SMA	GW2 Percolation (mm/hr)	0%	20
Muskingum	Muskingum X	0%	21
SCS Transform	Lag Time (min)	0%	22
SMA	Tension Storage (mm)	0%	22

The most sensitive parameters were observed to be soil storage, maximum infiltration, initial soil storage, and impervious area. When parameters are ranked according to sensitivity analysis, the top 4 sensitive parameters are from the SMA model, followed by recession constant from the baseflow model and surface storage from the surface model. The ranking of the parameters according to their sensitivity to model results is shown in Table 5-9.

5.3 Kalu Ganga Basin

First of all, terrain data is loaded into the HEC-HMS model and then a basin model is developed with three (3) sub-basins and one (1) reaches.

Figure 5-9: Kalu Ganga basin model with sub-basins developed in HEC-HMS

5.3.1 Canopy and Surface Storage

The canopy and surface storage values for the sub-basin were obtained complying with the process explained in Section 5.2.1. The canopy raster map for the Kalu Ganga basin obtained by classifying different land use categories is as shown in Figure 5-10 below.

The surface storage calculated processing a terrain slope obtained from the digital elevation model (DEM) using ArcGIS is obtained as shown in Figure 5-11.

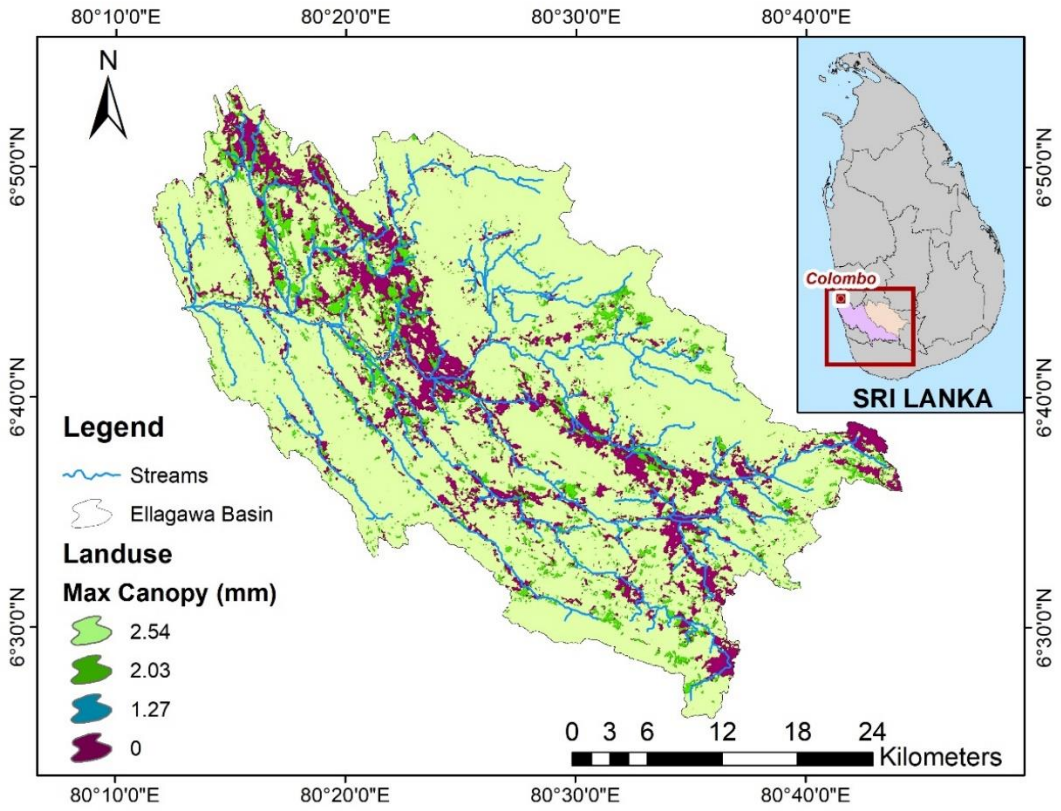

Figure 5-10: Canopy storage in the Kalu Ganga basin

The summary of canopy storage and surface storage for sub-basins in Kalu Ganga used as input in the model is mentioned in Table 5-10.

Table 5-10: Values of canopy storage and surface storage in Kalu Ganga basin

Sub Basin	Canopy Storage (mm)	Surface Storage (mm)
Sub Basin 1	2.32	18.17
Sub Basin 2	2.03	25.89
Sub Basin 3	2.11	47.70

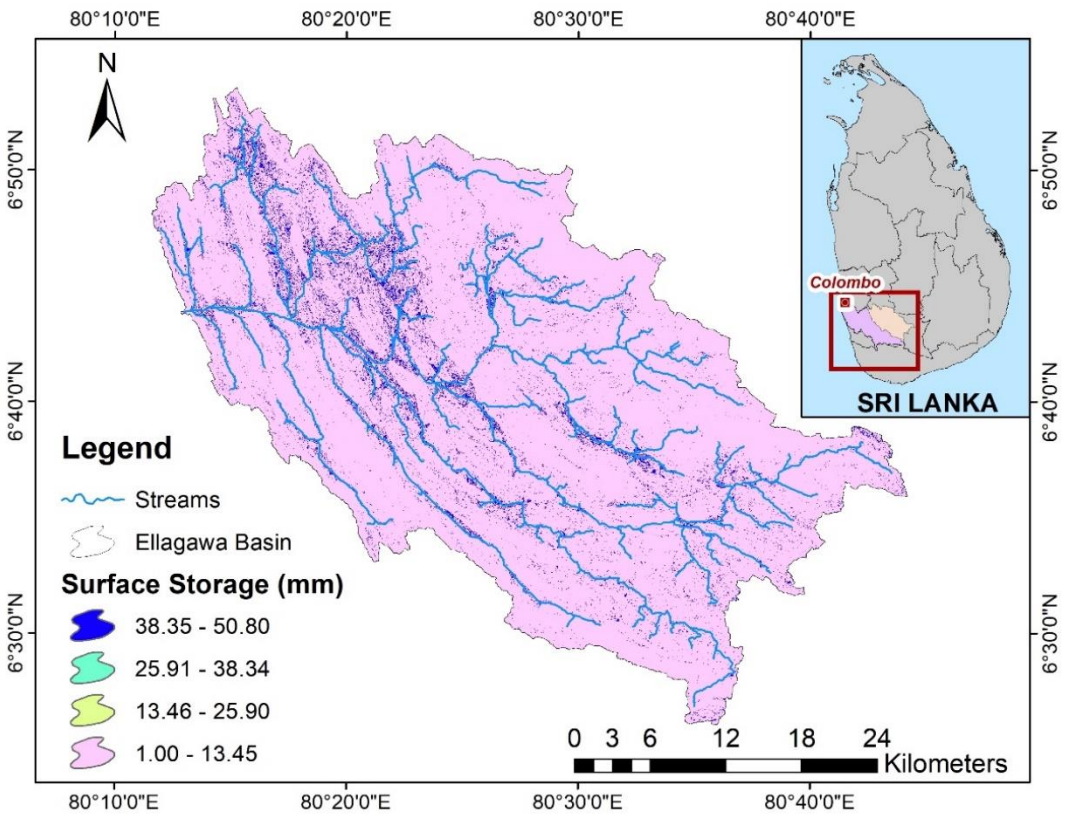

Figure 5-11: Surface storage in the Kalu Ganga basin

5.3.2 Soil Moisture Accounting Loss Method

The parameters related to SMA have been estimated referring to Section 5.2.2. The parameters calculated are listed in the succeeding sub-sections below. Other remaining parameters mentioned in Annexure 2 are obtained during the calibration process.

5.3.2.1 Top Soil Layer

The topsoil layer consists of storage and conveyance parameters which will simultaneously store water and then relay it to the lower soil layers depending on the saturation level of lower layers. The calculated parameters for the topsoil layer are as presented in Table 5-11. The values of maximum infiltration obtained was around 5 mm/hr and soil storage was around 284 mm with a maximum impervious area of 16% in Sub-basin 3.

Table 5-11: Topsoil layer physical parameters for Kalu Ganga basin

Sub Basin	Maximum Infiltration (mm/hr)	Soil Storage (mm)	Impervious Area
Sub Basin 1	5.80	284.82	3.95%
Sub Basin 2	5.69	284.43	9.47%
Sub Basin 3	5.74	285.09	15.19%

5.3.2.2 Groundwater 1 and Groundwater 2 Layers

The parameters associated with Groundwater 1 and Groundwater 2 layers are calculated using streamflow recession analysis as suggested by Bennett and Peters (2004) and the procedure explained in Section 5.2.2.

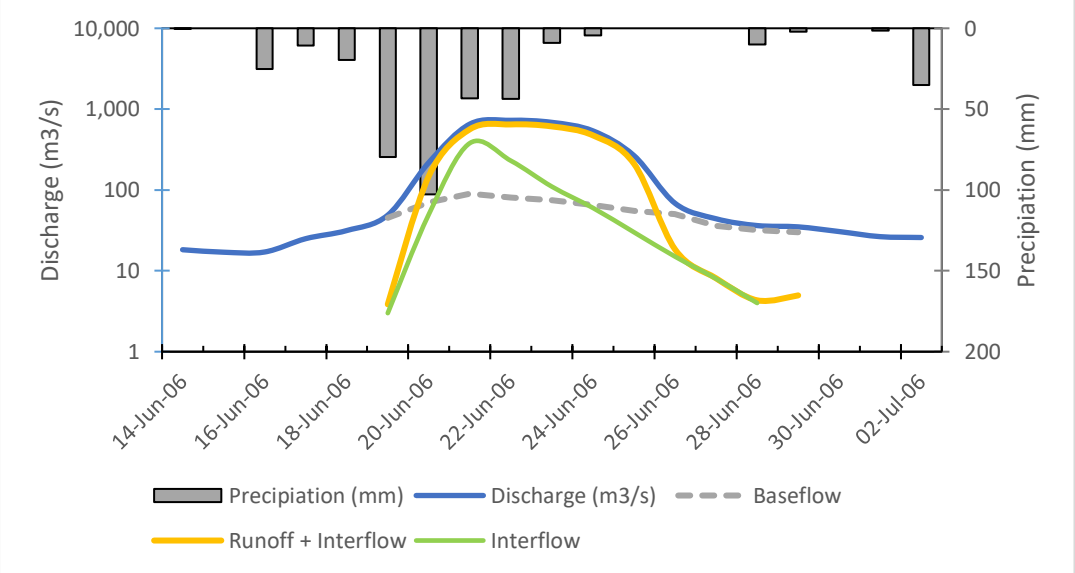

Figure 5-12: Streamflow recession analysis for the year 2006 in Kalu Ganga Basin

The parameters obtained are listed in Table 5-12 where average GW1 and GW2 storage values are 176 and 475 mm, respectively. The GW1 constant was obtained to be 1.4 hr and the GW2 constant to be 7 hr.

Table 5-12: Groundwater layers parameters obtained from streamflow recession analysis

S.N	Time Period		GW1 Storage (mm)	GW1 Constant (hr)	GW2 Storage (mm)	GW2 Constant (hr)
	From	To				
1	4/13/1999	5/5/1999	138.54	1.32	744.13	9.79
2	6/14/2006	7/2/2006	112.80	1.54	499.44	7.28
3	4/19/2008	5/13/2008	430.87	1.88	433.15	6.50
4	5/7/2013	5/19/2013	22.45	0.69	222.32	4.15
		Average	**176.16**	**1.36**	**474.76**	**6.93**

5.3.3 SCS Unit Hydrograph Transform

Time of concentration is calculated using the Kirpich equation as explained in Section 2.4.3. Required channel flow length and main channel slope were obtained from the sub-basin characteristics window of the HEC-HMS model. Time of concentration calculated from the Kirpich equation is then relayed to the basin lag time by dividing t_c by 1.67. The maximum lag time obtained for the basin is 2,069 min for the Sub-basin 3.

5.3.4 Development of Baseflow and Routing Model

Recession constant and ratio to peak parameters are calculated from streamflow recession analysis of observed streamflow data. The calculated parameters are listed in Table 5-13. Muskingum *K* is calculated using the reach length which is divided by the velocity of a flood wave in the reach. In the case of Muskingum *X*, it is first assumed to be 0.25 and then adjusted further in the calibration process.

Table 5-13: Calculation of recession parameters for Kalu Ganga through streamflow recession analysis

S.N.	Period		Recession constant (*k*)	Ratio to peak
	From	To		
1	4/13/1999	5/5/1999	0.9132	0.0692
2	6/2/2006	7/2/2006	0.9457	0.0941
3	4/19/2008	5/13/2008	0.8616	0.0550
4	5/7/2013	5/19/2013	0.8488	0.1241
	Average		**0.8923**	**0.0856**

5.3.5 Model Warmup

The model warmup is carried out for 1 year and the model delivered a good response as shown in Figure 5-13. After the successful warmup of the model, the model is now ready for the simulation of the events selected for the simulation.

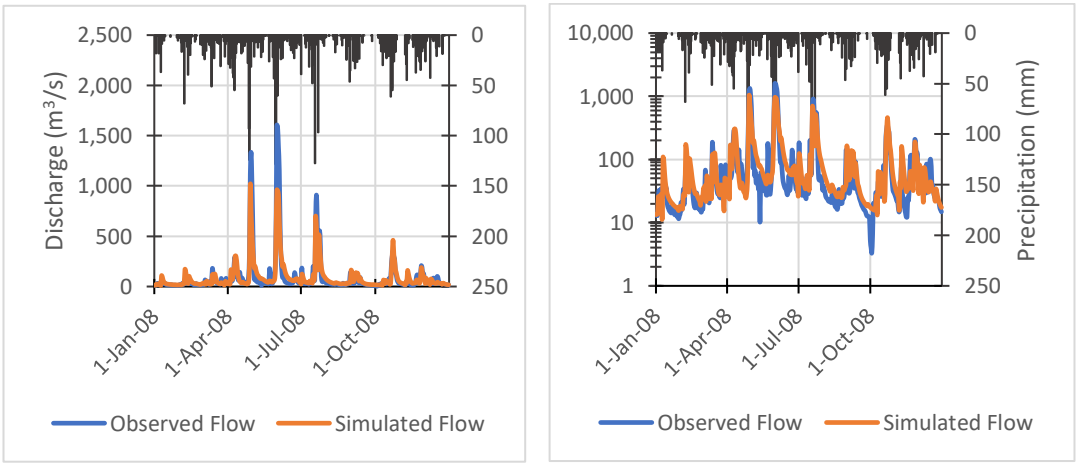

a) b)

Figure 5-13: Simulated vs observed discharge a) normal plot, b) semi-log plot during the warmup period

CHAPTER 6

6 RESULTS AND ANALYSIS

6.1 Kirindi Oya Basin

6.1.1 Model Calibration

Five (5) events selected for the different periods in different seasons (Maha and Yala) are used to calibrate the model performance. Calibration was carried out adjusting the parameters of each sub-basin using the optimization tool available in HEC-HMS. The calibration of all five (5) events yielded satisfactory to very good results in terms of different objective functions as shown in Table 6-1.

Table 6-1: Summary of objective functions during calibration of events in Kirindi Oya

Event Number	Event Code	RMSE std dev	NSE	Percent Bias	R^2
1	1D-56W-Oct/Dec12	0.40	0.80	17.40%	0.84
2	1D-14W-Dec14	0.10	0.99	-2.41%	0.99
3	1D-10W-Nov/Dec05	0.40	0.89	3.04%	0.96
8	3D-12W-Apr/May08	0.60	0.63	-0.24%	0.65
9	7D-11W-Apr/May13	0.50	0.71	0.71%	0.75

The hydrograph of simulated and observed discharge of calibration events are presented along with the flow duration curve (FDC) of simulated and observed discharge in the pages below starting from Figure 6-1 to Figure 6-10 for different events. The calibrated parameters for the events are attached in Annexure 2.

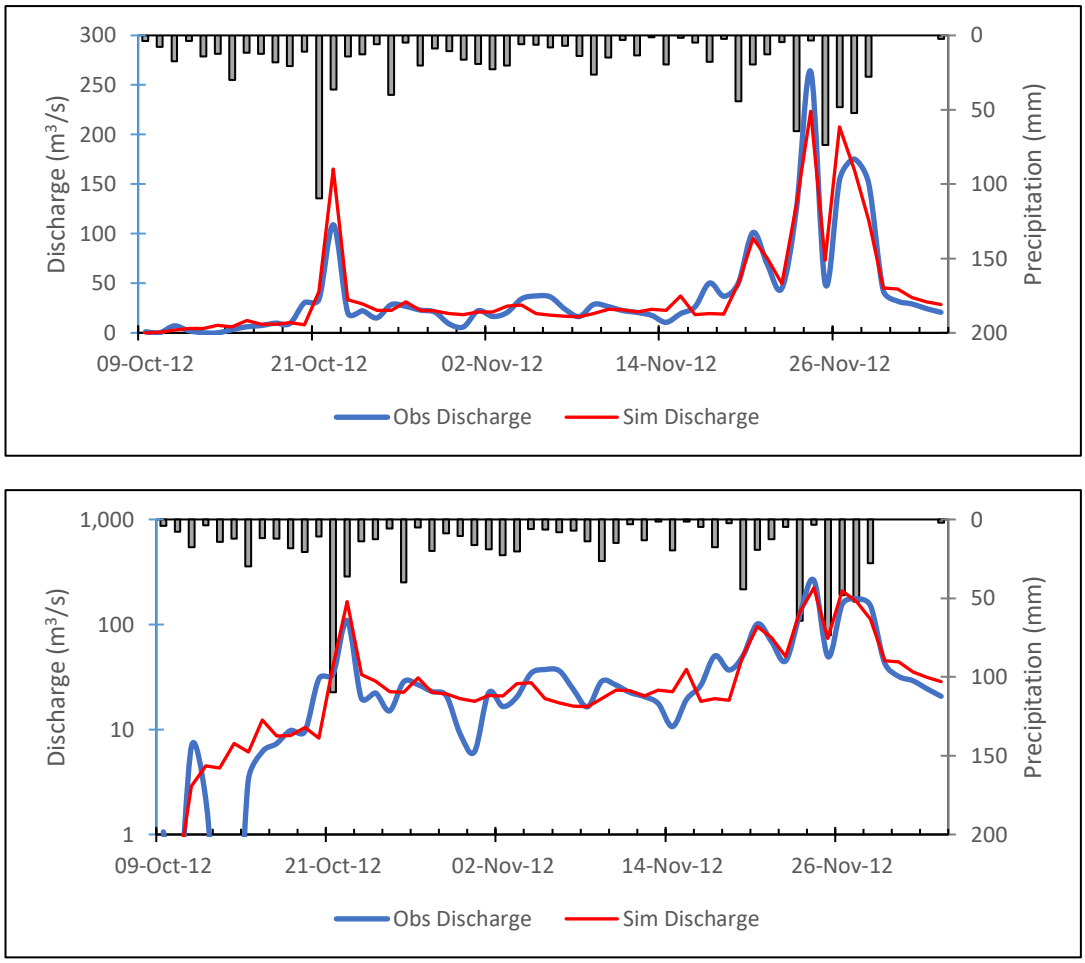

Figure 6-1: Simulated vs observed hydrograph for calibration Event 1 a) normal scale, b) semi-log scale

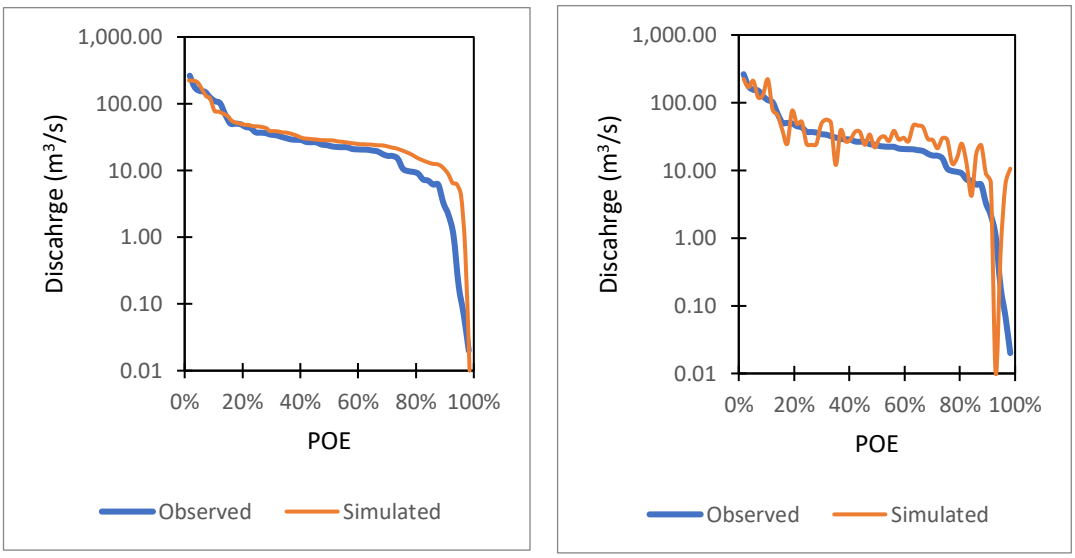

Figure 6-2: Event 1 FDC a) simulated sorted high to low, b) simulated sorted with observed

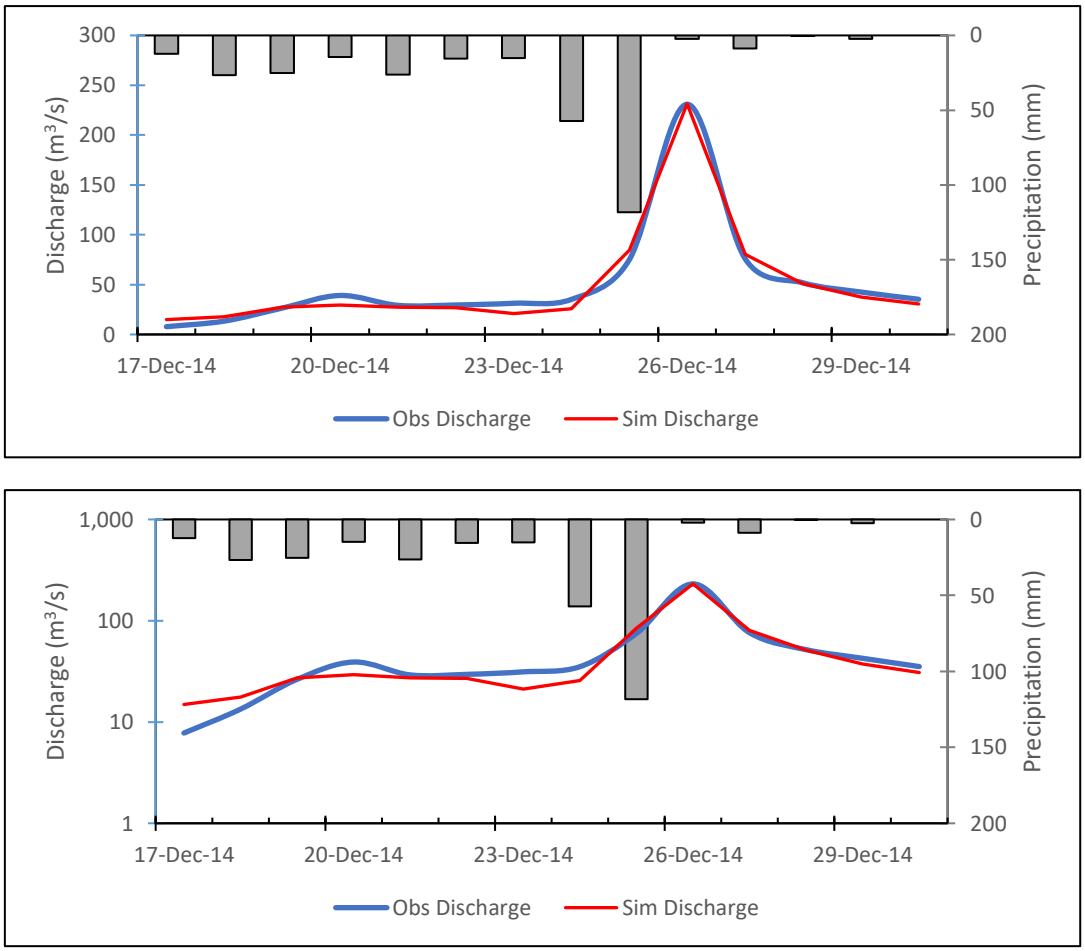

Figure 6-3: Simulated vs observed hydrograph for calibration Event 2 a) normal scale, b) semi-log scale

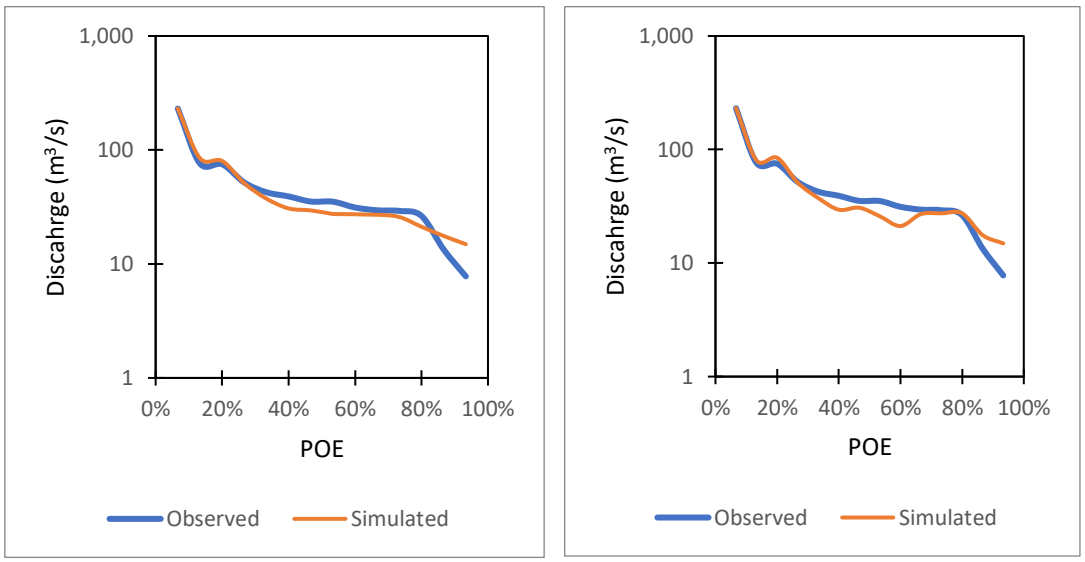

Figure 6-4: Event 2 FDC a) simulated sorted high to low, b) simulated sorted with observed

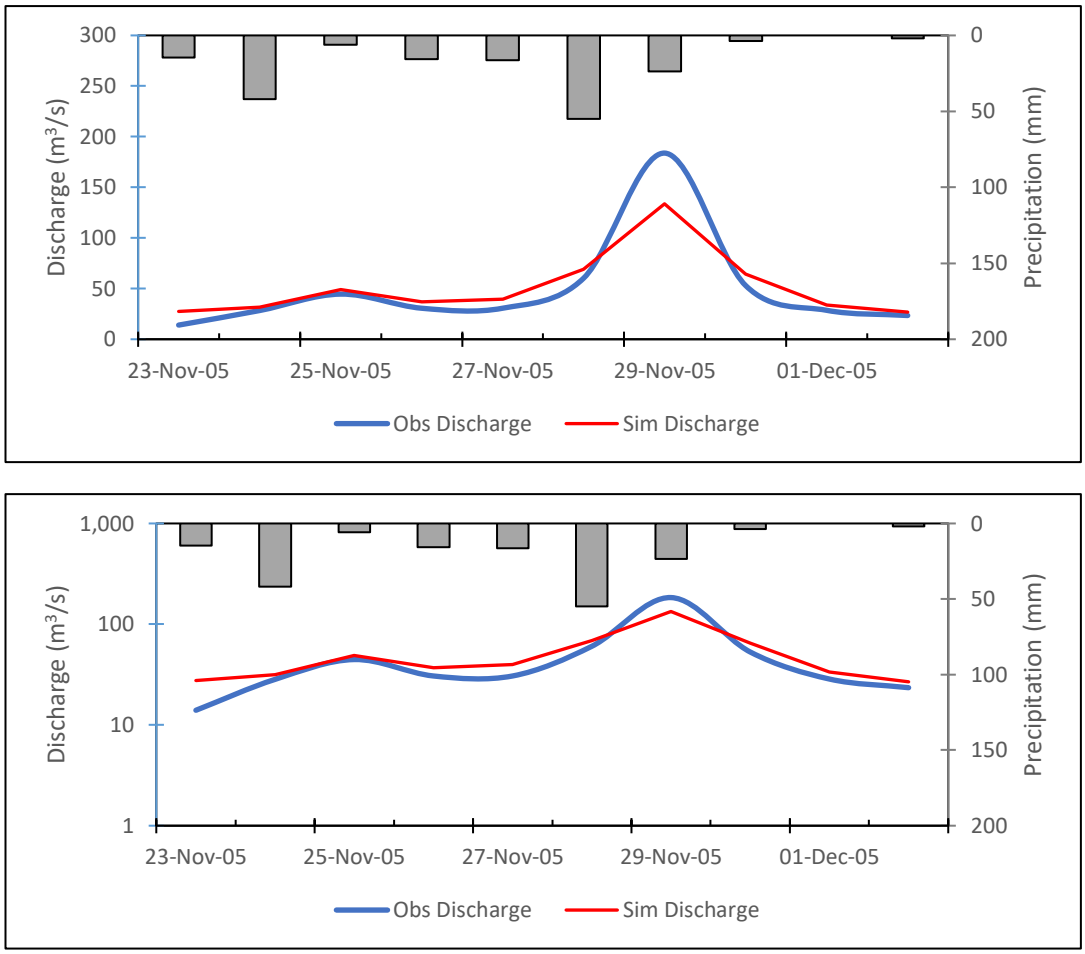

Figure 6-5: Simulated vs observed hydrograph for calibration Event 3 a) normal scale, b) semi-log scale

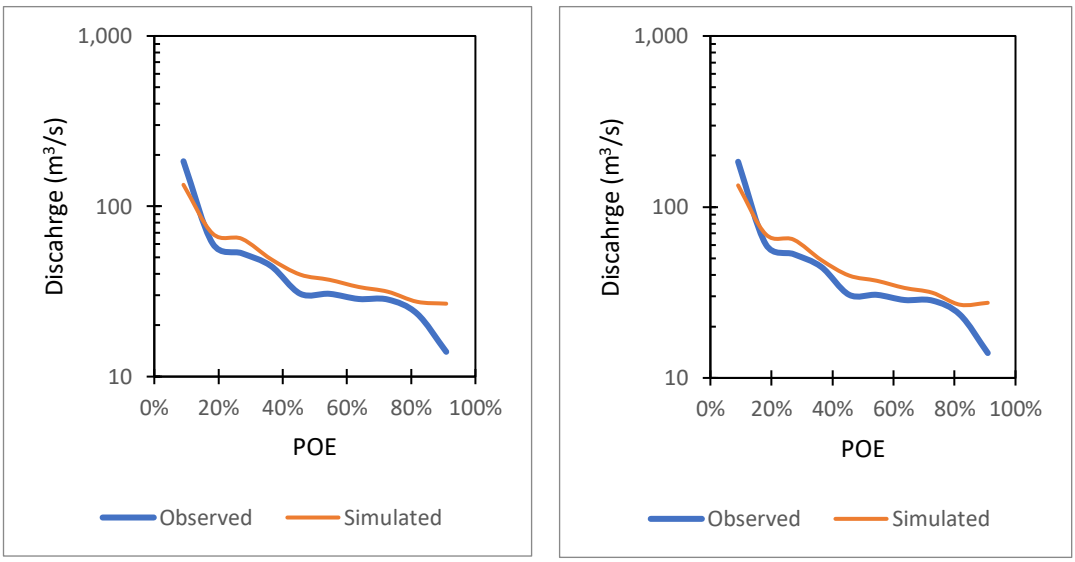

Figure 6-6: Event 3 FDC a) simulated sorted high to low, b) simulated sorted with observed

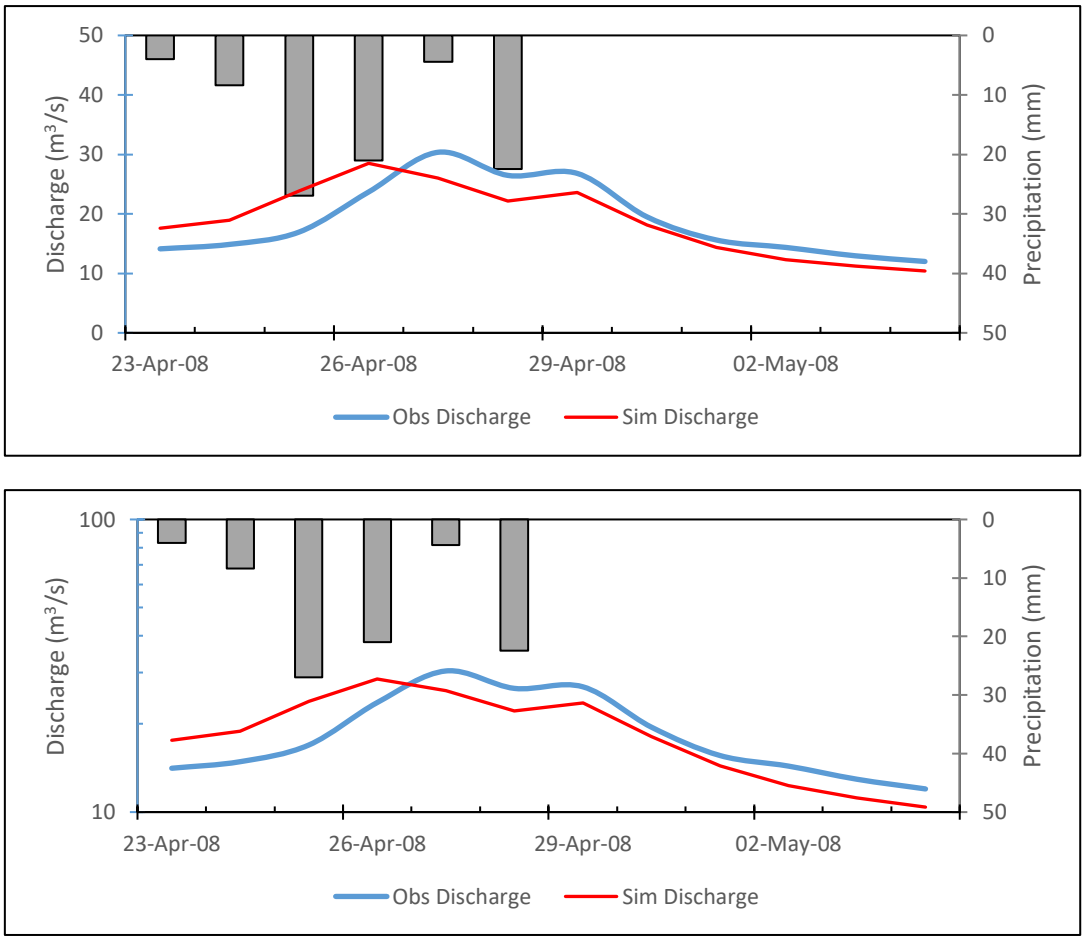

Figure 6-7: Simulated vs observed hydrograph for calibration Event 8 a) normal scale, b) semi-log scale

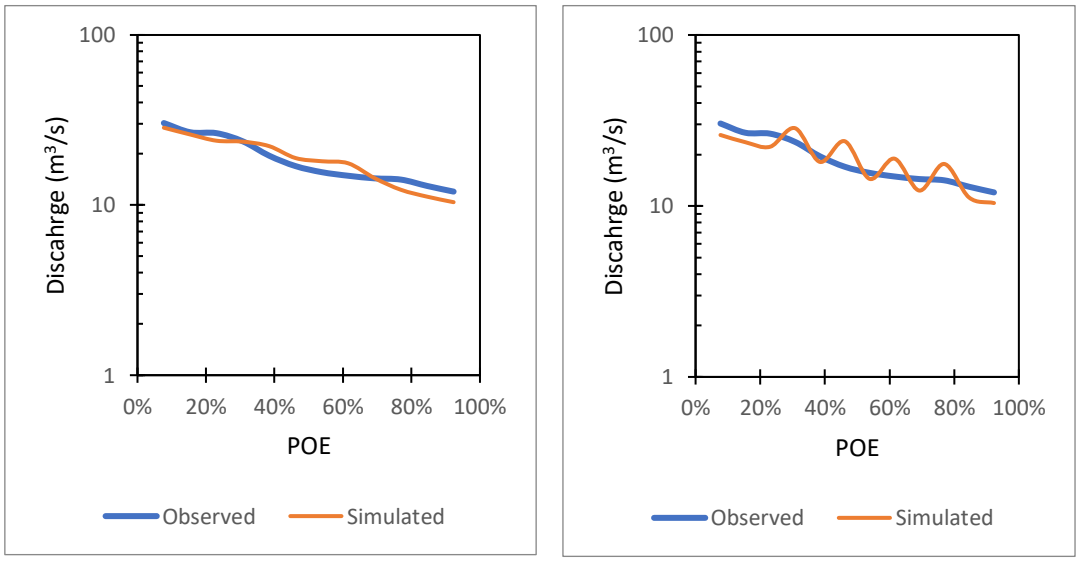

Figure 6-8: Event 8 FDC a) simulated sorted high to low, b) simulated sorted with observed

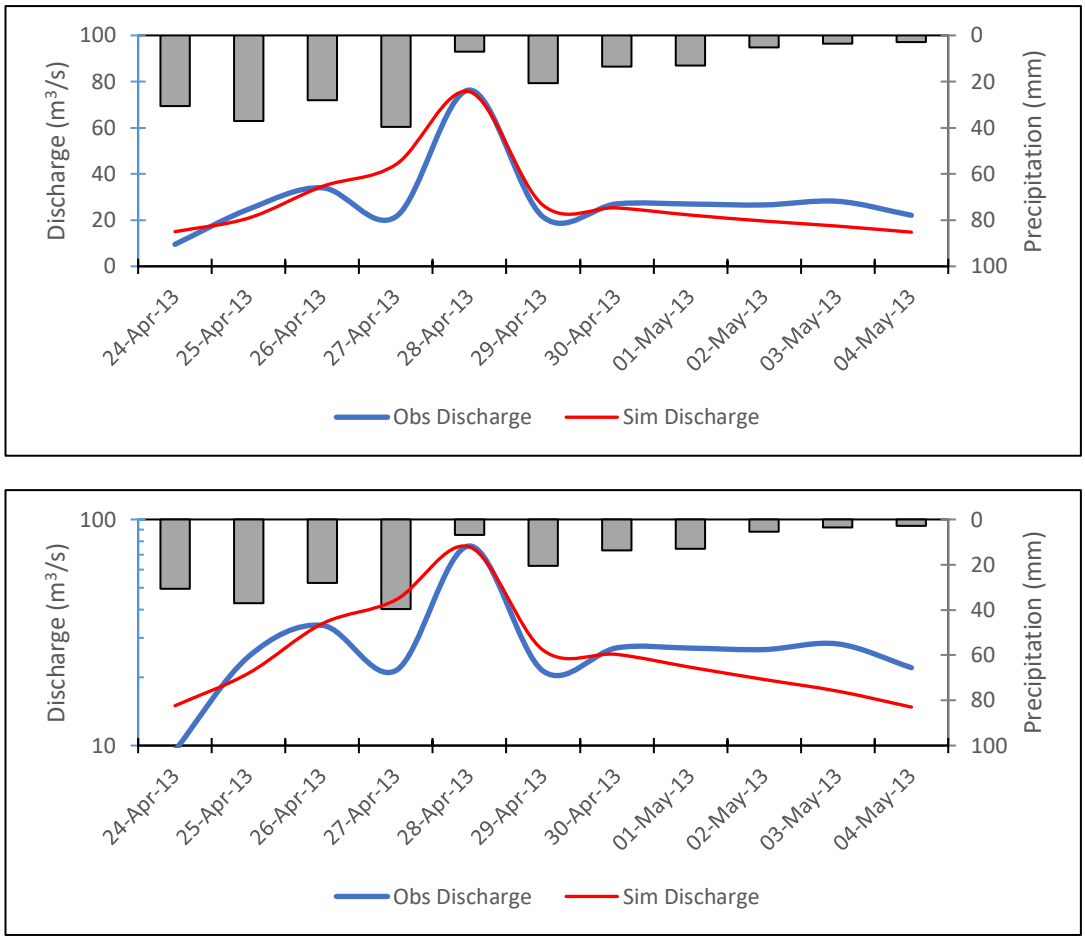

Figure 6-9: Simulated vs observed hydrograph for calibration Event 8 a) normal scale, b) semi-log scale

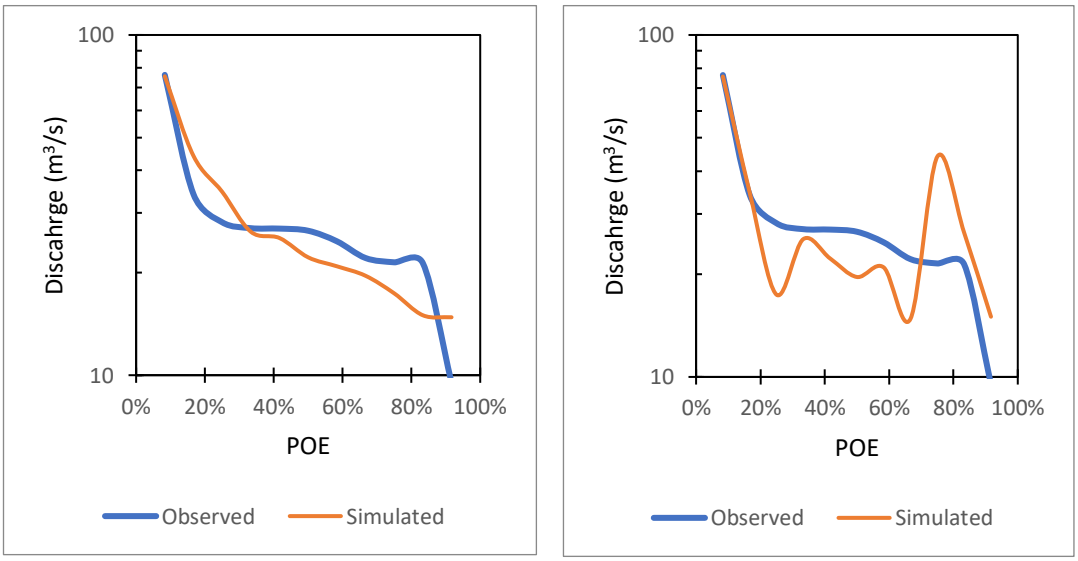

Figure 6-10: Event 9 FDC a) simulated sorted high to low, b) simulated sorted with observed

6.1.2 Model Validation

Four (4) events selected for the validation purpose were simulated in the HEC-HMS model using the optimized parameters obtained during the optimization process. The validation of all four (4) events yielded satisfactory to very good results in terms of different objective functions as presented in Table 6-2. During the validation process, initial soil content, initial groundwater content and initial discharge parameters are varied compared to calibrated parameters since these initial conditions vary with respect to the time of the simulation.

Table 6-2: Summary of objective functions during validation of events in Kirindi Oya

Event Number	Event Code	RMSE std dev	NSE	Percent Bias (%)	R^2
4	1D-13W-Dec17	0.60	0.60	11.17%	0.95
5	2D-31W-Nov/Dec19	0.50	0.76	-5.74%	0.77
6	1D-12W-May16	0.40	0.85	-1.75%	0.96
7	1D-13W-May17	0.40	0.80	7.65%	0.82

The hydrograph of simulated and observed discharge and flow duration curve of observed and simulated discharge (high-low sorted and sorted with observed) of events considered during the validation period is shown in Figure 6-11 to Figure 6-18. The parameters used during validation for the events are attached in Annexure 2. During the simulation, two (2) events underestimated runoff volume while the other two (2) events overestimated the runoff volume of the discharge.

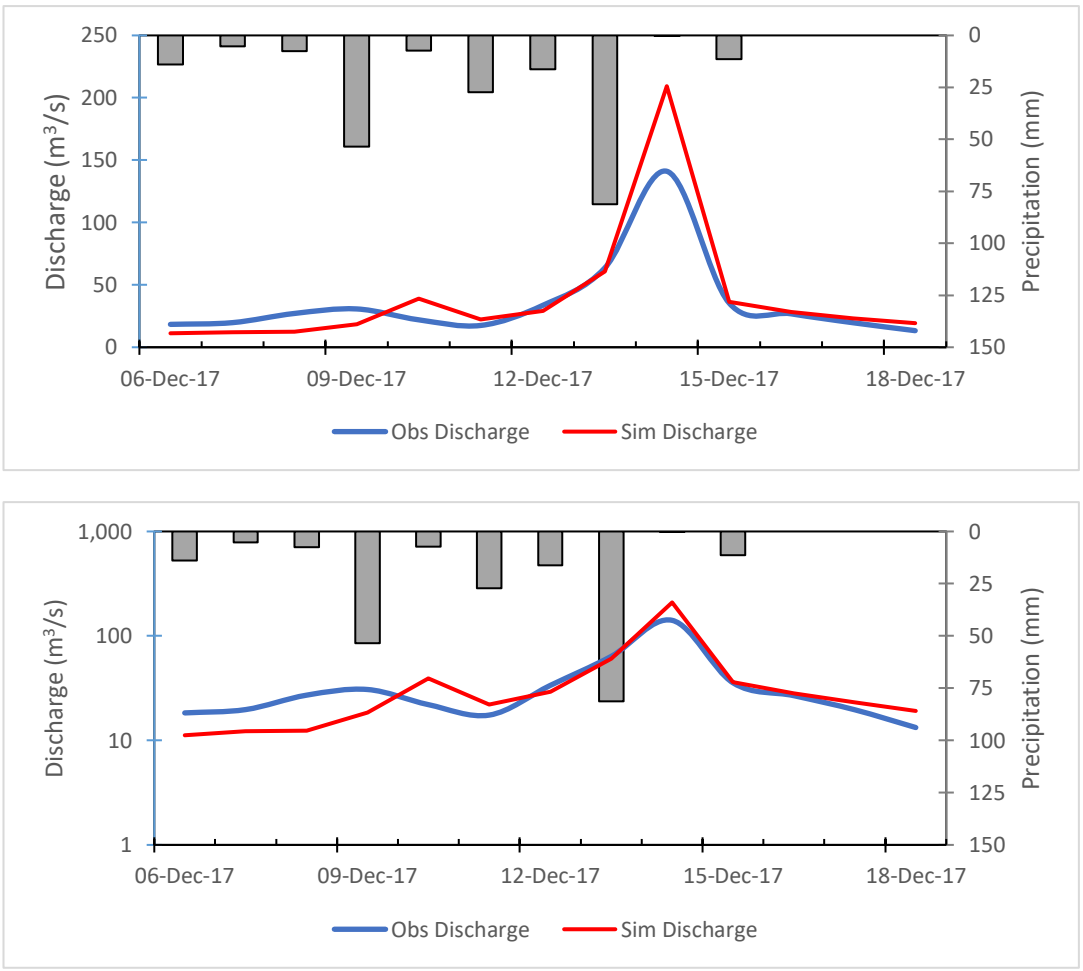

Figure 6-11: Simulated vs observed hydrograph for validation Event 4 a) normal scale, b) semi-log scale

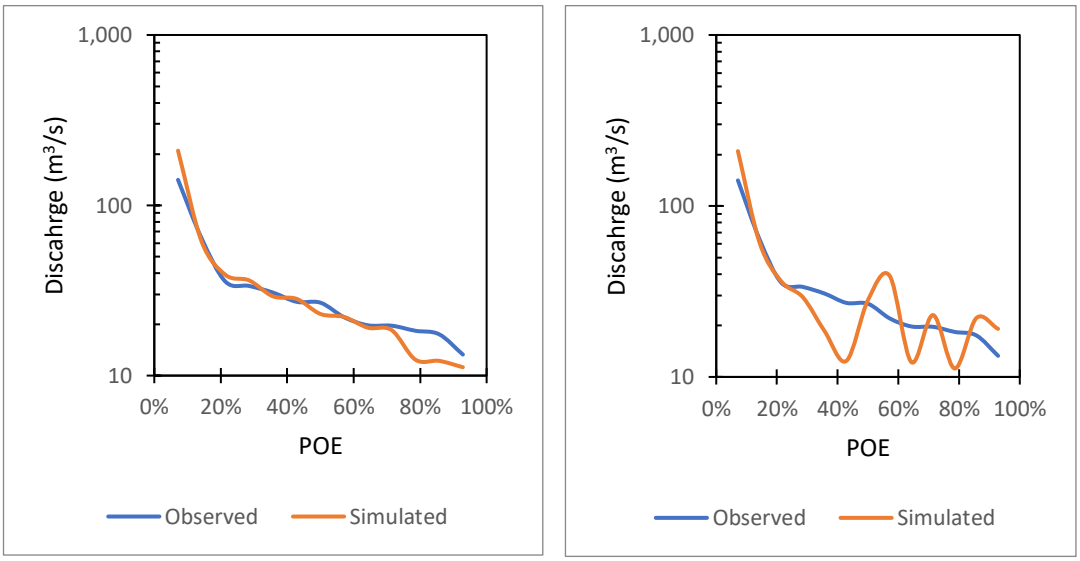

Figure 6-12: Event 4 FDC a) simulated sorted high to low, b) simulated sorted with observed

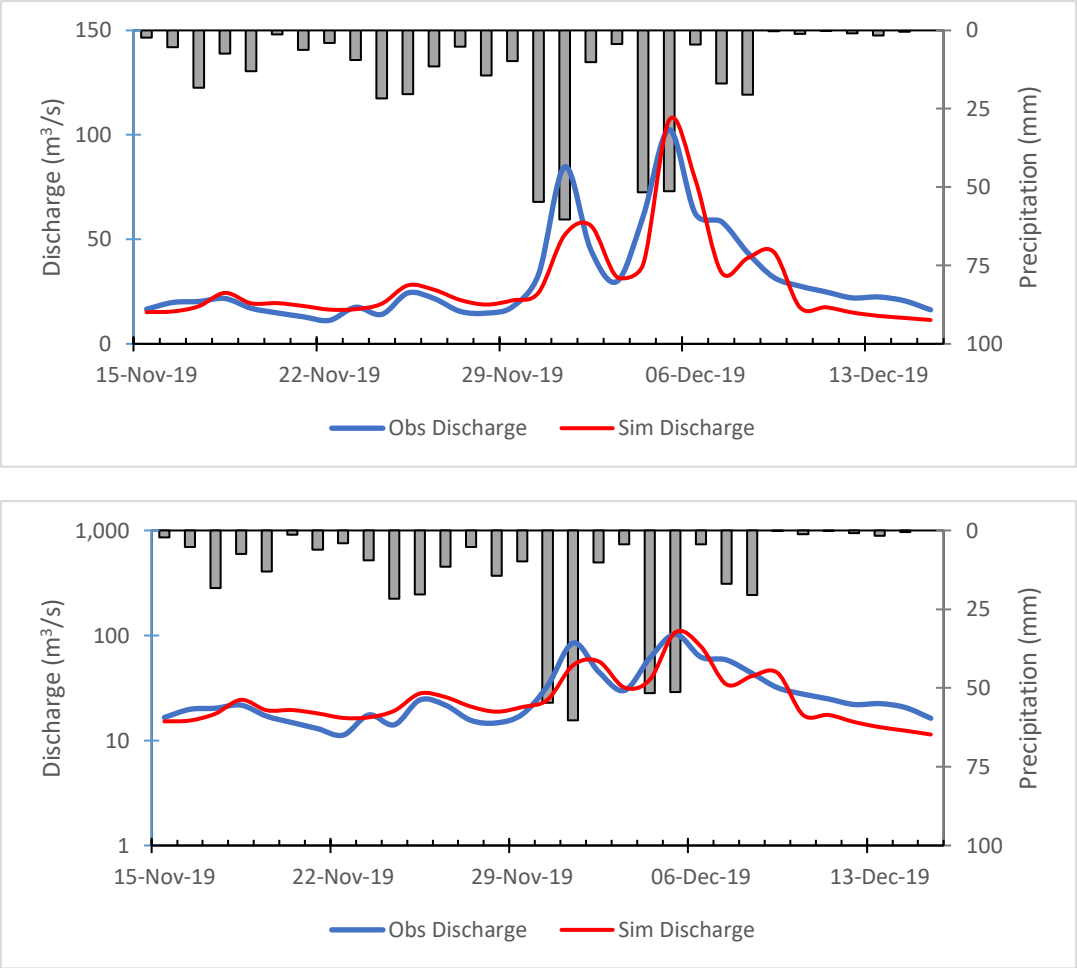

Figure 6-13: Simulated vs observed hydrograph for validation Event 5 a) normal scale, b) semi-log scale

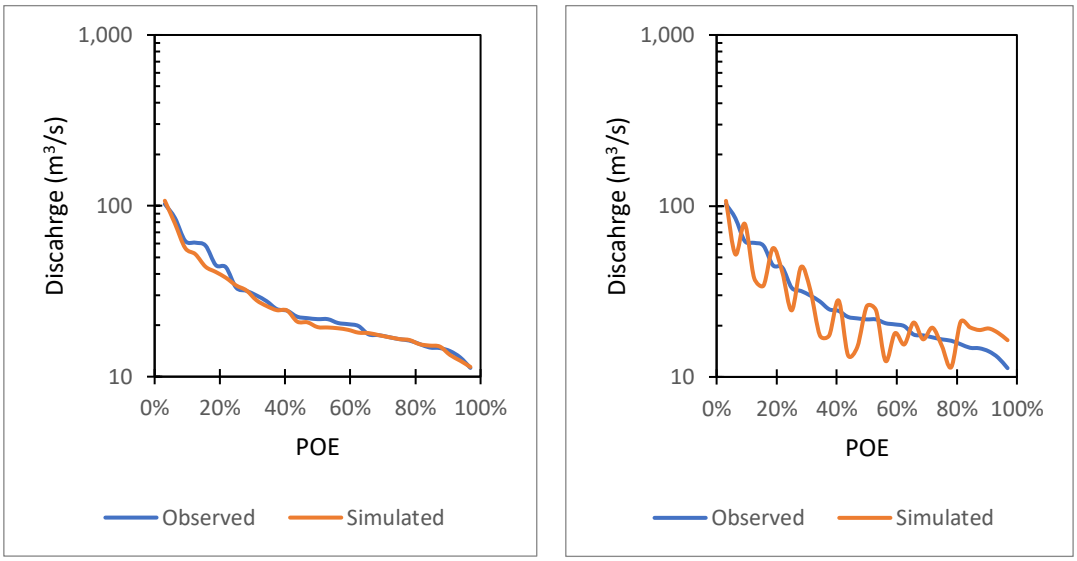

Figure 6-14: Event 5 FDC a) simulated sorted high to low, b) simulated sorted with observed

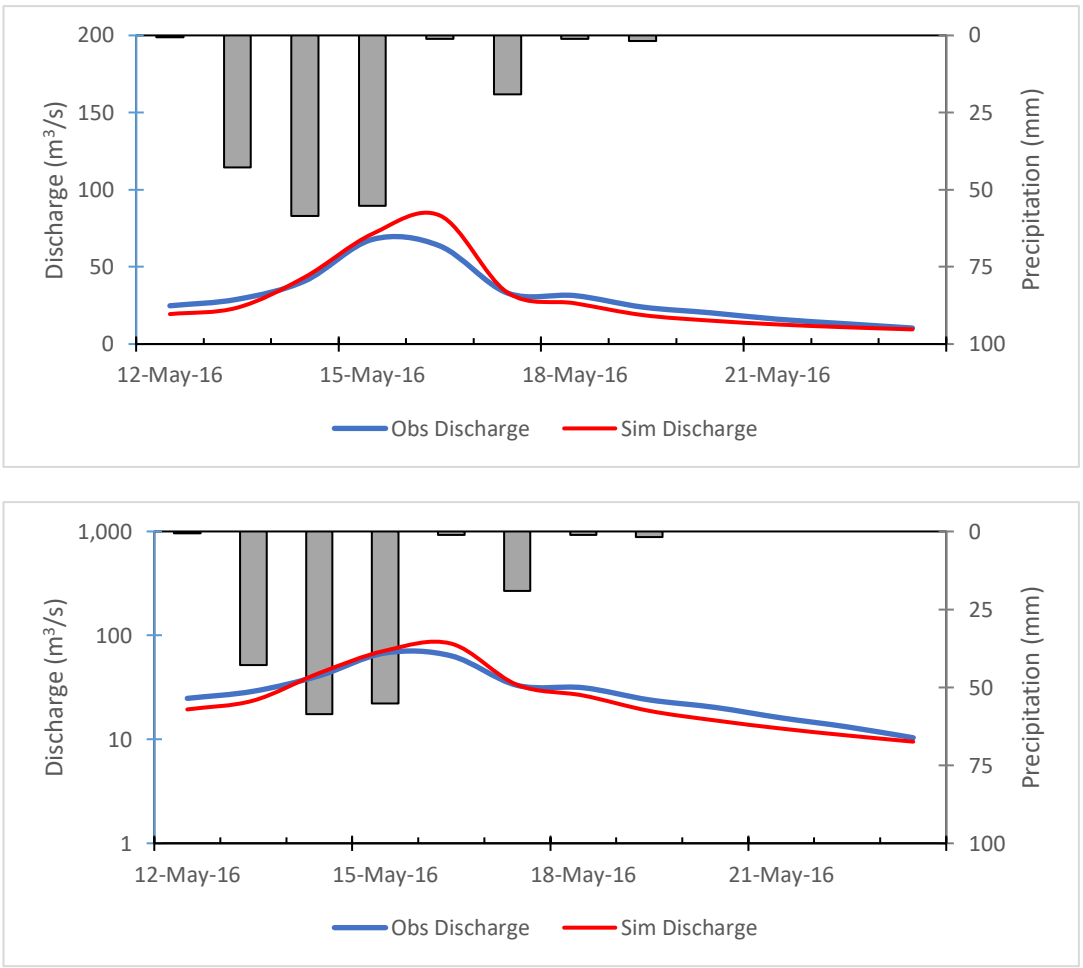

Figure 6-15: Simulated vs observed hydrograph for validation Event 6 a) normal scale, b) semi-log scale

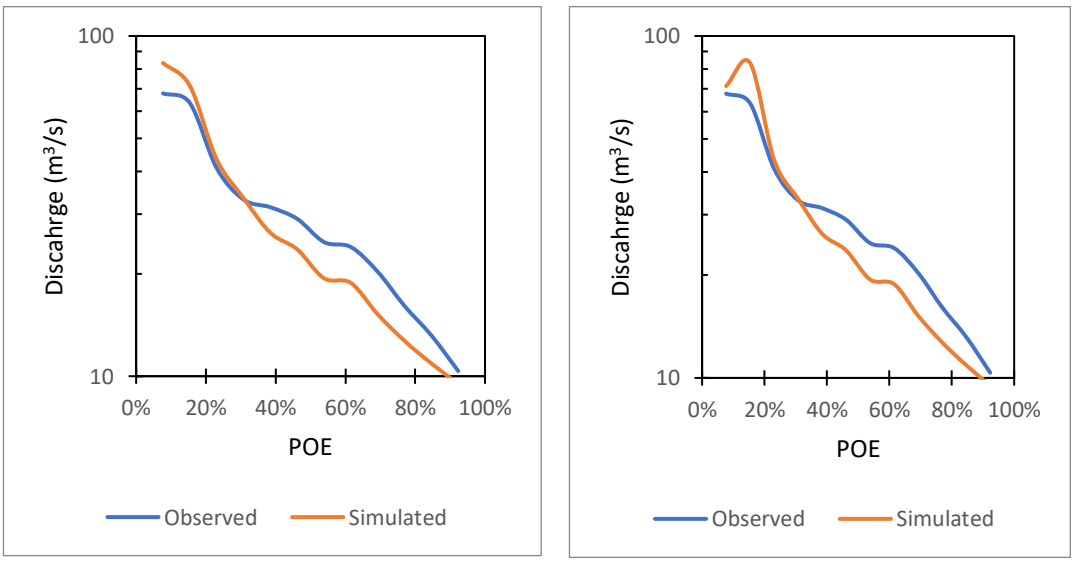

Figure 6-16: Event 6 FDC a) simulated sorted high to low, b) simulated sorted with observed

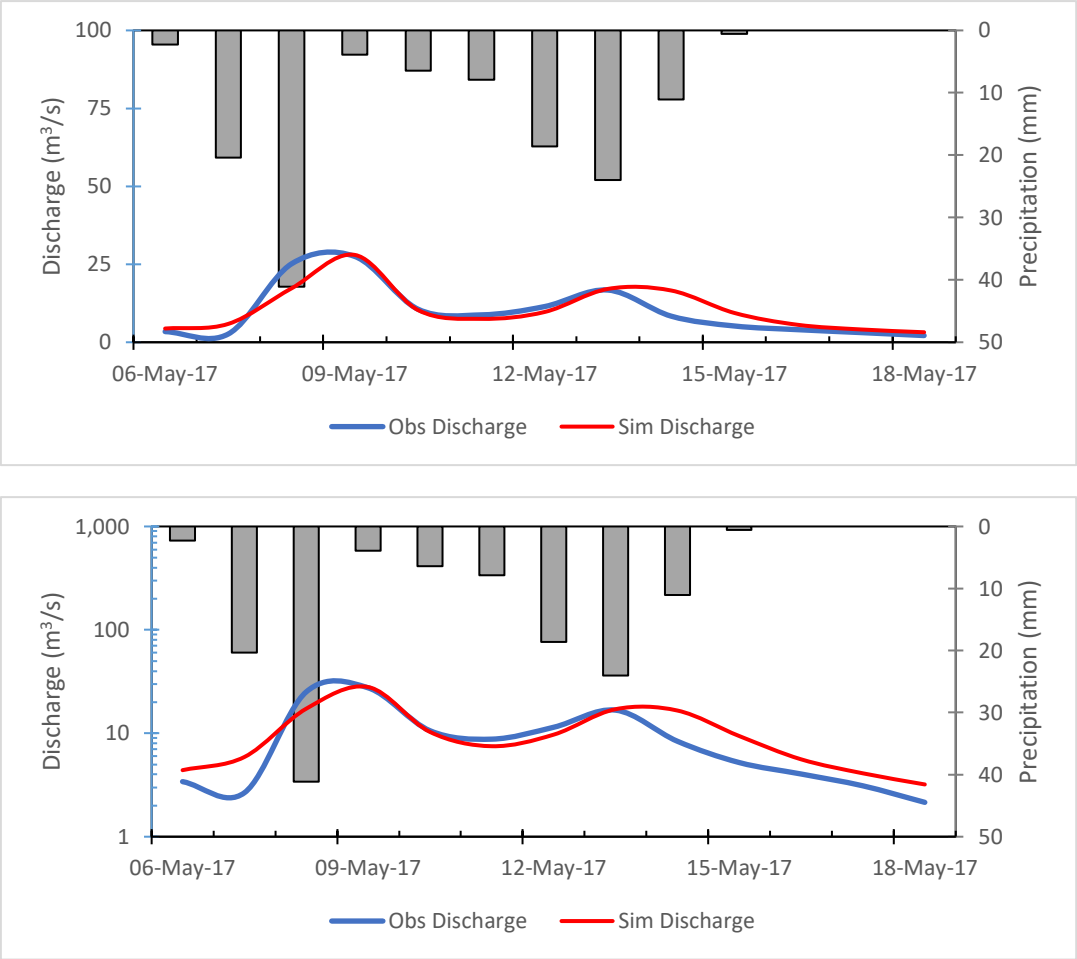

Figure 6-17: Simulated vs observed hydrograph for validation Event 7 a) normal scale, b) semi-log scale

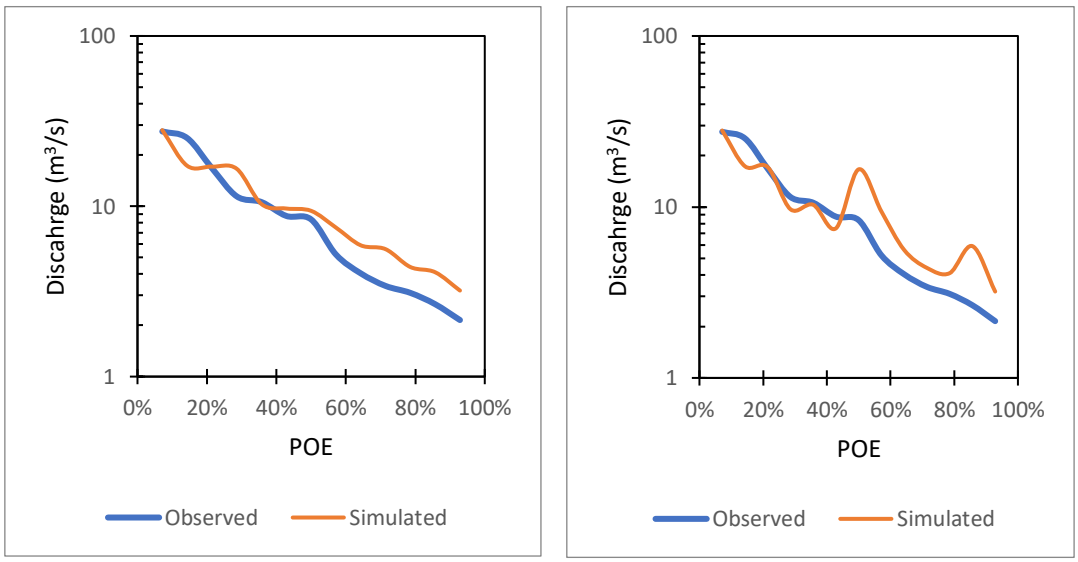

Figure 6-18: Event 7 FDC a) simulated sorted high to low, b) simulated sorted with observed

6.1.3 Validation of Satellite Soil Moisture Data

Four (4) events selected for the validation run were simulated once again with the initial soil moisture parameters derived from the SMAP satellite soil moisture product.

Using the ArcGIS, the gridded soil moisture product was converted to grid points, then was used to overlay with the sub-basin polygons to calculate average soil moisture as presented in Figure 6-19.

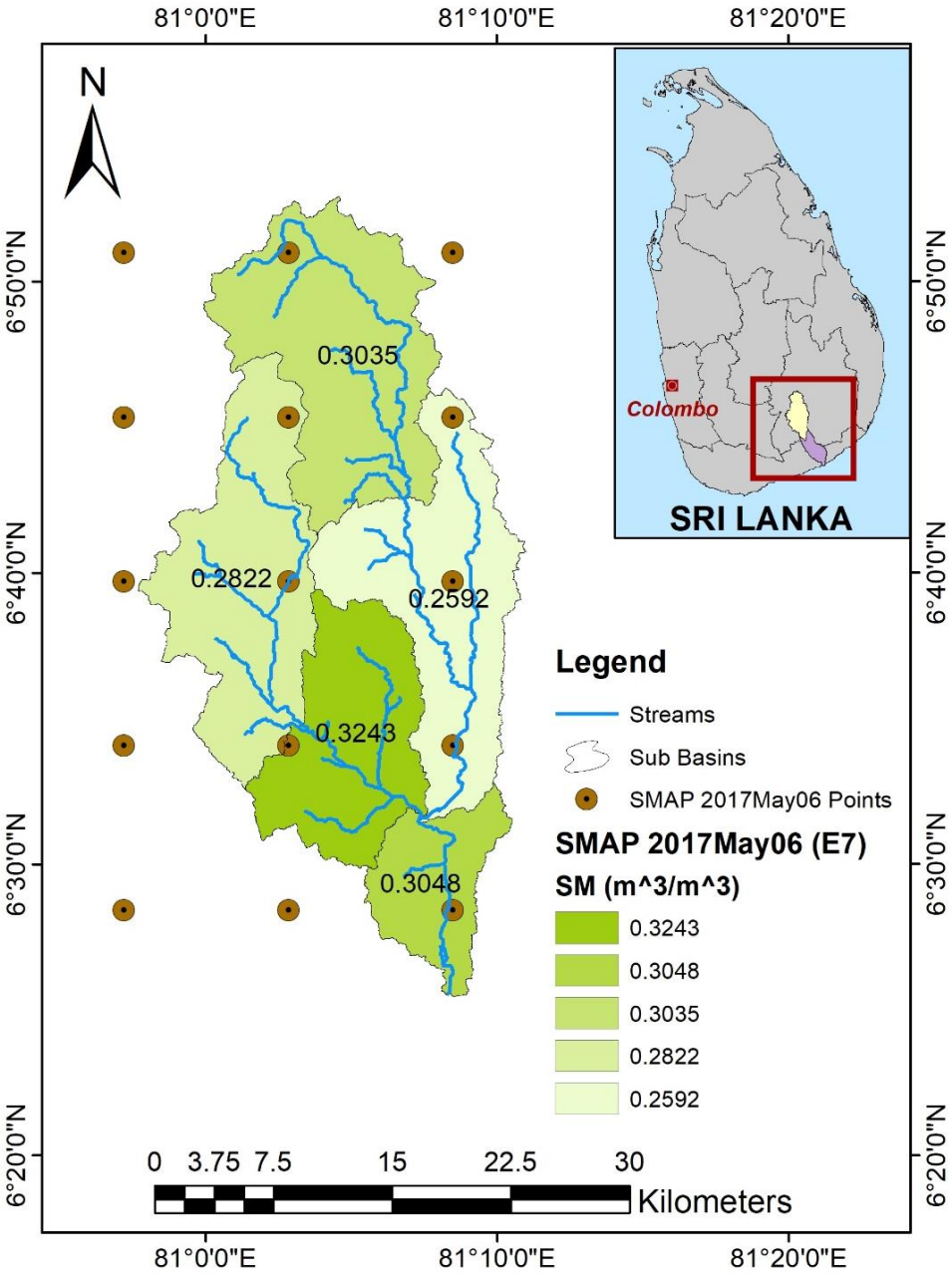

Figure 6-19: SMAP SM grid points and average volumetric soil moisture in sub-basins

The gridded soil moisture data was processed and then average soil moisture in each sub-basin was obtained. The estimated soil moisture ranges between 0.2592 m^3/m^3 and 0.3243 m^3/m^3 over the area for an event of 6th May 2017. The values of soil moisture vary with the time considered which is as presented in Figure 6-20.

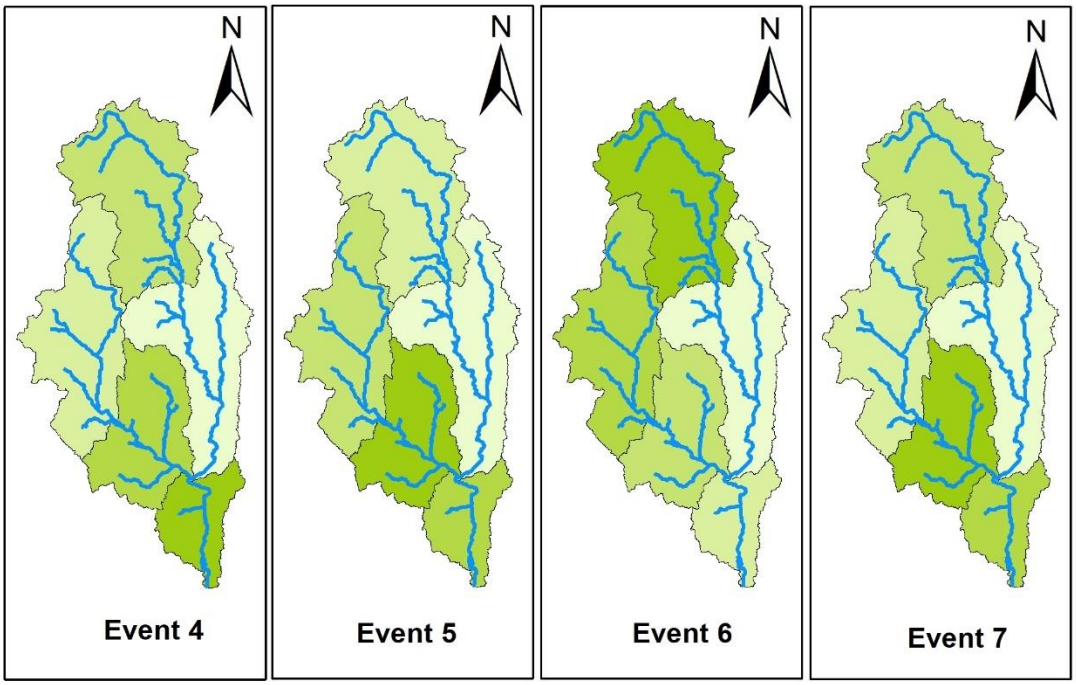

Figure 6-20: Soil moisture value of sub-basins during different events

The SSM data obtained from the satellite was converted to initial soil moisture (%) using Equation [6-1] obtained from Bhuiyan et al. (2017) which utilizes the ratio of volumetric soil moisture and porosity as shown by

$$S = \frac{\theta}{\phi} * 100 \qquad [6\text{-}1]$$

where S is the saturation percentage, θ is the volumetric soil moisture obtained from SMAP data and ϕ is the porosity of the soil. The above mentioned equation is used to calculate the saturation percentage for each sub-basin. The values of saturation percentage (initial soil saturation) obtained for different events are presented in Table 6-3.

Table 6-3: Sub-basin initial soil saturation (%) extracted from SMAP data for different events

Event	Event code	Sub Basin					Average
		1	2	3	4	5	
Event 4	1D-13W-Dec17	89%	81%	85%	87%	82%	**84%**
Event 5	2D-31W-Nov/Dec19	86%	84%	86%	93%	92%	**88%**
Event 6	1D-12W-May16	72%	62%	72%	75%	70%	**70%**
Event 7	1D-13W-May17	68%	57%	62%	71%	67%	**65%**

The initial run with the above-mentioned saturation values overestimated the results of four (4) events allocated to the validation of the model. It can be observed that the initial moisture values obtained from the SMAP SM product are comparatively higher than the moisture values of the calibrated model. The performance of the model indicated below satisfactory results in most of the cases. Summary of the objective functions for the initial run using SSM are presented in Table 6-4. Although, the value of R^2 was obtained greater than 0.80 in all simulations indicating a strong correlation, the runoff volume was highly overestimated with a maximum percentage bias of 44.71 % and a minimum of 7.99 %. This indicates that the soil is saturated and can not take further moisture and pass it to lower layers. The simulated vs. observed hydrographs are presented in Figure 6-21. Bearing this in mind, soil storage and groundwater storage values were optimized to observe a change in the results.

Table 6-4: Summary of the objective functions for the initial run using SSM

Event Number	Event Code	RMSE std dev	NSE	Percent Bias (%)	R^2
4	1D-13W-Dec17	1.00	-0.05	44.71%	0.93
5	2D-31W-Nov/Dec19	0.60	0.66	7.99%	0.81
6	1D-12W-May16	1.20	-0.35	25.75%	0.95
7	1D-13W-May17	0.60	0.68	24.35%	0.80

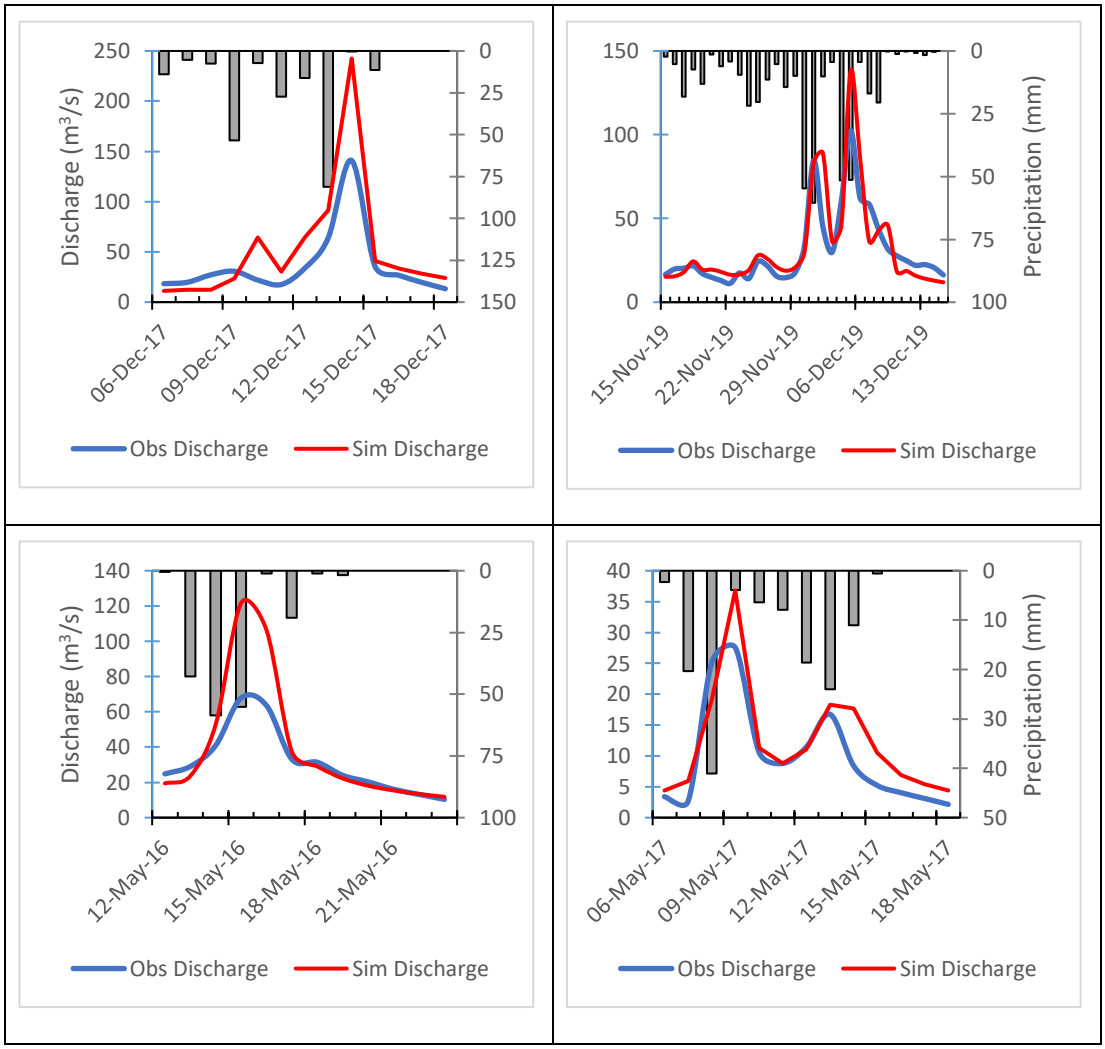

Figure 6-21: Results of the initial run of events with satellite soil moisture

The optimization of the soil Storage and Groundwater 1 (GW1) storage yielded better results compared to the initial run using SSM only. The GW1 storage was increased in all of the events which enhanced the model performance. The RMSE std dev was below 0.4 and NSE was above 0.8 indicating the very good performance of the model. The value of R^2 was obtained greater than 0.81 in all simulations indicating a strong correlation. The overestimated peak discharge was reduced by 28 % (maximum) and the overestimated runoff volume was reduced by 18% (maximum). The objective functions indicated enhanced performance compared to the validation of the model and the summary of objective functions are presented in Table 6-5. The simulated vs. observed hydrographs are presented in Figure 6-22.

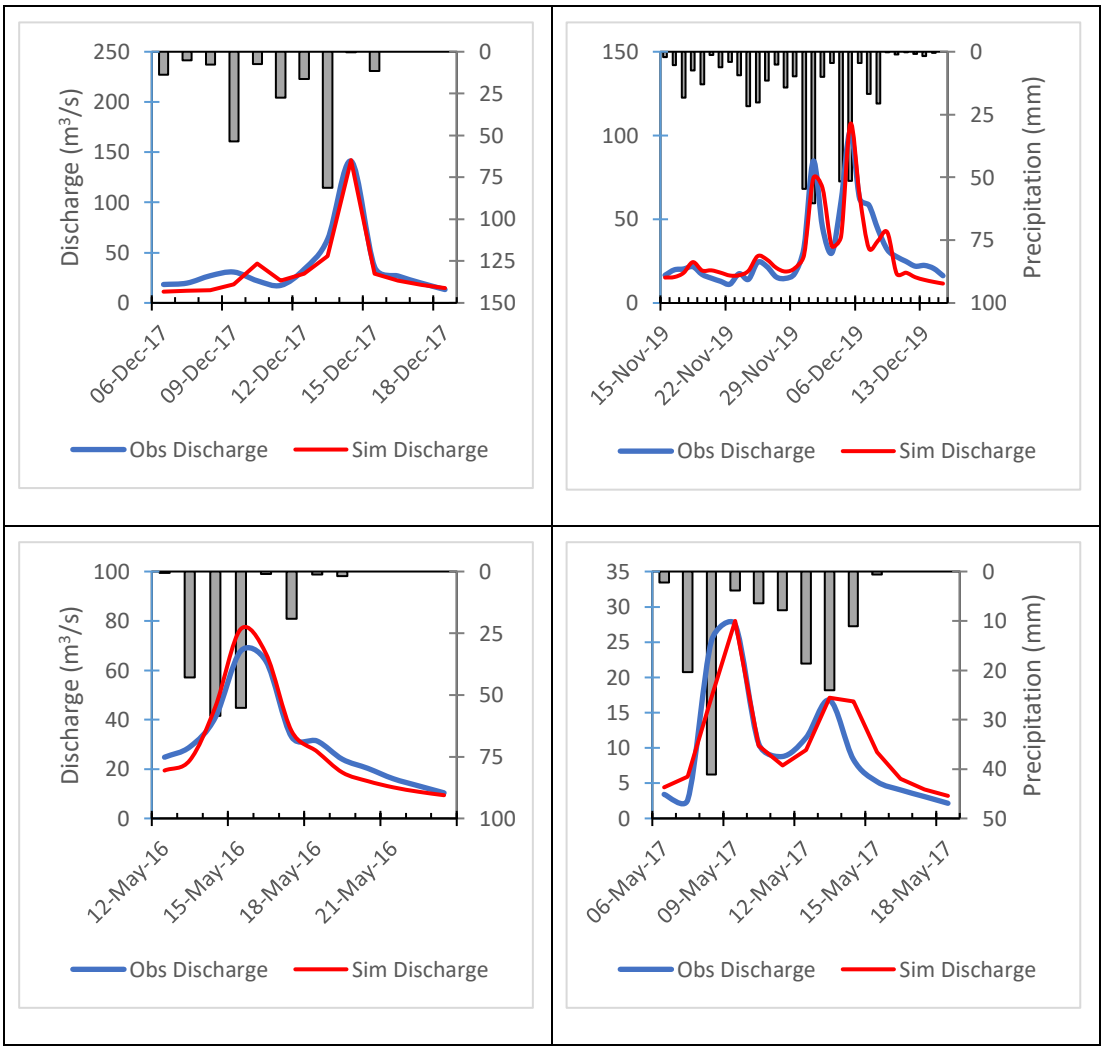

Figure 6-22: Enhanced results of the validation run after incorporating SMAP SM

Table 6-5: Summary of the objective functions for the final run using SSM

Event Number	Event Code	RMSE std dev	NSE	Percent Bias (%)	R^2
4	1D-13W-Dec17	0.30	0.92	-11.01%	0.93
5	2D-31W-Nov/Dec19	0.40	0.82	-3.43%	0.83
6	1D-12W-May16	0.30	0.90	-4.45%	0.98
7	1D-13W-May17	0.40	0.80	7.65%	0.81

6.2 Kalu Ganga Basin

6.2.1 Model Calibration

Two (2) events selected for the Maha and Yala seasons are used to calibrate the model performance. Calibration was performed adjusting the parameters of each sub-basins using the optimization tool available in HEC-HMS. The calibration of events yielded satisfactory to very good results in terms of different objective functions which is presented in Table 6-6.

Table 6-6: Summary of objective functions during calibration of events in Kalu Ganga

Event Number	Event Code	RMSE std dev	NSE	Percent Bias (%)	R^2
1	1D-24W-Sep/Oct97	0.60	0.68	3.16%	0.69
3	1D-11W-Apr/Mar99	0.50	0.78	-5.23%	0.88

The hydrograph of simulated and observed discharge and the flow duration curve (FDC) of simulated and observed discharge of calibration events are presented from Figure 6-23 to Figure 6-26. The calibrated parameters for the events are attached in Annexure 2. Both of the calibration events were underestimated by the model.

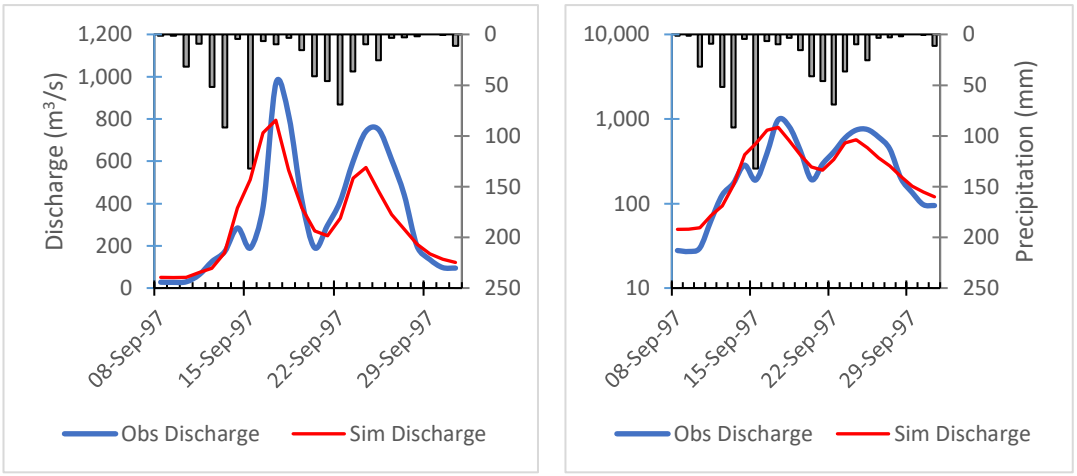

Figure 6-23: Simulated vs observed hydrograph for calibration Event 1 a) normal scale, b) semi-log scale

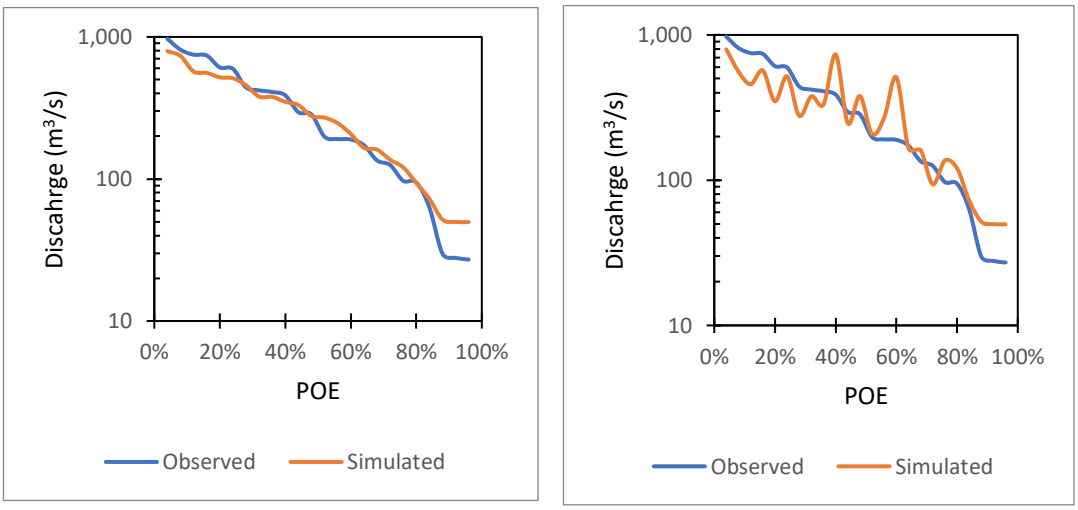

Figure 6-24: Event 1 FDC a) simulated sorted high to low, b) simulated sorted with observed

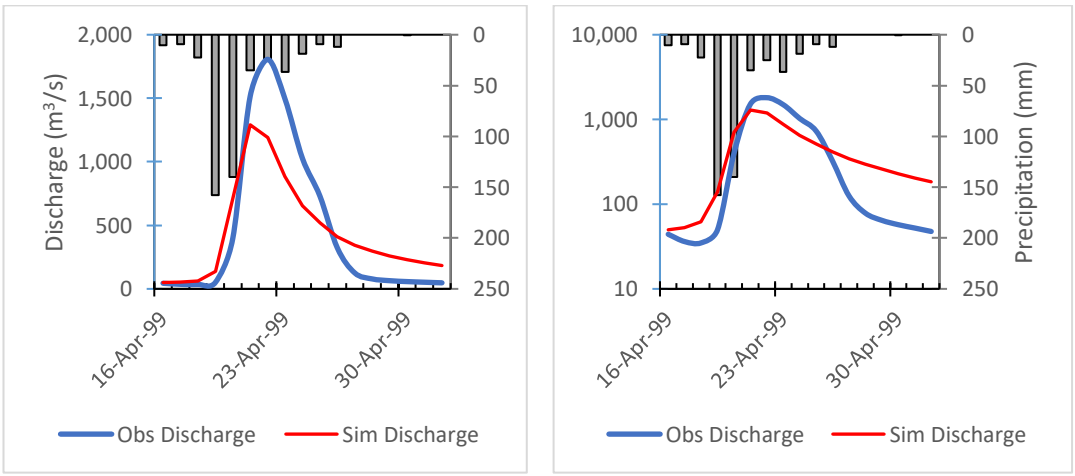

Figure 6-25: Simulated vs observed hydrograph for calibration Event 3 a) normal scale, b) semi-log scale

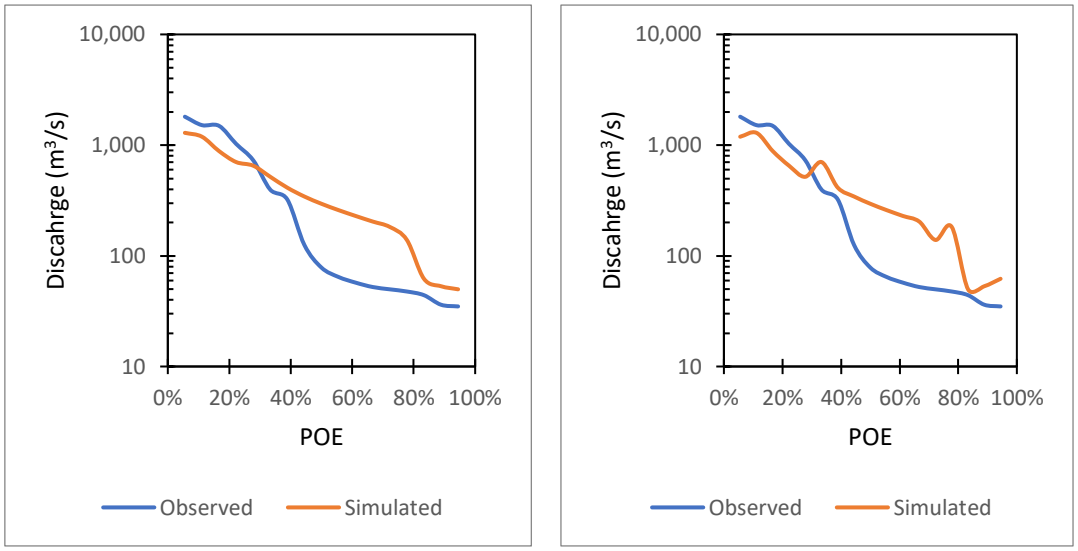

Figure 6-26: Event 3 FDC a) simulated sorted high to low, b) simulated sorted with observed

6.2.2 Model Validation

Two (2) events selected for the validation purpose were simulated in the HEC-HMS model using the optimized parameters obtained during the optimization process. The validation of events yielded satisfactory to very good results in terms of different objective functions. The hydrograph of simulated and observed discharge and flow duration curve of observed and simulated discharge (high-low sorted and sorted with observed) of events considered during the validation period are shown from Figure 6-27 to Figure 6-30 where POE represents the probability of exceedance.

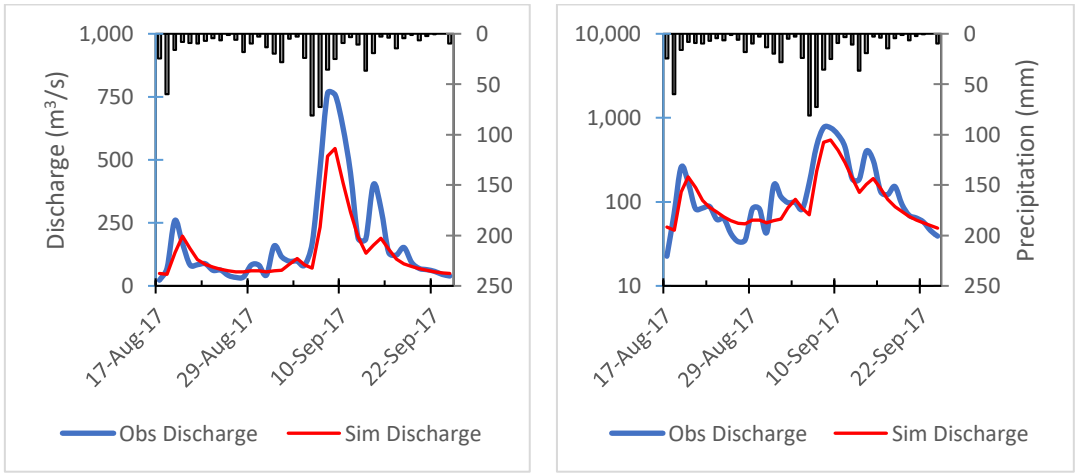

Figure 6-27: Simulated vs observed hydrograph for validation Event 3 a) normal scale, b) semi-log scale

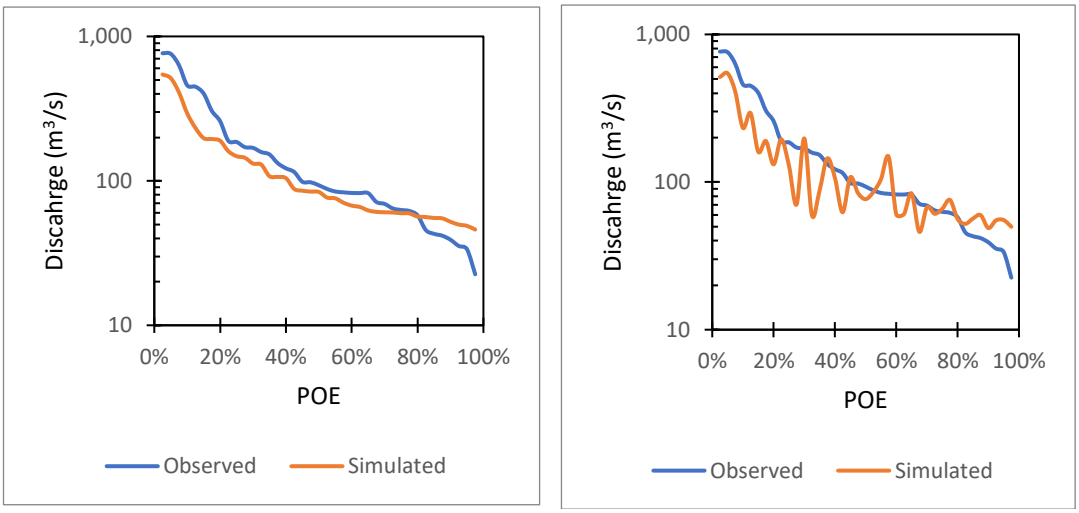

Figure 6-28: Event 4 FDC a) simulated sorted high to low, b) simulated sorted with observed

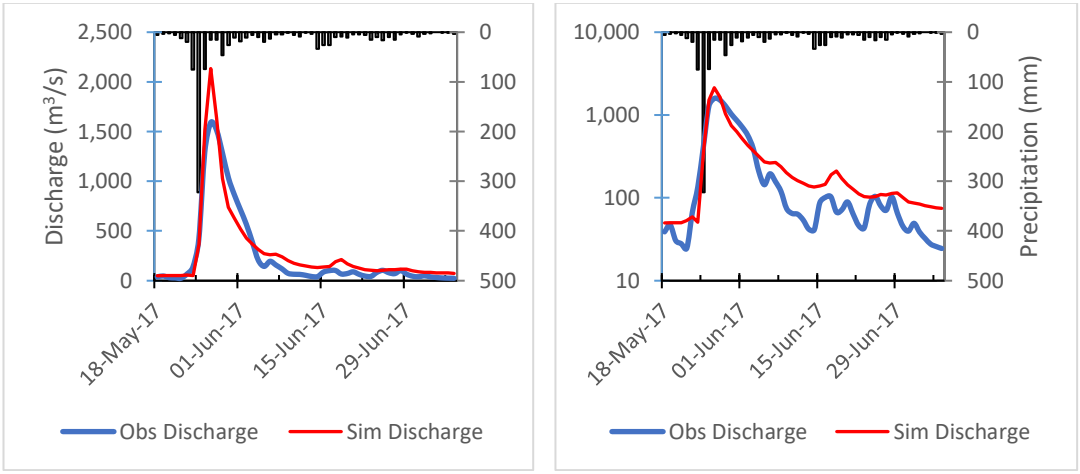

Figure 6-29: Simulated vs observed hydrograph for validation Event 2 a) normal scale, b) semi-log scale

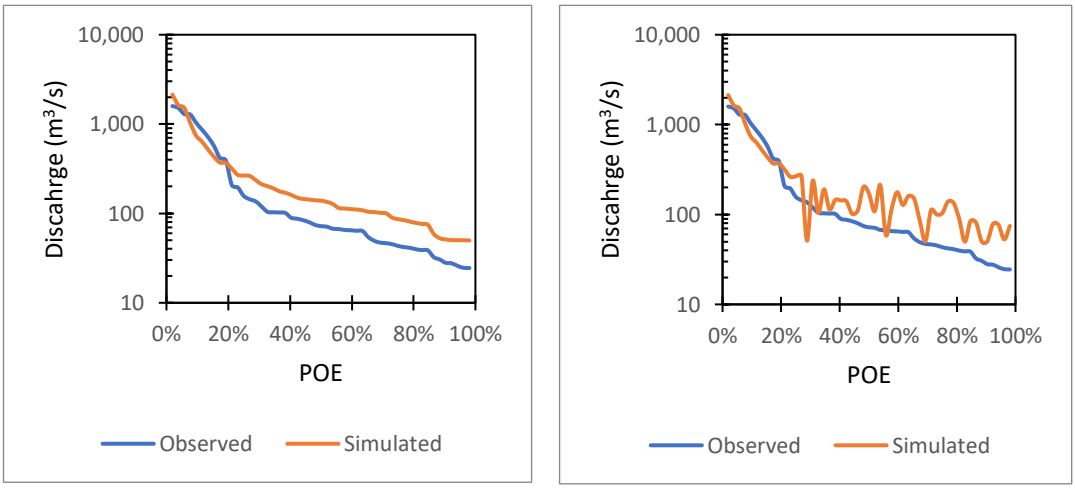

Figure 6-30: Event 2 FDC a) simulated sorted high to low, b) simulated sorted with observed

The parameters used during validation for the events are attached in Annexure 2. During the simulation, two (2) events underestimated the runoff volume while the other two (2) events overestimated the runoff volume at the outlet of the basin.

Table 6-7: Summary of objective functions during validation of events in Kalu Ganga basin

Event Number	Event Code	RMSE std dev	NSE	Percent Bias (%)	R^2
2	5D-39W-Aug/Sep17	0.50	0.74	-25.83%	0.91
4	1D-51W-May/Jul17	0.40	0.90	16.24%	0.92

6.2.3 Validation of Satellite Soil Moisture Data

Two (2) events selected for the validation run were simulated once again with the initial soil moisture parameters derived from the SMAP satellite soil moisture product. Using the ArcGIS, the gridded soil moisture product was converted to grid points, then was used to overlay with the sub-basin polygons to calculate average soil moisture as presented in Figure 6-31. The estimated soil moisture ranges between 0.2826 m^3m^{-3} and 0.3071 m^3m^{-3} over the area for an event of 18th Aug 2017.

The gridded soil moisture data was processed and then average soil moisture in each sub-basin was obtained. The values of saturation percentage (initial soil saturation) obtained for two (2) different events are presented in .

Table 6-8: Sub-basin initial soil saturation (%) extracted from SMAP data for different events in Kalu Ganga

Event	Event code	Sub Basin			Average
		1	2	3	
Event 2	5D-39W-Aug/Sep17	66%	66%	60%	**64%**
Event 4	1D-51W-May/Jul17	61%	58%	57%	**59%**

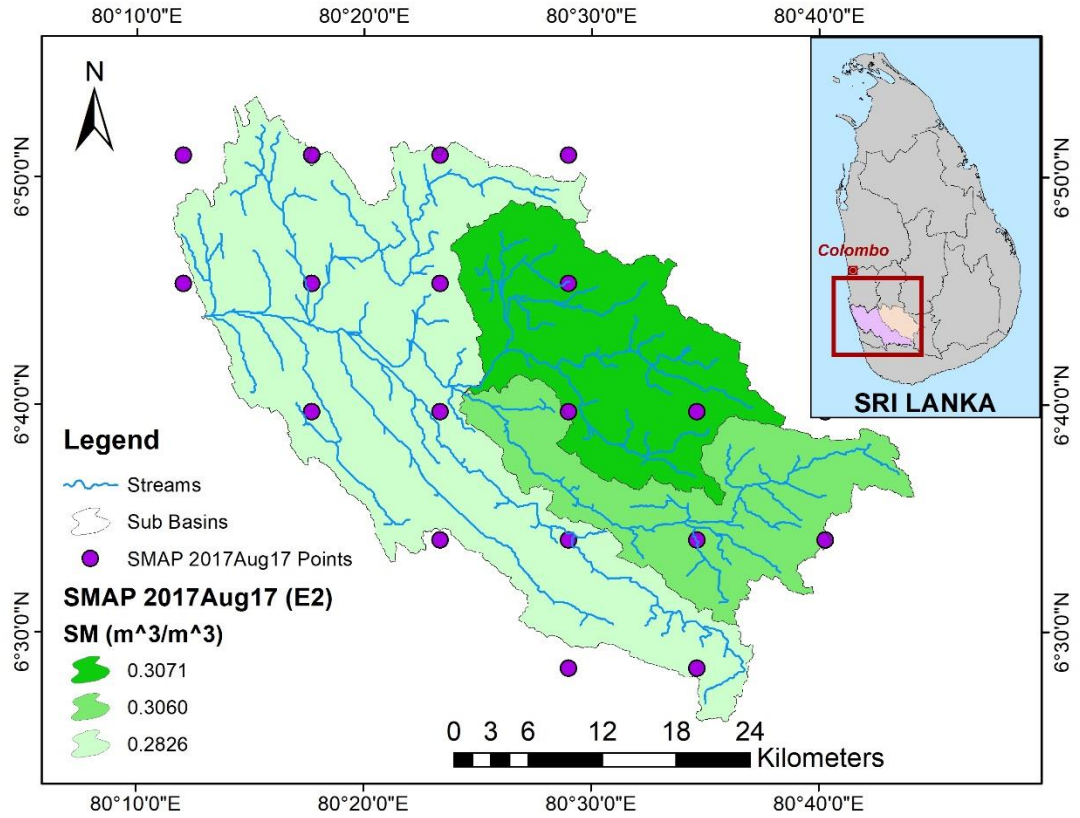

Figure 6-31: SMAP SM grid points and average volumetric soil moisture in sub-basins dated 2017 Aug 17 in Kalu Ganga

The initial run with the above-mentioned saturation values enhanced the performance of the model in simulating Event 4 by a small margin and deteriorated the performance of the model in simulating Event 2 by a small margin. Summary of the objective functions for the initial run using SSM are presented in Table 6-4. The simulated vs observed hydrographs are presented in Figure 6-21.

Table 6-9: Summary of the objective functions for the initial run using SSM

Event Number	Event Code	RMSE std dev	NSE	Percent Bias	R^2
2	5D-39W-Aug/Sep17	0.50	0.73	-26.76%	0.90
4	1D-51W-May/Jul17	0.30	0.90	15.94%	0.92

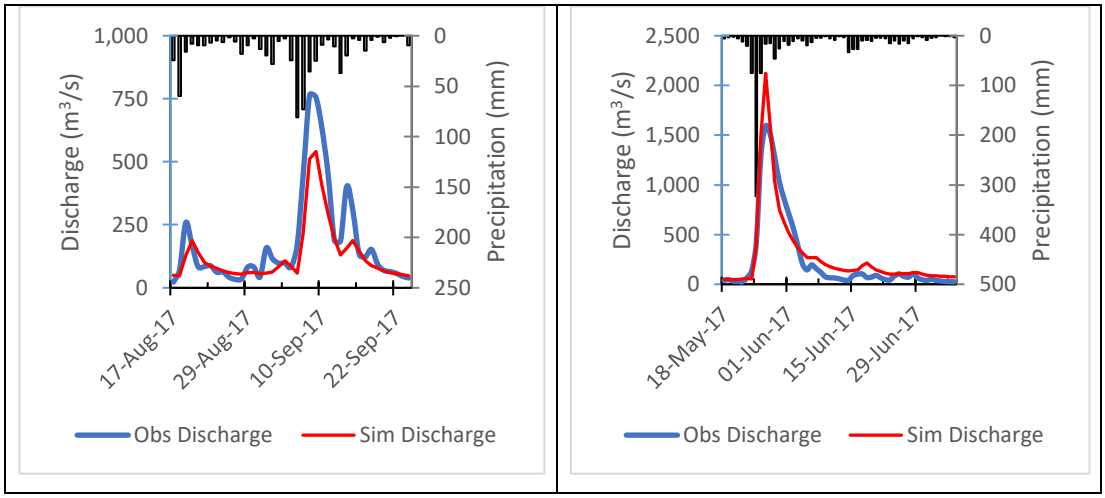

Figure 6-32: Results of the initial run of events with satellite soil moisture in Kalu Ganga

In both of the cases, the model simulated a lower runoff volume compared to normal validation. Bearing this in mind, soil storage value was optimized to observe a change in the results.

The optimization of the soil storage yielded better results compared to the initial run using SSM only. Event 2 was underestimated, for which enhanced performance was obtained after decreasing the soil storage. For Event 4, enhanced results were achieved on increasing the soil storage which had earlier overestimated runoff volume results. The objective functions indicated enhanced performance compared to the validation of the model and the summary of objective functions are presented in Table 6-5.

Table 6-10: Summary of the objective functions for the final run using SSM

Event Number	Event Code	RMSE std dev	NSE	Percent Bias	R^2
4	1D-13W-Dec17	0.30	0.92	-11.01%	0.93
7	1D-13W-May17	0.40	0.80	7.65%	0.81

The RMSE std dev was below 0.4 and NSE was above 0.8 indicating the very good performance of the model. The value of R^2 was obtained greater than 0.81 in all simulations indicating a strong correlation. The underestimated peak discharge was increased by 37 % and the underestimated runoff volume was increased by 43 %.

Although Event 4 was overestimated in terms of peak discharge and runoff volume, the results were enhanced when compared to normal validation. In the case of overestimated results, the peak discharge was reduced by 2 % and the runoff volume was reduced by 1 %. The simulated vs observed hydrographs are presented in Figure 6-22.

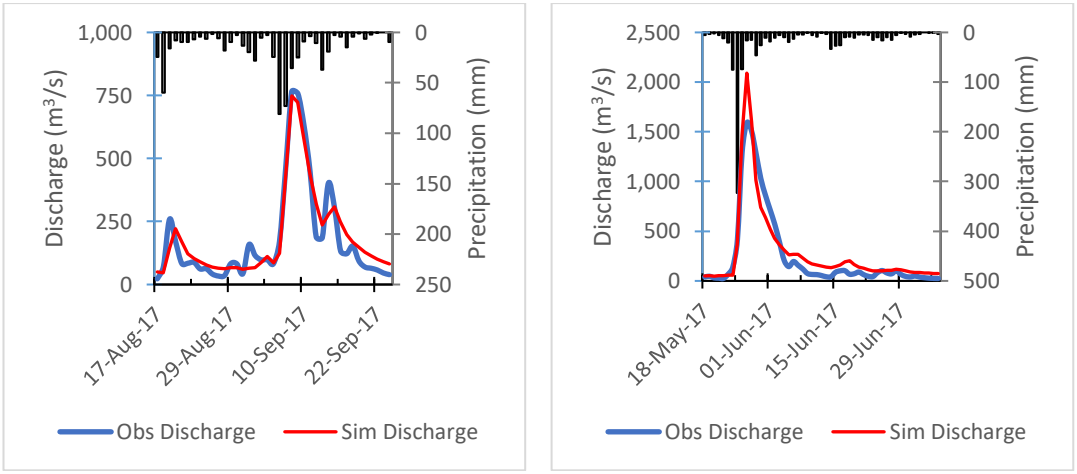

Figure 6-33: Enhanced results of the validation run after incorporating SMAP SM in Kalu Ganga

CHAPTER 7

7 DISCUSSION

7.1 Climate Extremes and Trends in the Basin

The dynamic nature of climate fabricates extremes and the long-term analysis of the climate data provides a perception of trends exhibited by climate indices. The climate is changing and the world is experiencing more frequent extremes than before (Zhai et al., 2021). A study by Dissanayaka and Rajapakse (2018) in the Kelani River Basin in Sri Lanka concluded that the annual temperature and precipitation extremes on the basin are increasing but the annual average precipitation is decreasing on the basin. Furthermore, streamflow trends in Kirindi Oya for 1994 to 2010 were studied by Abeysingha et al. (2017) identified that annual precipitation and streamflow at the basin were exhibiting a decreasing trend. The author further pointed out that the trend is upwards during the first inter-monsoon (FIM) where most of the extreme events are witnessed. This study mainly focused on the extremes of precipitation and streamflow which are further discussed in Section 7.1.1 and Section 7.1.2 below.

7.1.1 Kirindi Oya Basin

Analyzing the historical data, various indices of precipitation and streamflow are listed in Table 3-1 and Table 3-2 which are calculated for the two study basins. The summary of the precipitation indices and streamflow indices for the Kirindi Oya basin for the period of 2002 to 2020 are mentioned in Table 7-1 and Table 7-2, respectively. In the Kirindi Oya basin, it is observed that the total dry days (CDD) in a year is decreasing in three (3) stations (Bandaraeliya, Wellawaya, and Tanamalwila) whereas increasing in the Bandarawela station. Similarly, in the case of total wet days in a year, two (2) stations are indicating an increasing trend and two (2) stations (Bandaraeliya and Bandarawela) are indicating a decreasing trend. On average, the basin is experiencing a decrease in dry days by 0.42 days/year and an increase of wet days by 0.25 days/year.

Table 7-1: Trends of precipitation extreme indices in Kirindi Oya basin (2002 – 2020)

Station	CDD	CWD	R10	R20	RX1day	RX2day	RX5day
Bandaraeliya	-0.34	-0.35	-0.34	-0.06	2.42	3.37	4.58
Bandarawela	0.63	-0.63	-0.09	0.11	0.96	2.15	1.10
Wellawaya	-0.38	0.39	1.11	1.14	0.87	2.44	6.35
Tanamalwila	-1.57	1.58	-0.37	-0.36	-0.67	-0.46	-0.05
Average	**-0.42**	**0.25**	**0.08**	**0.21**	**0.90**	**1.87**	**3.00**

Table 7-2: Trends of streamflow extreme indices in Kirindi Oya basin (2002 – 2020)

Station	CDS	CWS	SX1day	SX2day	SX5day
Tanamalwila	1.90	0.57	0.74	0.34	0.19

The study revealed an increasing trend for heavy and very heavy rainfall days by 0.08 days/year and 0.21 days/year respectively. The heavy rainfall days (R10) are increasing in Wellawaya with high magnitude while decreasing with lower magnitude compared to Wellawaya in all other 3 stations. Days with very heavy rainfall (R20) are increasing in Bandarawela and Wellawaya whereas decreasing Bandaraeliya and Tanamalwila. The sharp increase in heavy and very heavy rainfall days in Wellawaya may be attributed to its location as it lies around the confluence of the intermediate zone and dry zone.

Considering annual extreme rainfall in the basin, the daily extreme rainfall, 2-day cumulative extreme rainfall, and 5-day cumulative rainfall are exhibiting an increasing trend. The 5-day cumulative rainfall is showing a sharp increase indicating a higher magnitude of extreme events in the recent period. Although one (1) station Tanamalwila is indicating a decreasing trend, this may be due to a large number of missing data between 2015 to 2020. The missing data which was filled using other station data might not truly represent extreme events in the particular station.

The streamflow data of the Tanamalwila station analyzed from 1988 to 2020 indicated an upward trend for both low flow days (CDS) and high flow days (CWS). In approaching recent years, the frequency of high flow and low flow days are increasing rapidly. Similarly, the magnitude of the annual extreme of daily flow (SX1day) is increasing at a rate of 0.74 m^3/s per year. The 2-day (SX2day) and 5-day (SX5day) extremes are also indicating an increasing trend.

The upward trend of streamflow can be justified by the increasing magnitude of precipitation in the basin as explained earlier. Although the 2-day and 5-day extreme rainfall is increasing at higher magnitudes, the 2-day and 5-day extreme flow is exhibiting an increase in lesser magnitude. This can be attributed to the climate change effect where there is heavy precipitation which gets drained faster allowing for lesser storage in the underlying groundwater layers in the basin. This will lead to severe drought in the future if the basin water management is not thought of.

7.1.2 Kalu Ganga Basin

Precipitation and streamflow data for the Kalu Ganga basin from 1995 to 2020 were analyzed and the results indicated that the precipitation extremes and streamflow extremes are decreasing in the basin as mentioned in Table 7-1 and Table 7-2, respectively.

Table 7-3: Trends of precipitation extreme indices in Kalu Ganga basin (1995 – 2020)

Station	CDD	CWD	R10	R20	RX1day	RX2day	RX5day
Halwatura	0.64	-0.64	-0.34	-0.69	-0.60	-0.95	-0.77
Galatura	-0.38	0.38	-0.10	-0.14	-2.00	-2.37	-3.21
Ratnapura	0.09	-0.08	0.06	-0.17	-0.51	-0.28	1.41
Depedena	0.26	-0.26	-0.35	-0.50	2.93	2.68	2.49
Average	**0.15**	**-0.15**	**-0.18**	**-0.38**	**-0.05**	**-0.23**	**-0.02**

Table 7-4: Trends of streamflow extreme indices in Kalu Ganga basin (1995 – 2020)

Station	CDS	CWS	SX1day	SX2day	SX5day
Ellagawa	2.80	-0.91	-5.60	-3.78	-0.77

The total dry days (CDD) in the Kalu Ganga basin is showing an upward trend except for the Galatura station. The Halwatura, Ratnapura, and Depedena are experiencing an increase of CDD by 0.64, 0.09, and 0.26 days/year, respectively, whereas Galatura is experiencing a decrease by 0.38 days/year. The trend of decreasing CWD for all 3 stations is within a similar magnitude of CDD except for Galatura station which is pointing towards an increasing trend. On average, the dry days are increasing by 0.15 days/year and wet days are decreasing by the same magnitude. The heavy rainfall days (R10) are decreasing by 0.18 days/year and very heavy rainfall days (R20) are decreasing rapidly by 0.38 days/year.

From the analysis of annual extreme rainfall in the basin, the daily extreme rainfall (RX1day), 2-day cumulative extreme rainfall (RX2day), and 5-day cumulative rainfall (RX5day) are exhibiting a decreasing trend in average with a magnitude of 0.05, 0.23, and 0.02 mm/year respectively. Although the three (3) stations; Halwatura, Galatura, and Ratnapura are experiencing a decreasing magnitude, Depedena station is exhibiting an increase in precipitation with higher magnitudes. This can be corroborated from a precipitation trend study carried out in Kalu Ganga by Ampitiyawatta and Guo (2010) for the data period of 1965 to 2004 that indicated a decreasing precipitation trend in the basin.

The streamflow data of the Ellagawa station analyzed from 1995 to 2020 indicated an upward trend for low flow days (CDS) and a downward trend for high flow days (CWS). The magnitude of the annual extreme of daily flow (SX1day) is decreasing at a rate of 5.60 m^3/s per year. The 2-day (SX2day) and 5-day (SX5day) extremes are also decreasing at the rate of 3.78 and 0.77 m^3/s per year respectively. This correlates well with the decreasing precipitation extremes in the basin. Although the overall precipitation is indicating a decreasing trend, daily extreme flow is highly affected compared to the 2-day and 5-day streamflow in the basin.

7.2 Parameter Estimation

For modeling streamflow, HEC-HMS with soil moisture accounting (SMA) was set up as a model for the simulation of events of various return periods to analyze both dry period flow and wet period flow in the basin. The physical parameters related to canopy storage and surface storage were estimated using the land use land cover data, slope data, and the road map of the basin. These storage values are assigned for different land-use types according to their storage capacity and do not vary much in magnitude. The lag time in the SCS transform was estimated using the Kirpich formula. The parameters related to baseflow were estimated from streamflow recession analysis. The parameters obtained vary depending on the period of streamflow analysis and the season considered for analysis. Proper care should be given while considering the hydrograph for the analysis of baseflow. The hydrograph should follow a dry period before it quickly rises to peak responding to the rainfall and then recedes slowly without any rainfall on the basin. This helps to identify the recession of baseflow and separate runoff from the baseflow.

There are 14 parameters in the SMA and they need to be estimated carefully with proper judgment. The maximum infiltration rates and soil storage are determined from the saturated hydraulic conductivity and porosity of the soil. The soil properties for Sri Lanka were adopted from Moormakn et al. (1961) and the parameters were estimated referring to Feldman (2000). The storage capacity of groundwater layers under the soil is estimated using streamflow recession analysis. The points mentioned in the above streamflow recession analysis for the calculation of recession parameters should be considered in this case too. The base flow is estimated based on the recession curve, thus, it should be estimated carefully by extending the recession line backward and intersecting it with a line on the day of the peak flow as shown in Figure 5-4. The baseflow parameters should be representative of all seasons as the recession characteristics vary depending on the season and the variability of precipitation in the basin.

7.3 Model Calibration

In Kirindi Oya, events were selected between the period of 2002 to 2014 to calibrate the model performance. Five (5) events of the different periods from two (2) seasons were identified and implied in the calibration process. First of all, a parameter sensitivity study is performed right after the model warmup to know about the sensitivity of the parameters to the model performance. Soil storage, soil percolation, and soil infiltration were the most sensitive parameters in the SMA method applied in the Sturgeon Creek basin in Canada and the Vamshadhara River basin in India (Bhuiyan et al., 2017; Singh & Jain, 2015).

The most sensitive parameter obtained for this study was soil storage (mm) followed by maximum infiltration rate (mm/hr) and initial soil storage (%). Since the study was focused on analyzing the effect of soil storage on runoff, the sensitivity analysis verified that the soil storage parameters are indeed very important in simulating the runoff from the catchment.

Depending on the sensitivity obtained, the most sensitive parameters were calibrated within the allowable range of the parameters using the automatic calibration found in the HEC-HMS. After automatic calibration, manual calibration was adopted to further enhance the model results. Special attention should be given to the parameter range selected during the calibration and should be justified with proper literature support. Since the initial moisture conditions and initial discharge vary with the events, these two (2) parameters were changed in each event throughout the calibration process.

The calibration of events yielded an average nash-sutcliffe efficiency (NSE) of 0.80 with the maximum and minimum ranging between 0.99 to 0.63. This indicated a very good performance of the model specifically in simulating the peak flows. The average RMSE std dev obtained was 0.40 with the upper and lower range of 0.10 to 0.60, respectively. Event 1, Event 3, and Event 9 were overestimated by the model while other Event 2 and Event 8 were slightly underestimated. Event 1 was highly overestimated with a percentage bias of 17.40 %. The average goodness of fit (R^2) is about 0.84 (upper and lower limit ranging from 0.99 to 0.65, respectively) which indicates an agreeable correlation of the results.

Event 8 yielded satisfactory objective function values because the lag of the peak flow compared to the peak rainfall was 2 days, which the model simulated 1 day earlier. The peak may have been achieved in the early period of the 2nd day which can not be justified through the daily data. Thus, the use of hourly data could have simulated the flow much better.

For the Kalu Ganga basin, a total of four (4) events were selected between 1995 to 2020 among which two (2) were from the Maha season and two (2) were from the Yala season. Each set of events from the maha and Yala season were considered for the calibration and validation process. The calibration of the events generated objective functions within the allowable range. The peak flow of both events was underestimated by the model. The average NSE was generated to be 0.73 (0.68 – 0.78) and the average RMSE std dev was obtained to be 0.55 (0.50 to 0.60). The percentage bias was obtained within a good range of 3.16 % to -5.23 %. A good correlation was obtained with an average R^2 of 0.79 (0.69 - 0.88).

7.4 Model Validation

In Kirindi Oya, the events identified for the validation of the model performance were obtained from 2015 to 2020 where four (4) events; two (2) from Maha and two (2) from Yala are considered. The parameters obtained from the calibration of events were used in the validation process. In the validation, a total of four (4) events were selected, two (2) from Maha season and two (2) from Yala season. Following the trend of calibration, two (2) parameters were changed in each event to provide an initial condition to the model as the event is considered to have different initial conditions.

The validation of events resulted in satisfactory to good performance in terms of objective functions. The average NSE was obtained 0.75 (0.60 – 0.85) indicating the good overall performance of the model in simulating the event runoff. The average RMSE std dev was 0.48 (0.40 – 0.60) and average PBIAS was 2.83 % (-5.74 % to 11.17 %) during the validation period. The average R^2 of 0.87 (0.77 – 0.96) indicated a good fit of the simulated flow with the observed flow.

The model simulated Event 4 peak flow 1 day late than the observed peak flow. The peak flow was observed on the same day of peak rainfall, but it was simulated late by

the model. The maximum lag time input in the model is 2,086 minutes which is comparable to 2,127 minutes adopted by Jayadeera and Wijesekera (2019) for study area up to Ratnapura and 240 minutes to 2,160 minutes used by Nandalal and Ratmayake (2010) for various sub-basins. In actual conditions, the rainfall may have occurred at the beginning of the day or near to outlet of the basin, causing runoff to reach the outlet at the end of the day. This hourly variation of the rainfall and discharge can not be captured in daily data thereby reducing the accuracy of the simulation.

For the validation of model simulation in Kalu Ganga, two (2) events identified were used. The parameters obtained from the model calibration were provided as an input to the model and the model yielded very good results. The average NSE of 0.82 (0.73 – 0.90) was obtained which suggested a good fit of simulation with the observed streamflow data. The RMSE std dev was obtained within a good range with an average of 0.40 (0.30 – 0.50). Event 2 volume was underestimated by -26.76 % whereas event 4 was overestimated by 15.94 % by the model. However, the R^2 indicated a very good fit of the model results with an average value of 0.91 (0.90 – 0.92).

7.5 Incorporation of Satellite Soil Moisture

One of the objectives of this study is to incorporate satellite soil moisture in the hydrologic model. The HEC-HMS does not allow the user to input soil moisture directly into the model. Thus, the soil moisture obtained from the SMAP data needs to be converted to the initial saturation condition of the simulation to feed as an input to the model. This is carried out by following the procedure described in Section 6.1.3. The soil moisture of each grid was averaged into each sub-basins using ArcGIS and the final soil moisture value was obtained.

7.5.1 Kirindi Oya Basin

The SSM was used as an input in the model of the Kirindi Oya basin for the validation of the same four (4) events used in the validation process earlier. The volumetric soil moisture values from SMAP data were obtained in the ranges between 0.25 m^3/m^3 to 0.43 m^3/m^3. The volumetric soil moisture in the Sturgeon Creek basin in Manitoba, Canada estimated from RADARSAT-2 were in the ranges of 0.029 m^3/m^3 and 0.550

m^3/m^3 (Bhuiyan et al., 2017). The soil moisture parameters obtained were higher in range compared to the initial soil saturation input to the calibrated model. Because of this, the model simulated results in the validation were overestimated. Examining the simulated results, the parameters related to soil storage and groundwater storage were adjusted to observe the change in the model performance. The summary of objective functions for different saturation scenarios is mentioned in Table 7-6.

Table 7-5: Changes in parameters while incorporating SSM in the model to enhance result in Kirindi Oya

Event Number	Initial Soil Storage (%)			GW1 Storage (mm)		
	Calibrated	SSM	Change	Calibrated	SSM	Change
4	32%	84%	52%	10.47	40.99	30.52
5	32%	88%	56%	10.47	33.91	23.44
6	32%	70%	38%	10.47	64.18	53.71
7	32%	65%	33%	10.47	64.18	53.71

The initial soil saturation obtained from the calibration was 32% and the saturation obtained from SSM was in the range of 65% to 84%. This excess moisture in the upper soil layer led to more runoff volume in the model. To adjust with the actual soil moisture obtained from the SMAP data, changes were made in the underlying groundwater layers. The enhanced results were obtained when the GW1 storage was increased in the range of 23 mm to 53 mm in the events. On increasing the GW1 storage, the model results were enhanced and very good objective functions were obtained.

Table 7-6: Performance of model in different saturation scenarios in Kirindi Oya basin

Event Number	Saturation Scenario	RMSE std dev	NSE	Percent Bias	R^2
	Calibration	0.60	0.60	11.17%	0.95
Event - 4	SSM	1.00	-0.05	44.71%	0.93
	Optimized SSM	***0.30***	***0.92***	***-11.01%***	***0.93***
	Calibration	0.50	0.76	-5.74%	0.77
Event - 5	SSM	0.60	0.66	7.99%	0.81
	Optimized SSM	***0.40***	***0.82***	***-3.43%***	***0.83***
	Calibration	0.40	0.85	-1.75%	0.96
Event - 6	SSM	1.20	-0.35	25.75%	0.95
	Optimized SSM	***0.30***	***0.90***	***-4.45%***	***0.98***
	Calibration	0.40	0.80	7.65%	0.81
Event - 7	SSM	0.60	0.68	24.35%	0.80
	Optimized SSM	***0.40***	***0.80***	***7.65%***	***0.81***

7.5.2 Kalu Ganga Basin

The SSM was used as an input in the model of the Kalu Ganga basin for the validation of the same two (2) events used in the validation process earlier. The volumetric soil moisture values from SMAP ranges between 0.28 m^3/m^3 to 0.31 m^3/m^3. The soil moisture parameters obtained were lower in magnitude compared to the initial soil saturation input to the calibrated model. The performance of Event 4 was slightly optimized when incorporating satellite soil moisture whereas the performance of Event 2 was deteriorated by a small margin. Analyzing the simulated results, the parameters

related to soil storage and groundwater storage were adjusted to observe the change in the model performance. The enhanced results were obtained after optimizing the soil storage parameter. For Event 2, soil moisture was decreased by 9.85 mm whereas increased by 9.66 mm for Event 4 to get enhanced results from the model.

Table 7-7: Changes in parameters while incorporating SSM in the model to enhance result in Kalu Ganga

Description	**Initial Soil Storage (%)**			**Soil Storage (mm)**		
Calibrated	**Calibrated**	**SSM**	**Change**	**Calibrated**	**SSM**	**Change**
Event 2	31%	64%	33%	27.03	17.17	-9.85
Event 4	31%	59%	28%	27.03	36.68	9.66

The summary of the objective functions obtained from the model with various scenarios of soil moisture is presented in Table 7-8. The NSE and R^2 obtained were above 0.90 for both the events after incorporation of SSM and optimization of soil storage parameters indicating better agreement of the simulated flow with the observed flow.

Table 7-8: Performance of model in different saturation scenarios in Kalu Ganga basin

Event Number	**Saturation Scenario**	**RMSE std dev**	**NSE**	**Percent Bias**	**R^2**
	Calibration	0.50	0.74	-25.83%	0.91
Event - 2	SSM	0.50	0.73	-26.76%	0.90
	Optimized SSM	***0.30***	***0.92***	***5.85%***	***0.92***
	Calibration	0.40	0.90	16.24%	0.92
Event - 4	SSM	0.30	0.90	15.94%	0.92
	Optimized SSM	***0.30***	***0.91***	***14.71%***	***0.92***

7.5.3 Soil Saturation and Runoff Relationship

The sensitivity analysis of the model in simulating the flow of various validation events was carried out which provided a significant understanding of the response of the soil storage to the runoff. In Kirindi Oya, soil saturation obtained from SSM is very high in Event 4 and Event 5, compared to events 6 and 7, where the GW1 storage parameter is very sensitive to both runoff volume and peak discharge as presented in Figure 7-1 and Figure 7-2. When GW1 storage is limited or reduced, it will lead to higher volume and much higher discharges in quick succession of time. The soil storage had minimum sensitivity on producing runoff on the higher saturation scenario as it was unable to store further water into it. This phenomenon can be practically related to the recent surge in flood and its effects on urban catchments where unplanned development that covers the soil with built-up areas that can barely take any water into the top-soil/ground storage. The surge in peak discharge observed in urban catchments despite the rainfall not being of extreme magnitude is due to the decreased groundwater storage. The available soil gets saturated quickly and is unable to pass the water to the lower groundwater layers due to a lack of land covers that would allow moisture to pass through it.

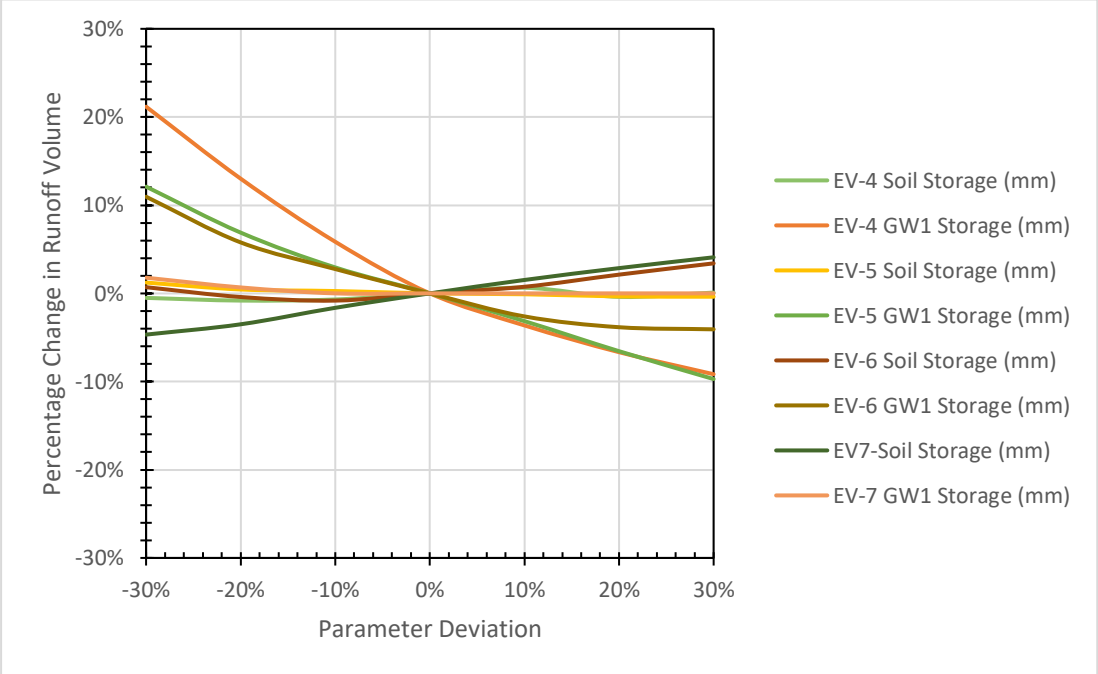

Figure 7-1: Sensitivity analysis of soil storage parameters of various events in simulating runoff volume in Kirindi Oya basin

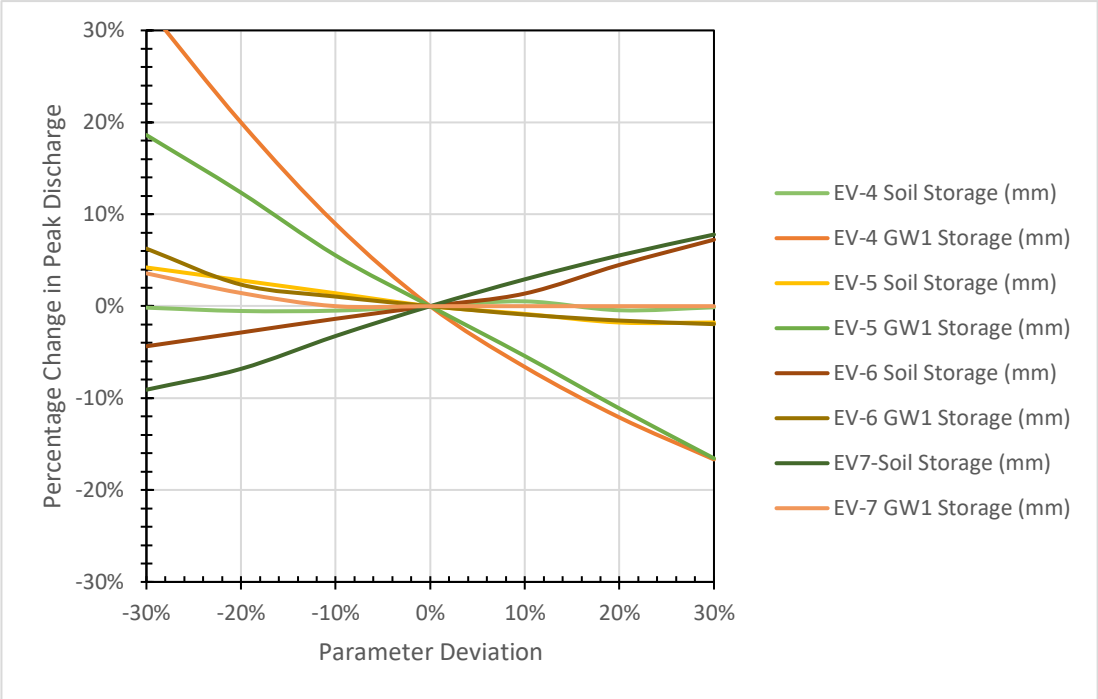

Figure 7-2: Sensitivity analysis of soil storage parameters of various events in simulating peak discharge in Kirindi Oya basin

Similarly, the soil saturation obtained from SSM for Event 6 and Event 7, used as an input to the simulation in the model is comparatively lower than the other two (2) events 4 and 5. The sensitivity analysis of these two events leads to a finding that the topsoil with a lower saturation/unsaturated state is sensitive in simulating the runoff in the catchment compared to the groundwater storage parameter. The sensitivity analysis is presented in Figure 7-1 and Figure 7-2. For soil with comparatively lower saturation levels, an increase in the soil storage will lead to a slight increase in runoff and peak discharge in the basin irrespective of changes in the groundwater storage.

The quick surge of floods is directly linked to the soil moisture condition which controls the runoff to the catchment. Bhuiyan et al. (2017) from their study on the Manitoba basin in Canada concluded that peak discharge from the basin is very sensitive to antecedent soil moisture conditions. Furthermore, Czigány et al. (2010) and Hegedüs et al. (2013) concluded that the soil moisture conditions are very sensitive in producing peak discharge and accumulated discharge which would contribute to the flash flooding in the basin.

In a catchment with a limited exposed soil surface, greater soil moisture will enable rapid runoff from the catchment slowing down the movement of moisture into the underlying layers. This justifies the importance of soil storage in the runoff from the catchment. Thus, the floods and their effects can be dampened through the enhanced understanding of the storage capacity of the soil layers and thereby increasing the ground recharge.

CHAPTER 8

8 CONCLUSIONS

a) According to the historical observation of precipitation data in the Kirindi Oya basin, the basin is experiencing an increase in wet days by 0.25 days per year along with an increase in very heavy precipitation days by 0.21 days/year. Daily extreme precipitation is indicating an increasing trend of 0.90 mm/year which is followed by extreme streamflow increasing at an annual rate of 0.74 m^3/s. Despite the 5-day rainfall increasing at a very high rate of 3.00 mm/year, the 5-day average streamflow is increasing annually at a mere rate of 0.19 m^3/s.

b) In the Kalu Ganga basin, observation of historical precipitation data revealed that dry days in the basin are increasing at a rate of 0.15 days annually with very high precipitation days decreasing at 0.38 days/year. The extreme daily precipitation is decreasing at a rate of 0.05 mm annually with the streamflow exhibiting a sharp decrease of 5.60 m^3/s annually. Also, the 5-day extreme precipitation and streamflow are showing a downward trend at an annual rate of 0.02 mm and 0.77 m^3/s.

c) The analysis of historical data in the basin revealed that the basin in the dry zone is getting wetter whereas the basin in the wet zone is getting drier.

d) The consideration of different return period discharge yielded well-distributed events with high and low flow magnitude (27 m^3/s to 263 m^3/s for Kirindi Oya and 764 m^3/s to 1,806 m^3/s for Kalu Ganga) from both Maha and Yala seasons. The model was successfully calibrated and validated using these events.

e) The SMA was found to be the most suitable loss method in HEC-HMS for simulating both low flows and high flows as the results obtained from the model nearly matched peaks and low flows in all the events selected.

f) The model for Kirindi Oya performed well with an average NSE of 0.80 for calibration and 0.75 for validation, respectively. Similarly, the average RMSE

std dev was below 0.48 for both the calibration and validation. The average R^2 was obtained above 0.84 which indicated a strong correlation.

g) The HEC-Model developed for the Kalu Ganga basin simulated good results with an average NSE of 0.73 in the calibration and 0.82 in the validation. The average RMSE std dev value was obtained 0.55 for calibration and 0.45 for validation. A good correlation was obtained with an average R^2 of 0.79 for the calibration period and 0.91 for the validation period.

h) The satellite soil moisture (SSM) data with different moisture scenarios was successfully used in both basins to enhance the performance of the developed HEC-HMS model. Initially, the use of SSM deteriorated the performance of the model in Kirindi Oya. Later the performance was enhanced with optimization of the Groundwater 1 (GW1) storage parameter. The model generated an average NSE of 0.80 and an average R^2 of above 0.90 with an average RMSE std dev of 0.35. The overestimated peak discharge was reduced by 28 % (maximum) and the runoff volume was reduced by 18% (maximum). The average variation in the peak discharge and runoff volume was obtained to be 6 % and -2 %, respectively.

i) Moreover, performance was slightly increased in the case of Kalu Ganga when SSM is incorporated into the model. The results were further enhanced by optimizing soil storage parameters generating the average NSE and R^2 above 0.90 indicating a very strong correlation and an average RMSE sd. dev. of 0.30. The underestimated peak discharge was increased by 37 % and the underestimated runoff volume was increased by 43 %. The average variation in the peak discharge and runoff volume was obtained to be 15 % and 10 %, respectively.

j) The SSM data was successfully used in both the basin and soil storage and groundwater storage parameters were identified to be the most sensitive parameters in the model. Thus, it was identified that soil moisture plays a key role in the generation of runoff affecting effective water resources management in the basin.

CHAPTER 9

9 RECOMMENDATIONS

a) The present study focused on the use of satellite-derived soil moisture as an initial condition in the simulation of the hydrologic model HEC-HMS. Further study should be carried out incorporating real-time SSM into the distributed model. Also, the availability of the ground measured SM data should be increased which would provide more accurate data and can be compared with satellite SM data for its usability.

b) The parameters used in the simulation of the model should be estimated with proper care as the model response is highly sensitive to the parameters. It should be well understood that a minor change in a single parameter would change other parameters as it was observed that a change in initial soil moisture led to higher runoff in the basin. Thus, an in-depth study should be carried out related to the estimation of soil parameters used in the models.

c) There were lots of missing rainfall data in many stations in both the basin which restrained the study to use with maximum stations data declining the accuracy of model simulation.

d) The event-based simulation was carried out using the daily data sets. For the increase in the accuracy of the model simulation, adopting hourly data sets would allow enhancing the performance of the model and provide a better understanding of the temporal response of soil moisture to the basin runoff.

e) In HEC-HMS, it is recommended to assess the effect of the soil moisture on producing the runoff through the development of the soil conservation service (SCS) curve number (CN) loss method and incorporating satellite soil moisture to relate the antecedent moisture conditions (AMC) of the soil.

BIBLIOGRAPHY

Abeysingha, N., Jayasekara, J., Abeysingha, N. S., Jayasekara, J. M. N. S., & Meegastenna, T. J. (2017). *Stream flow trends in up and midstream of Kirindi Oya river basin In Sri Lanka and its linkages to rainfall* (Vol. 68, Issue 1). https://www.researchgate.net/publication/313771386

Ahmad, J., Forman, B., & Kumar, S. (2021). SMAP retrieval assimilation improves soil moisture estimation across irrigated areas in South Asia. *Hydrology and Earth System Sciences Discussions*, 1–32. https://doi.org/10.5194/HESS-2021-460

Akbari, S., & Singh, R. (2012). *Hydrological modelling of catchments using MIKE SHE*. https://www.infona.pl//resource/bwmeta1.element.ieee-art-000006216284

Alvarez-Garreton, C., Ryu, D., Western, A. W., Su, C. H., Crow, W. T., Robertson, D. E., & Leahy, C. (2015). Improving operational flood ensemble prediction by the assimilation of satellite soil moisture: Comparison between lumped and semi-distributed schemes. *Hydrology and Earth System Sciences*, *19*(4), 1659–1676. https://doi.org/10.5194/HESS-19-1659-2015

Alvarez-Garreton, Ryu, D., Western, A. W., Crow, W. T., Su, C.-H., & Robertson, D. R. (2016). Dual assimilation of satellite soil moisture to improve streamflow prediction in data-scarce catchments. *Water Resources Research*, *52*(7), 5357–5375. https://doi.org/10.1002/2015WR018429

Ampitiyawatta, A., & Guo, S. (2010). Precipitation trends in the Kalu Ganga basin in Sri Lanka. *Journal of Agricultural Sciences*, *4*(1), 10. https://doi.org/10.4038/jas.v4i1.1641

Armanuos, A. M., Al-Ansari, N., & Yaseen, Z. M. (2020). Cross Assessment of Twenty-One Different Methods for Missing Precipitation Data Estimation. *Atmosphere 2020, Vol. 11, Page 389*, *11*(4), 389. https://doi.org/10.3390/ATMOS11040389

Aubert, D., Loumagne, C., & Oudin, L. (2003). Sequential assimilation of soil moisture and streamflow data in a conceptual rainfall–runoff model. *Journal of Hydrology*, *280*(1), 145–161. https://doi.org/10.1016/S0022-1694(03)00229-4

Bakker, M., Barker, R., Meinzen-Dick, R., & Konradsen, F. (Eds.). (1999). *Multiple uses of water in irrigated areas: A case study from Sri Lanka* (Vol. 8). IWMI.

Barnston, A. G. (1992). Correspondence among the Correlation, RMSE, and Heidke Forecast Verification Measures; Refinement of the Heidke Score. *Weather and Forecasting*, *7*(4), 699–709. https://doi.org/10.1175/1520-0434(1992)007

Baumbach, T., Burckhard, S. R., & Kant, J. M. (2015). *Watershed Modeling Using Arc Hydro Tools. Geo HMS, and HEC-HMS*. https://openprairie.sdstate.edu/cvlee_pubs

Bennett, T. H., & Peters, J. C. (2004). *Continuous Soil Moisture Accounting in the Hydrologic Engineering Center Hydrologic Modeling System (HEC-HMS)*.

Bhuiyan, H., McNairn, H., Powers, J., & Merzouki, A. (2017). Application of HEC-HMS in a Cold Region Watershed and Use of RADARSAT-2 Soil Moisture in Initializing the Model. *Hydrology*, *4*(1), 9. https://doi.org/10.3390/hydrology4010009

Brocca, Ciabatta, L., Massari, C., Camici, S., & Tarpanelli, A. (2017). Soil Moisture for Hydrological Applications: Open Questions and New Opportunities. *Water 2017, Vol. 9, Page 140*, *9*(2), 140. https://doi.org/10.3390/W9020140

Brocca, L., Melone, F., Moramarco, T., Wagner, W., Naeimi, V., Bartalis, Z., & Hasenauer, S. (2010). Improving runoff prediction through the assimilation of the ASCAT soil moisture product. *Hydrology and Earth System Sciences*, *14*(10), 1881–1893. https://doi.org/10.5194/HESS-14-1881-2010

Brocca, Moramarco, T., Melone, F., Wagner, W., Hasenauer, S., & Hahn, S. (2012). Assimilation of Surface- and Root-Zone ASCAT Soil Moisture Products Into Rainfall–Runoff Modeling. *IEEE Transactions on Geoscience and Remote Sensing*, *50*(7), 2542–2555. https://doi.org/10.1109/TGRS.2011.2177468

Buytaert, W., De Bièvre, B., Wyseure, G., & Deckers, J. (2004). The use of the linear

reservoir concept to quantify the impact of changes in land use on the hydrology of catchments in the Andes. *Hydrology and Earth System Sciences*, *8*(1), 108–114. https://doi.org/10.5194/HESS-8-108-2004

Cenci, L., Laiolo, P., Gabellani, S., Campo, L., Silvestro, F., Delogu, F., Boni, G., & Rudari, R. (2016). Assimilation of H-SAF Soil Moisture Products for Flash Flood Early Warning Systems. Case Study: Mediterranean Catchments. *IEEE Journal of Selected Topics in Applied Earth Observations and Remote Sensing*, *9*(12), 5634–5646. https://doi.org/10.1109/JSTARS.2016.2598475

Chandrasekara, S. S. K., Kwon, H. H., Vithanage, M., Obeysekera, J., & Kim, T. W. (2021). Drought in south asia: A review of drought assessment and prediction in south asian countries. *Atmosphere*, *12*(3). https://doi.org/10.3390/atmos12030369

Chien, H., Yeh, P. J. F., & Knouft, J. H. (2013). Modeling the potential impacts of climate change on streamflow in agricultural watersheds of the Midwestern United States. *Journal of Hydrology*, *491*(1), 73–88. https://doi.org/10.1016/J.JHYDROL.2013.03.026

Chow, V. Te, Maidment, D. R., & Mays, L. W. (1988). *Applied Hydrology*. McGraw-Hill, Inc.

Costa, M. H., Botta, A., & Cardille, J. A. (2003). Effects of large-scale changes in land cover on the discharge of the Tocantins River, Southeastern Amazonia. *Journal of Hydrology*, *283*(1–4), 206–217. https://doi.org/10.1016/S0022-1694(03)00267-1

Czigány, S., Pirkhoffer, E., & Geresdi, I. (2010). Impact of extreme rainfall and soil moisture on flash flood generation. *IDŐJÁRÁS Quarterly Journal of the Hungarian Meteorological Service*, *114*(2), 79–100. https://www.researchgate.net/publication/289445194

Davison, A. C., & Smith, R. L. (1990). Models for Exceedances Over High Thresholds. *Journal of the Royal Statistical Society: Series B (Methodological)*, *52*(3), 393–425. https://doi.org/10.1111/J.2517-6161.1990.TB01796.X

De Silva, M. M. G. T., Weerakoon, ; S B, & Herath, S. (2014). *Modeling of Event and Continuous Flow Hydrographs with HEC-HMS: Case Study in the Kelani River Basin, Sri Lanka*. https://doi.org/10.1061/(ASCE)HE.1943-5584.0000846

Devia, G. K., Ganasri, B. P., & Dwarakish, G. S. (2015). A Review on Hydrological Models. *Aquatic Procedia*, *4*, 1001–1007. https://doi.org/10.1016/J.AQPRO.2015.02.126

Di Bucchianico, A. (2008). Coefficient of Determination (R 2) . *Encyclopedia of Statistics in Quality and Reliability*. https://doi.org/10.1002/9780470061572.EQR173

Dissanayaka, K. D. C. R., & Rajapakse, R. L. H. L. (2018). Climate Extremes And Precipitation Trends In Kelani River Basin, Sri Lanka And Impacts On Streamflow Variability Under Climate Change. *Proceedings of The International Conference on Climate Change*, *2*(2), 1–17. https://doi.org/10.17501/2513258X.2018.2201

Dobson, M. C., Ulaby, F. T., Hallikainen, M. T., & El-Rayes, M. A. (1985). Microwave Dielectric Behavior of Wet Soil-Part II: Dielectric Mixing Models. *IEEE Transactions on Geoscience and Remote Sensing*, *GE-23*(1), 35–46. https://doi.org/10.1109/TGRS.1985.289498

Dorji, K. Y. (2018). *The Effect Of Antecedent Moisture Condition On Hec-Hms Model Performance: A Case Study In Kelani River Basin, Sri Lanka*. http://dl.lib.uom.lk/handle/123/15764

Du, J., Qian, L., Rui, H., Zuo, T., Zheng, D., Xu, Y., & Xu, C.-Y. (2012). Assessing the effects of urbanization on annual runoff and flood events using an integrated hydrological modeling system for Qinhuai River basin, China. *Journal of Hydrology*, *464*, 127–139.

Dunkerley, D. (2008a). Rain event properties in nature and in rainfall simulation experiments: a comparative review with recommendations for increasingly systematic study and reporting. *Process*, *22*, 4415–4435. https://doi.org/10.1002/hyp.7045

Dunkerley, D. (2008b). Identifying individual rain events from pluviograph records: a review with analysis of data from an Australian dryland site. *Hydrological Processes*, *22*(26), 5024–5036. https://doi.org/10.1002/HYP.7122

Enrekhabi, D., Yueh, Si., O'Neil, P. E., Kellogg, K. H., Allen, A., Bindlish, R., & Administration, N. A. and S. (2014). SMAP Handbook. *Mapping Soil Moisture and Freezs/Thaw from Space*, 192.

ESRI. (2017). *ArcGIS* (10.5). Environmental Systems Research Institute, United States of America. https://desktop.arcgis.com/en/arcmap/10.5/get-started/setup/arcgis-desktop-quick-start-guide.htm

Feldman, A. D. (2000). *Hydrologic modeling system HEC-HMS: technical reference manual*. US Army Corps of Engineers, Hydrologic Engineering Center.

Ferreira, P. M. de L., Paz, A. R. da, & Bravo, J. M. (2020). Objective functions used as performance metrics for hydrological models: state-of-the-art and critical analysis. *RBRH*, *25*. https://doi.org/10.1590/2318-0331.252020190155

Gabriel-Martin, I., Sordo-Ward, A., Garrote, L., & García, J. T. (2019). Dependence Between Extreme Rainfall Events and the Seasonality and Bivariate Properties of Floods. A Continuous Distributed Physically-Based Approach. *Water 2019, Vol. 11, Page 1896*, *11*(9), 1896. https://doi.org/10.3390/W11091896

Gebre, S. L. (2015). *Application of the HEC-HMS Model for Runoff Simulation of Upper Blue Nile River Basin Enset bacteria wilt distribution in Southern Ethiopia View project Hydro climatology on Omo-Gibe River Basin View project Application of the HEC-HMS Model for Runoff Sim*. https://doi.org/10.4172/2157-7587.1000199

Gleick, P. H., & Adams, D. B. (2000). *Water: the potential consequences of climate variability and change for the water resources of the United States* (P. H. Gleick, D. B. Adams, A. J. J. Busalacchi, T. Engman, D. K. Frederick, A. P. Georgakakos, B. P. Hayden, K. L. Jacobs, J. L. Meyer, M. J. Sale, J. C. Schaake, S. S. Seacrest, R. Kuzelka, & E. Z. Stakhiv (Eds.)).

Golkhatmi, N. S. N., Sanaeinejad, S. H., Ghahraman, B., & Pazhand, H. R. (2012).

Extended Modified Inverse Distance Method for Interpolation Rainfall. 57–65.

Green, I. R. A., & Stephenson, D. (2009). Criteria for comparison of single event models. *Https://Doi.Org/10.1080/02626668609491056*, *31*(3), 395–411. https://doi.org/10.1080/02626668609491056

Gupta, H. V., Sorooshian, S., & Yapo, P. O. (1999). Status of Automatic Calibration for Hydrologic Models: Comparison with Multilevel Expert Calibration. *Journal of Hydrologic Engineering*, *4*(2), 135–143. https://doi.org/10.1061/(ASCE)1084-0699(1999)4:2(135)

Gupta, H. V., Kling, H., Yilmaz, K. K., & Martinez, G. F. (2009). Decomposition of the mean squared error and NSE performance criteria: Implications for improving hydrological modelling. *Journal of Hydrology*, *377*(1–2), 80–91. https://doi.org/10.1016/J.JHYDROL.2009.08.003

Haile, A. T., Rientjes, T. H. M., Habib, E., Jetten, V., & Gebremichael, M. (2011). Hydrology and Earth System Sciences Rain event properties at the source of the Blue Nile River. *Hydrol. Earth Syst. Sci*, *15*, 1023–1034. https://doi.org/10.5194/hess-15-1023-2011

Halwatura, D., & Najim, M. M. M. (2013). Application of the HEC-HMS model for runoff simulation in a tropical catchment. *Environmental Modelling & Software*, *46*, 155–162. https://doi.org/10.1016/J.ENVSOFT.2013.03.006

Hegedüs, P., Czigány, S., Balatonyi, L., & Pirkhoffer, E. (2013). Analysis of soil boundary conditions of flash floods in a small basin in SW Hungary. *Central European Journal of Geosciences 2013 5:1*, *5*(1), 97–111. https://doi.org/10.2478/S13533-012-0119-6

Hendawitharana, S. U., Priyasad, M. K. D. D., & Rajapakse, R. L. H. L. (2020). Comparative Study of Spatial and Temporal Variation of Drought Using Remotely Sensed Data - A Case Study for Kirindi Oya Basin. In R. Dissanayake & P. Mendis (Eds.), *Lecture Notes in Civil Engineering* (Vol. 44, pp. 116–130). Springer Singapore. https://doi.org/10.1007/978-981-13-9749-3_11

Hossain, S., Hewa, G. A., & Wella-Hewage, S. (2019). A comparison of continuous

and event-based rainfall-runoff (RR) modelling using EPA-SWMM. *Water (Switzerland)*, *11*(3). https://doi.org/10.3390/w11030611

Hu, M., Sayama, T., Duan, W., Takara, K., He, B., & Luo, P. (2017). Assessment of hydrological extremes in the Kamo River Basin, Japan. *Https://Doi.Org/10.1080/02626667.2017.1319063*, *62*(8), 1255–1265. https://doi.org/10.1080/02626667.2017.1319063

Huo, J., & Liu, L. (2020). Evaluation Method of Multiobjective Functions' Combination and Its Application in Hydrological Model Evaluation. *Computational Intelligence and Neuroscience*, *2020*. https://doi.org/10.1155/2020/8594727

Hvitved-Jacobsen, T., & Yousef, Y. A. (1988). Analysis of rainfall series in the design of urban drainage control systems. *Water Research*, *22*(4), 491–496. https://doi.org/10.1016/0043-1354(88)90045-0

IPCC. (2007). *Climate Change 2007: Synthesis Report: An Assessment of the Intergovernmental Panel on Climate Change*.

Jackson, B., Mcintyre, N., Pechlivanidis, I. G., Jackson, B. M., Mcintyre, N. R., & Wheater, H. S. (2011). Catchment scale hydrological modelling: A review of model types, calibration approaches and uncertainty analysis methods in the context of recent developments in technology and applications. *Article in GlobalNEST International Journal*, *13*(3), 193–214. https://www.researchgate.net/publication/266341273

Jayadeera, P. M., & Wijesekera, N. T. S. (2019). A Diagnostic Application of HEC–HMS Model to Evaluate the Potential for Water Management in the Ratnapura Watershed of Kalu Ganga Sri Lanka. *Engineer: Journal of the Institution of Engineers, Sri Lanka*, *52*(3), 11. https://doi.org/10.4038/engineer.v52i3.7361

Jeong, D. Il, Sushama, L., Khaliq, M. N., & Roy, R. (2014). A copula-based multivariate analysis of Canadian RCM projected changes to flood characteristics for northeastern Canada. *Climate Dynamics*, *42*(7–8), 2045–2066. https://doi.org/10.1007/S00382-013-1851-4/FIGURES/11

Johnston, R., & Smakhtin, V. (2014). Hydrological Modeling of Large river Basins: How Much is Enough? *Water Resources Management*, *28*(10), 2695–2730. https://doi.org/10.1007/S11269-014-0637-8/TABLES/4

Kamali, B., Mousavi, S. J., & Abbaspour, K. C. (2013). Automatic calibration of HEC-HMS using single-objective and multi-objective PSO algorithms. *Hydrological Processes*, *27*(26), 4028–4042. https://doi.org/10.1002/HYP.9510

Kamran, M., & Rajapakse, R. H. L. (2018). Effect of Watershed Subdivision and Antecedent Moisture Condition on HEC-HMS Model Performance in the Maha Oya Basin, Sri Lanka. *Kamran & Rajapakse/International Journal of Engineering Technology and Sciences*, *5*(2), 22–37. https://doi.org/10.15282/ijets.5.2.2018.1004

Karnieli, A. (1990). Application of kriging technique to areal precipitation mapping in Arizona. *GeoJournal 1990 22:4*, *22*(4), 391–398. https://doi.org/10.1007/BF00174760

Karra, K., Kontgis, C., Statman-Weil, Z., Mazzariello, J. C., Mathis, M., & Brumby, S. P. (2021). *Global land use / land cover with Sentinel 2 and deep learning*. 4704–4707. https://doi.org/10.1109/IGARSS47720.2021.9553499

Knebl, M. R., Yang, Z.-L., Hutchison, K., & Maidment, D. R. (2005). Regional scale flood modeling using NEXRAD rainfall, GIS, and HEC-HMS/RAS: a case study for the San Antonio River Basin Summer 2002 storm event. *Journal of Environmental Management*, *75*(4), 325–336.

Krause, P., Boyle, D. P., & Bäse, F. (2005). Comparison of different efficiency criteria for hydrological model assessment. *Advances in Geosciences*, *5*, 89–97. https://doi.org/10.5194/ADGEO-5-89-2005

Kumar, N. (2011). Water Resources Systems Planning and Management:Simulation-ReservoirOperation Simulation [electronic resource]. *NPTEL, IISC BAnglore*, *iii*, 1–8. https://nptel.ac.in/courses/105108081/28

Lang, M., Ouarda, T. B. M. J., & Bobée, B. (1999). Towards operational guidelines for over-threshold modeling. *Journal of Hydrology*, *225*(3–4), 103–117.

https://doi.org/10.1016/S0022-1694(99)00167-5

Lettenmaier, D. P., Alsdorf, D., Dozier, J., Huffman, G. J., Pan, M., & Wood, E. F. (2015). Inroads of remote sensing into hydrologic science during the WRR era. *Water Resources Research*, *51*(9), 7309–7342. https://doi.org/10.1002/2015WR017616

Liang, B., Shao, Z., Li, H., Shao, M., & Lee, D. (2019). An automated threshold selection method based on the characteristic of extrapolated significant wave heights. *Coastal Engineering*, *144*, 22–32. https://doi.org/10.1016/J.COASTALENG.2018.12.001

López, Wanders, N., Schellekens, J., Renzullo, L. J., Sutanudjaja, E. H., & Bierkens, M. F. P. (2016). Improved large-scale hydrological modelling through the assimilation of streamflow and downscaled satellite soil moisture observations. *Hydrology and Earth System Sciences*, *20*(7), 3059–3076. https://doi.org/10.5194/hess-20-3059-2016

McGill, R., Tukey, J. W., & Larsen, W. A. (1978). Variations of Box Plots. *The American Statistician*, *32*(1), 12. https://doi.org/10.2307/2683468

Mckee, T. B., Doesken, N. J., & Kleist, J. (1993). The Relationship Of Drought Frequency And Duration To Time Scales. *Eighth Conference on Applied Climatology*, 17–22.

Mckee, T. B., Doesken, N. J., & Kleist, J. (1995). Drought monitoring with multiple time scales. *Proceedings of 9th Conference on Applied Climatology, Boston, 1995*. https://ci.nii.ac.jp/naid/10028178079

McMillan, H. K., & Srinivasan, M. S. (2015). Characteristics and controls of variability in soil moisture and groundwater in a headwater catchment. *Hydrology and Earth System Sciences*, *19*(4), 1767–1786. https://doi.org/10.5194/HESS-19-1767-2015

Medina-Cobo, M. T., García-Marín, A. P., Estévez, J., & Ayuso-Muñoz, J. L. (2016). *The identification of an appropriate Minimum Inter-event Time (MIT) based on multifractal characterization of rainfall data series*.

https://doi.org/10.1002/hyp.10875

Meinzen-Dick, R., & Bakker, M. (2000). Water Rights And Multiple Water Uses: Framework And Application To Kirindi Oya Irrigation System, Sri Lanka. *International Water and Resource Economics Consortium*, *17*.

Milzow, C., Krogh, P. E., & Bauer-Gottwein, P. (2011). Combining satellite radar altimetry, SAR surface soil moisture and GRACE total storage changes for hydrological model calibration in a large poorly gauged catchment. *Hydrology and Earth System Sciences*, *15*(6), 1729–1743. https://doi.org/10.5194/HESS-15-1729-2011

Ministry of Disaster Management. (2017). *Floods and Landslides Sri Lanka Rapid Post Disaster Needs Assessment Floods and Landslides*. www.disastermin.gov.lk

Molden, D. J., Starkloff, R., Sakthivadivel, R., & Keller, J. (2001). *Hydronomic Zones for Developing Basin Water Conservation Strategies*. https://books.google.lk/books?hl=en&lr=&id=s-Xw-uq9VGUC&oi=fnd&pg=PR5&dq=Molden,+D.+J.,+Keller,+J.+and+Sakthivadivel,+R.,+2001,+"Hydronomic+zones+for+developing+basin+water+conservation+strategies",+Research+Report+56,+Colombo,+Sri+Lanka:+International+Wa

Molina-Sanchis, I., Lázaro, R., Arnau-Rosalén, E., & Calvo-Cases, A. (2016). Rainfall timing and runoff: The influence of the criterion for rain event separation. *J. Hydrol. Hydromech*, *64*, 226–236. https://doi.org/10.1515/johh-2016-0024

Moormakn, F. R., Panäbokkt, C. R., & Moormann, F. R. (1961). *Soils Of Ceylon A New Approach To The Identification And Classification Of The Most Important Soil Groups Of Ceylon*.

Moriasi, D. N., Arnold, J. G., Liew, M. W. Van, Bingner, R. L., Harmel, R. D., & Veith, T. L. (1983). Model Evaluation Guidelines For Systematic Quantification Of Accuracy In Watershed Simulations. *Transactions of the ASABE*, *50*(3).

Nandalal, H. K., & Ratmayake, U. R. (2010). Event Based Modeling of a Watershed Using HEC-HMS. *Engineer: Journal of the Institution of Engineers, Sri Lanka*,

43(2), 28. https://doi.org/10.4038/engineer.v43i2.6979

Nash, J. E., & Sutcliffe, J. V. (1970). River flow forecasting through conceptual models part I — A discussion of principles. *Journal of Hydrology*, *10*(3), 282–290. https://doi.org/10.1016/0022-1694(70)90255-6

Nasimi, M. N. (2018). *Continuous Hydrological Modeling Using Soil Moisture Accounting for Water Resources Assessment in Kelani River Basin , Sri Lanka Using Soil Moisture Accounting for Water Resources Assessment in Kelani River Basin , Sri Lanka*. *May*.

Nguyen, H. T. T., Turner, S. W. D., Buckley, B. M., & Galelli, S. (2020). Coherent Streamflow Variability in Monsoon Asia Over the Past Eight Centuries—Links to Oceanic Drivers. *Water Resources Research*, *56*(12), e2020WR027883. https://doi.org/10.1029/2020WR027883

Njoku, E. G., & Kong, J.-A. (1977). Theory for passive microwave remote sensing of near-surface soil moisture. *Journal of Geophysical Research*, *82*(20), 3108–3118. https://doi.org/10.1029/JB082I020P03108

Nojumuddin, N. S., Yusof, F., & Yusop, Z. (2018). Determination of minimum inter-event time for storm characterisation in Johor, Malaysia. *Journal of Flood Risk Management*, *11*, S687–S699. https://doi.org/10.1111/JFR3.12242

Ondieki, C. M. (1997). Potential Of Episodic Flows In Some Four Representative Non-Perennial River Flow Catchments In Semi Arid Laikipia District, Kenya. *Environmental Monitoring and Assessment 1997 45:3*, *45*(3), 285–299. https://doi.org/10.1023/A:1005751331595

Parajka, J., Naeimi, V., Blöschl, G., Wagner, W., Merz, R., & Scipal, K. (2006). Assimilating scatterometer soil moisture data into conceptual hydrologic models at the regional scale. *Hydrology and Earth System Sciences*, *10*(3), 353–368. https://doi.org/10.5194/HESS-10-353-2006

Razmkhah, H. (2016). Comparing performance of different loss methods in rainfall-runoff modeling. *Water Resources 2016 43:1*, *43*(1), 207–224. https://doi.org/10.1134/S0097807816120058

Reichle, Ardizzone, J. V., Kim, G.-K., Lucchesi, R. A., Smith, E. B., & Weiss, B. H. (2018). *Soil Moisture Active Passive (SMAP) Mission Level 4 Surface and Root Zone Soil Moisture (L4_SM) Product Specification Document*. http://gmao.gsfc.nasa.gov/pubs/office_notes.

Reichle, de Lannoy, G. J. M., Liu, Q., Ardizzone, J. V., Colliander, A., Conaty, A., Crow, W., Jackson, T. J., Jones, L. A., Kimball, J. S., Koster, R. D., Mahanama, S. P., Smith, E. B., Berg, A., Bircher, S., Bosch, D., Caldwell, T. G., Cosh, M., González-Zamora, Á., … Zeng, Y. (2017). Assessment of the SMAP Level-4 Surface and Root-Zone Soil Moisture Product Using In Situ Measurements. *Journal of Hydrometeorology*, *18*(10), 2621–2645. https://doi.org/10.1175/JHM-D-17-0063.1

Reichle, de Lannoy, G. J. M., Liu, Q., Koster, R. D., Kimball, J. S., Crow, W. T., Ardizzone, J. V., Chakraborty, P., Collins, D. W., Conaty, A. L., Girotto, M., Jones, L. A., Kolassa, J., Lievens, H., Lucchesi, R. A., & Smith, E. B. (2017). Global assessment of the SMAP Level-4 surface and root-zone soil moisture product using assimilation diagnostics. *Journal of Hydrometeorology*, *18*(12), 3217–3237. https://doi.org/10.1175/JHM-D-17-0130.1

Reichle, G. De Lannoy, R. D. Koster, W. T. Crow, J. S. Kimball, & Q. Liu. (2020). *SMAP L4 Global 3-hourly 9 km EASE-Grid Surface and Root Zone Soil Moisture Analysis Update, Version 5*. NASA National Snow and Ice Data Center Distributed Active Archive Center. https://nsidc.org/data/SPL4SMAU/versions/5

Restrepo-Posada, P. J., & Eagleson, P. S. (1982). Identification of independent rainstorms. *Journal of Hydrology*, *55*(1–4), 303–319. https://doi.org/10.1016/0022-1694(82)90136-6

Rientjes, T. H. M., Muthuwatta, L. P., Bos, M. G., Booij, M. J., & Bhatti, H. A. (2013). Multi-variable calibration of a semi-distributed hydrological model using streamflow data and satellite-based evapotranspiration. *Journal of Hydrology*, *505*, 276–290. https://doi.org/10.1016/J.JHYDROL.2013.10.006

Rostami, N., & Khalighi, S. (2016). *Calibration of loss estimation methods in HEC-HMS for simulation of surface runoff (case study: Amirkabir dam watershed,*

Iran). https://www.researchgate.net/publication/289917089

Rwetabula, J., De Smedt, F., & Rebhun, M. (2012). Simulation of hydrological processes in the Simiyu River, tributary of Lake Victoria, Tanzania. *Water SA*, *38*(4), 623–632. https://doi.org/10.4314/wsa.v38i4.18

Samady, K. (2017). Continuous Hydrologic Modeling For Analyzing The Effects Of Drought On The Lower Colorado River In Texas. *Dissertations, Master's Theses and Master's Reports*. https://doi.org/10.37099/mtu.dc.etdr/460

Sarkar, A., Kumar, R., Sarkar, A., & Kumar, R. (2012). Artificial Neural Networks for Event Based Rainfall-Runoff Modeling. *Journal of Water Resource and Protection*, *4*(10), 891–897. https://doi.org/10.4236/JWARP.2012.410105

Schaffenberg, W., & Fleming, M. (2013). Hydrologic Modeling System HEC-HMS, User Manual: Version 4.0. *US Army Corps of Engineers, Hydrologic Engineering Center HEC, 609*.

Sheffield, J., & Wood, E. F. (2007). Characteristics of global and regional drought, 1950–2000: Analysis of soil moisture data from off-line simulation of the terrestrial hydrologic cycle. *Journal of Geophysical Research: Atmospheres*, *112*(D17). https://doi.org/10.1029/2006JD008288

Shelton, S., & Lin, Z. (2019). Streamflow Variability in Mahaweli River Basin of Sri Lanka during 1990–2014 and Its Possible Mechanisms. *Water 2019, Vol. 11, Page 2485*, *11*(12), 2485. https://doi.org/10.3390/W11122485

Singh, W. R., & Jain, M. K. (2015). Continuous Hydrological Modeling using Soil Moisture Accounting Algorithm in Vamsadhara River Basin, India. *Journal of Water Resource and Hydraulic*, *4*(4), 398–408. https://doi.org/10.5963/JWRHE0404011

Sirisena, M. (2008). Basin scale drought management in Kirindi Oya River system. *Kirindi Oya Project Office, Sri Lanka. Retrieved on June, 20*, 2015.

Solari, S., & Losada, M. A. (2012). A unified statistical model for hydrological variables including the selection of threshold for the peak over threshold method. *Water Resources Research*, *48*(10), 10541.

https://doi.org/10.1029/2011WR011475

Stillman, S., & Zeng, X. (2018). Evaluation of SMAP soil moisture relative to five other satellite products using the climate reference network measurements over USA. *IEEE Transactions on Geoscience and Remote Sensing*, *56*(11), 6296–6305. https://doi.org/10.1109/TGRS.2018.2835316

Suman, S., Srivastava, P. K., Petropoulos, G. P., Pandey, D. K., & O'Neill, P. E. (2020). Appraisal of SMAP operational soil moisture product from a global perspective. *Remote Sensing*, *12*(12), 1977. https://doi.org/10.3390/rs12121977

Tavakol, A., Rahmani, V., Quiring, S. M., & Kumar, S. V. (2019). Evaluation analysis of NASA SMAP L3 and L4 and SPoRT-LIS soil moisture data in the United States. *Remote Sensing of Environment*, *229*, 234–246. https://doi.org/10.1016/j.rse.2019.05.006

Tramblay, Y., Bouvier, C., Martin, C., Didon-Lescot, J.-F., Todorovik, D., & Domergue, J.-M. (2010). Assessment of initial soil moisture conditions for event-based rainfall–runoff modelling. *Journal of Hydrology*, *387*(3), 176–187. https://doi.org/10.1016/j.jhydrol.2010.04.006

Ud Din, A. M. (2018). *Analysis of the Effect of Loss and Baseflow Methods and Catchment Scale on Performance of HEC-HMS Model for Kelani River Basin , Sri Lanka*. *June*.

USACE. (2008). Hydrologic modeling system (HEC-HMS) application guide: version 3.1. 0. *Institute for Water Resources, Davis*.

Valent, P., Szolgay, J., & Riverso, C. (2013). Assessment of The Uncertainties of a Conceptual Hydrologic Model By Using Artificially Generated Flows. *Slovak Journal of Civil Engineering*, *20*(4), 35–43. https://doi.org/10.2478/V10189-012-0020-9

Vereecken, H., Huisman, J. A., Bogena, H., Vanderborght, J., Vrugt, J. A., & Hopmans, J. W. (2008). On the value of soil moisture measurements in vadose zone hydrology: A review. *Water Resources Research*, *44*(4). https://doi.org/10.1029/2008WR006829

Vrugt, J. A., Gupta, H. V, Dekker, S. C., Sorooshian, S., Wagener, T., & Bouten, W. (2006). Application of stochastic parameter optimization to the Sacramento Soil Moisture Accounting model. *Journal of Hydrology*, *325*(1–4), 288–307. https://doi.org/10.1016/j.jhydrol.2005.10.041

Westerberg, I. K., Guerrero, J. L., Younger, P. M., Beven, K. J., Seibert, J., Halldin, S., Freer, J. E., & Xu, C. Y. (2011). Calibration of hydrological models using flow-duration curves. *Hydrology and Earth System Sciences*, *15*(7), 2205–2227. https://doi.org/10.5194/HESS-15-2205-2011

Wheater, H., Sorooshian, S., & Sharma, K. D. (2008). Hydrological modelling in arid and semi-arid areas. *Hydrological Modelling in Arid and Semi-Arid Areas.*

Wöhling, T., Samaniego, L., & Kumar, R. (2013). Evaluating multiple performance criteria to calibrate the distributed hydrological model of the upper Neckar catchment. *Environmental Earth Sciences 2013 69:2*, *69*(2), 453–468. https://doi.org/10.1007/S12665-013-2306-2

Xuefeng, C., & Alan, S. (2009). Event and Continuous Hydrologic Modeling with HEC-HMS. *Journal of Irrigation and Drainage Engineering*, *135*(1), 119–124. https://doi.org/10.1061/(ASCE)0733-9437(2009)135:1(119)

Xuereb, K., & Green, J. (2012). Defining Independence of Rainfall Events with a Partial Duration Series Approach. *Hydrology and Water Resources Symposium 2012, 34th*, 169–176.

Yang, H., Xiong, L., Ma, Q., Xia, J., Chen, J., & Xu, C. Y. (2019). Utilizing satellite surface soil moisture data in calibrating a distributed hydrological model applied in humid regions through a multi-objective Bayesian hierarchical framework. *Remote Sensing*, *11*(11), 1335. https://doi.org/10.3390/rs11111335

Zeinivand, H. (2015). Comparison of interpolation methods for precipitation fields using the physically based and spatially distributed model of river runoff on the example of the Gharesou basin, Iran. *Russian Meteorology and Hydrology 2015 40:7*, *40*(7), 480–488. https://doi.org/10.3103/S1068373915070079

Zhai, P., Pirani, A., Connors, S., Péan, C., Berger, S., Caud, N., Chen, Y., Goldfarb,

L., Gomis, M., Huang, M., Leitzell, K., Lonnoy, E., Matthews, J., Maycock, T., Waterfield, T., Yelekçi, O., Yu, R., Zhou, B., Bellouin, N., … Zickfeld, K. (2021). *IPCC, 2021: Climate Change 2021: The Physical Science Basis*. https://www.ipcc.ch/

Zhang, X., Zhang, T., Zhou, P., Shao, Y., & Gao, S. (2017). Validation Analysis of SMAP and AMSR2 Soil Moisture Products over the United States Using Ground-Based Measurements. *Remote Sensing*, *9*(2), 104. https://doi.org/10.3390/rs9020104

Zhuo, L., & Han, D. (2017). Hydrological Evaluation of Satellite Soil Moisture Data in Two Basins of Different Climate and Vegetation Density Conditions. In *Advances in Meteorology*. https://www.hindawi.com/journals/amete/2017/1086456/

ANNEXURE 1

CLIMATE EXTREMES AND TRENDS

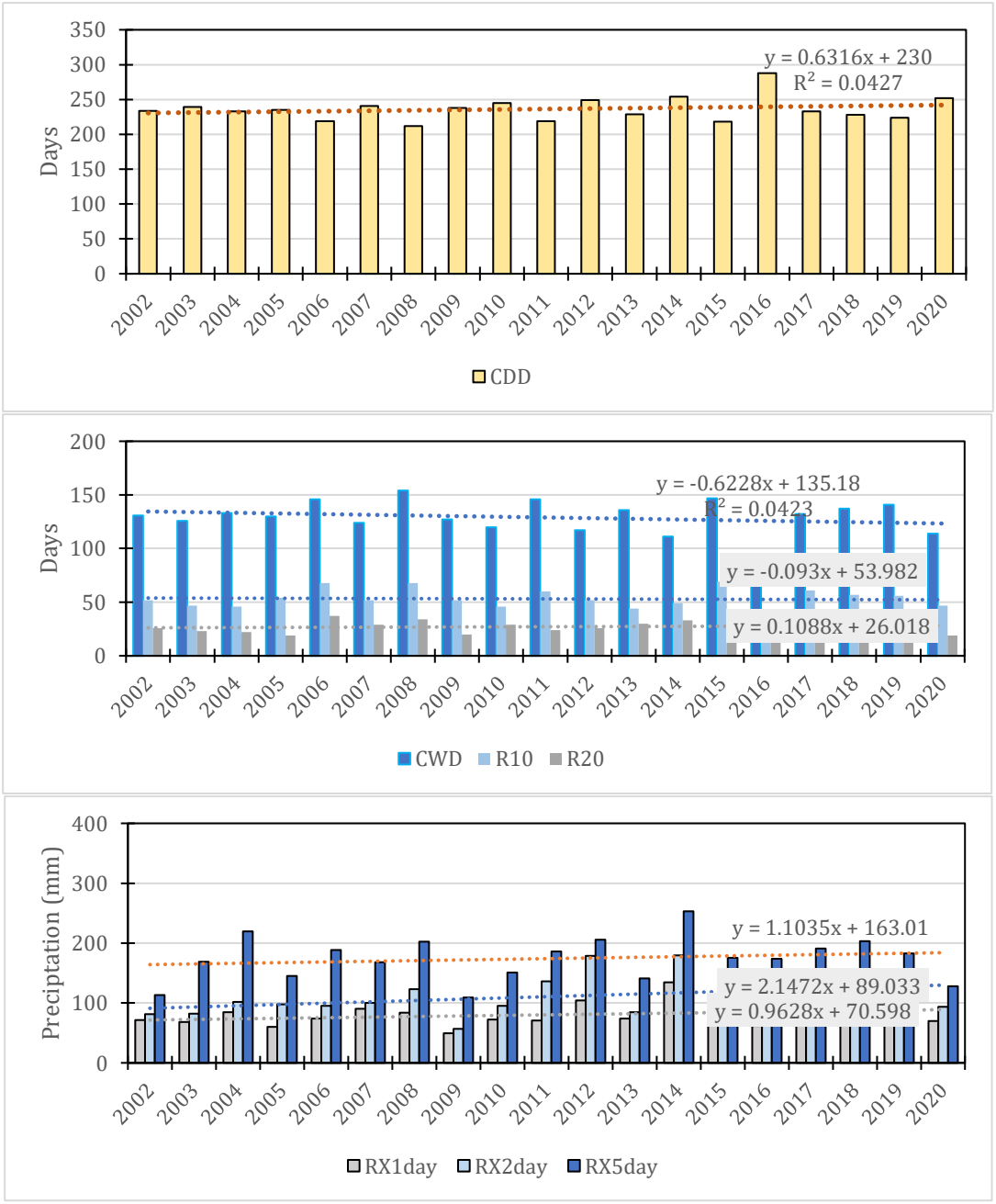

Figure A - 1: Extreme precipitation indices in Bandarawela station in Kirindi Oya basin

Figure A - 2: Extreme precipitation indices in Wellawaya station in Kirindi Oya basin

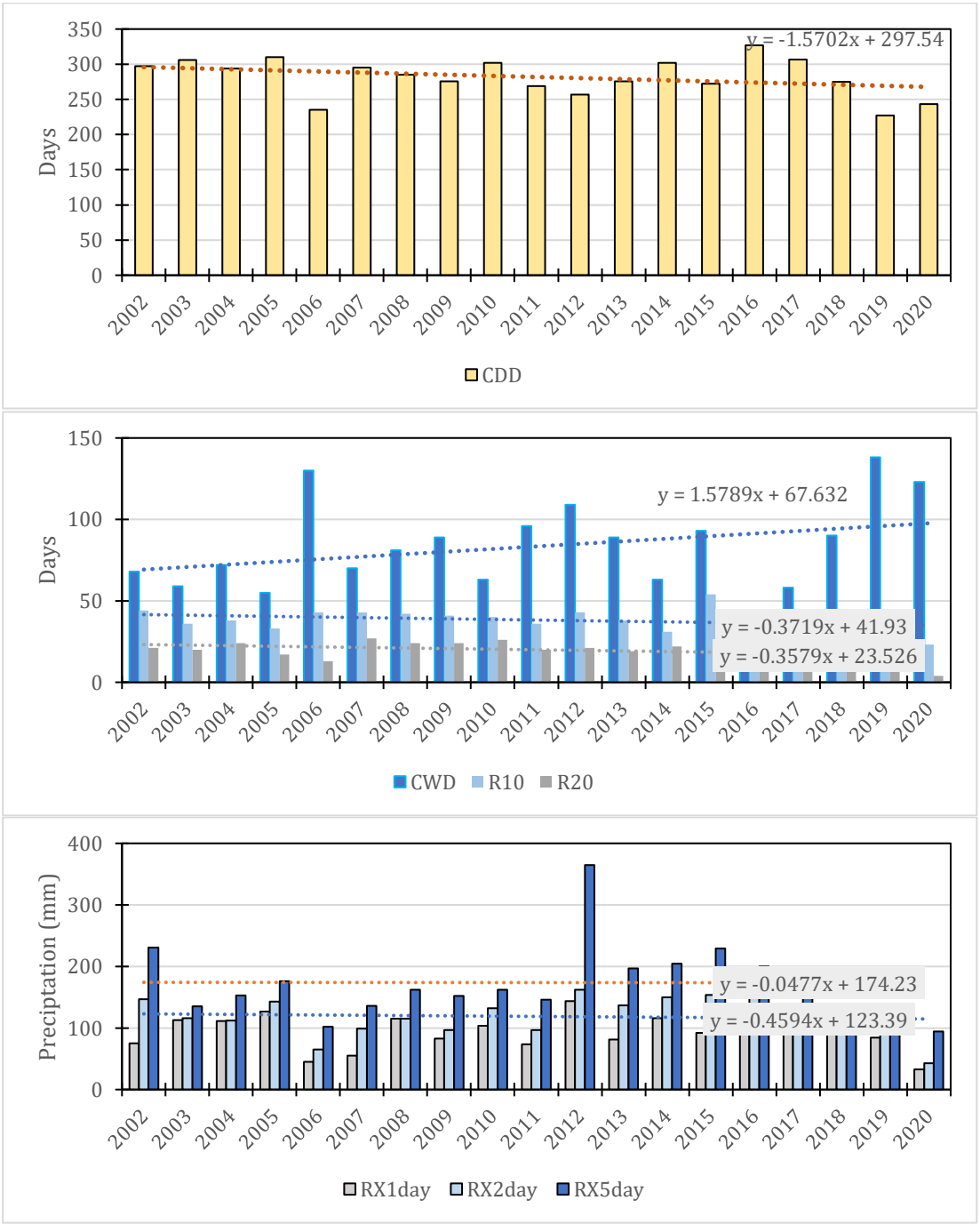

Figure A - 3: Extreme precipitation indices in Tanamalwila station in Kirindi Oya basin

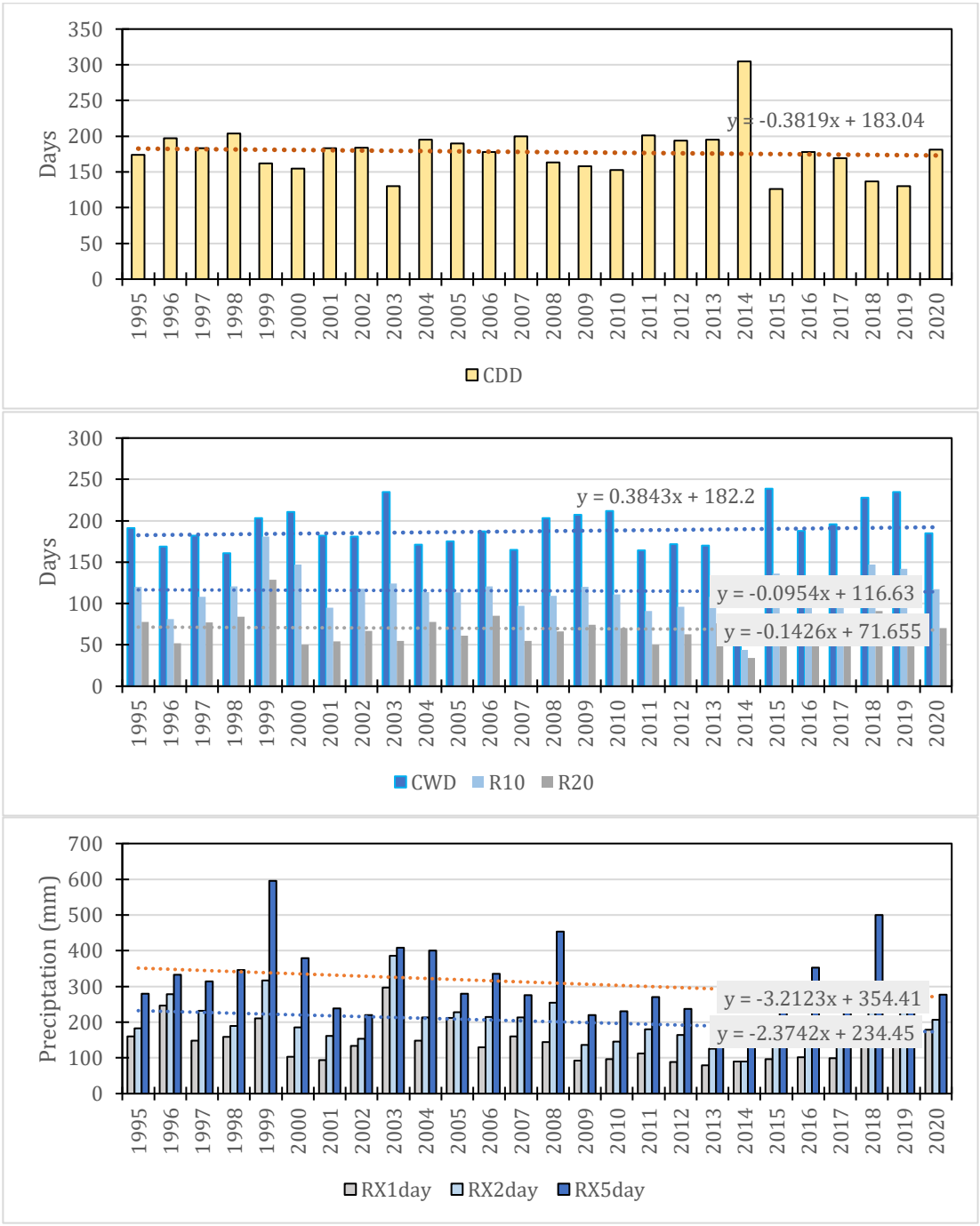

Figure A - 4: Extreme precipitation indices in Galatura station in Kalu Ganga basin

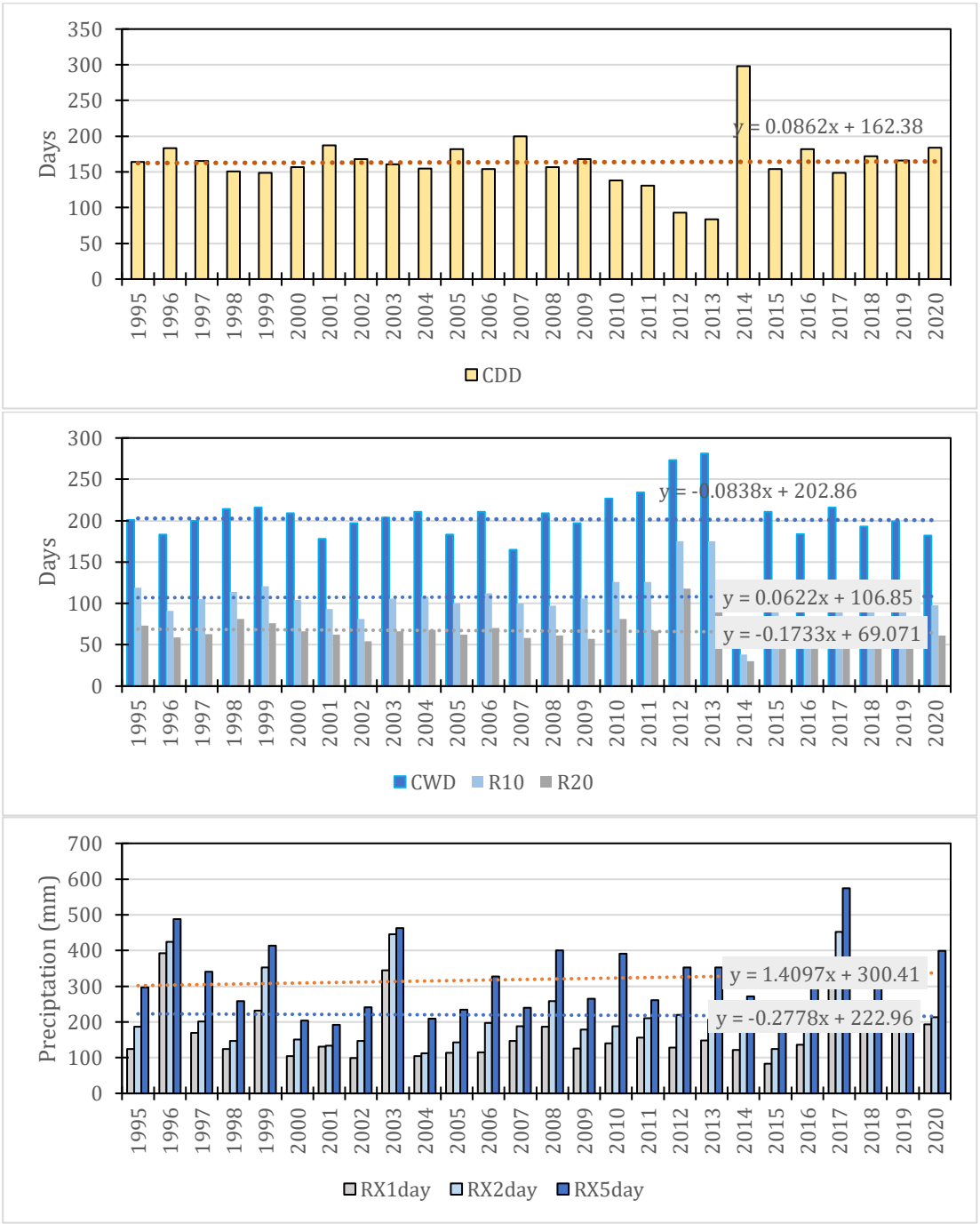

Figure A - 5: Extreme precipitation indices in Ratnapura station in Kalu Ganga basin

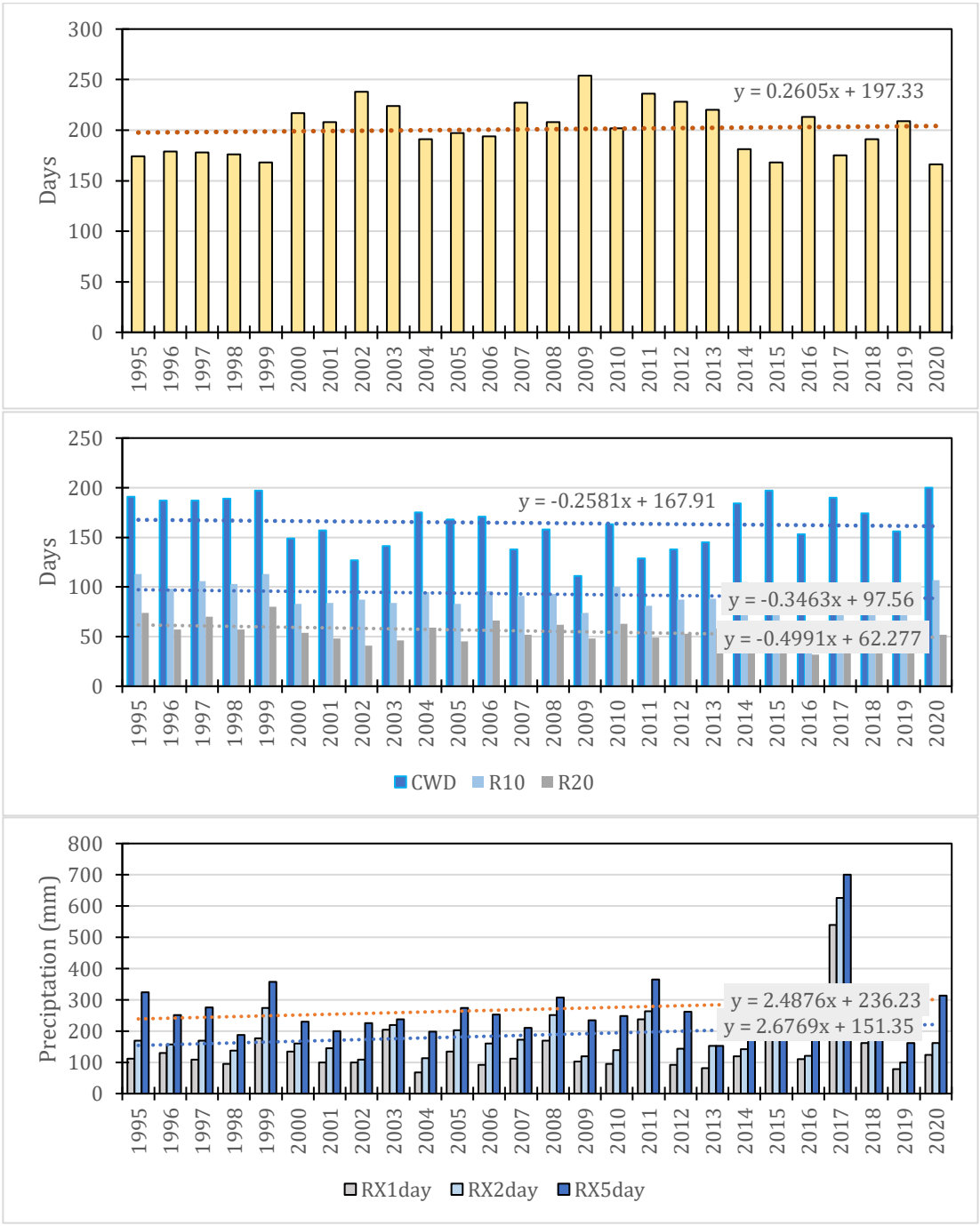

Figure A - 6: Extreme precipitation indices in Depedena station in Kalu Ganga basin

ANNEXURE 2

MODEL PARAMETERS

Different model parameters values obtained to develop the model are explained in Table A - 1 to Table A - 4 below. The methods used for calculating those parameters are also mentioned in Table A - 1 below.

Table A - 1: Parameters involved in HEC-HMS and their method of calculation

S.N.	Parameters	Description	Methods
1	Canopy max storage (mm)	Precipitation intercepted by the vegetation	Landuse map
2	Surface max storage (mm)	Water stored in the ground surface	Landuse map & DEM
3	Max infiltration rate (mm/hr)	Maximum infiltration from the surface storage into soil	Literature & calibration
4	Max soil storage (%)	Percentage of water in soil layer at beginning of simulation	Satellite SM (SMAP)
5	Groundwater 1 (%)	Percentage of water in soil layer at beginning of simulation	Literature & calibration
6	Groundwater 2 (%)	Percentage of water in soil layer at beginning of simulation	Literature & calibration
7	Soil storage (mm)	Total storage available in the upper zone of soil layer	Literature & calibration
8	Soil percolation rate (mm/hr)	Percolation from the upper zone of soil storage to the upper groundwater zone	Literature & calibration
9	Tension Storage (mm)	Amount of water storage in the soil that does not drain under the effects of gravity	Literature & calibration
10	Impervious (%)	Percentage of impervious area in the basin/subbasin	Landuse map
11	GW1 storage (mm)	Total storage in the upper groundwater layer	Streamflow recession
12	GW1 max percolation rate (mm/hr)	Percolation from the upper groundwater zone to the lower groundwater zone	Literature & calibration
13	GW1 storage coefficient (hr)	Time lag on a linear reservoir for transforming water in storage to become lateral outflow	Streamflow recession
14	GW2 storage (mm)	Total storage in the lower groundwater layer	Streamflow recession
15	GW2 max percolation rate (mm/hr)	Deep percolation out of the system	Calibration
16	GW2 storage coefficient (hr)	Time lag on a linear reservoir for transforming water in storage to become lateral outflow	Streamflow recession
17	Time of concentration	Time taken by water to flow from remote point of basin to its outlet	Kirpich Formula

Table A - 2: Parameters used for calibration of events in Kirindi Oya Basin

Parameters	Event 1	Event 2	Event 3	Event 8	Event 9
Initial Storage (%)*	10.50	10.50	10.50	10.50	10.50
Max Storage (mm)*	0.98	0.98	0.98	0.98	0.98
Initial Storage (%)**	19.48	19.48	19.48	19.48	19.48
Max Storage (mm)**	28.57	28.57	28.57	28.57	28.57
Soil (%)	3.14	23.69	37.20	32.22	32.22
GW 1 (%)	5.00	5.00	5.00	5.00	5.00
GW 2 (%)	8.00	8.00	8.00	8.00	8.00
Maximum Infiltration (mm/hr)	8.90	8.90	8.90	8.90	8.90
Impervious (%)	10.84	10.84	10.84	10.84	10.84
Soil Storage (mm)	214.05	214.05	214.05	214.05	214.05
Tension Storage (mm)	7.10	7.10	7.10	7.10	7.10
Soil Percolation (mm/hr)	6.75	6.75	6.75	6.75	6.75
GW1 Storage (mm)	10.47	10.47	10.47	10.47	10.47
GW1 Percolation (mm/hr)	0.45	0.45	0.45	0.45	0.45
GW1 Coefficient (hr)	30.67	30.67	30.67	30.67	30.67
GW2 Storage (mm)	231.63	231.63	231.63	231.63	231.63
GW2 Percolation (mm/hr)	0.20	0.20	0.20	0.20	0.20
GW2 Coefficient (hr)	305.74	305.74	305.74	305.74	305.74
Lag Time (min)	166.20	166.20	166.20	166.20	166.20
Initial Discharge (m3/s)	0.00	2.99	5.51	3.53	3.00
Recession Constant	0.88	0.88	0.88	0.88	0.88
Ratio to peak	0.11	0.11	0.11	0.11	0.11
Muskingum K (hr)	23.97	23.97	23.97	23.97	23.97
Muskingum X	0.18	0.18	0.18	0.18	0.18

* Canopy Storage

**Surface Storage

Table A - 3: Parameters used for validation of events in Kalu Ganga Basin

Parameters	Event 4	Event 5	Event 6	Event 7
Initial Storage (%)*	10.50	10.50	10.50	10.50
Max Storage (mm)*	0.98	0.98	0.98	0.98
Initial Storage (%)**	19.48	19.48	19.48	19.48
Max Storage (mm)**	28.57	28.57	28.57	28.57
Soil (%)	32.22	32.22	32.22	32.22
GW 1 (%)	5.00	5.00	5.00	5.00
GW 2 (%)	8.00	8.00	8.00	8.00
Maximum Infiltration (mm/hr)	8.90	8.90	8.90	8.90
Impervious (%)	10.84	10.84	10.84	10.84
Soil Storage (mm)	214.05	214.05	214.05	214.05
Tension Storage (mm)	7.10	7.10	7.10	7.10
Soil Percolation (mm/hr)	6.75	6.75	6.75	6.75
GW1 Storage (mm)	10.47	10.47	10.47	10.47
GW1 Percolation (mm/hr)	0.45	0.45	0.45	0.45
GW1 Coefficient (hr)	30.67	30.67	30.67	30.67
GW2 Storage (mm)	231.63	231.63	231.63	231.63
GW2 Percolation (mm/hr)	0.20	0.20	0.20	0.20
GW2 Coefficient (hr)	305.74	305.74	305.74	305.74
Lag Time (min)	166.20	166.20	166.20	166.20
Initial Discharge (m3/s)	2.24	3.03	3.87	0.88
Recession Constant	0.88	0.88	0.88	0.88
Ratio to peak	0.11	0.11	0.11	0.11
Muskingum K (hr)	23.97	23.97	23.97	23.97
Muskingum X	0.18	0.18	0.18	0.18

* Canopy Storage

**Surface Storage

Table A - 4: Parameters used for calibration and validation of events in Kalu Ganga Basin

Parameters	Calibration		Validation	
	Event 1	Event 3	Event 2	Event 4
Initial Storage (%)*	19.44	19.44	19.44	19.44
Max Storage (mm)*	2.15	2.15	2.15	2.15
Initial Storage (%)**	25.00	25.00	25.00	25.00
Max Storage (mm)**	30.59	30.59	30.59	30.59
Soil (%)	84.44	84.44	84.44	84.44
GW 1 (%)	25.00	25.00	25.00	25.00
GW 2 (%)	25.00	25.00	25.00	25.00
Maximum Infiltration (mm/hr)	9.30	9.30	9.30	9.30
Impervious (%)	9.54	9.54	9.54	9.54
Soil Storage (mm)	27.03	27.03	27.03	27.03
Tension Storage (mm)	6.15	6.15	6.15	6.15
Soil Percolation (mm/hr)	3.24	3.24	3.24	3.24
GW1 Storage (mm)	31.81	31.81	31.81	31.81
GW1 Percolation (mm/hr)	0.57	0.57	0.57	0.57
GW1 Coefficient (hr)	217.17	217.17	217.17	217.17
GW2 Storage (mm)	300.00	300.00	300.00	300.00
GW2 Percolation (mm/hr)	10.00	10.00	10.00	10.00
GW2 Coefficient (hr)	302.27	302.27	302.27	302.27
Lag Time (min)	1872.33	1872.33	1872.33	1872.33
Initial Discharge (m3/s)	16.59	16.59	16.59	16.59
Recession Constant	0.95	0.95	0.95	0.95
Ratio to peak	0.33	0.33	0.33	0.33
Muskingum K (hr)	36.23	36.23	36.23	36.23
Muskingum X	0.50	0.50	0.50	0.50

* Canopy Storage

**Surface Storage

ANNEXURE 3

EVENTS IDENTIFIED

Table A - 5: Details of events identified for calibration and validation in Kalu Ganga basin

ID	Dry days	Total Event RF (mm)	Wet days	Season	Max RF (mm)	Max 2 day RF	Peak flow (m^3/s)	Event period	Return Period (years)	5 day AMC RF (mm)	AMC type
1	1	606.7	24	Maha	132.3	143.3	971.0	08-Sep-1997 to 01-Oct-1997	2	7.6	AMC III
2	5	605.6	39	Maha	80.9	153.7	764.9	17-Aug-2017 to 24-Sep-2017	2	0.0	AMC I
3	1	477.1	11	Yala	157.9	298.1	1806.0	16-Apr-1999 to 02-Mar-1999	15	49.3	AMC III
4	1	959.8	51	Yala	322.6	397.5	1590.6	18-May-2017 to 07-Jul-2017	10	58.0	AMC III

Table A - 6: Details of events identified for calibration and validation in the Kirindi Oya basin

ID	Dry days	Total Event RF (mm)	Wet days	Season	Max RF (mm)	Max 2 day RF	Peak flow (m^3/s)	Event period	Return Period (years)	5 day AMC RF (mm)	AMC type
1	1	991.8	56	Maha	109.58	145.85	263.41	9-Oct-2012 to 3-Dec-2012	25	5.7	AMC III
2	1	324.3	14	Maha	118.29	175.4	230.95	17-Dec-2014 to 30-Dec-2014	15	6.1	AMC III
3	1	148	10	Maha	41.89	56.37	183.79	23-Nov-2005 to 2-Dec-2005	5	54.5	AMC III
4	1	223.6	13	Maha	81.25	97.43	141.05	6-Dec-2017 to 18-Dec-2017	5	37.6	AMC III
5	2	428.8	24	Maha	60.34	115.02	102.49	15-Nov-2019 to 8-Dec-2019	2	79.8	AMC III
6	1	180.3	12	Yala	58.56	113.79	67.81	12-May-2016 to 23-May-2016	1	154.6	AMC III
7	1	136.1	13	Yala	41.1	61.46	27.51	6-May-2017 to 18-May-2017	1	37.6	AMC III
8	3	87.22	12	Yala	26.98	47.98	30.36	23-Apr-2008 to 4-May-2008	1	4.1	AMC III
9	7	201.2	11	Yala	39.7	67.84	76.34	24-Apr-2013 to 4-May-2013	1	0.8	AMC I

ANNEXURE 4

COMPARISON OF SATELLITE SOIL MOISTURE, PRECIPITATION, AND DISCHARGE

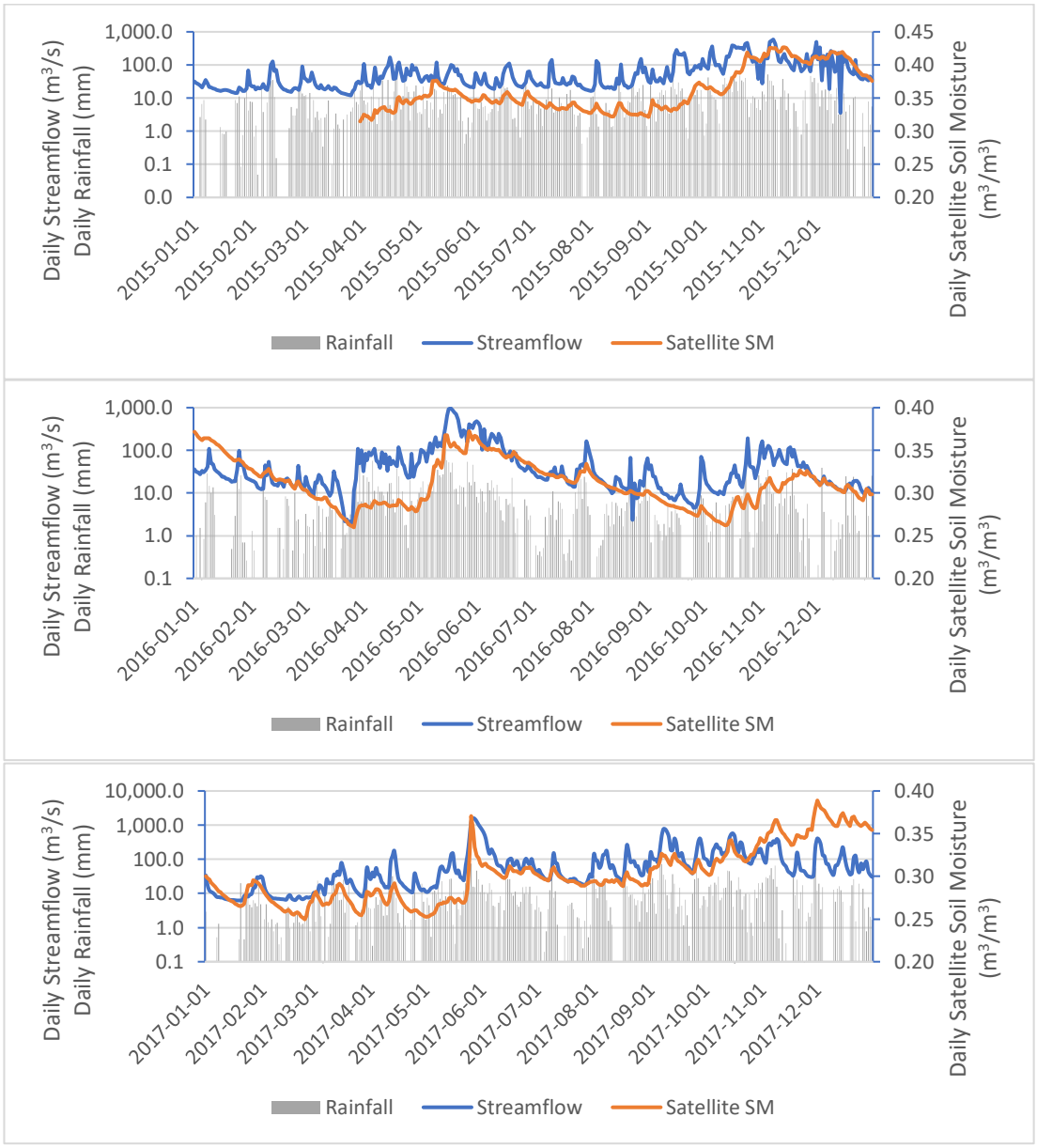

Figure A - 7: Daily root zone soil moisture (m^3/m^3) along with daily rainfall and streamflow from 2015 to 2017 in Kalu Ganga

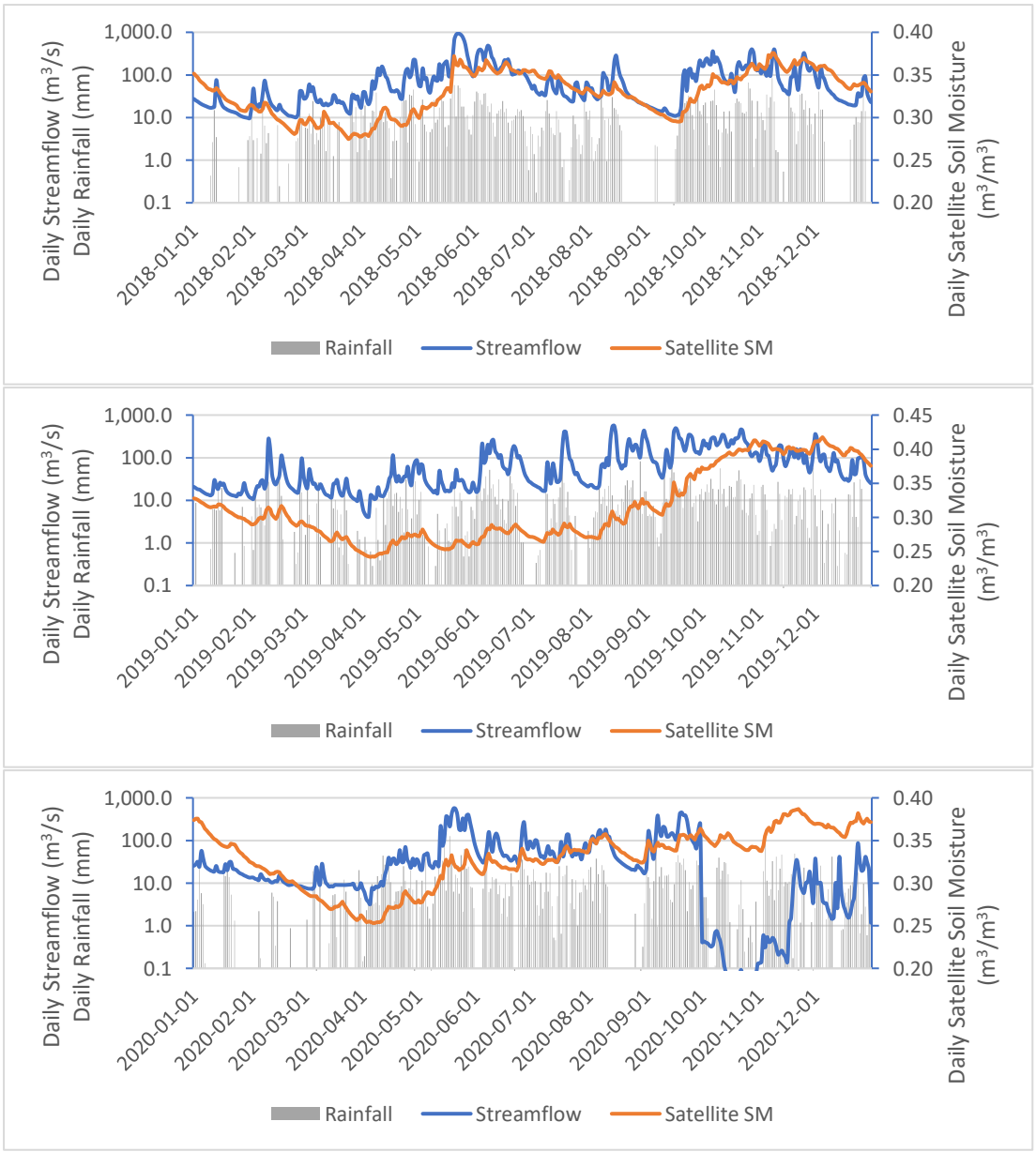

Figure A - 8: Daily root zone soil moisture (m^3/m^3) along with daily rainfall and streamflow from 2018 to 2020 in Kalu Ganga

The findings, interpretations and conclusions expressed in this thesis are entirely based on the results of the individual research study and should not be attributed in any manner to or do neither necessarily reflect the views of UNESCO Madanjeet Singh Centre for South Asia Water Management (UMCSAWM), nor of the individual members of the MSc panel, nor of their respective organizations.